Author:
Smith, Phil

Title:
A systems biology approach using electrophysiology and modelling to determine the membrane clock

A systems biology approach using electrophysiology and modelling to determine the membrane clock

By

Philip Smith

"A dissertation submitted to the University of Bristol in accordance with the requirements for award of the degree of Doctor of Philosophy in the Faculty of Life Sciences."

School of Physiology, Pharmacology, and Neuroscience

University of Bristol

September 2018

Word Count: 33,310

Abstract

Circadian rhythms (endogenous 24-hour rhythms of physiology and behaviour) are vital to health and wellbeing; disruption of these rhythms has been linked with health problems such as depression, diabetes, and cancer. Modern times have seen an increase in the use of artificial lighting at night, which has been associated with growing circadian disruption in the general population. This means that understanding of the circadian machinery is increasingly important. Previous studies have shown that clock neurons in the fruit fly *Drosophila melanogaster* called the lateral neurons ventral (LNvs) are an important part of the circadian system and display electrical properties that vary with the time of day, particularly in action potential firing rate. However, the mechanism of how these neurons produce this change is not yet fully understood.

To address this, we investigated the role of voltage-gated potassium channels in generating different activity profiles during the day and night. We utilised electrophysiological techniques, computational modelling, and behavioural assays to show that changes in the current of certain ion channels, namely Shaw (Kv3) current being highest at dawn and Shal (Kv4) current being highest at dusk, support a shift between the more active morning state and the less active evening state of LNv neuronal activity. These ion channels are key in the generation of functional circadian rhythms, where disruption is detrimental to sleep patterns, and in supporting good overall health of the fly. Computational modelling of these channels led to a model of the LNv neuronal activity that allowed the first implementation of an electrophysiological and modelling technique called dynamic clamp in *Drosophila*. The model was subsequently applied to investigation of human essential tremor and the associated channel Kv9 showing increased neuronal hyperexcitation. These results enhance the understanding of how the LNvs function and potentially offer more insight into their physiological importance.

Dedication and acknowledgments

There are numerous people who have supported this project and generously given their time and advice. First of all, thanks to my two supervisors, Dr James Hodge and Prof Krasimira Tsaneva-Atanasova who have lent invaluable help over the course of this project. Also, Prof Neil Marrion and Prof Elek Molnar, whose feedback and insight helped to shape the project.

Many thanks also go to the lab technicians as well as current and previous members of the Hodge lab: Jack Curran, Kiah Tasman, Hannah Julienne, Amanda Deakin, Simon Lowe, James Higham, and especially Edgar Buhl for help in setting up the electrophysiology and behaviour experiments.

Additional thanks go to Prof Lorraine Clark and members of her lab for the opportunity to collaborate on the essential tremor project and all the hard-work that went into making that happen.

Author’s declaration

I declare that the work in this dissertation was carried out in accordance with the requirements of the University's Regulations and Code of Practice for Research Degree Programmes and that it has not been submitted for any other academic award. Except where indicated by specific reference in the text, the work is the candidate's own work. Work done in collaboration with, or with the assistance of, others, is indicated as such. Any views expressed in the dissertation are those of the author.

SIGNED: ..... DATE:.....

Table of contents

List of figures

List of tables

List of abbreviations

ANOVA	Analysis of variance
BDS	Blood depressing substance
cAMP	Cyclic adenosine monophosphate
CLK	Clock
CREB	cAMP response element-binding protein
CRY	Cryptochrome
CYC	Cycle
CyO	Curly O balancer chromosome
DAM	*Drosophila* Activity Monitor
DD	Constant darkness
DN1-3	Dorsal neuron groups 1-3
D/NI	Diurnal/nocturnal index
DSPD	Delayed sleep-phase disorder
DTX	α-dendrotoxin
EGTA	ethylene glycol-bis(β-aminoethyl ether)-N,N,N',N'-tetraacetic acid
ET	Essential tremor
GABA	γ-aminobutyric acid
GAL4	Galactose transcription factor 4
$GAL80^{ts}$	Temperature-sensitive galactose transcription factor 80
GxTX	Guangxitoxin-1E
HH	Hodgkin-Huxley
I_A	A-type current
ipRGC	Intrinsically photosensitive retinal ganglion cells
KCNS2	Human Kv9 gene
KChIPs	Kv channel interacting proteins
Kv channel	Voltage-gated potassium channel
LD	12 h:12 h light/dark cycle
l-LNv	Large lateral neurons ventral
LNd	Lateral neurons dorsal
LNv	Lateral neurons ventral

LPN	Lateral posterior neurons
NA	Narrow abdomen
NaChBac	Bacillus sodium channel
NMJ	Neuromuscular junction
mCD8	Mammalian cluster of differentiation 8
MKRS	Balancer chromosome
PaTX	Phrixotoxin-1
PDF	Pigment-dispersing factor
PER	Period
PSO	Particle swarm optimisation
RFP	Red fluorescent protein
RNAi	RNA interference
R_S	Series resistance
RS	Rhythmicity statistic
SCN	Suprachiasmatic nucleus
SEM	Standard error of the mean
s-LNv	Small lateral neurons ventral
Slob	Slowpoke-binding protein
TIM	Timeless
TM6b	Balancer chromosome
TTFL	Transcription-translation feedback loop
TTX	Tetrodotoxin
UAS	Upstream activation site
VPAC2	Vasoactive intestinal peptide receptor
ZT	Zeitgeber Time

Chapter 1 – Introduction

1.1 Circadian rhythms

Circadian rhythms are cycles of physiology and behaviour that oscillate on a roughly 24-hour period ('circa' meaning around, and 'diem' meaning day), often in response to the periodic alternation of day and night. External inputs such as light and temperature act as 'zeitgebers' (time-givers, zeitgeber time where ZT0 indicates the zeitgeber cue of lights-on and ZT12 indicates lights-off in a 12 hours light: 12 hours dark (LD) cycle) to synchronise or entrain these rhythms to the outside environment. However, in the absence of these external time cues, these rhythms persist on a free-running basis driven by the endogenous clock.

The earliest record of study of circadian rhythms dates back to 1729 with Jean de Mairan observing that the plant *Mimosa pudica* opens and closes its leaves in a daily cycle, even when kept in constant darkness (De Mairan 1729). Since then, circadian rhythms have been found in various animals, plants, and even cyanobacteria. The importance of circadian rhythms is increasingly being acknowledged as they are found to affect a wide range of physiology and behaviours. Indeed, this culminated in the 2017 Nobel Prize for Professors Jeff Hall, Michael Rosbash, and Mike Young for their work on circadian rhythms.

The clinical importance of circadian rhythms is also gaining appreciation. It has been observed that various conditions have circadian components, such as the circadian variation in the likelihood of asthma attacks (Burioka et al. 2010) or the severity of pain in rheumatoid arthritis (Gibbs and Ray 2013). However, misalignment between a person's behaviour and their circadian clock also has health consequences. This can be seen most clearly with shift work and jet lag, where links have been made to diabetes (Knutsson and Kempe 2014), effective nursing (Harris et al. 2015), and certain cancers (Masri et al. 2015). Indeed, circadian rhythm disorders such as delayed sleep

phase disorder (DSPD) and non-24-hour sleep-wake disorder can have a major detrimental effect on patients and have been linked to increased prevalence of depression (Murray et al. 2017). The rising use of bright light in the form of phones and computer screens outside of physiologically normal times means that circadian misalignment is becoming an ever-greater issue.

1.2 Molecular regulation of circadian rhythms in *Drosophila* and mammals

The mechanism of circadian rhythm generation is perhaps best understood in molecular terms through negative feedback loops (for review see Hurley et al. 2016; Buhr and Takahashi 2013) (Figure 1.1). *Drosophila* display circadian rhythms in multiple behaviours including the sleep/wake cycle, which is similar to that of mammals (Panda et al. 2002). Here, the transcription factors *CLOCK* (*CLK*) and *CYCLE* (*CYC*) are expressed and form into heterodimers at high levels (Harbour et al. 2014). These dimers then drive the transcription and subsequent translation of *PERIOD* (*PER*) and *TIMELESS* (*TIM*), which in turn repress the expression of *CLK* and *CYC*. Degradation of *PER* and *TIM* allows the cycle to begin anew by releasing the inhibition of *CLK* and *CYC*; this degradation is regulated by phosphorylation such as by casein kinase 1ε (*CK1ε*).

In mammals, the same system applies. Here *CLK* and *BMAL1* (the mammalian ortholog of *CYC*) form the positive arm of the feedback loop driving transcription of *PER* and *CRY* (taking the place of *TIM*), which form the negative arm and inhibit *CLK* and *BMAL1*. This core transcription-translation feedback loop (TTFL) allows for the generation of circadian rhythms on an individual cell-by-cell basis and numerous additional components, such as *REV-ERB*, allow for fine-tuning.

Nevertheless, some cells do not contain a molecular clock. A particular example of this is the human red blood cells, which do not contain a nucleus. In this case, important regulators of the circadian clock were found to be a

cytosolic clock including redox reactions (O'Neill and Reddy 2011) and a membrane clock involving the transport of potassium into and out of the cells (Henslee et al. 2017).

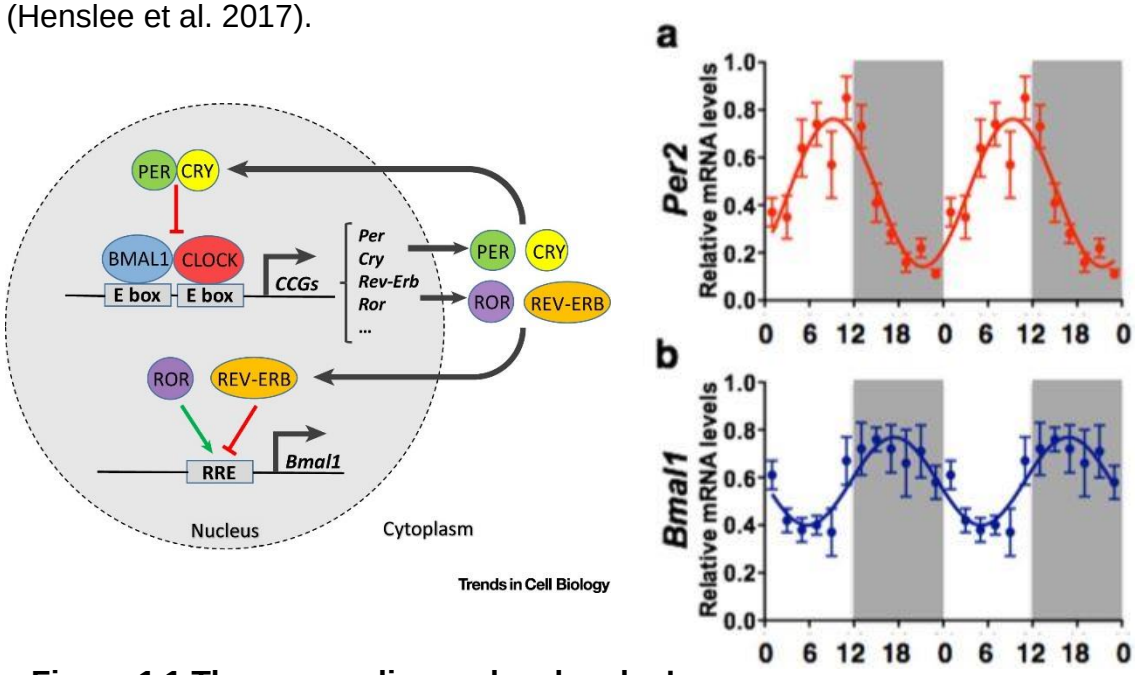

Figure 1.1 The mammalian molecular clock

Left panel: The canonical transcription-translation feedback loop (TTFL) in mammals. The core feedback loop of BMAL1/CLK and PER/CRY is shown along with a modulatory loop of REV-ERB. Reproduced from Gaucher 2018 with permission from Elsevier. BMAL1: brain and muscle ARNT-like protein, CLOCK: circadian locomotor output cycles kaput, PER: period, CRY: cryptochrome, E box: circadian regulatory element, CCGS: clock-controlled genes, REV-ERB: family of nuclear receptors, ROR: retinoic acid receptor-related orphan receptors, RRE: REV-ERB/ROR-response elements.

Right panel: mRNA expression of two genes, PER2 (a) and BMAL1 (b), in the mammalian SCN (Harbour et al. 2014). PER2 peaks during the day whereas BMAL1 peaks during the night.

1.3 Neuronal regulation of rhythms in *Drosophila* and mammals

A wide range of clocks exist throughout the human body, including in peripheral tissues, often termed 'peripheral clocks', which are regulated by the TTFL. However, to function in a cohesive manner these clocks must be synchronised and work in tandem. This is often achieved by the use of a

'master clock', sometimes called the central clock, which in mammals is termed the suprachiasmatic nucleus (SCN) (Buhr and Takahashi 2013). The SCN is located in the hypothalamus immediately superior to the optic chiasm and collates information, such as light inputs from intrinsically-photosensitive retinal ganglion cells (ipRGCs), to determine the time of day (Pickard and Sollars 2012). This is then communicated throughout the body to peripheral clocks. The SCN itself is also involved in the timing of a range of other functions beyond the sleep/wake cycle, such as cognitive performance, metabolism, and hormone secretion (Hastings et al. 2018). Certainly, flies also have a 'master clock' (Figure 1.2). The difference here is that rather than being a discrete nucleus, the fly clock consists of ~150 neurons spread throughout the fly brain (Rieger 2006; Helfrich-Förster et al. 2007; Tomchik and Davis 2008).

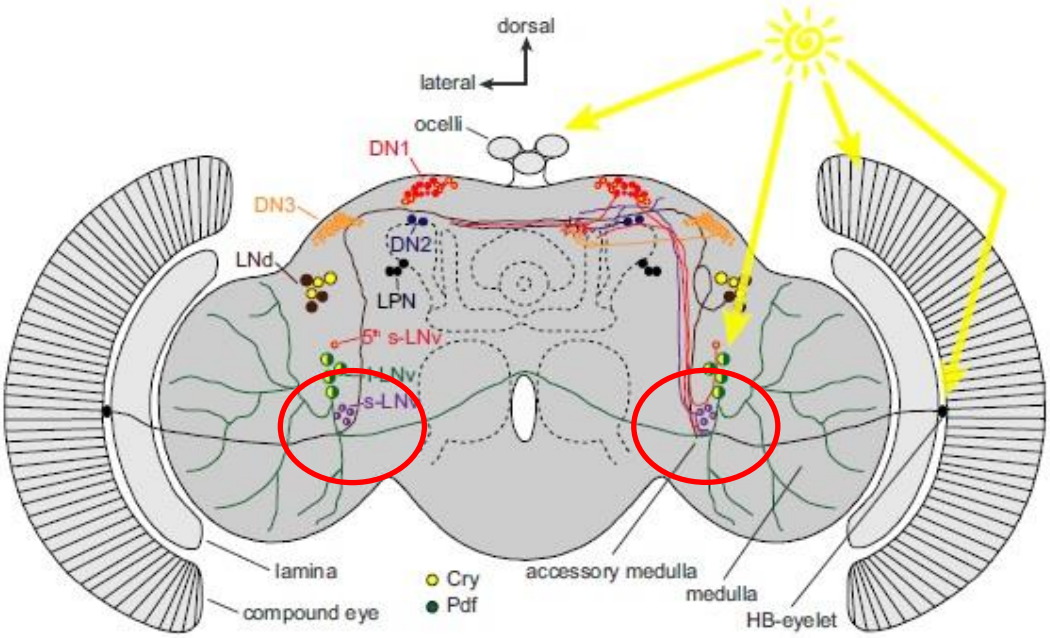

Figure 1.2 Anatomy of the fly clock

Anterior view of the *Drosophila* brain situated between the two compound eyes. Individual clock neuron clusters are indicated, particularly the lateral neurons ventral (LNvs) that are highlighted in the red circles. Reproduced from Buhl et al. 2016 with permission from PNAS. LNvs: lateral ventral neurons, LNds: lateral dorsal neurons, LPN: lateral posterior neurons, DN1-3: dorsal neurons groups 1-3, Cry: cryptochrome, Pdf: pigment dispersing factor, HB-eyelet: Hofbauer-Buchner eyelet.

The *Drosophila* clock neuron network is commonly subdivided on the basis of anatomical location. The two broad divisions are between the lateral clusters and the dorsal clusters. These then further subdivide with the lateral cluster separating into the lateral ventral neurons (LNvs), the lateral dorsal neurons (LNds), the lateral posterior neurons (LPNs), and the dorsal cluster splitting into three clusters of dorsal neurons (DN1-3). The dorsal neurons (DN1-3) have more of a modulatory function (Vosshall and Young 1995; Frisch et al. 1994; Zhang et al. 2011; Maguire and Sehgal 2015) as opposed to the core pacemakers of the lateral neurons (Grima et al. 2004; Stoleru et al. 2004).

Of particular interest are the LNvs, which are also known as the PDF neurons due to their production of the neuropeptide pigment-dispersing factor (PDF) that has a role in maintaining rhythms in constant conditions and synchronising the clock neurons (Shafer and Yao 2014; Taghert and Shafer 2006). The LNvs are particularly notable for their expression of PDF since the removal of functional PDF in the pdf^{01} mutants causes a loss of rhythms in constant darkness (Peng et al. 2003; Lin et al. 2004), placing the LNvs as important clock neurons. However, in addition to the PDF-containing dense-core vesicles, small clear vesicles have also been observed in the PDF terminals (Miskiewicz et al. 2004; Yasuyama and Meinertzhagen 2010) although the neurotransmitter contained within is still unclear. The LNvs also have a further subdivision between the more dorsally located large LNvs (l-LNvs) and the more ventral small LNvs (s-LNvs). The l-LNvs are particularly tractable for electrophysiological research and so have been more extensively examined.

Previous studies have identified that the resting membrane potential (RMP) and spontaneous action potential firing rate of the LNvs change throughout the day (Cao and Nitabach 2008; Sheeba, Gu, et al. 2008), with a higher frequency and more positive RMP at dawn compared with dusk. This circadian rhythm of electrical activity (for review see Belle and Diekman, 2018) is also seen in neurons of the mammalian SCN (Brown and Piggins 2007; Belle 2015) and persists even when dissociated (Shirakawa et al.

2000; Webb et al. 2009). The LNvs additionally show a relationship between electrical activity changes and the molecular clock in that imposing an electrical activity state causes a change in the transcriptional state (Mizrak et al. 2012). Moreover, disrupting the firing of the LNvs leads to disturbances in circadian locomotor activity (Nitabach et al. 2002; Park and Griffith 2006).

1.4 Voltage-gated potassium channels and other ion channels

Previous studies have indicated the possibility that voltage-gated potassium (Kv) channels play an important role in this phenomenon of circadian electrical activity (Itri et al. 2010; Kuhlman and McMahon 2004) and in regulation of neuronal activity (Peng and Wu 2007). The major *Drosophila* voltage-gated potassium channels are Shaker, Shab, Shaw, and Shal; homologues of the mammalian channels Kv1-4 (summarised in table 1.1).

Kv channels share a common structure of four α-subunits, each containing six transmembrane segments, combined in a tetramer that forms the functional channel. The α-subunits generally form into homotetramers within individual channel families (Covarrubias et al. 1991). In *Drosophila*, the first Kv channel identified was Shaker and this lead to identification of the related channels Shab, Shaw, and Shal (Wicher et al. 2001). Other Kv channels present in *Drosophila* are KCNQ (Kv7), ether-à-go-go also known as eag (Kv10), eag-related-gene (Kv11), and eag-like potassium channel (Kv12). Cloning of the *Drosophila* Shaker potassium channels soon led to cloning of the mammalian orthologue Kv1.1 thanks to the high degree of their sequence conservation (Tempel et al. 1988; Coetzee et al. 1999).

The Shaker channel (Kv1) conducts a rapidly activating and inactivating current (I_A current) (Peng and Wu 2007; Salkoff and Wyman 1981). Shaker associates with a β-subunit called Hyperkinetic that modulates channel properties such as activation and inactivation (Wang and Wu 1996) and mutants of Hyperkinetic have reduced sleep and impaired memory (Bushey et al. 2007). Shab channels (Kv2) contribute a sustained potassium current

and are expressed in neurons and muscle (Tsunoda and Salkoff 1995b; Hegde et al. 1999; Peng and Wu 2007). There are two genes in the Shaw (Kv3) subfamily: Shaw itself and Shawl (Hodge et al. 2005). Shaw is associated with a slowly inactivating current and is important in the *Drosophila* circadian clock (Tsunoda and Salkoff 1995a; Hodge and Stanewsky 2008). Shal channels (Kv4) also conduct a rapidly activating and inactivating I_A current that is important in a range of neuronal tissues for functions such as memory (Gasque et al. 2005; Yu et al. 1999; Ping et al. 2011).

The different kinetics of different channels such as Shaker, Shab, Shaw, and Shal lead to different roles in action potential generation. For example, some channels may activate early in the depolarisation phase whilst others may activate much later in the repolarisation phase (Figure 1.3) (Johnston et al. 2010).

Transcriptomic analyses have also shown some evidence for changes in the expression of these channels in the *Drosophila* clock neurons (Claridge-Chang et al. 2001; Kula-Eversole et al. 2010; Huang et al. 2013). This phenomenon of circadian expression of ion channels is again conserved in the mammalian SCN, where transcription or function has been shown to vary in various ion channels such as voltage-gates calcium channels, voltage-gated sodium channels, and sodium leak channels (Kudo et al. 2011; Colwell 2011; Belle 2015; Flourakis et al. 2015). In some cases, these are directly regulated by components of the circadian molecular clock, as in the case of L-type calcium channels (Schmutz et al. 2015).

Mammals	***Drosophila***
Kv1	Shaker
Kv2	Shab
Kv3.1 (and Kv3.2)	Shaw (and Shawl)
Kv4	Shal
Kv5/6	Not present
Kv7	KCNQ
Kv8/9	Not present
Kv10	ether-à-go-go (eag)
Kv11	eag-related-gene (erg)
Kv12	eag-like potassium (elk)
BK	Slowpoke (slo)
SK	dSK
Ca_V1 (L-type)	Dmca1D
Ca_V2 (N-type)	Cacophony (cac), Dmca1A
Ca_V3 (T-type)	Dmca1T
Na_V1-10	Paralytic (para)

Table 1.1 Ion channel nomenclature of mammals and *Drosophila*

A summary of major ion channel names between mammals and *Drosophila*.

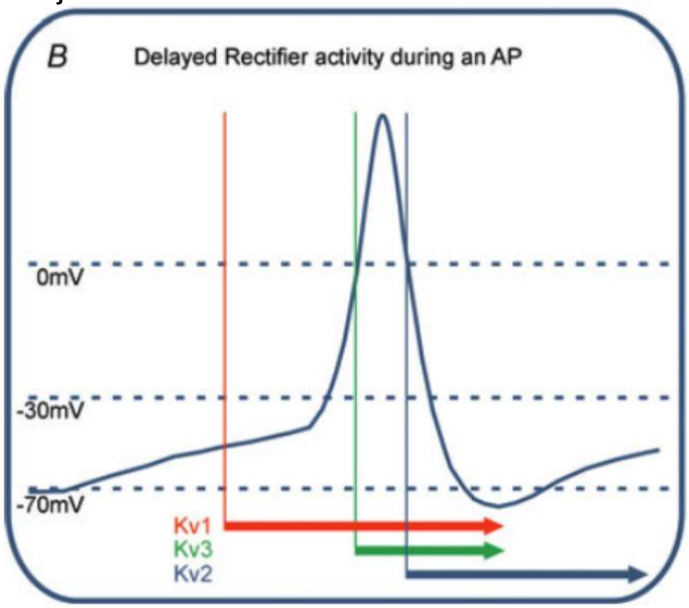

Figure 1.3 Ion channel activation in an action potential

Kv channel kinetics cause different channels to activate during different parts of an action potential waveform. Shown is an example of Kv1, Kv2, and Kv3 activating at different points of a mammalian action potential as indicated by the coloured arrows. Reproduced from Johnston et al. 2010 with permission from Elsevier.

1.5 *Drosophila* as a model organism for circadian research

The *GAL4/UAS* system is a commonly used binary expression system in *Drosophila* (Fischer et al. 1988; Brand and Perrimon 1993; Duffy 2002). The system uses a yeast transcription activator (*GAL4*) inserted into the fly genome under the control of a specific promoter. Upon transcription of the *GAL4* in those cells expressing the promoter region, this activates the transcription of a *UAS* sequence that is also inserted into the genome along with a gene of interest. This means that mating of a *GAL4* fly strain and a *UAS* fly strain will cause spatially-restricted expression of a gene in the progeny. *GAL4* and *UAS* strains are commonly available, allowing expression of a wide variety of genes in a range of cell types. Notable examples are *Elav-GAL4*, which expresses in all neurons, *tim-GAL4*, which expresses in all clock neurons, and *PDF-GAL4*, which expresses in LNvs.

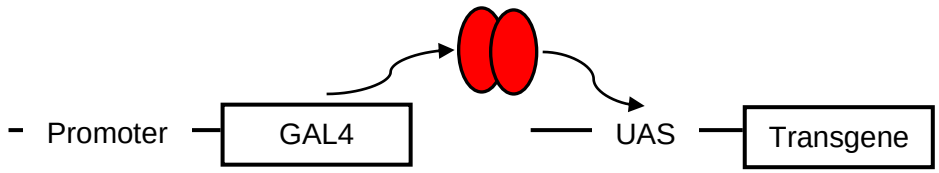

Figure 1.4 *GAL4/UAS* Gene expression system

Diagrammatic representation of the *GAL4/UAS* system, whereby a promoter controls expression of the transcription factor *GAL4*. Once expressed, *GAL4* activates the *UAS* region, enhancing expression of a transgene.

1.6 Aims of the thesis

The aim of this thesis is to investigate the mechanism underpinning circadian variation of LNv electrical activity, as well as the physiological consequences of disrupting this variation. In order to do this, three lines of research were undertaken: electrophysiological examination of the LNvs, mathematical modelling of electrophysiological data, and investigation of circadian behaviour and longevity. The over-arching hypothesis is that circadian

changes in voltage-gated potassium channels lead to the observed changes in electrical activity of the LNv and that these changes are important for the overall health of the animal.

Chapter 2 details the materials and methods used throughout the thesis. Chapter 3 presents electrophysiological data from whole-cell patch clamping of the LNvs, particularly pertaining to voltage-gated potassium channels where circadian changes were detected in the channels Shaw and Shal. Chapter 4 uses the electrophysiological data of chapter 3 to generate a model of the activity of the LNvs and subsequently use this to implement dynamic clamp. Here, the circadian variation of Shaw and Shal is sufficient to recapitulate the variation in electrical behaviour. Chapter 5 illustrates changes in circadian behaviour and longevity due to manipulation of the system. Dominant negative block of Shaw and Shal causes changes in activity and longevity that are similar to dominant negative block of the clock genes *cycle* and *clock*. Chapter 6 combines these approaches in the study of human essential tremor. Chapter 7 discusses the significance of these results.

Chapter 2 - Materials & methods

This chapter describes the materials and methods used throughout this thesis. Section 2.1 outlines the fly stocks used and the conditions under which they were maintained. Section 2.2 introduces the electrophysiological techniques used including the voltage protocols, solutions, and drugs used in the assays. Section 2.3 describes the behavioural assays looking at longevity and circadian locomotor behaviour. Section 2.4 outlines the computational methods used in modelling the system. Finally, section 2.5 describes the statistical analysis methods.

2.1 Flies

The fruit fly *Drosophila* melanogaster was used as the model organism in this thesis. Section 2.1.1 outlines the conditions they were kept in. Section 2.1.2 gives an overview of the fly lines used along with brief explanations of the transgenes they carried.

2.1.1 Fly husbandry

Flies were raised in standard plastic vials or bottles containing standard fly food. The fly food was prepared in 5l batches consisting of: agar (35 g), soya flour (50 g), polenta (400 g), dried yeast (90 g), malt extract (400 g), molasses (200 g), proprionic acid (40 ml), nipagin (100 ml), and water. The food cooled and set overnight before addition of a cotton ball top (flug) to avoid build-up of condensation.

Flies were maintained in standard conditions of a 12h: 12h light/dark cycle (LD), at a temperature of 25°C and humidity of 60% unless otherwise stated. Before handling, flies were anaesthetised using CO_2 as required.

2.1.2 Fly stocks

The main fly line used was +; *PDF-RFP*/*CyO*; *MKRS*/*TM6b* as used in other studies (Buhl et al. 2016). This fly line expresses red fluorescent protein (RFP) using the promoter of the pigment-dispersing factor (PDF) neuropeptide gene. Thus, the LNvs, which primarily use PDF as their neuropeptide, are selectively labelled allowing targeted study.

For spatially-restricted expression of genes the *GAL4/UAS* system was employed (see Chapter 1, Figure 1.4). For expression within the LNvs, the *PDF-GAL4* line was used (Renn et al. 1999; Park et al. 2000); this line also included *UAS-mCD8-RFP* for visualisation of these neurons (Bloomington stock centre number BL27392) or the fusion protein PDF-RFP for similar purposes (Ruben et al. 2012). Expression throughout the clock neurons was achieved through use of *tim-GAL4* (Stanewsky et al. 1998). The *UAS-ShawTR332* (Hodge et al. 2005) and *UAS-Shal pore 14* (Ping et al. 2011) transgenes are dominant negative subunits of the Shaw and Shal channels, respectively. These encode dominant negative subunits that, when assembled with endogenous Shaw and Shal subunits, form heteromeric channels that are rendered unable to conduct potassium ions. Manipulation of Shab was attained through the use of a total Shab null line (Hegde et al. 1999) as well as through the use of RNA interference (*RNAi*) (Ni *et al.*, 2011, Bloomington's BL55682). Shaker similarly was manipulated by *RNAi* (Vienna KK104474). Essential tremor genes KCNS2 and KCNS2-D379E (Liu et al. 2016; Smith et al. 2018) were used to simulate ET pathology and to affect the Shab current in more subtle ways. A fly line where the endogenous Shab gene was knocked out and replaced by a Shab gene including a similar mutation to the KCNS2-D379E mutation was also used (Shab-D658E). The molecular clock of the neurons was also altered by the use of dominant negative clock genes *UAS-CLK-Δ5* and *UAS-CYC-Δ103* (Tanoue et al. 2004). These lines are summarised in table 2.1.

Table 2.1 Transgenic fly lines

Gene Name (Chromosome)	Function of gene	Source
PDF-RFP (II)	Fusion protein of PDF and RFP for visualisation of LNvs	(Ruben et al. 2012)
PDF-GAL4 (II)	Drives expression in LNvs	(Renn et al. 1999; Park et al. 2000)
tim-GAL4 (II)	Drives expression in clock neurons	(Stanewsky et al. 1998)
UAS-mCD8-RFP (III)	Allows visualisation of target	BL27392
UAS-ShawTR332 (III)	Expresses the Shaw dominant negative subunit	(Hodge et al. 2005) BDSC 55748
UAS-Shal pore 14 (III)	Expresses the Shal dominant negative subunit	(Ping et al. 2011)
Shab 507	Shab knock-out	(Hegde et al. 1999)
UAS-Shab RNAi (III)	Knocks down Shab	(Ni et al. 2011) BL55682
UAS-Shaker RNAi (II)	Knocks down Shaker	KK104474
UAS-KCNS2 (II)	Expresses the human wild-type KCNS2 (Kv9)	(Liu et al. 2016; Smith et al. 2018)
UAS-KCNS2-D379E (II)	Expresses the human ET mutant KCNS2 (Kv9)	(Liu et al. 2016; Smith et al. 2018)
UAS-CLK-Δ5 (II)	Expresses a CLK dominant negative	(Tanoue et al. 2004) BDSC 36318
UAS-CYC-Δ103 (II)	Expresses a CYC dominant negative	(Tanoue et al. 2004)BDSC 36317

Table 2.1 Transgenic fly Lines

A summary of the main transgenes used and their function.

2.2 Electrophysiology

The electrical activity of the LNvs was assayed by whole cell patch-clamp, whereby the neuron is connected to a pipette tip and the intervening cell membrane is ruptured by the use of negative pressure, resulting in the cell cytosol and the intracellular solution in the pipette becoming continuous. Section 2.2.1 introduces the procedure of removing the explant *Drosophila* brain. Section 2.2.2 outlines the methods and apparatus used in the whole cell patch-clamp set-up. Section 2.2.3 describes the voltage clamp protocol utilised in assaying the current response of the various ion channels. Section 2.2.4 lays out the extracellular and intracellular solutions used. Section 2.2.5 gives detail on the pharmacological drugs used. Finally, section 2.2.6 describes the set-up used for dynamic clamp.

2.2.1 Brain dissection

Adult flies aged 0-5 days post-eclosion (hatching) were anaesthetised by CO_2 and dissected prior to patch clamping using an establish method (Buhl et al. 2016; Chen et al. 2015) after entrainment to a 12:12 LD cycle, unless otherwise stated. Brain dissection was performed in a Petri dish with standard *Drosophila* external recording solution consisting of (in mM): 101 NaCl, 1 $CaCl_2$, 4 $MgCl_2$, 3 KCl, 5 glucose, 1.25 NaH_2PO_4, and 20.7 $NaHCO_3$ with a pH of 7.2 and an osmolality of 250mOsm. The dissection involves removal of the full head cuticle along with photoreceptors and lamina; the air sacs and trachea are also removed. The preparation was discarded if the LNvs were visibly damaged. Once the brain is fully accessible, it is transferred to a recording chamber of fresh extracellular solution and secured with a brain harp with the anterior-side facing upwards (Figure 2.1).

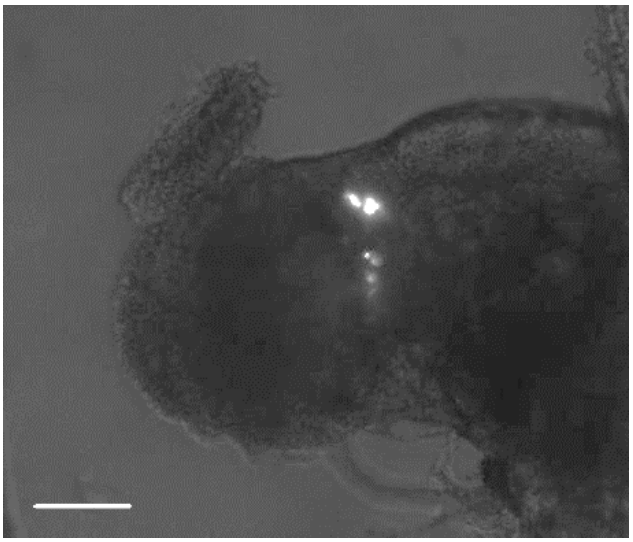

Figure 2.1 Adult fly brain with LNvs fluorescently labelled.

Anterior view of the *Drosophila* brain. The LNvs can be seen by visualisation of red fluorescent protein (RFP) fluorescence; the large LNvs can be seen more dorsally with the small LNvs more ventrally. Scale bar = 50 µm.

2.2.2 Whole cell patch clamp

LNvs were visualised by red fluorescent protein (RFP) fluorescence with a 555 nm LED light source and distinguished by size and anatomical location for separation of the LNvs into the two subpopulations of s- and l-LNv (small and large); l-LNvs are located dorsal to the s-LNvs and have a diameter of approximately 10-11 µm, whereas the s-LNvs have a diameter of approximately 7 µm (Schubert et al. 2018).

Whole cell patch clamp of visualised neurons was performed using standard borosilicate capillary glass pipettes (World Precision Instruments), which were pulled using a Sutter P-1000 pipette puller to a resistance of 8–15 MΩ. Whole cell currents peak around the mean of 250 pA and series resistance was compensated to approximately 70%, thus the maximum voltage error for an access resistance of 40 MΩ was roughly 3 mV. Recordings were not used if the access resistance was above 50 MΩ or if it increased by more than 20% during recordings.

Data were acquired using a Multiclamp 700B amplifier and Axon Digidata 1440A digitiser through pClamp10 software (Axon Instruments). A sampling rate of 20 kHz was used, and signals were filtered using a 10 kHz low-pass Bessel filter; this filter frequency represents the Nyquist frequency.

2.2.3 Voltage protocol

Voltage-clamp recording protocols were based on previous studies (Solc and Aldrich 1988; Wei et al. 1990; Peng and Wu 2007). Neurons were held during resting periods at a resting membrane potential of -63 mV, below the normal resting membrane potential of -50 to -55 mV (Cao and Nitabach 2008). During voltage step protocols, the holding membrane potential was -93 mV. To generate I-V relationships, a standard protocol was used consisting of a hyperpolarising step of -40 mV to -133 mV for 500 ms and then subsequently depolarising steps in increments of 10 mV to between -93 mV and -3 mV, covering the physiological range observed, for a duration of 200 ms before a return to the holding potential. This is summarised in Figure 2.3. Where peak currents are used this refers to the maximum current recorded during the depolarisation step.

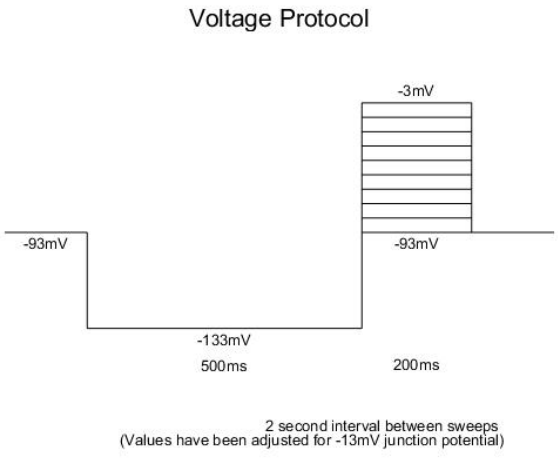

Figure 2.2 Voltage-clamp protocol

Diagrammatic scheme of voltage steps utilised in generating IV relationships. The initial holding potential of -93 mV is hyperpolarised to -133 mV for 500 ms before a range of depolarising steps between -93 mV and -3 mV for 200 ms.

2.2.4 Recording solutions

The standard *Drosophila* external recording solution consisted of (in mM): 101 NaCl, 1 $CaCl_2$, 4 $MgCl_2$, 3 KCl, 5 glucose, 1.25 NaH_2PO_4, and 20.7 $NaHCO_3$ with a pH of 7.2 and an osmolality of 250 mOsm. The recording pipettes were filled with standard intracellular solution consisting of (in mM): 102 K-gluconate, 0.085 $CaCl_2$ (free calcium concentration 29 nM), 1.7 $MgCl_2$, 17 NaCl, 0.94 EGTA, and 8.5 HEPES with a pH of 7.2 and an osmolality of 235 mOsm (Chen et al. 2015; Buhl et al. 2016). The solutions used in this thesis have been utilised in the study of *Drosophila* previously for a variety of neuronal groups such as the LNvs, other clock neurons and other non-clock neurons (Gu and O'Dowd 2006; Wilson et al. 2004; Sheeba, Gu, et al. 2008; Cao and Nitabach 2008).

The resulting junction potential between the two solutions has been calculated and measured as being 13 mV (data shown in this thesis has been adjusted to account for this).

In assays examining sodium or calcium currents a different intracellular solution is used consisting of (in mM): 102 Cs-gluconate, 0.085 $CaCl_2$, 1.7 $MgCl_2$, 17 NaCl, 0.94 EGTA, and 8.5 HEPES with a pH of 7.2 and an osmolality of 235 mOsm. Here the use of caesium instead of potassium ions blocks the voltage-gated potassium channels. The liquid junction potential was calculated as 13.1 mV.

2.2.5 Pharmacology

In order to isolate individual ion channel currents, Kv channel specific blockers were used. Stock solutions of α-dendrotoxin (DTX), blood depressing substance I (BDS), guangxitoxin-1E (GxTX), phrixotoxin-1 (PaTX), and tetrodotoxin (TTX) were made up using extracellular solution; all drugs were purchased from Alomone labs. During recordings, the stock drug solutions were bath applied by pipette to 1 mL of external solution in the

recording chamber to achieve final drug concentrations of 100 nM for DTX, 20 nM for GxTX, 300 nM for BDS, 100 nM for PaTX, and 6 µM for TTX before bathing for a minimum of 2 minutes before further recording. For recovery experiments, a perfusion system was utilised to wash extracellular solution through the recording chamber in order to wash out drugs.

The toxin DTX is a blocker of the voltage-gated potassium channel Shaker, the homologue of Kv1 in mammals (Baumann et al. 1988). DTX itself is one of several toxins derived from the green mamba *Dendroaspis angusticeps* (Harvey and Karlsson 1980). It was later found that there are actually four dendrotoxins: α, β, γ, and δ (Benishin et al. 1988) that are similar to the black mamba toxins I and K (Botes et al. 1974). A subsequent structure of α-DTX was solved (Skarzyński 1992). The effect of DTX on mammalian cells and Xenopus oocytes shows that the IC_{50} for Kv1 channels is between 1 to 150 nM depending on the system (Harvey 2001).

GxTX is a blocker of the Shab channel, the ortholog of Kv2 in mammals. Derived from the Chinese tarantula *Plesiophrictus guangxiensis*, there are two forms of guangxitoxin that differ by a single N-terminal residue. Both forms inhibit Kv2 channels in the low nanomolar range with an IC_{50} of roughly 3 nM (Herrington et al. 2006) reaching almost complete inhibition at approximately 10 nM (Tilley et al. 2014). GxTX was also found to have some effect on Kv4.3 channels, but with a lower sensitivity resulting in an IC_{50} roughly ten times that of Kv2 channels (Herrington et al. 2006). The mechanism of action has been suggested to be based in alteration of the activation voltage-dependence (Herrington 2007). This was reported to be through modulation of the voltage sensor domain of the channel leading to a higher threshold for activation (Gupta et al. 2015). Hanatoxin derived from the Chilean tarantula *Phrixotrichus spatulata* is another toxin selective for Kv2 channels, however it is less widely available than GxTX due to more difficulty in synthesis.

BDS is a blocker of the Shaw channel, the homologue of Kv3 in mammals; although recent studies have suggested the toxin acts more as a modulator

of Kv3 activity than as a blocker by shifting activation to more positive voltages (Yeung 2005). BDS-I and -II are derived from the sea anemone *Anemonia sulcata* and differ by only two amino acids. In COS cells transfected with voltage-gated potassium channels it was observed that Kv3.4 current was reversibly inhibited by BDS-I with an IC_{50} of around 47 nM (Diochot et al. 1998). This finding has been corroborated in other systems such as rat brains where micromolar concentrations of BDS-I broadened action potentials and reduced spike frequency (Baranauskas et al. 2003). BDS-I has also been shown to affect Kv3.1 and Kv3.2 channels by modulation of gating kinetics (Yeung 2005).

PaTX is a blocker of the Shal channel, the ortholog of Kv4 in mammals with 82% amino acid identity between *Drosophila* and mouse (Pak et al. 1991). PaTX is isolated from the venom of the Chilean copper tarantula *Phrixotrichus auratus*. It has been shown to block potently A-type potassium currents, with notable specificity for Kv4 channels with an IC_{50} of between 5 and 70 nM while no significant effect was observed on Kv1, Kv2, or Kv3 channels in the micromolar range (Diochot et al. 1999). The structure has been solved and is fairly similar to other venoms such as ScTx1 and HmTX, which also modify voltage-gated potassium channels (Chagot et al. 2004). *Drosophila* Shal has been shown to be sensitive to PaTX in the low micromolar range (Gasque et al. 2005).

TTX is a potent blocker of the voltage-gated sodium channels (Narahashi et al. 1964) in the nanomolar range. This was later verified on systems such as squid giant axon, eel electric organ, and frog myelinated axons (Nakamura et al. 1965; Hille 1966; Hille 1967; Hille 1968). Its name derives from the tetraodontiformes, the order of puffer fish that notably carry this toxin (Lago et al. 2015). However, many different species such as octopus and certain worms have been found to possess this toxin. It has been indicated that the toxin is actually a product of some *Pseudomonas* and *Vibrio* bacteria; indeed, it does occur in those bacteria and explains the independent emergence of the toxin in widely different species. TTX is particularly useful in studying neuronal function through the block of action potential firing.

2.2.6 Dynamic clamp

Virtual voltage-gated ion channel conductance, with kinetics based on the Hodgkin-Huxley formalism (equations 2.1-2.4), were introduced to patch clamp recordings by use of the CED Power 1401 system (Cambridge Electronic Design) and recordings made using Signal (version 6.05, Cambridge Electronic Design) in the same manner as standard patch clamp recordings (section 2.2.2). Maximal conductance of the models was adjusted in accordance with variation in cell membrane capacitance (Table 2.2).

Table 2.2 Conductances used in dynamic clamp experiments

Conductance (nS)	Shaker (Kv1)	Shab (Kv2)	Shaw (Kv3)	Shal (Kv4)
	2.35	0.86	1.40	0.8
	2.05	0.66	1.40	0.8
	1.90	0.66	1.30	0.8
	1.60	0.44	1.30	0.8
	1.55	0.44	1.30	0.8

Conductance (nS)	Shaw (Kv3)	Shal (Kv4)
Day to Night	-1.4	1.25
	-1.2	1.15
	-1.1	1.00
	-0.8	0.90
Night to Day	1.4	-1.25
	1.2	-1.1

Table 2.2 Conductances used in dynamic clamp experiments

Conductances used for each of the Kv channel models in dynamic clamp experiments to rescue pharmacological block (top) and to switch between morning and evening states of neuronal activity (bottom). Rows indicate separate experiments and negative conductances are shown as used in Signal to remove ion channel current.

2.3 Behavioural assays

The behaviour of flies was examined by standard assays. Section 2.4.1 outlines the longitudinal study of fly longevity. Section 2.4.2 describes the set-up for measuring the circadian locomotor activity of flies.

2.3.1 Longevity assay

The longevity of different genotypes of fly was assayed by a standard longevity assay (Metaxakis and Partridge 2013; Linford et al. 2013). Flies were collected daily and separated into single sex vials of around 10 male or females flies per day per genotype allowing for close monitoring. Flies were flipped into vials of fresh food (Section 2.1.1) every 3-4 days, maintained at 25°C, and examined daily to identify any mortality.

2.3.2 *Drosophila* activity monitor (DAM)

Circadian locomotion of flies was studied through the recording of locomotor activity of individual flies in the presence or absence of external time cues such as light. The apparatus used was the Trikinetics *Drosophila* Activity Monitor (DAM2, Trikinetics Inc., Waltham, MA, USA) system as in other studies (Julienne et al. 2017; Kumar et al. 2012; Sheeba et al. 2008). This system utilises small glass tubes housing individual flies. Each monitor has 32 horizontal tubes intersected by an infrared beam which, when broken by the movement of the fly, records the locomotor activity. The DAM monitors were located inside a light- and temperature-controlled incubator (Percival Scientific Inc., Perry, IA, USA).

Figure 2.3 *Drosophila* activity monitor (DAM)

Standard *Drosophila* Activity Monitor (DAM) set-up. Each glass tube is sealed with a plastic cap and cotton bung to contain an individual fly. The monitor holds 32 of these tubes, passing an infrared beam through each to monitor locomotor activity.

Loading of flies into the tubes was achieved under CO_2 anaesthesia. Only males were used to prevent the confounding effect of eggs and larvae. Care was taken to ensure flies were not damaged during loading and were under minimal anaesthesia. Monitors were connected to a computer and placed in an incubator maintained at 25°C and 60% humidity. Light cycles of 12 h:12 h light/dark (LD, lights on/off at 8am/pm, respectively) were used initially for five days to fully entrain the flies. This was then switched to constant darkness (DD) for a further seven days (unless indicated otherwise). Activity counts were recorded in 1 min bins.

The analysis of resulting data was performed in Matlab using the Flytoolbox (Levine et al. 2002). Data were initially visually scrutinised to exclude flies that died during the recording period. The data for individual flies or averaged groups were visualised by activity actograms to show broad rhythms of activity.

Quantitative analysis of rhythms was performed by standard autocorrelation analysis. Simply, the activity is compared to itself and a correlation is

calculated. The activity is then moved out of phase to itself and the correlation re-calculated. This process is repeated giving correlations in the data at different time intervals; this is plotted as an autocorrelogram. Peaks in the plot indicate strong rhythms in the data (Figure 2.4). Conventionally, the height of the third peak of the autocorrelogram is used to determine the rhythmicity index (RI). From this, a rhythmicity statistic (RS) can be calculated that is the ratio of the RI value to the absolute value of the 95% confidence line as is used widely in fly circadian literature (RS, see Figure 2.4) (Chen et al. 2011; Cirelli et al. 2005). For the purposes of this thesis, arrhythmic flies are identified as having RS<1 and subsequently visually confirmed. Weakly rhythmic flies are those with RS values between 1 and 1.25, while strongly rhythmic flies have RS values of greater than 1.25.

Circadian locomotor behaviour was recorded in 1-minute bins. This allowed analysis of sleep as sleep in *Drosophila* is taken as inactivity for periods of 5 minutes or longer (Shaw et al. 2000). Analysis of sleep behaviour was achieved in Matlab through the use of the SCAMP toolbox.

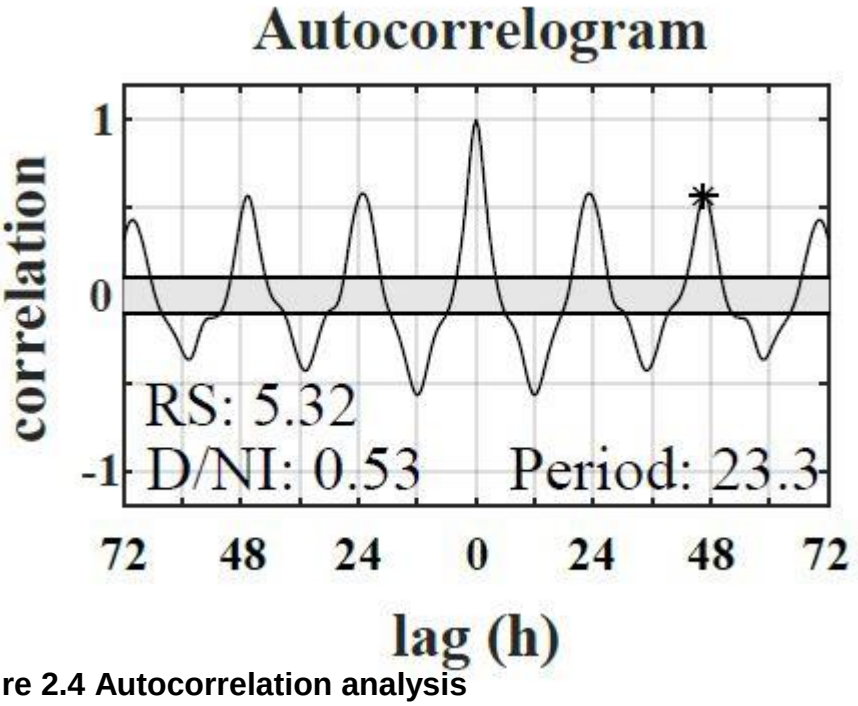

Figure 2.4 Autocorrelation analysis

Autocorrelogram of circadian locomotor behaviour. Each peak represents a peak in activity, hence the peak at 24 hours indicates a 24-hour period. The third peak used for the rhythmicity index is indicated by the asterisk. This peak gives the rhythmicity index (RI). The ratio of this to the 95% confidence line (grey band) gives the rhythmicity statistic (RS).

The use of RS in this thesis is complimented by the reporting of the period of the rhythm as well as the day and night activity. The difference in activity between the daytime and night-time can be quantified by the diurnal/nocturnal index (D/NI) (Julienne et al. 2017; Kumar et al. 2012).

$$DNI = \frac{Day\ activity - Night\ activity}{Total\ activity}$$

For this measure a value of 1 indicates a fly that is exclusively diurnal whereas a value of -1 indicates a fly that is exclusively nocturnal. Under DD the subjective day and night are defined by the period of their rhythmicity as determined by autocorrelation analysis.

2.4 Computational modelling

Computational modelling of channels and neurons was achieved in Matlab (MATLAB Release 2015a, The Mathworks Inc., Natick, Massachusetts, US). Section 2.4.1 looks at the modelling of individual ion channels. Section 2.4.2 combines the individual ion channel models to create a model describing the whole cell activity of the LNvs.

2.4.1 Channel models

The classic equations for modelling ion channel currents are those initially proposed by Hodgkin and Huxley (Hodgkin and Huxley 1952a). These have since been integrated with thermodynamics to yield the following equations (for full derivation see Section 4.1.2).

$$I = g_{max} * (n^P * h^Q) * (V - E) \quad \text{Eq. 2.1}$$

$$\frac{dx}{dt} = \frac{x_\infty - x}{\tau_x} \quad \text{Eq. 2.2}$$

$$x_\infty = \frac{1}{1 + e^{-\frac{V - V_h}{k}}} \quad \text{Eq. 2.3}$$

$$\tau_x = Amp * e^{-\frac{V - V_{max}}{\sigma}} \quad \text{Eq. 2.4}$$

where g_{max} denotes the maximal conductance, and x the state of the activation and inactivation gates, n and h respectively, as well as the driving force which is the difference between the membrane voltage, V, and the reversal potential, E. The activation (m and n) and inactivation gates (h) are subsets of the gating variables, x, and are modelled by a differential equation (Eq. 2.2) that uses an assortment of variables specific to that ion channel.

The reversal potentials are calculated using the Nernst equation.

$$E = \frac{RT}{zF} \ln\left(\frac{[X]_{out}}{[X]_{in}}\right) \quad \text{Eq. 2.5}$$

Where R is the gas constant, T is the temperature in °K, z is the charge of the ion, and F is Faraday's constant. X represents the concentration of the ion, so for voltage-gated potassium channels this is the concentration of potassium outside and inside the cell. Hence, the potassium reversal potential is -90 mV and for sodium it is 52 mV. The reversal potential for calcium is more complicated as calcium ions are buffered by the use of EGTA in the solutions. Calculation of the free calcium concentration in the intracellular solution by the algorithm Chelator (Schoenmakers et al. 1992) gives a concentration of 29 nM. Using this free calcium, the reversal potential is then 132 mV.

These equations can be fit to experimental data for each individual channel to determine the parameters that will describe that data. A standard Hill climbing search-based optimisation procedure was originally used to narrow the parameter-space for searching. This procedure generated a random number in a constrained range for each parameter to be fitted. This created a random parameter set that was entered into the Hodgkin-Huxley equations and compared to the experimental data to give a score of the fit. This score was then minimised by varying each parameter in turn to eventually reach an estimation of the optimal set of parameters describing that channel behaviour. However, this approach can often give local minimums rather than global minimums. This means that the algorithm starts in one part of the parameter-space and finds the nearest good fit, missing a much better fit that is further away.

To solve this problem, a particle swarm optimisation (PSO) was employed. This works by generating many particles, each of which is a parameter set as in the previous method. Each particle is assessed for a score of the fit and the best fitting particle is designated as the global best. Each particle then moves toward the global best (along with some randomness), searching the

parameter-space as they move. This gives a much better chance of finding the best fit in the parameter space without getting stuck in a local minimum. The movement of the particles is governed by an iterative calculation.

$$x'_i = x_i + v_i \qquad \text{Eq. 2.6}$$

$$v'_i = \omega v_i + \psi U_1(x_{gi} - x_i) + \psi U_2(x_{pi} - x_i) \qquad \text{Eq. 2.7}$$

This means that the parameter, x, for a given particle, I, is updated by its velocity, v. The velocity of a particle depends on the position of the global best particle, x_g, and the best iteration of that particle, x_p. This is altered by a weighting, ψ, and some randomness, U, as well as the inertia of the particle, ω. Essentially, a particle will travel towards the global best but is also pulled towards the best fit it has experienced. The algorithm gives the global best as the optimal parameter set once all particles have converged. The difference between the PSO and the original algorithm can be seen in the example of Figure 2.5. The parameters generated for the four main voltage-gated potassium channels are summarised in Table 2.2.

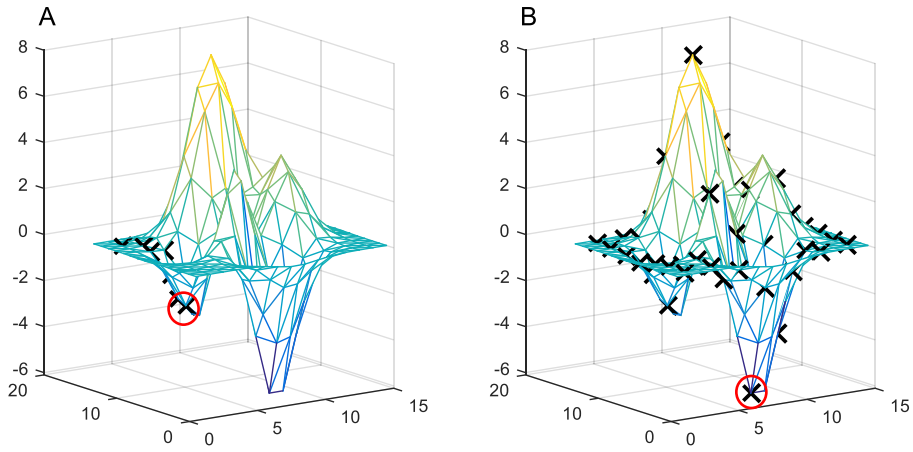

Figure 2.5 General search algorithm and particle swarm optimisation (PSO)

A) Original algorithm starts in a random position and moves towards a local minimum ending at the red-circled point as the best fit, or minimum, but has missed the global minimum. **B)** Particle swarm optimisation has generated particles throughout the parameter-space and has found the global minimum at the red-circled point. All other points now move towards this point until they converge, scanning the parameter-space as they move.

2.4.2 Whole cell model

The individual ion channels were then combined along with a previous model of the mammalian SCN (Sim and Forger 2007; Belle et al. 2009) to generate a model describing the whole cell activity of the LNvs. The current balance equation for the whole cell is:

$$C\frac{dV}{dt} = I_{app} - g_{Na}m^3h(V - E_{Na}) - g_{Ca}mh(V - E_{Ca}) \quad \text{Eq. 2.8}$$
$$- g_{Kv1}m^4h(V - E_K) - g_{Kv2}m^4(V - E_K)$$
$$- g_{Kv3}m^4h(V - E_K) - g_{Kv4}m^4h(V - E_K)$$
$$- g_{leak}(V - E_{leak})$$

This equation uses the capacitance of the cell body, C (which is 3.7 pF in accordance with recordings), along with the applied current, I_{app}, and the currents of the sodium, calcium, potassium, and leak channels to calculate the change in the membrane voltage, V. The sodium, calcium, and leak channels are used unaltered from the previous Sim-Forger model (Sim and Forger 2007). Kv channel model parameters are given in Table 4.2. Whole cell activity simulations are performed by use of the Euler-Maruyama method.

The Matlab scripts used for generating the whole cell model and the fitting algorithms are given in the Appendix. Bifurcation analysis was performed with the matcont6p1 toolbox in Matlab (Dhooge et al. 2003).

2.5 Statistics

All statistical analyses were performed in Matlab. For the simple comparison of two population sets, an unpaired t-test was commonly used. For the comparison of three or more sets, one-way analysis of variance (ANOVA) was used with post-hoc comparisons using Bonferroni's multiple

comparisons, selected to correct for multiple comparisons. Kolmogorov-Smirnov tests were used to check normality of datasets.

Throughout the thesis statistical analyses are presented in the figure legends and indicated on the figure by standard notation such that * is $p<0.05$, ** is $p<0.01$, *** is $p<0.001$. Bars represent the mean and error bars represent the standard error (SEM) unless otherwise stated.

A notable exception to the analysis is in the longevity assay. Due to the need to compare longitudinal data the non-parametric Mantel-Cox log-rank test was used (Peto et al. 1977; Clark et al. 2003) alongside the Gehan-Breslow-Wilcoxon test (Prentice and Marek 1979); this analysis was performed in GraphPad Prism. Briefly, two populations are compared to determine whether a certain event happens at the same or a different rate in each population. In the context of *Drosophila* longevity data, this means that each day the proportion of flies that died overall is compared with the proportion that died in each population; if the two populations are the same then the proportion of flies that died in each should remain the same. The difference between the expected deaths (equal between the two populations) and the overall deaths (in both populations) on each day is then combined to give a score that is then used in a chi-squared test to determine significance. This method has been previously criticised as being too permissive and an alternative of the F* test has been suggested (Berty et al. 2010) but has yet to see widespread use.

Chapter 3 – Electrophysiology

This chapter describes the electrophysiological techniques used to explore the *Drosophila* LNvs. Section 3.1.1 introduces the background of electrophysiology, section 3.1.2 explains various electrophysiological concepts and practical considerations, and section 3.1.3 looks at some specific aspects of *Drosophila* electrophysiology. Section 3.2 provides the results of a range of electrophysiological experiments studying the function of ion channels, primarily voltage-gated potassium channels, in the LNvs. Section 3.3 discusses these results in the context of the LNv function in regulating circadian rhythms.

3.1 Electrophysiology theory

3.1.1 Historical development of electrophysiological techniques

The early foundations of electrophysiology can be found as back as the 1660s when Dutch scientist Jan Swammerdam developed a preparation of the frog leg; allowing him to trigger muscle contractions by stimulation of the attached nerve (Cobb 2002). It was not until more than a century later when Luigi Galvani published his observations of the frog leg preparation and truly advanced the field (Galvani 1791). He described a relationship between intensity of stimulation and muscle contraction, a refractory period where contractions decrease until a period of rest, and most importantly, that stimulation of one nerve could transmit down a second connected nerve. This was one of the first demonstrations of a propagating action potential (Verkhratsky et al. 2006; Rubaiy 2017).

In the 1930s and 40s, the Atlantic squid (*Loligo pealii*) became the model of choice for both Cole and Curtis (Curtis and Cole 1940) as well as Hodgkin and Huxley (Hodgkin and Huxley 1939) to develop intracellular electrodes for the recording of action potentials. This all lead to the landmark development

of the voltage-clamp technique showing that membrane excitability is determined by ion fluxes (Hodgkin and Huxley 1952b). These experiments also demonstrated the action potential overshoot and refractory period. While this suggested the existence of transmembrane ionic pathways, evidence of ion channels themselves did not really happen until the observation that certain antibiotics and proteins created ionic conductances in membranes (Hladky and Haydon 1970; Bean et al. 1969).

However, conventional intracellular microelectrode recordings of the time had a background noise too high for observations of the single ion channels that had been proposed to allow this selective permeability of ions. Neher and Sakmann then followed up previous work pressing a smooth electrode tip to the surface of a muscle fibre and isolated a patch of membrane (Neher and Sakmann 1976). The discovery of a high-resistance seal, termed the gigaseal, a few years later (Sigworth and Neher 1980) brought the field to the form of the whole-cell patch-clamp technique used today.

3.1.2 Practical principles of the patch-clamp technique

The patch clamp technique involves, as previously mentioned, a smooth glass or borosilicate pipette tip contacting the membrane of the target cell. Application of a small suction pressure ensures a tight seal (gigaseal) between the pipette and the cell to avoid current leakage.

At this point several variations of the technique can be utilised. The cell-attached configuration can be changed into the whole-cell configuration by further application of pressure or electrical shock to rupture the membrane and make the cell cytoplasm continuous with the pipette solution. This can lead to the loss of intracellular components however and so, instead of membrane rupture, certain pore-forming drugs such as amphotericin-B or nystatin can be used to make the membrane highly permeable; this is the perforated patch set-up. Instead of retaining the whole cell, a small portion of the membrane can also be excised. When this occurs, it is known as inside-

out or outside-out depending on the orientation of the membrane with respect to the pipette (for a review of these configurations see Gandini, Sandoval and Felix, 2014).

For patch-clamping, the formation of the pipette tip is crucial in generating good electrophysiological data. Using the widest possible pipette tip, without aspirating the cell, creates a small series resistance – that is the resistance between the cell and the recording electrode caused by the pipette; it is synonymous with access resistance.

There are two main issues surrounding series resistance. Firstly, series resistance creates a voltage divider with the membrane resistance and so creates a voltage error that can influence accuracy of the voltage-clamp. Secondly, the series resistance also sets up a low-pass filtering effect with the membrane capacitance. The capacitance of the membrane charges depending on the rate of voltage change and so at higher frequencies the membrane capacitor draws more current and so takes longer to reach the command voltage. Thus, high frequency signals, such as voltage-gated sodium channels, are more heavily filtered.

These problems are illustrated when looking at a theoretical current (Fig 3.1). For a cell of 5 pF membrane capacitance and a series resistance of 50 MΩ the output recorded relative to the true output drops rapidly (Fig 3.1A) but this can be ameliorated by series resistance compensation. In the case of 60% compensation (where the series resistance is effectively reduced by 60%), the filtering is much less drastic. For the voltage-gated potassium channel Shal, the peak activation is within roughly 2-4 ms (Tsunoda and Salkoff 1995a). With uncompensated series resistance this severely attenuates the peak of the current recorded, whereas a 60%-compensated current is much closer to the original Shal current (fig 3.1B). In terms of the LNvs studied in this thesis, this example represents a higher capacitance and series resistance and hence the filtering in experiments is likely to be much lower.

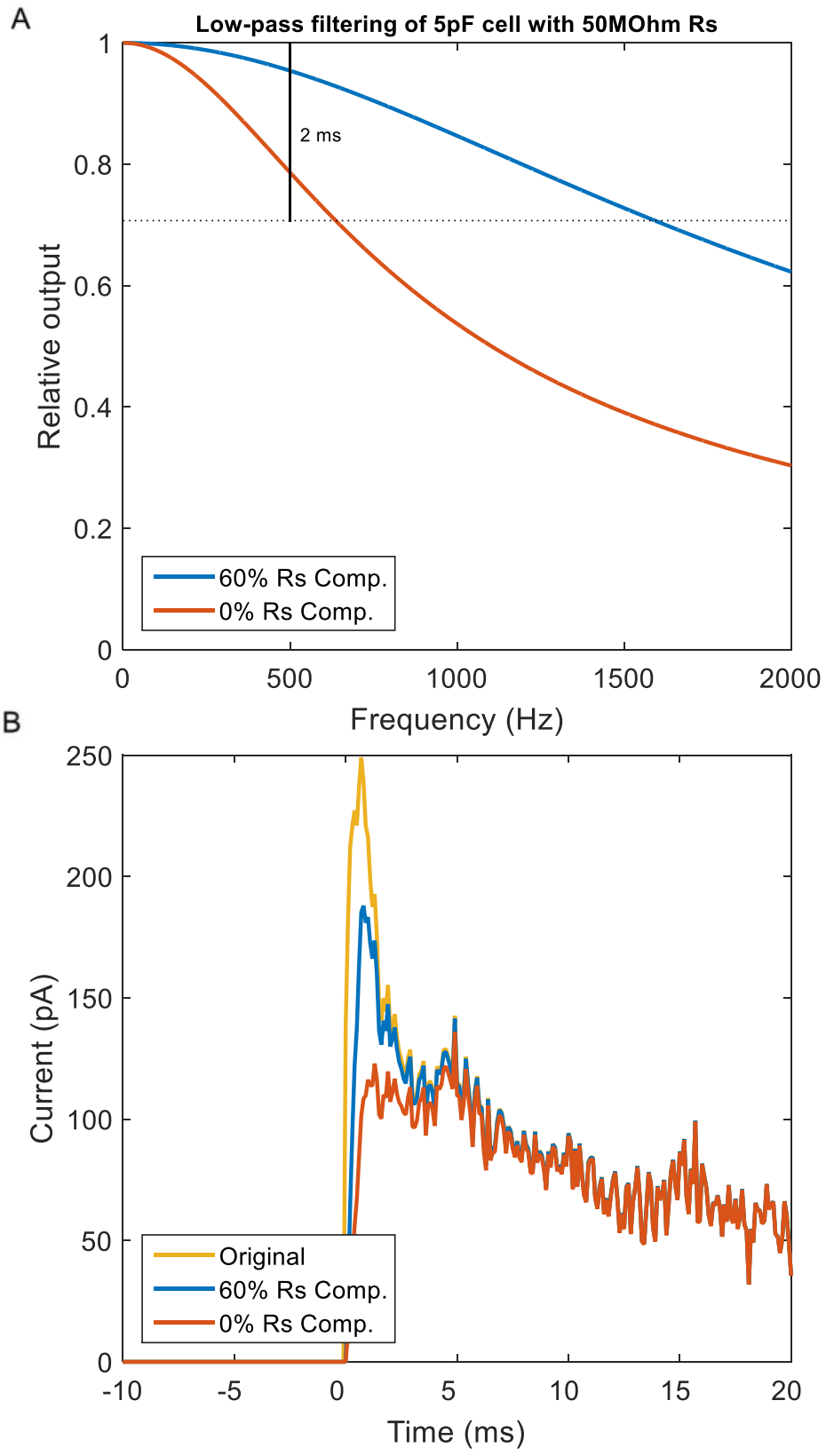

Figure 3.1 Low-Pass filtering effects of access resistance.

A) Model simulation of low-pass filtering in a 5 pF capacitance cell with an access resistance of 50 MΩ with either 0% or 60% access resistance compensation. **B)** A theoretical true Shal current (original), or after applying low-pass filtering as if the true current were being recorded at either 0% or 60% access resistance compensation. Filtering greatly reduces the observed current peak.

3.1.3 Electrophysiology of *Drosophila* and mammals

The original electrophysiological recording of the *Drosophila* LNvs did not identify spontaneous action potentials, only action potentials in response to current injection (Park and Griffith 2006). However, subsequent studies modified the recording solutions and did identify spontaneous action potentials and presented the idea that the LNvs exhibit a strong time-of-day dependence in the firing rate of these spontaneous action potentials, being faster at dawn than at dusk (Sheeba et al. 2008; Cao and Nitabach 2008).

Electrical activity of the LNvs is vital to rhythmicity of the fly. Indeed, affecting the excitability of these PDF neurons leads to complex rhythmic patterns (Sheeba, Fogle, et al. 2008; Nitabach et al. 2006) and behavioural arrhythmicity (Nitabach et al. 2002; Nitabach et al. 2005). In addition, hyperexcitation of the LNvs leads to disruption of nocturnal sleep (Wu et al. 2008). The interplay between the electrical activity of the neurons and the rhythmicity of the molecular clock is less clear. There does appear to be reciprocal interaction whereby the molecular and membrane clocks affect each other, as seen by specific electrical activity inducing changes in the phase of the molecular clock (Mizrak et al. 2012). Although, while electrical silencing of the LNvs has been indicated to have some effect on core clock proteins (Nitabach et al. 2002), in general oscillations remain unaltered (Depetris-chauvin et al. 2011).

The electrical activity of the LNvs is somewhat similar to that of the SCN. SCN neurons maintain rhythms of spontaneous firing rate in culture and slices (Noguchi et al. 2017; Liu et al. 2007; Patton et al. 2016). Here the activity is high in the day and low in the night, varying between roughly 10 and 1 Hz, respectively (Meijer and Stephan Michel 2015). Indeed, the PDF receptor shows remarkable similarity to the vasoactive intestinal peptide receptor (VPAC2), both being type II G-protein coupled receptors (GPCRs) coupled to cAMP (Mertens et al. 2005). In addition, both are vital to clock function as VPAC2 mutants are arrhythmic under constant conditions

(Mertens et al. 2005; Hyun et al. 2005; Lear et al. 2005) and so are *pdf*^{01} mutants (Peng et al. 2003; Lin et al. 2004)

The mechanisms underlying the rhythmic changes in neuronal activity are not well understood. The excitatory and inhibitory ion channels that drive rhythmicity are sometimes referred to as the 'membrane clock' and a variety of channels have been implicated as part of the membrane clock, including the sodium leak channel *narrow abdomen* (NA) in the *Drosophila* dorsal clock neurons (Flourakis et al. 2015) and voltage-gated L-type calcium channels in the SCN (Diekman et al. 2013). But comprehensive knowledge of the membrane clock is lacking in both systems.

As mentioned previously, transcriptomic analyses have suggested the voltage-gated potassium (Kv) channels to be of importance to the LNv membrane clock (Kula-Eversole et al. 2010), in particular the channels Shaw and Shal (Kv3 and Kv4 homologues, respectively). This is again similar to the mammalian SCN where Kv3.1b and Kv3.2 expression peaks during the day (Itri et al. 2005) and the I_A current associated with Kv4 is also circadian (Itri et al. 2010). These candidates are well-placed to regulate changes in neuronal activity as both channels have been previously shown to regulate firing rates in *Drosophila* (Tsunoda and Salkoff 1995b; Hodge et al. 2005; Ping et al. 2011; Hodge and Stanewsky 2008) and mammals (Martina et al. 1998; Lien and Jonas 2003; Granados-Fuentes et al. 2012; Granados-Fuentes et al. 2015; Hermanstyne et al. 2017). In addition, a recent study suggested that the block of Shal current in the *Drosophila* LNvs was preferentially effective around dusk, although only the composite I_A current was assayed as opposed to the specific Shal current and so current cycling was not identified (Feng et al. 2018).

In terms of voltage-gated sodium and calcium channels in the *Drosophila* clock neurons, much less is known. Application of either TTX to block sodium channels or $CoCl_2$ to block calcium channels abolished spontaneous action potential firing in the LNvs (Sheeba, Gu, et al. 2008). Therefore, both sodium and calcium fluxes are important depolarising currents in the generation of

action potentials in the LNvs. The sodium channel *paralytic* (*para*) and calcium channel *cacophony* (*cac*) are also indicated to be expressed in the LNvs (Kula-Eversole et al. 2010). However, characterisation of sodium channel activity has mostly been done in heterologous systems (Lin et al. 2009).

In similar fashion, the larval clock is much less studied than it is in the adult. The larval circadian clock appears to function from the very early first instar stage immediately after hatching (Sehgal et al. 1992). Expression of the core clock components *per* and *tim* can be detected in a subset of larval neurons (Kaneko et al. 1997) and among these, some neurons are positive for expression of PDF. These larval PDF-positive neurons are precursors to the adult s-LNvs (Helfrich-Förster et al. 1998). Nevertheless, the larval clock neurons are more inaccessible for electrophysiological examination and have received much less study. However, while the adult LNvs have a wide arborisation covering most of the adult brain, the larval LNvs have a smaller arborisation pattern (Schubert et al. 2018).

3.2 Results

3.2.1 Potassium channels of the LNvs

Using whole cell patch clamp, electrical activity was recorded from the LNv clock neurons of the explant *Drosophila* brain at a selection of time-points across the circadian day. Current-clamp recordings show variations in spontaneous action potential firing rate (Figure 3.2A) consistent with previous studies (Cao and Nitabach 2008; Sheeba et al. 2008). Voltage-clamp experiments at similar time-points also show variation in peak and sustained currents, indicating potential differences in ion channel function (Figure 3.2B).

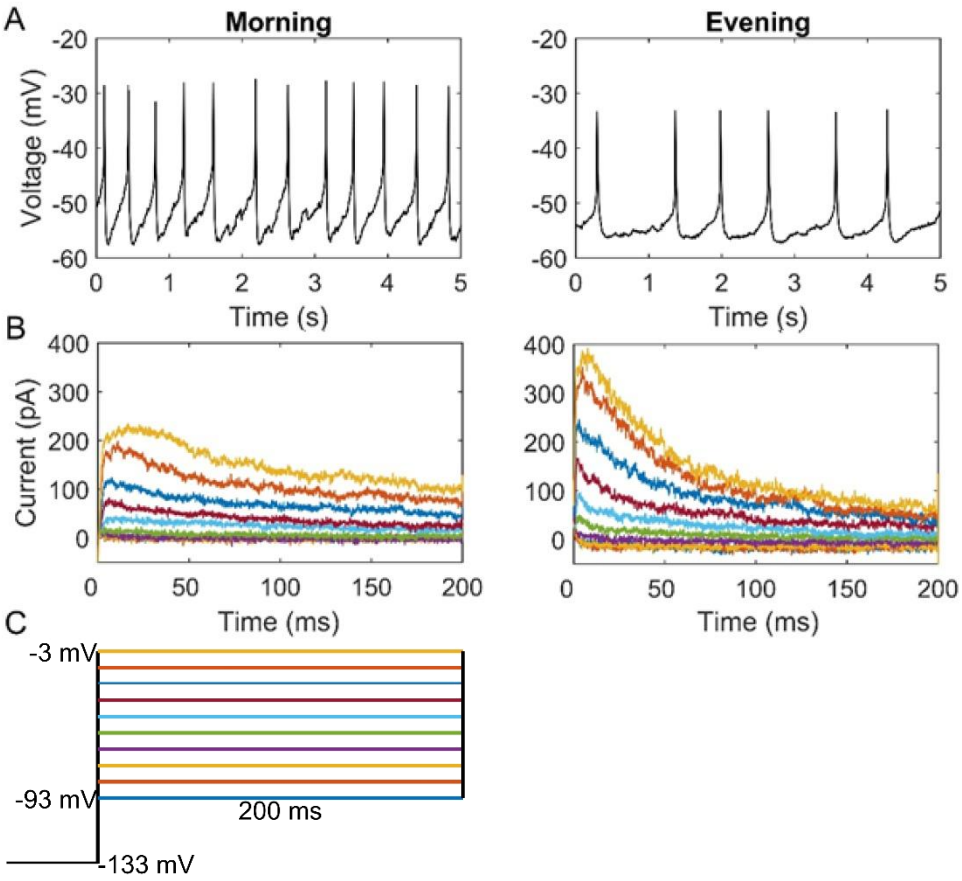

Figure 3.2 Morning and evening electrical activity of LNvs.

A) Current-clamp recordings in the morning (ZT0, left panel) and the evening (ZT12, right panel) show variations in spontaneous action potential firing rate. **B)** Mean voltage-clamp recordings of LNvs show differences in the morning (ZT0, left panel, n=6) compared with the evening (ZT12, right panel, n=6) in overall current response without pharmacological blocking to a standard depolarisation step protocol. **C)** Voltage-clamp protocol used, for reference resting membrane potential is -50 to -55 mV.

Application of various drugs allowed the separation of these composite currents into individual ion channels. Briefly, currents in response to a standard depolarising pulse protocol were obtained before and after application of the drugs; the difference between the conditions is the current sensitive to that drug. Dendrotoxin was used for separation of Shaker (Kv1), guangxitoxin for Shab (Kv2), BDS for Shaw (Kv3), and phrixotoxin for Shal (Kv4) (for more information see Section 2.2.5). Current profiles (Figure 3.3A) show that Shaker and Shal are particularly inactivating, with Shal being much faster, Shaw is slowly inactivating , and Shab is non-inactivating (Tsunoda and Salkoff 1995a). Channel block by drugs was specific since in flies expressing Shaker *RNAi*, Shab *RNAi*, or Shaw or Shal dominant negative transgenes, the respective drug effects were abolished (Figure 3.3B). Drug effects were also reversible as wash-out of the drug recovered most of the channel currents (DTX 90.15%, GxTX 88.64%, BDS 78.54%, PaTX 83.80% data not shown).

Plotting the peak current obtained during each depolarisation against the voltage of that depolarisation for each of the four channels gives the I-V relationships for each (Figure 3.4). It is apparent from this that Shaker and Shab activate at higher voltages during initiation of the action potential, whereas Shaw and Shal activate at more negative voltages near the resting potential. Shaw and Shal currents are based on their peak currents during peak expression, for Shaw this is during dawn at ZT0 and for Shal this is during dusk at ZT12 (Figure 3.8). Shal currents during dusk are the largest potassium currents, accounting for the majority of fast-activating currents.

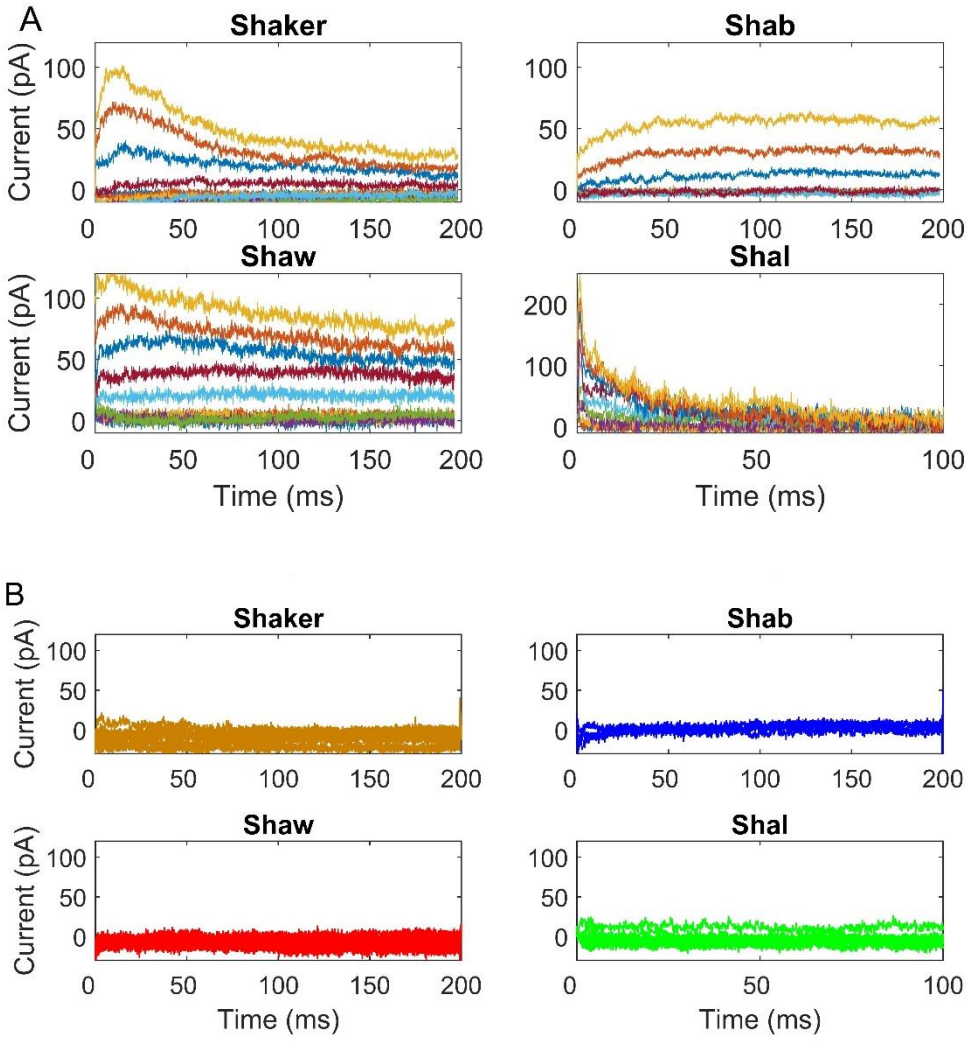

Figure 3.3 Individual voltage-gated potassium channel kinetics.

A) Mean current difference in control LNvs due to selective ion channel blockers used to block either Shaker (n=10), Shab (n=12), Shaw (n=6), or Shal (n=6) during a 200 ms depolarisation step to between -93mV and -3 mV (Figure 3.2C). Shaker and Shab assays performed at ZT6, Shaw at ZT0, and Shal at ZT12. **B)** Mean current difference in flies expressing either Shaker *RNAi* (n=3), Shab *RNAi* (n=3), Shaw dominant negative (n=3), or Shal dominant (n=3) negative transgenes due to the respective ion channel blocker in the same protocol. There is no difference between before and after drug application. Hence, drug-sensitive currents are abolished by channel knock-down.

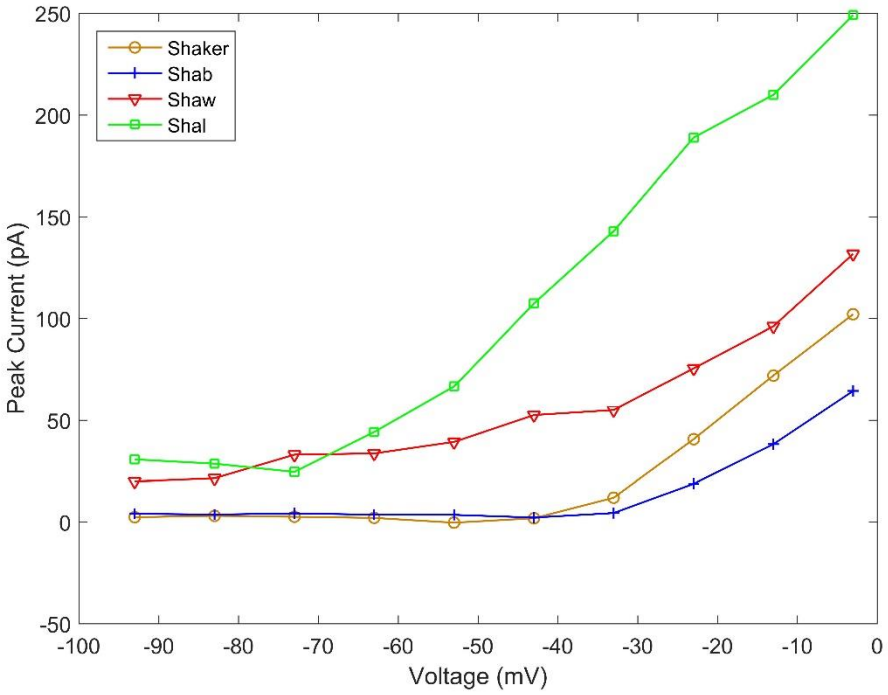

Figure 3.4 I-V relationships

Mean peak current obtained for each ion channel at each depolarisation step as detailed previously (Figure 3.3) plotted against the voltage of the depolarisation step. Activation thresholds vary among the channels with Shaker (n=10) and Shab (n=12) being at more positive values, whereas Shaw (n=6) and Shal (n=6) are at more negative near the resting membrane potential. Shaker and Shab assays performed at ZT6, Shaw at ZT0, and Shal at ZT12.

Current-clamp recordings of spontaneous action potentials were recorded as done previously (Figure 3.2) with addition of various ion channel blockers during recording (Figure 3.5A). Addition of DTX to target the Shaker channel in general was associated with an increase in spontaneous action potential firing rate. Application of GxTX targeting Shab caused a smaller increase in firing rate. Utilising BDS to block Shaw resulted in an overall slow-down of firing rate. Use of PaTX to block Shal caused a small increase in action potential frequency.

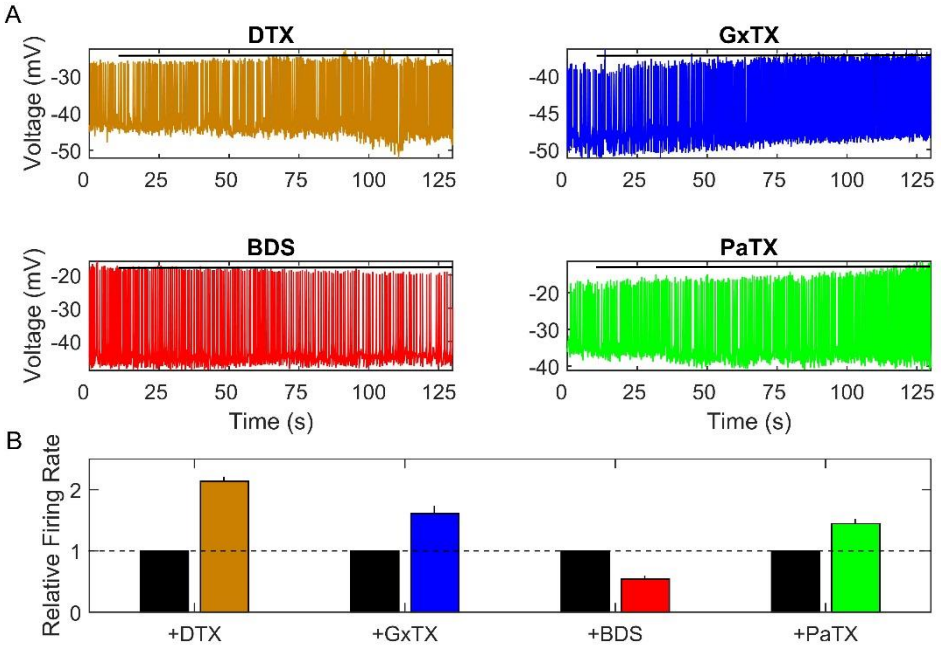

Figure 3.5 Application of ion channel blockers during spontaneous action potential firing has effects on firing rate.

A) Action potential firing behaviour during application of dendrotoxin (DTX), guangxitoxin (GxTX), blood depressing factor (BDS), and phrixotoxin (PaTX). Drugs were applied at 10 seconds, application is indicated by the black bar. Recordings made at ZT6 for DTX and GxTX, ZT0 for BDS, and ZT12 for PaTX. **B)** Quantification of action potential firing rate after application of drug (coloured right bar of each pair of bars) relative to firing rate before application (black left bar of each pair of bars). DTX (n=4, $p<0.0001$), GxTX (n=5, $p=0.0185$), and PaTX (n=9, $p=0.0025$) caused increases in firing rate whereas BDS (n=4, $p=0.004$) caused a decrease.

Current-clamp recordings of LNvs expressing Shaw or Shal dominant negative transgenes also showed changes in action potential firing rate (Figure 3.6). At dawn (ZT0), when Shaw is highest, the firing rate is high at just over 2 Hz. But, with expression of the Shaw dominant negative (ShawTR), this decreases significantly. At dusk (ZT12), when Shal is highest, the firing rate is lower at roughly 1 Hz. When the Shal dominant negative is expressed, the firing rate increases.

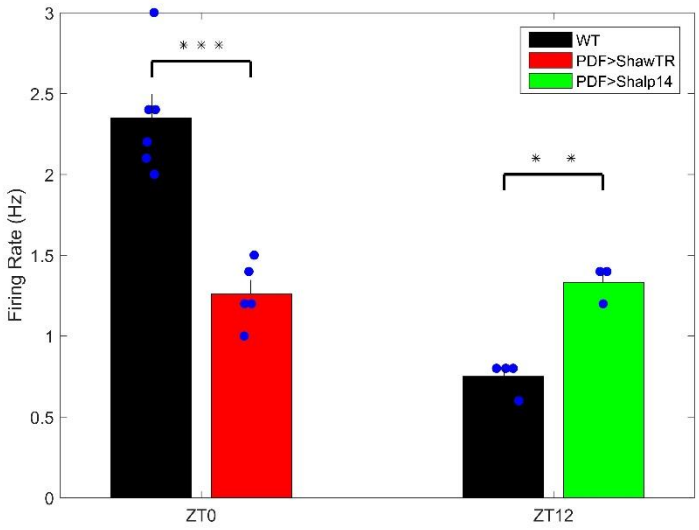

Figure 3.6 Action potential firing rate with Shaw and Shal dominant negatives.

At ZT0 control LNvs exhibit a roughly 2.3 Hz firing rate, when Shaw dominant negative is expressed this results in a reduction to roughly 1Hz ($p<0.001$). At ZT12 control LNvs exhibit a roughly 1Hz firing rate, when Shal dominant negative is expressed this increases to around 1.3 Hz ($p=0.0021$). Blue dots indicate individual data-points.

Progressive addition of channel blockers (Figure 3.7) shows the relative contribution of each ion channel to the overall current profile (Figure 3.2B). Time-of-day dependent effects can be seen particularly in the PaTX-sensitive current of Shal, having high current around ZT12 and low current around ZT0.

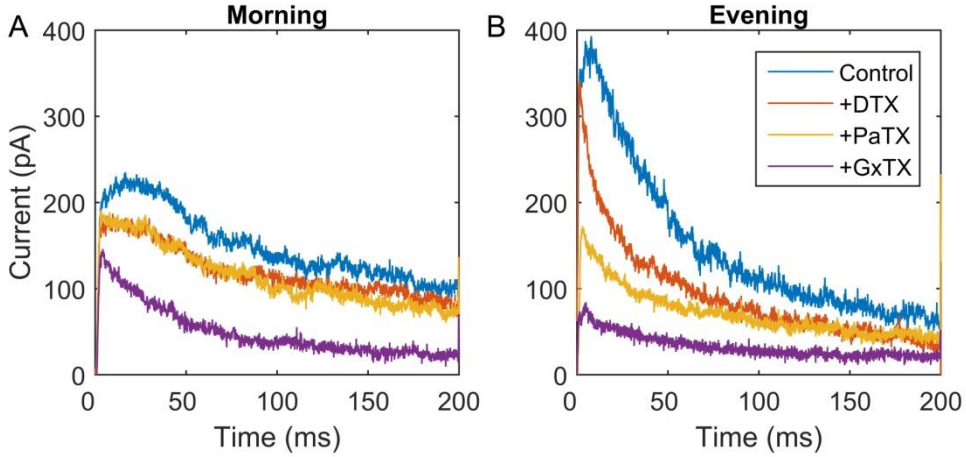

Figure 3.7 Progressive application of ion channel blockers during the morning and evening show differential ion channel currents.

A) Progressive application of DTX, PaTX, and GxTX at ZT0 (n=3) to target Shaker, Shal, and Shab, respectively, with depolarisation to -3 mV. All assayed channel currents are present. **B)** Identical application of channel blockers at ZT12 (n=3) with depolarisation to -3 mV. Shaker and Shab currents are unaffected, whereas Shal current is greatly diminished.

3.2.2 Circadian changes in potassium channels

Currents for individual ion channels (Figure 3.8) were obtained at four times of day: ZT2 (early morning), ZT8 (late day), ZT14 (early night), and ZT20 (late night) where ZT denotes the zeitgeber time, or number of hours after lights-on. Flies were maintained in a normal 12:12 LD cycle and so ZT0 indicates lights-on, and ZT12 indicates lights-off. Results show that Shaker and Shab remain constant throughout the circadian day, whereas Shaw and Shal vary. Shaw has a higher peak current at ZT2 than at ZT14, and Shal has a higher peak current at ZT8 than at ZT20.

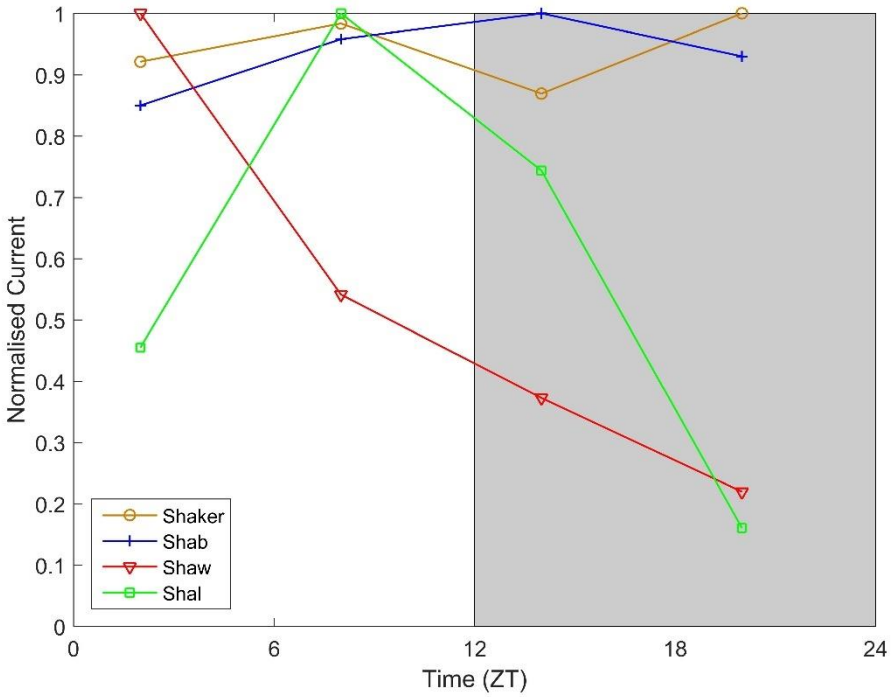

Figure 3.8 Peak ion channel currents vary at different times of day.

Mean peak ion channel currents obtained at each of ZT2, ZT8, ZT14, and ZT20 for each of the channels Shaker (n=12), Shab (n=14), Shaw (n=13), and Shal (n=12); the white box denotes day-time while the grey box denotes night-time. Shaker ($p=0.9813$) and Shab ($p=0.9181$) do not significantly vary with time of day, whereas Shaw ($p<0.0001$) and Shal ($p<0.0001$) exhibit distinct time-of-day variation. Shaw peaks in the early morning at ZT2 and Shal peaks in the late day at ZT8. Peak channel current was measured at -3mV and the same general pattern occurs at lower voltages.

Since flies were kept in standard 12:12 LD cycles it was reasonable to posit that the variation in Shaw and Shal peak current may be effects of light exposure rather than true circadian variations. To test this, flies were kept in 12:12 LD for 3 days to entrain them and transferred to constant darkness (DD) to remove acute light exposure effects. Currents were obtained for Shaw and Shal at different time-points as described previously (Figure 3.8) in LD and DD (Figure 3.9). In the s-LNvs, which are associated with driving rhythmicity in constant conditions such as DD (Grima et al. 2004; Stoleru et al. 2004), the peak current of Shaw and Shal continues to vary; this is consistent with LD conditions. In the l-LNvs this cycling of ion channel current is abolished and there is no cycling in Shaw or Shal currents.

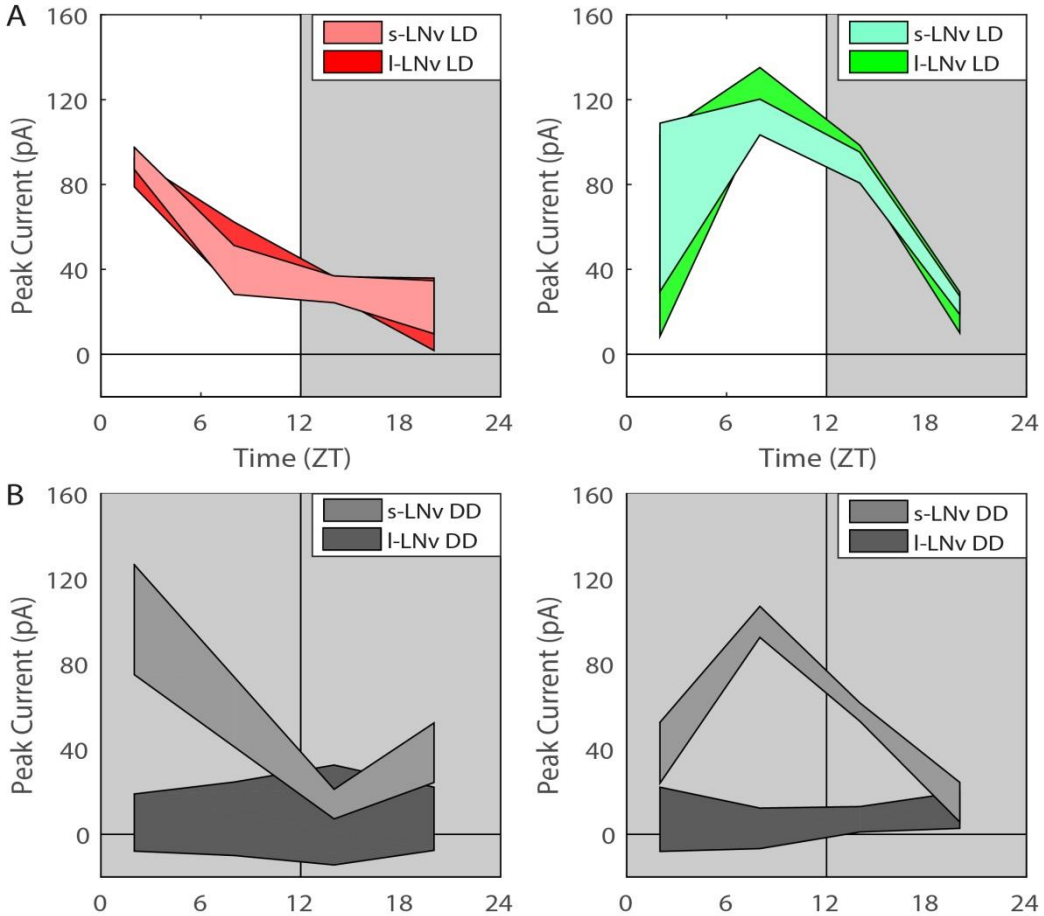

Figure 3.9 Peak ion channel currents of Shaw and Shal are circadian.

Peak ion channel currents obtained at ZT2, ZT8, ZT14, and ZT20 for each of the channels Shaw (left panel, s-LNv: n=12, l-LNv: n=13) and Shal (right panel, s-LNv: n=12, l-LNv: n=12). **A)** Currents cycle in LD in both s-LNvs and l-LNvs. **B)** Cycling is present in constant darkness (DD) in s-LNvs for both Shaw ($p=0.0229$, n=12) and Shal ($p<0.001$, n=12), but not in the l-LNvs in DD for either Shaw ($p=0.7982$, n=13) or Shal ($p=0.4149$, n=12). Peak channel current was measured at -3mV and the same general pattern occurs at lower voltages. Ranges plotted indicate the mean ± SEM.

Voltage-clamp recordings in flies expressing dominant negative transgenes for the circadian proteins CLK or CYC also affect channel cycling in a similar manner (Figure 3.10). Disruption of the molecular clock by this intervention abolished rhythms of Shaw and Shal in all LNvs for both *CLK* and *CYC* mutants.

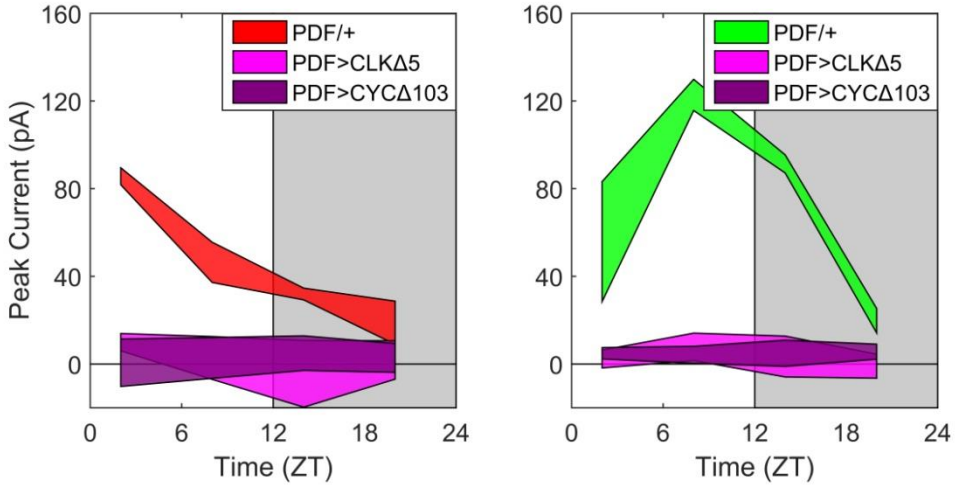

Figure 3.10 Cycling of peak ion channel currents requires the molecular clock.

Peak ion channel currents obtained at ZT2, ZT8, ZT14, and ZT20 for each of the channels Shaw (left panel) and Shal (right panel) in flies expressing dominant negative *CLK* or *CYC* transgenes in all LNvs; the white box denotes day-time while the grey box denotes night-time. Currents cycle in LD in controls for Shaw (n=13) and Shal (n=12). Cycling is not present in *CLK* mutant for Shaw (p=0.2386, n=12) or Shal (p=0.2379, n=12), or in *CYC* mutants for Shaw (p=0.6024, n=12) or Shal (p=0.7306, n=12). Peak channel current was measured at -3mV and the same general pattern occurs at lower voltages. Ranges plotted indicate the mean ± SEM.

3.2.3 Sodium and calcium channels of the LNvs

To investigate the sodium and calcium channels present in the LNvs, voltage-clamp recordings were conducted in caesium intracellular solution (see Section 2.2.4) in order to block potassium currents. Using the same protocol as for the separation of potassium currents (Figure 3.3A), tetrodotoxin (TTX) was utilised to selectively block voltage-gated sodium

channels (Figure 3.11A). This revealed a particularly small transient current visible upon depolarisation, occurring earlier with higher depolarisation. The amplitude of the response is voltage-independent and is absent from some preparations. In these cases, no notable current is observed (Figure 3.11B). These results indicate particularly poor space clamp and are unfit for computational modelling. Other factors include the particularly large and convoluted arborisation of the LNvs and the location of the spike initiating zones being distal to the cell soma.

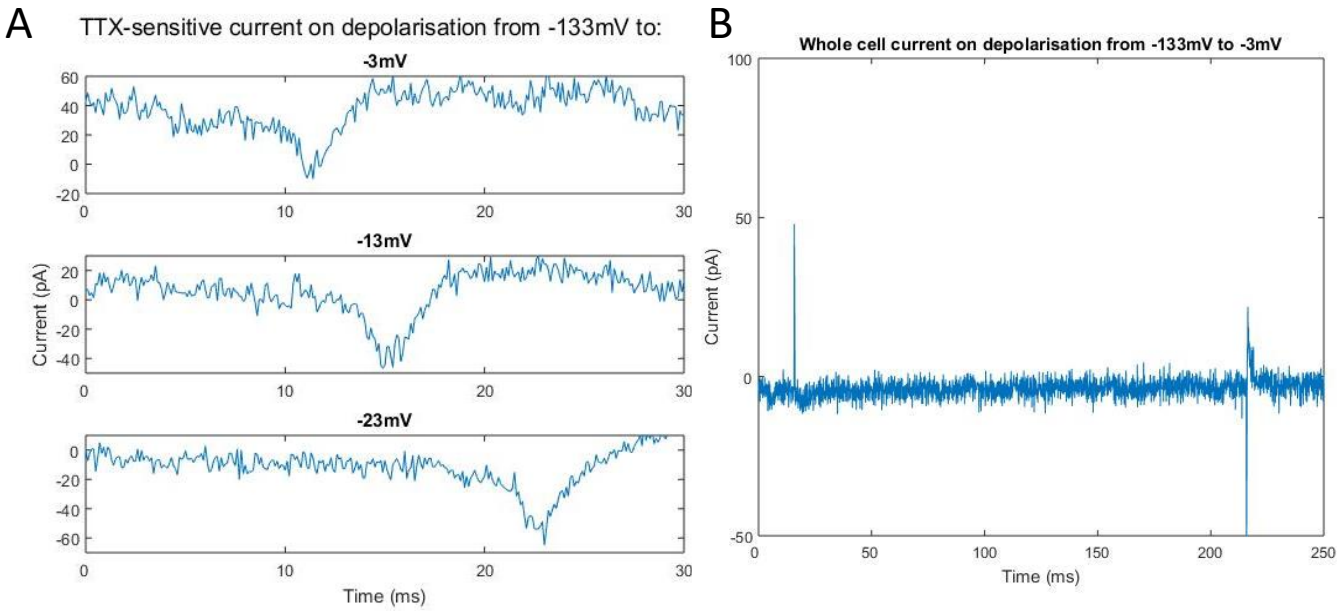

Figure 3.11 Sodium and calcium channel currents are not easily visible in LNvs.

A) Voltage-clamp depolarising step protocol shows small currents when using caesium intracellular solution. 30 ms epochs begin from the onset of depolarisation and show currents occurring earlier at higher voltages. **B)** Mean 200 ms depolarisation protocol in caesium intracellular solution shows no discernible currents beyond artefacts of depolarisation onset and offset.

The s-LNvs are known to persist from larval development into the adult stage (Kaneko et al. 1997; Helfrich-Förster 1997) and potentially present an alternative avenue to investigate depolarising currents. Initial recordings of the larval LNvs were performed with similar methodology to previous current-clamp recordings (Section 2.2) on wandering third-instar larvae prior to

pupation (Figure 3.12). Preliminary results indicate similar spiking behaviour in the larval LNvs compared with adult LNvs, albeit at a higher action potential firing rate than is expected. The larval LNvs are less widely arborised than in the adult (Kaneko et al. 1997) and so may present an opportunity to study sodium currents. However, more examination is needed to determine whether this is a viable approach and how applicable this is to the adult stage. Therefore, the sodium currents that cannot be obtained in the adult LNvs might be studied in the larval LNvs in the future.

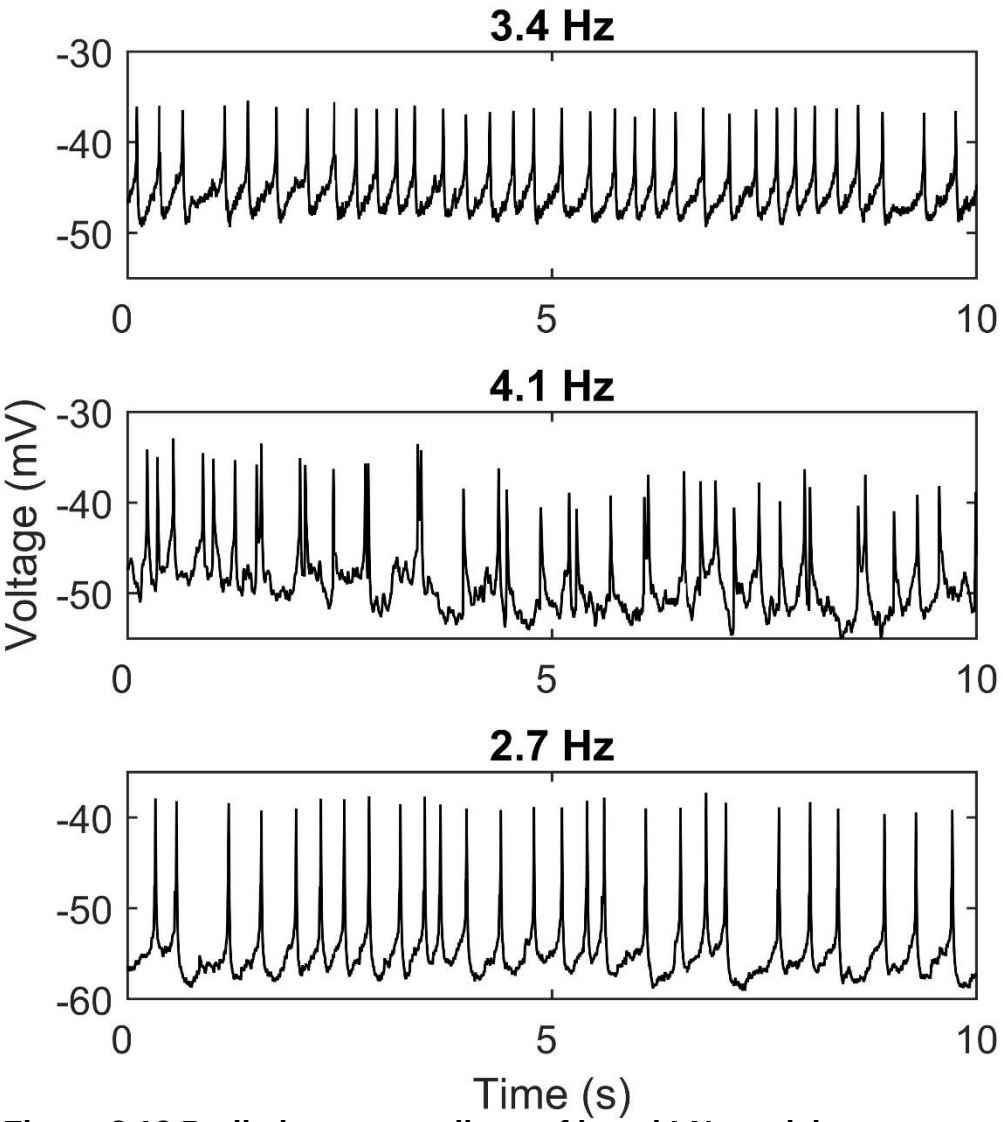

Figure 3.12 Preliminary recordings of larval LNv activity

Representative current-clamp recordings of wandering third-instar larval LNvs during late afternoon (ZT6-10). Spontaneous action potential firing rates are higher than would be expected for this time-of-day (approximately 1.5 Hz).

3.3 Discussion

3.3.1 Function of Kv channels in the *Drosophila* LNvs

The kinetics of the channels Shaker, Shab, Shaw, and Shal (Figure 3.3) are similar to those reported elsewhere; the transient currents of Shaker and Shal have been shown previously in *Xenopus* oocytes (Wei et al. 1990). In the present study Shal was found to be much more quickly inactivating, however this is more in line with later reports (Pak et al. 1991; Jegla and Salkoff 1997; Wang et al. 2004) and the observation that certain channel subunits present may make the inactivation much quicker; something that would not occur in the *Xenopus* oocyte. The inactivation constant here is also similar to that reported for embryonic *Drosophila* neurons (Tsunoda and Salkoff 1995a) and for flight motoneurons (Ryglewski and Duch 2009) as well as in the clock neurons (Feng et al. 2018). Shab as a non-inactivating channel contributing to sustained currents has been observed in *Drosophila* neurons and muscles (Hegde et al. 1999; Singh and Singh 1999). Shaw has been known as a channel that is often open around resting potential, driving the cell towards more hyperpolarised states (Tsunoda and Salkoff 1995b; Hodge 2009; Hodge et al. 2005). Shaw is however slightly different in that there is a second gene in the family known as Shawl (Hodge et al. 2005), but much less is known about the functions of Shawl.

The effect of each channel blocker on the electrical behaviour of the neuron is also interesting (Figure 3.5). Effects of blocker can often be counter-intuitive as blockade of one ion channel may result in different behaviour of another ion channel, confounding the observed effects. The effect of GxTX on Shab current to increase firing rate mirrors previous neuronal studies (Frazzini et al. 2016; Kimm et al. 2015).

In general, application of blockers resulted in increases in firing rate as might be expected for inhibition of a potassium current. However, the exception here is Shaw, which shows a decrease in firing rate. This is particularly interesting in the case of BDS affecting Shaw current as Shaw is active

around the resting membrane potential and is known to be involved in setting it (Hodge 2009). Thus, blockade of the channel should make the resting potential more positive and lead to an increase in excitability. However, other studies have indicated that in some systems Kv3 currents can confer "fast-spiking phenotypes" and the blockade of those currents reduces excitability (Martina et al. 1998; Lien and Jonas 2003) similar to the effect seen in this study (Figure 3.5). This may perhaps be due to a role of Kv3/Shaw channels in repolarisation of the action potential, meaning that the current allows faster re-setting of the membrane potential and hence faster action potential trains. This is also reflected in the lower firing rate observed in the Shaw dominant negative recordings (Figure 3.6).

There may also be a role of the related channel Shawl, which encodes the *Drosophila* homolog of Kv3.2 (Hodge et al. 2005; Bergquist et al. 2011). While Shaw and Shawl are highly similar, the relative lack of information on Shawl specifically means that the two channels may have subtly different kinetics or sensitivity to BDS. Hence, while Shaw accounts for the remaining current seen in the morning after removal of Shaker and Shab (Figure 3.7A), Shawl may account for some of the remaining current in the late day (Figure 3.7B). Although, it is likely that KCNQ (Kv7) is at least partially involved in the remaining dusk current.

3.3.2 Circadian variation in Kv Channels

The important finding of this study is that the voltage-gated potassium channels Shaw and Shal cycle in a circadian fashion (Figure 3.8). It is indeed a circadian effect rather than an effect of light exposure since the removal of light cues does not abolish the rhythms in the s-LNvs (Figure 3.9). The disruption of core circadian proteins CLK and CYC does however abolish the rhythms further indicating a requirement of a functioning circadian clock for the rhythms of these ion channel currents (Figure 3.10). The observation that the rhythms do not cycle in the l-LNvs during DD is likely due to the fact that the l-LNvs were assayed within two days of their transition to DD. It has been

noted previously that the molecular clock stops cycling soon after the transition (Yang and Sehgal 2001; Shafer et al. 2002; Stanewsky et al. 1998; Cao and Nitabach 2008) and only resumes much later (Peng et al. 2003; Stoleru et al. 2004; Sheeba, Fogle, et al. 2008) after several days.

This sets up the concept that Shaw and Shal cycle in the LNvs in an anti-phase manner and are regulated by the circadian clock. Shaw is highest in the morning and underlies the faster ~2 Hz firing rate of spontaneous action potentials, whereas Shal is highest at dusk and underlies the ~1 Hz firing rate. A recent study of the LNvs also supports this cycling of Shal current as block of Shal current is selectively effective at dusk as opposed to dawn (Feng et al. 2018). Shaw has been associated with a fast-spiking phenotype (Martina et al. 2007), where its kinetics are well-suited to narrow action potentials and short refractory periods (Erisir et al. 1999; Lien et al. 2002; Rudy and McBain 2001). Shal has similarly been linked to the maintenance of excitability during repetitive firing (Ping et al. 2011) but has also been used to rescue hyperexcitability (Ping et al. 2015). Hence, while each channel has been linked to fast-spiking phenotypes, it is likely the balance of each channel and their particular kinetics that give rise to the particular spiking patterns observed.

A previous study did report that over-expression of Shaw in the LNvs drives the neurons towards an evening-like firing rate (Buhl et al. 2016), seemingly in conflict with the data presented here. It must however be reiterated that it is the balance of the channels that is important. The data shown in this chapter previously indicates that the shift from dawn to dusk behaviour occurs because of the concurrent decrease in Shaw current and increase in Shal current. Over-expression of Shaw alone might be predicted to drive the neurons towards an evening-like state because of its role near the resting membrane in hyperpolarising the neuron.

It must also be noted that the circadian rhythms found were in ion channel current in response to depolarisation. The data presented does not indicate the mechanism behind this oscillation, only that there is a change in function.

A possible mechanism underlying this may be rhythms in transcription and translation; rhythms in mRNA production and subsequent translation could give rise to oscillating levels of ion channel expression within the neuron and so varying currents.

It has been previously reported that Shaw and Shal transcripts vary in expression while Shaker and Shab remain constant (Kula-Eversole et al. 2010). Here, Shaw transcript is highest in the morning around ZT0 while Shal is highest towards dusk around ZT12. This is consistent with the findings in this thesis, although the exact relationship between mRNA and protein level peaks is not clear. However, RNA-seq data has also been reported that shows Shab to cycle while Shaw and Shal remain constant (Abruzzi et al. 2017). Some research into the translatome has also reported that none of the voltage-gated potassium channels cycle, instead only the calcium channel *cacophony* (Huang et al. 2013). Many other transcriptomic studies focus on the whole fly head, and so are of limited use in focusing on the LNvs (McDonald and Rosbash 2001; Ceriani et al. 2002).

This conflicting set of results from different sources of transcriptomics has made the issue of which channels are cycling very unclear. Yet, it should also be noted that rhythms in the transcriptome do not necessarily directly correlate with rhythms in protein expression. In the mouse liver and SCN, many rhythmic proteins were not encoded by rhythmic mRNAs (Mauvoisin et al. 2014; Robles et al. 2014). In the mouse SCN, Kv4.1 (Shal) was found to be expressed without variation over the course of the day, yet the I_A current mediated by Kv4.1 was significantly higher in magnitude during the day compared with the night (Itri et al. 2010). Other studies have also reported circadian variation in Kv4.1 (Hermanstyne et al. 2017). Thus, transcriptomic analysis must be considered with caution in relation to circadian expression of proteins. Additionally, neither Shaw nor Shal genes include a pattern of E-box or E-box-like elements that are known to confer a circadian rhythm of gene transcription (Nakahata et al. 2008). Yet, many genes found to have a cycling mRNA level do not contain known circadian transcription elements (Claridge-Chang et al. 2001; McDonald and Rosbash 2001).

Other possible mechanisms for the cycling of ion channel currents are post-translational regulation, such as phosphorylation or association with accessory subunits, and trafficking of ion channels in and out of the membrane or between different areas of the neuron. One possibility is that the redox state of the neuron varies across time-of-day and that this leads to a non-transcriptional modulation of the potassium channels. Indeed, this has been reported to happen in the mammalian SCN (Wang et al. 2012) and in human red blood cells (Henslee et al. 2017; O'Neill and Reddy 2011) but is not well-studied in *Drosophila* as of yet. Another possibility is that the channel itself changes over the course of a day through differential splicing or RNA editing. Adenosine-to-inosine RNA editing has been reported in channels such as $Ca_V1.3$ requiring ADAR2 (Huang et al. 2012), and indeed ADAR2 has been indicated to have rhythmic expression in mice leading to rhythms of RNA populations (Terajima et al. 2017). Likewise, Shaker and Shab have been shown to undergo differential splicing in the LNvs and other clock neurons (Ryan et al. 2008; Ingleby et al. 2009; Jan and Jan 2012; Wang et al. 2018).

The voltage-independent sodium channel *narrow abdomen* (NA) is also of particular interest as measurement of the NA current in the DN1p clock neurons indicates a circadian modulation of current, being higher in the morning than in the evening (Flourakis et al. 2015); this rhythm was abolished in *per* mutants. Subsequent RNA-seq analysis showed that NA did not itself cycle, but rhythms were detected in the *Drosophila* ortholog of the localisation factor NLF-1 that persist in DD. This means that it is likely that circadian regulation of membrane properties by NA are mediated by a circadian regulation of its localisation by NLF-1, providing a link between the membrane clock and the molecular clock. In a similar fashion, potassium channel interacting proteins (KChIPs) have been placed as an integral component of Kv4 channels, particularly DPP6 in the rat (Nadal et al. 2003), suggesting that accessory subunits are well placed to mediate this circadian regulation (Maffie and Rudy 2008).

The *Drosophila* homologue of the big conductance calcium-activated potassium channel BK is known as *slowpoke*; the accessory subunit of the *slowpoke* binding protein (*slob*) has been previously reported to have circadian oscillating mRNA and protein levels and this cycling is altered in clock gene mutants (Jaramillo et al. 2004). Indeed, over-expression of *slowpoke* alters circadian locomotor behaviour. Similarly, Shaker has been implicated since a mutation, termed *minisleep*, causes shortened sleep periods and reduced lifespan (Cirelli et al. 2005). This however is likely separate from cycling of ion channel currents, as the mutation may simply be disrupting the function of neurons involved in the regulation of sleep without any link to circadian cycling of ion channels. In the case of Shaw, it has been observed that over-expression in *Drosophila* clock neurons leads to arrhythmic locomotor behaviour (Hodge and Stanewsky 2008). Again, Shaw is known to regulate membrane resting potential and so may simply be continuously disrupting neuronal function in this situation of over-expression.

3.3.3 Linking the molecular and membrane clocks

Links from the molecular clock to the membrane clock have indicated that the core clock proteins, such as CLK and CYC, have roles in regulating expression of membrane proteins such as ion channels. This has been previously mentioned in terms of NA, KChIPs, and *slob*. However, the inverse relationship, that of the membrane clock affecting the molecular clock, is less well understood.

Electrical silencing of the LNvs has been shown to leave rhythmic cycling of core clock proteins such as PER intact (Depetris-chauvin et al. 2011). However, hyperexcitation of the LNvs has been reported to create a shift in the transcriptome towards a morning-like state whereas hyperexcitation shifts towards an evening-like state (Mizrak et al. 2012; Emery 2012). The link for this was proposed to be the cAMP response element-binding (CREB) family of proteins reacting to electrical activity to affect change in molecular clock pathways. This fits with the observation that PDF feedback is required

for normal oscillatory patterns of transcription (Mezan et al. 2016) and that PDF autoreceptors can shift the balance of circadian activity from evening to morning, with the change mediated by cAMP (Choi et al. 2012). Hence, electrical activity may work through the release of PDF from LNvs and a feedback onto their own autoreceptors to influence the molecular clock through cAMP and CREB, although this may serve more of a modulatory function rather than being required.

This link between the molecular and membrane clocks could also link to the ion channels Shaw and Shal themselves. PDF is known to rhythmically accumulate in the dorsal terminals of the LNvs with more PDF during the day than at night (Park et al. 2000). Previous reports (Hodge and Stanewsky 2008) indicate that expression of the Shaw dominant negative transgene throughout the *Drosophila* clock network results in lower PDF levels across the day with a reduced strength of oscillation. The same effect is seen with expression of Shaw *RNAi* and the opposite effect is seen with over-expression of Shaw. That is, an increase in overall PDF levels and a loss of rhythm. Together this indicates that reduction of Shaw function depolarises the LNvs leading to a depletion of PDF, and hence changes in PDF signalling. However, when expression was restricted to the LNvs only, rhythmic accumulation of PDF was unaffected. This in turn suggests that the effect on accumulation of PDF is not due to the LNvs themselves but is a network effect possibly arising from other clock neurons such as the dorsal neurons (DN). Nevertheless, Shaw and Shal oscillations may link to PDF rhythms or the molecular clock. Future studies may benefit from investigating how manipulating the membrane clock affects the molecular clock such as *CLK* or *CYC* expression; this may show a reciprocal nature between the two clocks. In addition, the circadian remodelling of LNv dorsal terminals (Gorostiza et al. 2014; Fernandez et al. 2008) may serve as a useful output for investigating the effects of the membrane clock on the molecular clock.

3.3.4 Sodium and calcium channels of the LNvs

The discussion has so far focused entirely on potassium channels as experiments looking at sodium and calcium currents in the LNvs were unfortunately poor (Figure 3.12). The LNvs themselves are highly arborised neurons with projections ranging from the cell body to the medulla or the dorsal cerebrum (Peng et al. 2011; Schubert et al. 2018), thus spanning a length of perhaps approximately 400 µm. Such convoluted neurons are particularly hard to investigate due to the difficulty of obtaining a suitable space-clamp over the neuron, which usually only guarantees accurate electrical control over the cell body itself. This coupled with the fact that the invertebrate action potential initiating segment tends to be more distal to the cell body and can change position (Goodman and Heitler 1979; Melinek and Muller 1996), means that the voltage control over the sodium channels was not good. This situation may also be exacerbated by the relatively high access resistances needed to study neurons the size of the LNvs, since the access resistance will exert a low-pass filtering effect and reduce fast signals such as sodium channels whilst also reducing control over them (Section 3.1.2).

Previous reports have briefly looked at sodium and calcium channels in the LNvs. The threshold for spontaneous action potentials is close to activation of the *Drosophila* voltage-gated sodium channel *para* (O'Dowd and Aldrich 1988) and spontaneous action potentials are abolished on bath application of TTX (Sheeba et al. 2008). This indicates that the action potentials are largely sodium-dependent and likely through *para* channels. Also, while *Drosophila para* has many splice forms, *para* remains the main voltage-gated sodium channel. Heterologous expression of these splice forms in *Xenopus* oocytes (Lin et al. 2009) has allowed detailed investigation of kinetics and presents an opportunity to understand these channels even without suitable patch-clamp data.

Bath application of cobalt has also shown to modulate the firing state of the neurons, switching between burst firing, tonic firing, and silence (Sheeba, Gu, et al. 2008). The *cacophony* locus encodes the *Drosophila* homologue of the N-type voltage-gated calcium channel expressed in a variety of neurons (Peng and Wu 2007; Kawasaki et al. 2000; Rieckhof et al. 2003). It has also been shown to be present in the LNvs (Huang et al. 2013). This suggests that the calcium channel involved in the modulation of firing state is likely *cacophony*.

One potential avenue for investigating the depolarising currents of the LNvs was to use the larval brain rather than the adult brain. The *Drosophila* larval brain contains fewer PDF neurons than the adult brain, which are more difficult to patch-clamp due to a deeper anatomical position within the larval brain. Preliminary investigations (Figure 3.12) succeeded in obtaining some electrophysiological data from the larval LNvs, including the observation of spontaneous action potential firing similar to the adult LNvs. However, larval LNv arborisations are still fairly convoluted and more examination is needed to determine whether depolarising currents are detectable and how relevant this is to the adult LNvs. If sodium currents are detectable and well-controlled in voltage-clamp experiments, it would be reasonable to relate this information to the *para* splice forms mentioned previously (Lin et al. 2009) to determine whether they are likely to remain unchanged during development.

In summary, the electrical activity of the LNvs is regulated by voltage-gated potassium channels. Shaker and Shab remain constant throughout the day, whereas Shaw and Shal oscillate in anti-phase. These oscillations are truly circadian and contribute to creating a circadian rhythm in firing rate in the LNvs. Indeed, disruption of either the membrane clock or the molecular clock has effects on the other.

Chapter 4 – Using electrophysiological data to generate a computational model of the LNvs

This chapter details the mathematical modelling of the electrophysiological data presented in chapter 3 towards the generation of a model describing electrical activity of the LNv clock neurons. It begins with introduction to the computational modelling of neuronal activity; particularly the classical Hodgkin-Huxley formalism in section 4.1.1, the subsequent thermodynamics equivalents in section 4.1.2, whole-cell models in section 4.1.3 and other useful forms of models in section 4.1.4 with section 4.1.5 detailing the dynamic clamp approach. Section 4.2 presents results of modelling using the electrophysiological data shown previously in section 3.2. The model is developed in section 4.2.1, analysed in section 4.2.2, and used for real-time manipulation of neurons in dynamic clamp in section 4.2.3. Discussion of this model and its potential uses are given in section 4.3.

4.1 Introduction

4.1.1 Foundations of neuronal modelling

More than 60 years ago, Drs Alan Hodgkin and Andrew Huxley published their seminal works in the squid giant axon, proposing a mathematical model of electrical activity based on their experimental data (Hodgkin and Huxley 1952a). The Nobel Prize winning research of Hodgkin and Huxley laid the foundation for computational modelling of action potentials and channel currents, which has been steadily developed and expanded over the past decades.

The classical Hodgkin-Huxley (HH) model assumes that the number of ion channels in the membrane is sufficiently large, such that their activity (in terms of ionic currents conducted by these channels) can be modelled at population level. The ion channel population are also assumed to only have two states: an open or 'permissive' state through which ions can flow, and a closed or 'restrictive' state. This can be represented as follows:

$$\begin{matrix} & \beta & \\ C & \leftrightarrows & O \\ 1-n & \alpha & n \end{matrix} \qquad \text{Eq. 4.1}$$

Where C denotes the closed state, O the open state, ***α*** is the transition rate from closed to open (activation), ***β*** is the transition rate from open to closed (inactivation), and *n* is the proportion of channels in the open state, such that 1-*n* is the proportion of channels in the closed state. Looking at the proportion of channels in the open state allows us to formulate a differential equation as follows:

$$\frac{dn}{dt} = \alpha(1-n) - \beta n \qquad \text{Eq. 4.2}$$

Considering the steady-state condition, where the fraction of open channels is not changing with time, and hence *dn/dt* = 0, allows us to derive the following relationship between rate constants ***α*** and ***β*** and the steady-state activation function of the respective channel under investigation:

$$n_{\infty} = \frac{\alpha}{\alpha + \beta} \qquad \text{Eq. 4.3}$$

In other words, n_{∞} is the proportion of channels open at the steady-state. Indeed, if we solve this differential for *n* we find that:

$$n(t) = Ae^{-(\alpha+\beta)\tau} + \frac{\alpha}{\alpha + \beta} \qquad \text{Eq. 4.4}$$

This shows that the time constant, τ, for the change in *n* can be expressed as:

$$\tau_n = \frac{1}{\alpha + \beta} \qquad \text{Eq. 4.5}$$

Hence substituting eqs. 4.3 and 4.5 into eqn. 4.2 we obtain:

$$\frac{dn}{dt} = \frac{n_\infty - n}{\tau_n} \qquad \text{Eq. 4.6}$$

This forms the crux of the HH formalism. While we have so far been viewing *n* as the proportion of *channels* in an open configuration, we can instead view *n* as the proportion of *particles in a certain position*, either permissive or restrictive to ion flow. Thus, we can consider that *α* represents a movement of the particle that allows conduction of ions and *β* is a movement that restricts this conduction. In their original works Hodgkin and Huxley fitted these functions to the activation of a voltage-gated potassium channel conductance and found that *n* needed to be raised to a power of 4 in order to adequately fit the initial activation. Hence, they proposed:

$$g_K = \bar{g}_K n^4 \qquad \text{Eq. 4.7}$$

Where g_K is the conductance of the open population of voltage-gated potassium channels and $\bar{g}_K$ is the maximum conductance of the entire population of voltage-gated potassium channels.

This was surprisingly forward-thinking at the time as Hodgkin and Huxley wrote in their paper:

> *These equations may be given a physical basis if we assume that potassium ions can only cross the membrane when four similar particles occupy a certain region of the membrane.*
>
> *Hodgkin & Huxley, 1952*

This idea preceded the identification of voltage-gated potassium channels as tetrameric (MacKinnon 1991) and thus each of the four subunits can conceptually correspond to the n^4 kinetics proposed. Although this is a highly simplified view and has been expanded and complicated significantly by subsequent studies (for review see Pallotta and Wagoner, 1992), the core principle was essentially correct.

Hodgkin and Huxley also suggested m^3h kinetics, as opposed to n^4, for sodium channels. This allowed activation through the *m* particle and inactivation through the *h* particle, however again this is a case of fitting equations rather than imposing physical interpretations. Indeed, other schemes have been proposed to account for effects that the HH n^4 scheme cannot. For example, Cole and Moore (Cole and Moore 1960) described how strong hyperpolarisation followed by depolarisation delayed the rise of potassium conductance and suggested n^{25} kinetics. Nevertheless, the original n^4 scheme has remained the simplest and most common form used in modelling potassium channel conductances.

This description of the kinetics of the gating particle *n* allows computational modelling of an ion channel's current by relating this to certain other electrophysiological properties. The current is described as:

$$I_x = g_x * n^4 * (V - E_x) \qquad \text{Eq. 4.8}$$

Where I_x is the current of the channel being modelled, g_x is the conductance of that channel, *n* is the gating particle as described previously, *V* is the voltage of the cell, and E_x is the reversal potential of the ions conducted by the channel.

4.1.2 Thermodynamics of the HH formalism

In the original HH formalism, the rate constants of α and β were fit to experimental data empirically. Thus, while n^4 kinetics had a physical interpretation, individual parameters for the model did not. Thermodynamic models sought to offer a physical basis for the rate-constants in order to develop understanding of these models.

Consider the transition of an entity from an initial state (*I*) to an end state (*E*) at a rate (*r*) that is voltage-dependent:

$$I \xrightarrow{r(V)} E \qquad \text{Eq. 4.9}$$

The rate-constant, *r(V)*, depends on the free energy barrier between the initial and end states (Johnson et al. 1974) such that:

$$r(V) = r_0 e^{\frac{-\Delta G(V)}{RT}} \qquad \text{Eq. 4.10}$$

Where *R* is the gas constant (8.31 J mol^{-1} K^{-1}), *T* is the temperature in degrees Kelvin, and $\Delta G(V)$ is the difference in free energy of each state, which can be expressed as:

$$G_i(V) = A_i + B_i V + C_i V^2 + \cdots \qquad \text{Eq. 4.11}$$

Where A_i, B_i, C_i, … are constants that depend on the conformational state. Each separate term relates to free energy from different effects such as the electrical field from isolated charges and dipoles represented by the linear voltage term B_iV (Tsien and Noble 1969; Hill and Chen 1972; Andersen and Koeppe 1992). However, the physiological reality of neurons involves relatively small voltage changes and so a 'low field limit' can be used to simplify this nonlinear model (Destexhe and Huguenard 2000) to a linear thermodynamic model by excluding higher order terms. Combining the previous equations gives us the rate-constant:

$$r(V) = r_0 e^{\frac{-(a+bV)}{RT}} \qquad \text{Eq. 4.12}$$

Where *a* and *b* represent the difference of the voltage-independent terms (A_i, B_i) between the intermediate and initial states.

Returning to the original HH formalism model (eq. 1), we can now consider the equivalent of the activation rate-constant *α* in the linear thermodynamic model as:

$$\alpha(V) = \alpha_0 e^{\frac{-(a_1+b_1V)}{RT}} \qquad \text{Eq. 4.13}$$

Further simplifying this uses the conformational change of a particle with charge *q* (Borg-Graham 1991):

$$\alpha(V) = \alpha_0 e^{\frac{-\gamma qF\Delta V}{RT}} \qquad \text{Eq. 4.14}$$

Where *γ* is the relative position of the energy barrier (corresponding to the position of a charge in the ion channel which, when moved, causes conformational change between open and closed states). This form is particularly helpful as a fixed constant, *A*, can be introduced using the half-activation voltage, $V_{1/2}$, and the various parameters simplified for both activation, *α*, and inactivation, *β*, of the channel such that:

$$\alpha(V) = A_\alpha e^{-B_\alpha(V-V_{1/2})} \qquad \beta(V) = A_\beta e^{-B_\beta(V-V_{1/2})}$$

$$B_\alpha = \frac{\gamma qF}{RT} \qquad B_\beta = \frac{(\gamma-1)qF}{RT} \qquad \text{Eq. 4.15}$$

This can now be applied to eq. 4.3, to form the new thermodynamic equivalent of the HH formalism:

$$n_\infty = \frac{\alpha}{\alpha+\beta} \qquad \text{Eq. 4.3}$$

$$n_\infty = \frac{1}{1+e^{\frac{-(V-V_h)}{k}}}$$ Eq. 4.16

This means that our equations make use of physically measurable quantities such as the half-maximal activation and the temperature. In this thesis we will make use of this form. In summary the main equations involved are:

$$\frac{dn}{dt} = \frac{n_\infty - n}{\tau_n}$$ Eq. 4.6

$$n_\infty = \frac{1}{1 + e^{\frac{-(V-V_h)}{k}}}$$ Eq. 4.16

$$\tau_n = Amp * e^{-\frac{V-V_{max}}{\sigma}}$$ Eq. 4.17

4.1.3 Whole-cell HH models of activity

The activity of whole cells can be modelled using individual ion channel models. This modelling approach requires the simplifying assumption that the cell is represented by a single compartment and is isopotential and spatially uniform, where each ion channel model is combined to give the sum of the ionic current moving across the cell membrane. Taking the capacitance of the cell into account, this allows the membrane potential rate of change to be modelled as follows:

$$C\frac{dV}{dt} = I_{app} - g_{Na}m^3h(V - E_{Na}) - g_{Ca}mh(V - E_{Ca}) - g_{Kv1}m^4h(V - E_K) - g_{Kv2}m^4(V - E_K) - g_{Kv3}m^4h(V - E_K) - g_{Kv4}m^4h(V - E_K) - g_{leak}(V - E_{leak})$$ Eq. 4.18

Where C is the capacitance of the cell, I_{app} is the current applied to the cell, and each ion channel model is shown in the form of eqn. 4.8. The equation shown is the whole-cell model used in this thesis and features a voltage-gated sodium channel (g_{Na}), a voltage-gated calcium channel (g_{Ca}), four voltage-gated potassium channels ($g_{Kv1\text{-}4}$), and a leak channel (g_{leak}).

4.1.4 Other models of neuronal activity

It was remarked by the statistician George Box that, ‘Essentially, all models are wrong, but some are useful.’ (Box and Draper 1987). This comment relates to the idea that all models are a simplification of reality in an attempt to produce an easily interpretable model that could provide useful insight into the question under investigation. It also relates to how many models can describe the exact same problem or system in completely different ways. Indeed, while the Hodgkin-Huxley formalism is very common in electrophysiology, there is a wide range of other modelling approaches that have their own advantages and disadvantages. The goal is a model that exhibits: face validity - the model recapitulates features of the experimental data; - mechanistic validity – it uses mechanistic details such as ion channels to describe the behaviour; – and predictive validity – the model can predict novel behaviours and can respond correctly to perturbations that were not used to develop the model.

A computational model of neuronal activity that is simpler than the HH formalism is termed the ‘integrate-and-fire’ model. This is one of the first models of neuronal activity that was proposed before the mechanisms of voltage-gated ion channels were known (Lapicque 1907). The model is essentially based on a simple circuit of a capacitor and resistor in parallel; the capacitor slowly charges until a threshold level and then discharges as an action potential, somewhat mimicking the all-or-nothing concept of action potential thresholds and thus displaying some face validity. As a result, the model typically tends to linearly increase firing rate with stimulation and cannot capture more complex behaviour and hence has limited predictive validity. However, the integrate-and-fire model has been important, for example, in the understanding of large-scale networks and in response variability in cortical neurons (Softky and Koch 1993; Troyer and Miller 1997).

The Hodgkin-Huxley formalism is often thought to be physiologically relevant in its use of voltage-gated ion channels rather than mathematical constructs. However, the complex nature of the model makes it difficult to analyse its mathematical behaviour. Originally called the “Bonhoeffer-van der Pol oscillator” (FitzHugh 1955; FitzHugh 1961; Nagumo et al. 1962), the FitzHugh-Nagumo model is a simplified two-dimensional form of the original four-dimensional Hodgkin-Huxley formalism. Instead of modelling the gating particles, the FitzHugh-Nagumo model uses two differential equations describing the gating dynamics of membrane voltage by means of a relaxation variable and the membrane voltage dynamics by means of an excitation variable. This makes the model much more tractable for mathematical analysis. It is particularly notable for its use of phase-plane analysis showing how changes in the model variables can alter behaviour to create different dynamics, such as equilibria and limit cycles.

The Morris-Lecar model (Morris and Lecar 1981) is another simplified version of the Hodgkin-Huxley formalism similar to the FitzHugh-Nagumo model. However, in this case the model uses the membrane potential and a voltage-dependent potassium current for recovery. This retains the tractability of analysis for the system whilst also being more physiologically relevant than FitzHugh-Nagumo. Both the FitzHugh-Nagumo and Morris-Lecar models are thus preferred for analytical studies of the model behaviour over the more complex Hodgkin-Huxley model. However, the simplification of the dynamics and the loss of physiological mechanisms in the model mean it is often difficult to relate the analysis directly to physiological effects.

Contrary to the simplification of the FitzHugh-Nagumo and Morris-Lecar models, multicompartment models seek to more fully understand neuronal behaviour by creating more complex systems (Forrest 2015). Whereas the original Hodgkin-Huxley model defines the axon as a single isopotential compartment, multicompartment models define the neuron as a series of compartments each utilising the Hodgkin-Huxley equations. The compartments are then coupled by applying cable theory, allowing action potentials to propagate between compartments. This offers the innate

advantage of being able to vary the localisation of certain ion channels to certain compartments of the neuron such as the dendrites, cell body, or axon hillock; displaying perhaps the most mechanistic validity of the models. Nevertheless, the added complexity of multicompartment models means that analytical methods cannot be easily applied to study the behaviour of the system and hence this is achieved numerically by varying certain parameters in a computational model and observing the subsequent effects. Such analysis is often referred to as bifurcation analysis (for review see Guckenheimer and Labouriau, 1993), where smooth changes in parameters causes sudden dramatic changes in the behaviour of the system at bifurcation (or tipping) points. A clear example of this is where increasing input current causes a neuron to switch from silent (equilibrium) to spiking behaviour (limit cycle).

The Sim-Forger model (Sim and Forger 2007; Belle et al. 2009; Diekman et al. 2013) is a Hodgkin-Huxley-type model relating to neurons of the suprachiasmatic nucleus (SCN), which is the master circadian clock of the mammalian brain. It utilises the Hodgkin-Huxley formalism to model sodium, calcium, potassium, and leak currents using the wealth of experimental data available. The channel models are based on the thermodynamics Hodgkin-Huxley equations with some simplification on certain parameters to aid in computation and clarity: the potassium channel is based on experimental data from SCN slices (Bouskila and Dudek 1995) and represents a composite of the potassium currents expressed in those cells while the sodium and leak channels of the model originate from dissociated SCN dorsomedial neurons (Jackson 2004; Kononenko and Dudek 2006). The calcium channel modelled is based on an L-type calcium channel (Lindblad et al. 1996; Pennartz et al. 2002). Interestingly, the changes in calcium levels in the neuron (Ikeda et al. 2003) are modelled as a change in E_{Ca} within physiological range (Nygren et al. 1998; Baxter et al. 1999). The Sim-Forger model has also been used previously to model the *Drosophila* dorsal clock neurons (DN1p) (Flourakis et al. 2015) and represents a good starting point for development of a model of lateral clock neurons (LNv) activity.

4.1.5 Dynamic clamp

The term dynamic clamp refers to a collection of techniques that introduce artificial conductances into cells to simulate a variety of states (for review see Prinz, Abbott and Marder, 2004; Goaillard and Marder, 2006; Wilders, 2006). Dynamic clamp can be used for such purposes as creating electrical coupling between two cells, to simulate chemical synapses, or to add or remove voltage-dependent conductances such as ion channels. It does this by using the measured membrane potential of a neuron and calculating the appropriate current to inject as described by mathematical models, often the classical Hodgkin-Huxley formalism described previously. This allows for a specific modulation of neuronal activity in real-time.

Dynamic clamp has been a powerful tool, particularly in cardiac electrophysiology. However, it has not yet been implemented in *Drosophila* or utilised in circadian rhythm research.

4.2 Results

4.2.1 Generating models of potassium channels and LNv activity

Using the electrophysiological data described previously (see Chapter 3), Hodgkin-Huxley equations were fitted to data for each of the voltage-gated potassium channels: Shaker, Shab, Shaw, and Shal. Fitting was initially performed for each ion channel by a standard Hill climbing (or direct search) search-based optimisation procedure (Kolda et al. 2003) to determine approximate parameter sets. Briefly, this involved random generation of a parameter set, which was then evaluated for fitness against experimental data before random perturbations were applied to search the surrounding parameter space, forming an iterative local search. However, a limitation of this method is that it often finds only local optima, solutions that are the best in that region but not overall.

Successive fits were refined by particle swarm optimisation (PSO). This means that a parameter space was defined as the region surrounding the parameter set identified by the search-based optimisation previously. This parameter space was then populated with numerous parameter sets (particles), which then search through the parameter space towards the optimal solution. This approach allows more reliable identification of a global minimum over local minima. Models were fitted to equations 4.16 and 4.17 for activation and inactivation gating particles. This produces five parameters describing activation, five parameters describing inactivation, and a conductance parameter for the channel. The channel models are consistent with the experimental data (Figure 4.1) and the parameters obtained and used in subsequent modelling are listed (Table 4.1).

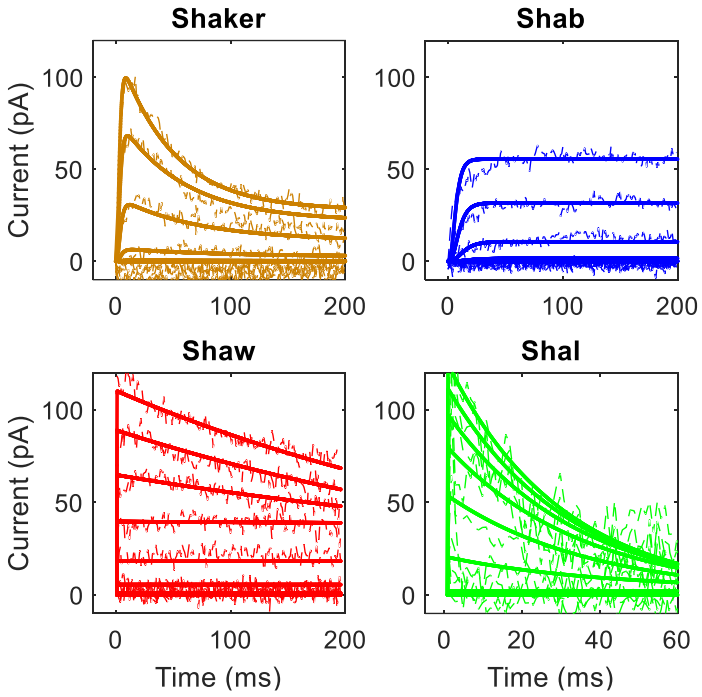

Figure 4.1 Model fits of voltage-gated potassium channel models.

Experimental voltage-clamp data (dotted lines) were fitted to Hodgkin-Huxley equations (eqns. 4.16 and 4.17, solid lines) for each of the voltage-gated potassium channels Shaker, Shab, Shaw, and Shal individually. Voltage protocol shown in Figures 2.2 and 3.2.

Activation	Shaker (Kv1)	Shab (Kv2)	Shaw (Kv3)	Shal (Kv4)
Vh (mV)	-34.18	-29.69	-57.30	-48.63
K (mV^{-1})	9.75	10.49	14.63	7.65
Amp (s^{-1})	1.79	30.72	0.03	0.05
Vmax (mV)	-4.07	-63.69	20.03	-74.86
σ (mV^{-1})	73.88	28.54	238.58	61.54
Inactivation				
Vh (mV)	-93.19	NA	-25.82	-43.05
K (mV^{-1})	54.49	NA	2.5	1.73
Amp (s^{-1})	22.49	NA	154.83	44.52
Vmax (mV)	35.81	NA	159.82	-66.24
σ (mV^{-1})	52.04	NA	167.10	180.11
Conductance (nS)	2.35	0.86	1.40	1.25

Table 4.1 Parameters of channel models.

Tabulation of parameters obtained from fitting of Hodgkin-Huxley equations (section 4.1.2, equations. 4.6, 4.16, and 4.17). Activation and inactivation are modelled using the following parameters: *Vh* (voltage of half-maximal activation/inactivation), K (slope of activation/inactivation), Amp (scaling of time-constant), V_{max} (voltage at which time-constant is equal to Amp), and σ (gradient of voltage-dependence of time-constant).

Individual channel models obtained from fitting behave similarly to known potassium channels (Figure 4.2). The activation curves show increases within physiologically relevant ranges for standard LNv activity. In particular, Shaw activates at particularly negative voltages. Inactivation curves show some variation between the steep voltage-dependence of Shaw and Shal and the shallower voltage-dependence of Shaker. The Shab channel model does not include inactivation as in other reports (Berger and Crook 2015).

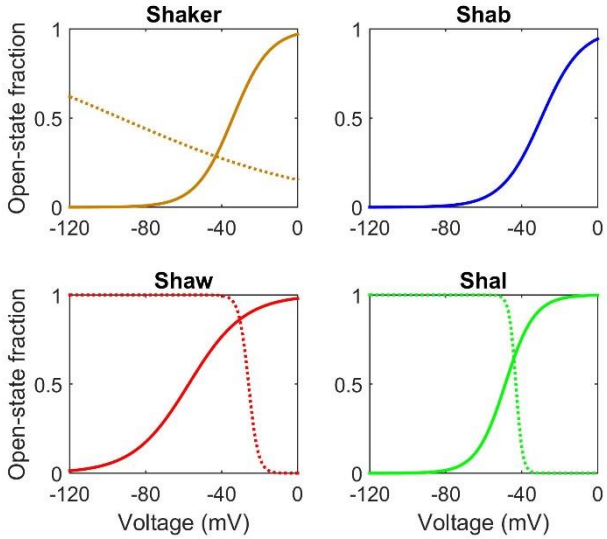

Figure 4.2 Activation and inactivation behaviour of channel models.

Activation (solid lines) and inactivation (dotted lines) of models of each channel Shaker, Shab, Shaw, and Shal. Activation curves show similar gradients between channels, with Shaw having the highest activation at particularly negative voltages. Inactivation curves show a very low gradient for Shaker whereas Shaw and Shal have very steep curves indicating rapid onset of inactivation, particularly for Shal.

The Sim-Forger model was used as the basis for producing a whole cell model of activity. This model features a composite potassium current, a sodium channel, an L-type calcium channel, and leak currents. In order to create the whole-cell model, the Sim-Forger composite potassium current was replaced with the channel models for Shaker, Shab, Shaw, and Shal described previously. As a result, the altered LNv model features four potassium channels, a sodium channel, a calcium channel, and a composite leak channel. In order to model the circadian changes in Shaw and Shal

current, the conductance of the channel was described by a cosine wave recapitulating the variation in peak current described previously (Figure 3.8). Due to the shifting balance of potassium channels, the potassium current varies depending on time-of-day. Whole cell potassium current was recorded at dawn and at dusk in response to a depolarising pulse to -3 mV (Figure 4.3A, similar to Figure 3.2B) and compared to the model prediction for each time-point (Figure 4.3B). The model prediction closely resembles the experimental data, indicating a good fit of the current variation.

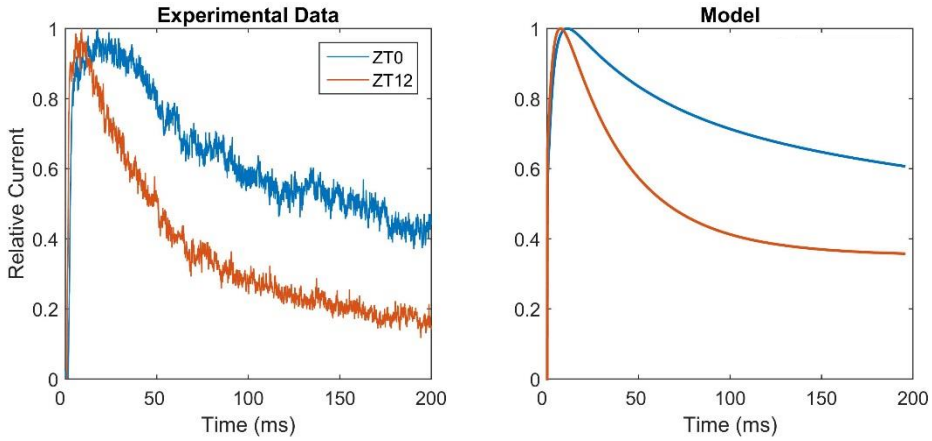

Figure 4.3 Whole cell total potassium currents in the morning and evening.

A) Whole cell potassium current response to depolarisation from -133 mV to -3 mV at either ZT0 (dawn) or ZT12 (dusk). **B)** Model description of whole cell potassium current in response to depolarisation from -133 mV to -3 mV at either ZT0 (dawn) or ZT12 (dusk).

The LNvs themselves display circadian variations in spontaneous action potential firing rate (Figure 3.2). The whole cell LNv model similarly displays action potential firing rates consistent with the experimental current-clamp recordings (Figure 4.4) varying between approximately 2 Hz at dawn and 1 Hz at dusk in both data and model.

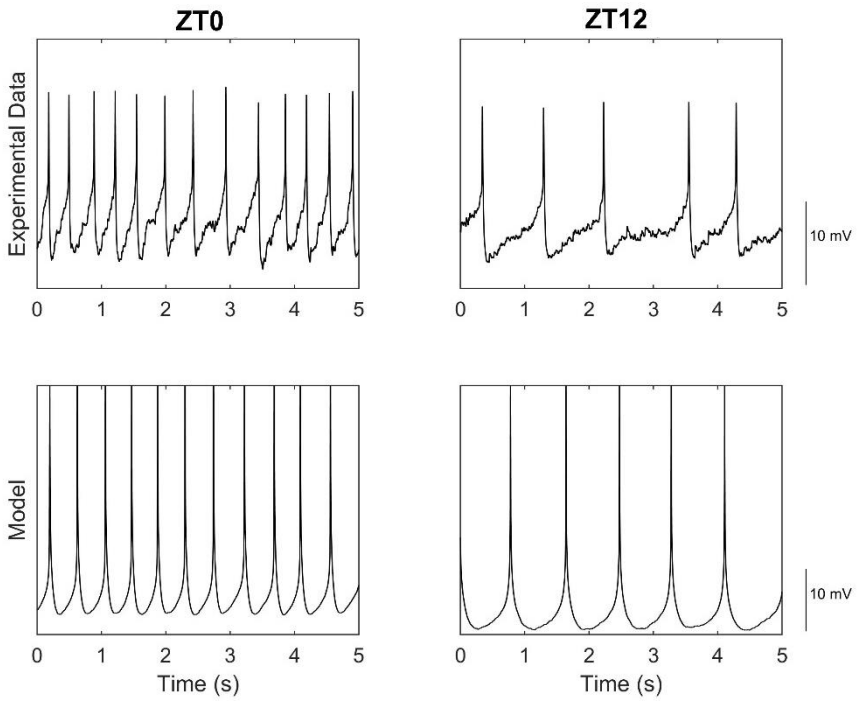

Figure 4.4 Whole cell action potentials.

Representative 5 second epochs of whole cell activity from experimental recordings (top row) against the model description (bottom row) at either ZT0 (left column) or ZT12 (right column). Model descriptions show similar action potential firing rates to those experimentally observed. The whole-cell model utilises equation 4.18 as well as equations 4.6, 4.16, and 4.17 for the individual ion channels. Resting membrane potential is roughly -50 mV to -55 mV.

4.2.2 Analysis of the whole-cell model

An advantage of computational modelling of patch clamp data is the ability to investigate the relationship between membrane voltage and currents. Patch clamp experiments are traditionally constrained to either following membrane voltage in current-clamp or recording ion channel currents in voltage clamp. However, the model can show how ion channel currents act during action potentials (Figure 4.5). Model simulations reveal that, at dawn, Shaw and Shaker are the main contributors to current during an action potential; Shaw is active earlier in the spike while Shaker activates afterwards. It can also be seen that Shaw remains active outside of the action potential, consistent with its role in resting membrane potential regulation. At dusk, the main contributors are Shal and Shaker, with Shal being active earlier during an action potential.

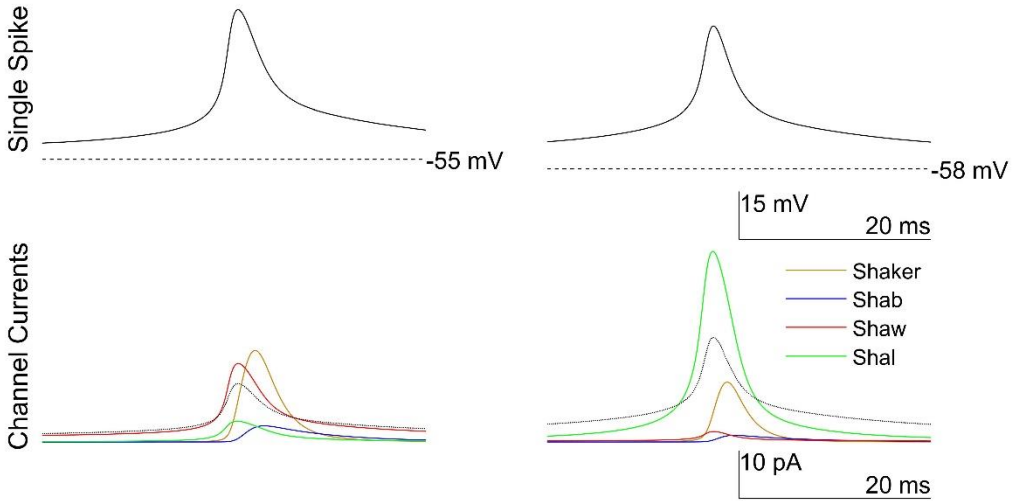

Figure 4.5 Ion channel currents during action potentials.

Representative 40 ms epochs of a single action potential from model descriptions (top row) with the current of each of the potassium channels (bottom row) at either dawn/ZT0 (left column) or dusk/ZT12 (right column). This shows high Shaw currents at dawn and high Shal currents at dusk. The shape of the voltage trace of the action potential is overlaid onto currents (black dotted line, not to scale) to aid in illustrating the phase of the action potential in which each channel is active. Dashed lines (top row panels) indicate resting membrane potential of recording.

Another way to look at ion channel kinetics during spiking behaviour is to examine activation and inactivation states (Figure 4.6). Plotting the trajectory of the activation or inactivation variable against the membrane voltage generates a phase portrait, or phase-plane. This is particularly useful for analysis of Hodgkin-Huxley equations because their complexity precludes simpler analyses. The phase-portraits of activation and inactivation kinetics against membrane voltage for each of the ion channel models shows a stable limit cycle, indicating stable, repetitive action potential firing without deviations. For example, it can be seen that Shaw and Shal activation is voltage-dependent whereas Shaker and Shaw inactivation are highly voltage-independent.

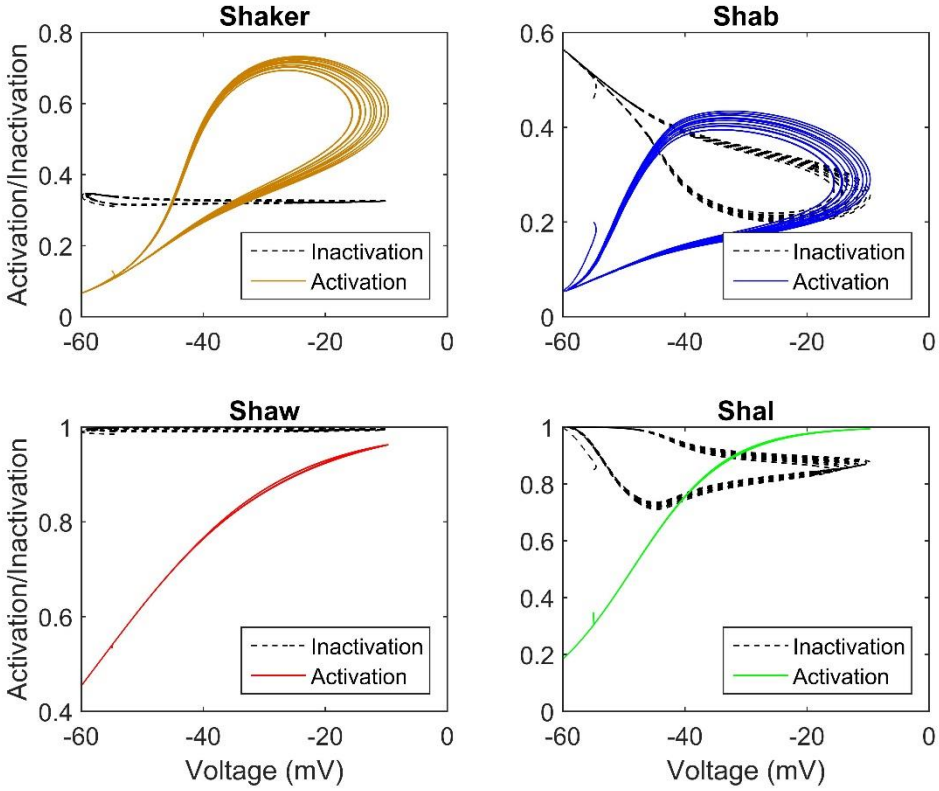

Figure 4.6 Phase portraits of channel model kinetics.

Activation and inactivation dynamics for each of the channel models Shaker, Shab, Shaw, and Shal at ZT12 (dusk) plotted against membrane voltage. Similar results are obtained at ZT0 (dawn). The plots indicate stable limit cycles of action potential firing, and stable, repetitive cycles of the activation and inactivation variables.

Plotting phase-portraits of the membrane voltage against the derivative of voltage (*dV/dt*, Figure 4.7) illustrates some aspects of the action potential more clearly (Bean 2007). The threshold for the action potential is particularly evident as the voltage at which the derivative rises rapidly. Some reports of such phase-portraits in other systems have observed a 'kink' in the plot (Shu et al. 2007), which has been suggested to be related to initiation of the action potential in the axonal initial segment (AIS). However, the plot here is remarkably smooth; potentially due to the convoluted nature of the LNv arborisation and loss of information from the AIS (see Section 3.2.3). It can also be seen that the resting membrane potential is slightly more negative at dusk (ZT12) (Figure 4.7B) than at dawn (ZT0) (Figure 4.7A) and that the peak rate of change of membrane voltage is higher in the morning, indicating faster and higher amplitude spikes. Some variation in the trajectories can also be seen, which is due to the noise added into the system.

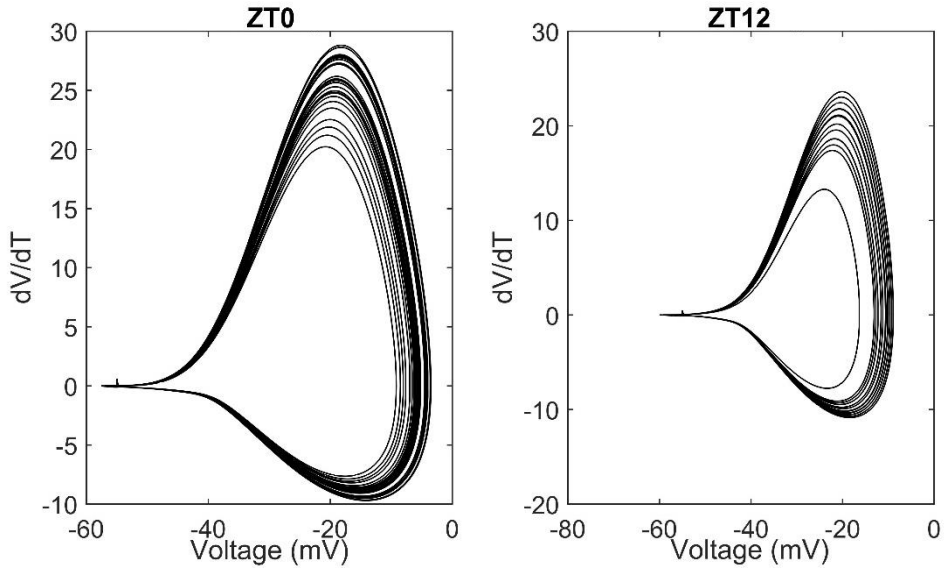

Figure 4.7 Phase portraits of membrane voltage dynamics.

(**A**) Dawn and (**B**) dusk simulations of whole cell action potential firing activity. Peak rate of change of membrane voltage is higher at dawn than dusk.

Complex dynamical systems like this are often difficult to analyse; other models like the FitzHugh-Nagamo model are used precisely because of their relative tractability for analysis. However, one approach for studying the performance of the model is to vary a parameter and observe how that changes the qualitative behaviour, this is called bifurcation analysis (Figure 4.8 and 4.9).

Varying the input current applied (I_{app}, equation 4.18) to the system (Figure 4.8) shows that as the applied current is increased in the morning (ZT0) the action potential firing rate of the system increases (Figure 4.8A). The range of voltages covered by the membrane during firing of action potentials (Figure 4.8B) also varies, gradually becoming slightly narrower as the current increases. However, the model is only active within a narrow range of the applied current, experiencing either depolarising block at more positive currents or simply becoming silent due to insufficient stimulation at more negative currents. During dusk (ZT12), varying the applied current has a similar effect on firing rate (Figure 4.8C) and membrane voltage (Figure 4.8D). However, the overall frequency is lower, and the model is active over a narrower range of currents compared with the morning.

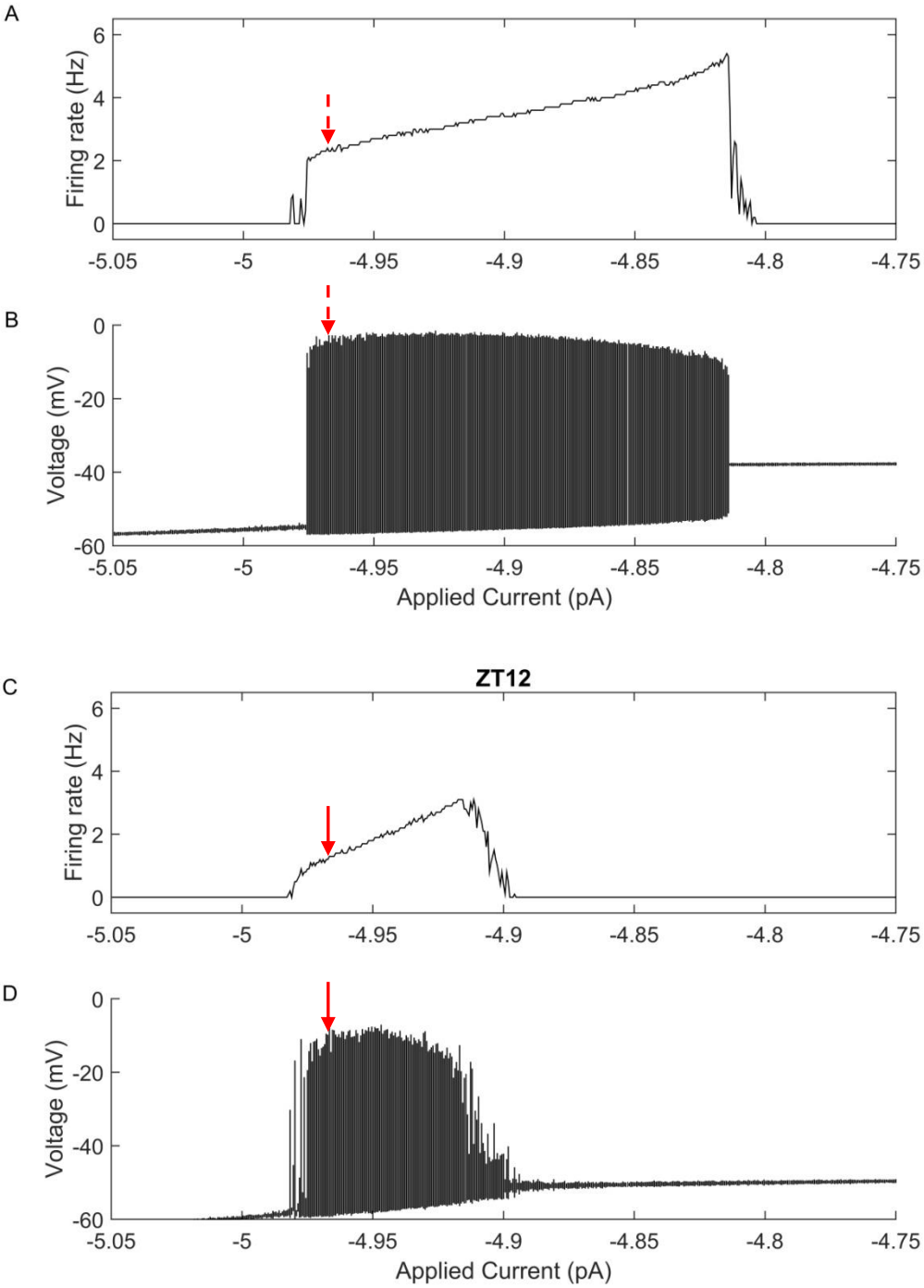

Figure 4.8 Bifurcations of neuronal activity when varying applied current.

(**A**) Action potential firing rate and (**B**) voltage range of the membrane over a range of applied currents modelled at ZT0. (**C**) Action potential firing rate and (**D**) voltage range of the membrane over a range of applied currents modelled at ZT12. Note the arrow indicating the normal applied current of the model.

Due to the circadian oscillation of Shaw and Shal currents, the conductance of the two channels becomes a natural bifurcation parameter (Figure 4.9). Varying the conductance of Shaw and Shal concurrently shows a similar effect whereby the model is active over a narrow range of values (Figure 4.9A). Either side of the active region is a silent region characterised by either a constantly hyperpolarised or depolarised state (Figure 4.9B). Action potential amplitude is remarkably consistent over the range (Figure 4.9A), but frequency does vary between approximately 1-3 Hz (Figure 4.9B).

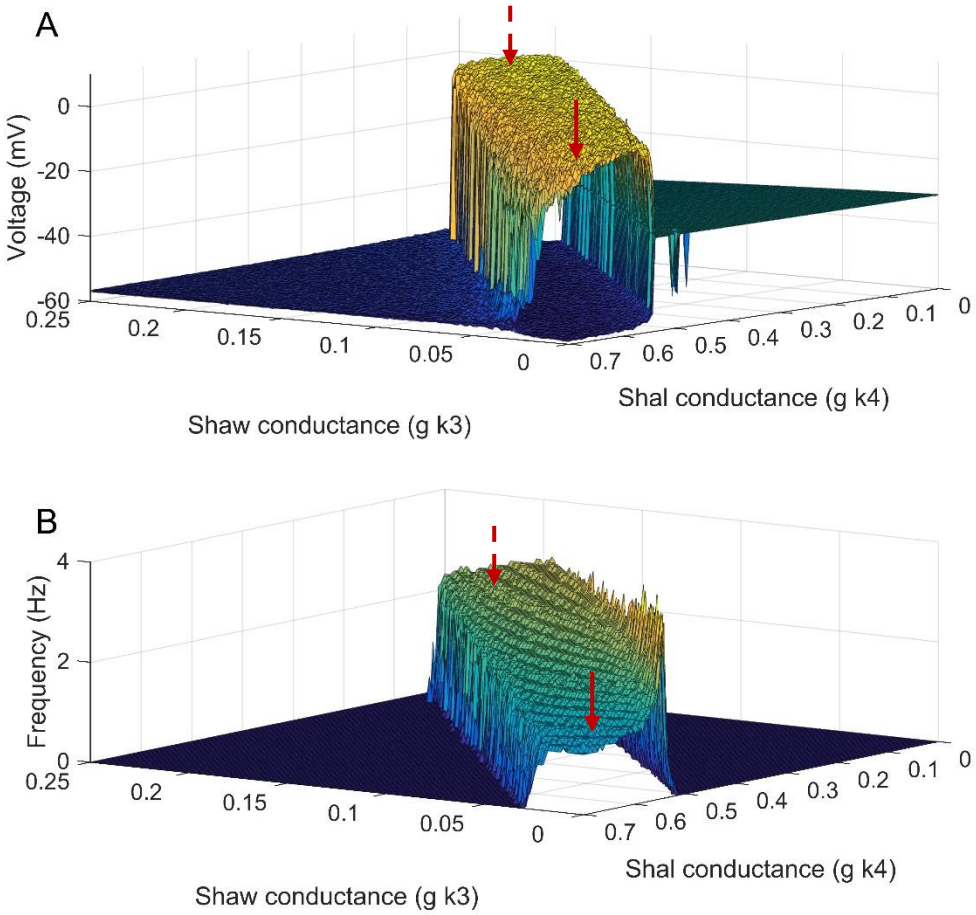

Figure 4.9 Bifurcations of neuronal activity when varying Shaw and Shal.

(**A**) Voltage range and (**B**) action potential firing rate of the membrane over a range of Shaw (g k3) and Shal (g k4) conductances. The model is active over a narrow range of values. Note the arrows indicating the normal dawn (ZT0, dashed arrow) and dusk (ZT12, solid arrow) positions of the model. The colours reinforce the z-axis value (i.e. voltage (A) or frequency (B)).

4.2.3 Implementation of dynamic clamp

Using the Kv channel models generated previously, dynamic clamp was implemented. In order to validate the channel models in a physiological setting, the Kv channels were individually blocked by the appropriate drug and re-introduced by the dynamic clamp model (Figure 4.10). This showed that initial changes in spike frequency (Figure 4.10A first row) induced by application of the drug could be rescued computationally, suggesting that the channel models can replace the channels themselves and describe their current (Figure 4.10A second row) accurately.

To accomplish this, the LNv is patch-clamped as previously (Chapter 3) in current-clamp. To achieve stable action potential firing, minimal current was injected. This was adjusted between control and drug addition (+DTX) before remaining constant between the drug addition (+DTX) and model application states (+DTX +Model).

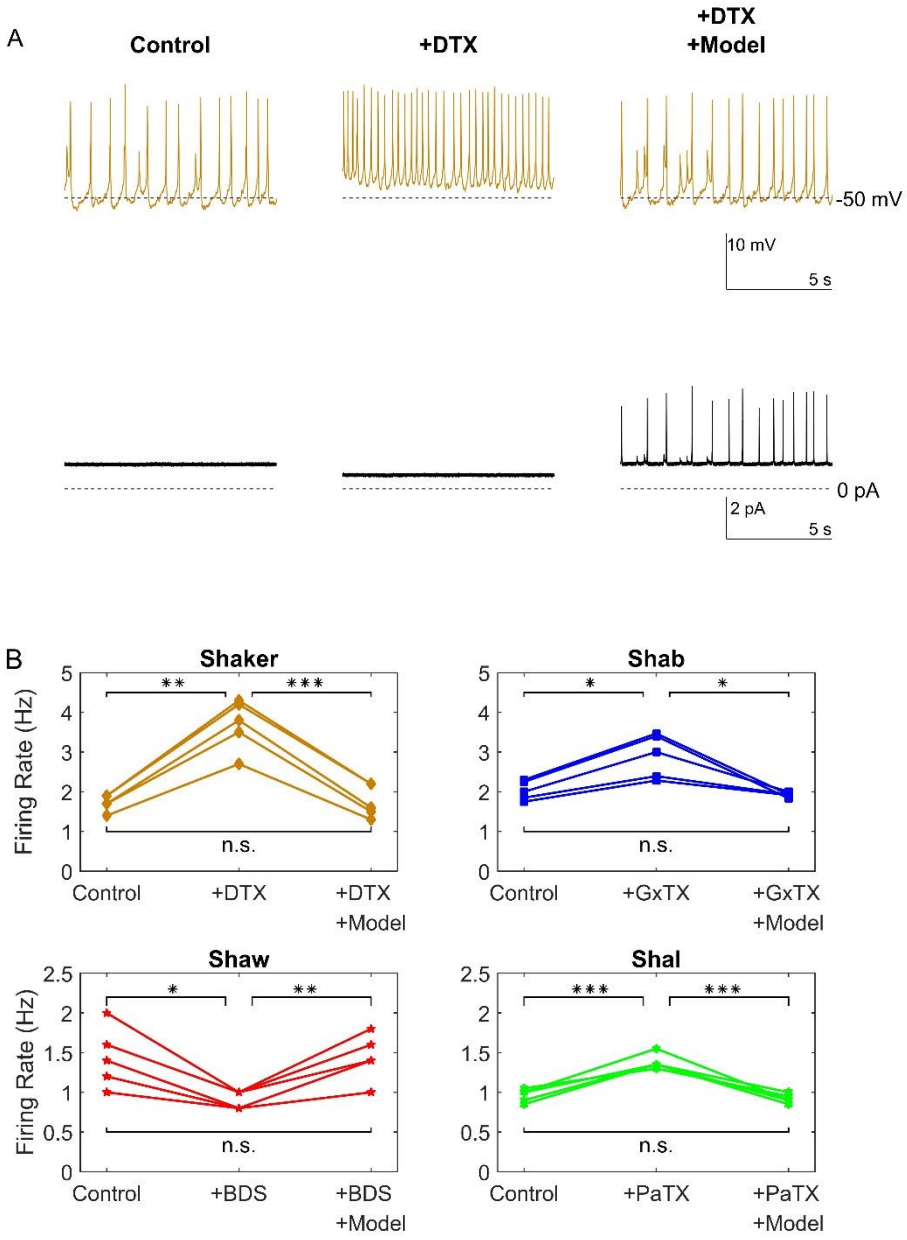

Figure 4.10 Dynamic-clamp rescue of pharmacological channel block.

(**A**) An example trace showing 10 second epochs of the control condition (left panel), after application of the Shaker channel blocker DTX (middle panel), and after subsequent addition of the Shaker channel model (right panel) at ZT0-3. The voltage trace (first row) and total current trace including dynamic clamp current output and current-clamp (second row) are shown. (**B**) Quantification of action potential firing rate before (left point) and after (middle point) channel block and subsequent rescue by dynamic-clamp (right point) for each of the Kv channels Shaker, Shab, Shaw, and Shal. Shaker, Shab, and Shaw recordings were performed at ZT0-3. Shal recordings were performed at ZT12-15. Conductances used are given in Table 2.2 (top). Firings rate change on drug application (Shaker: p=0.0014, Shab: p=0.0197, Shaw: p=0.0120, Shal: p<0.0001) and are rescued by appropriate models (Shaker: p=0.0008, Shab: p=0.0159, Shaw: p=0.0030, Shal: p<0.0001).

Expression of the Shaw and Shal dominant negative transgenes caused changes in action potential firing rate similar to that seen with the application of BDS and PaTX, respectively. Subsequent introduction of the Shaw channel models (Figure 4.11) rescued the changes similar to the rescue of pharmacological block.

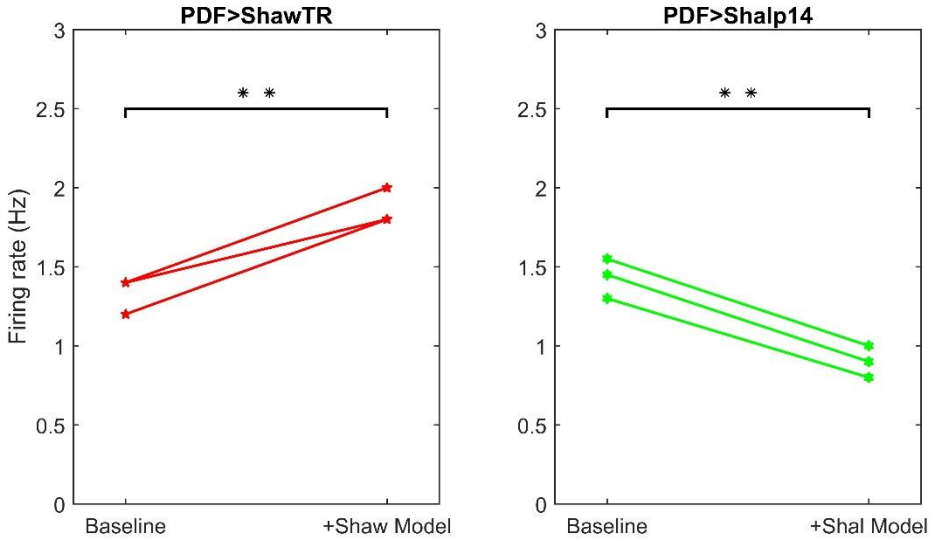

Figure 4.11 Dynamic-clamp rescue of dominant negative phenotypes.

Quantification of action potential firing rate before (left point) and after (right point) rescue by dynamic-clamp of LNvs expressing either Shaw (left panel) or Shal (right panel) dominant negative transgenes. Firing rate is rescued to wild-type levels at the appropriate time-point (see figure 3.2) similar to dynamic-clamp rescue of pharmacological block (see figure 4.10). Shaw recordings were made at ZT0-3 whereas Shal recordings were made at ZT12-15. PDF>ShawTR recordings increase firing rate on model introduction ($p=0.0048$) returning to the normal ZT0 level of ~2 Hz. PDF>Shalp14 recordings decrease firing rate ($p=0.0053$) towards the normal ZT12 level of ~1 Hz.

As the circadian variation in action potential firing rate is likely underpinned by changes in the Shaw and Shal channels, the modulation of Shaw and Shal current by dynamic clamp should recapitulate the circadian variation. Similar to previously (Figure 4.10), LNvs were patch-clamped and current injected to ensure stable repetitive action potential firing behaviour. This current remained constant between the controls and model application (+Model). By taking a dawn cell and removing the Shaw current whilst

increasing the Shal current (Figure 4.12A), the neuronal activity switched from a dawn to a dusk state. The converse situation at dusk (Figure 4.12B) also allows a switch from a dusk state to a dawn state.

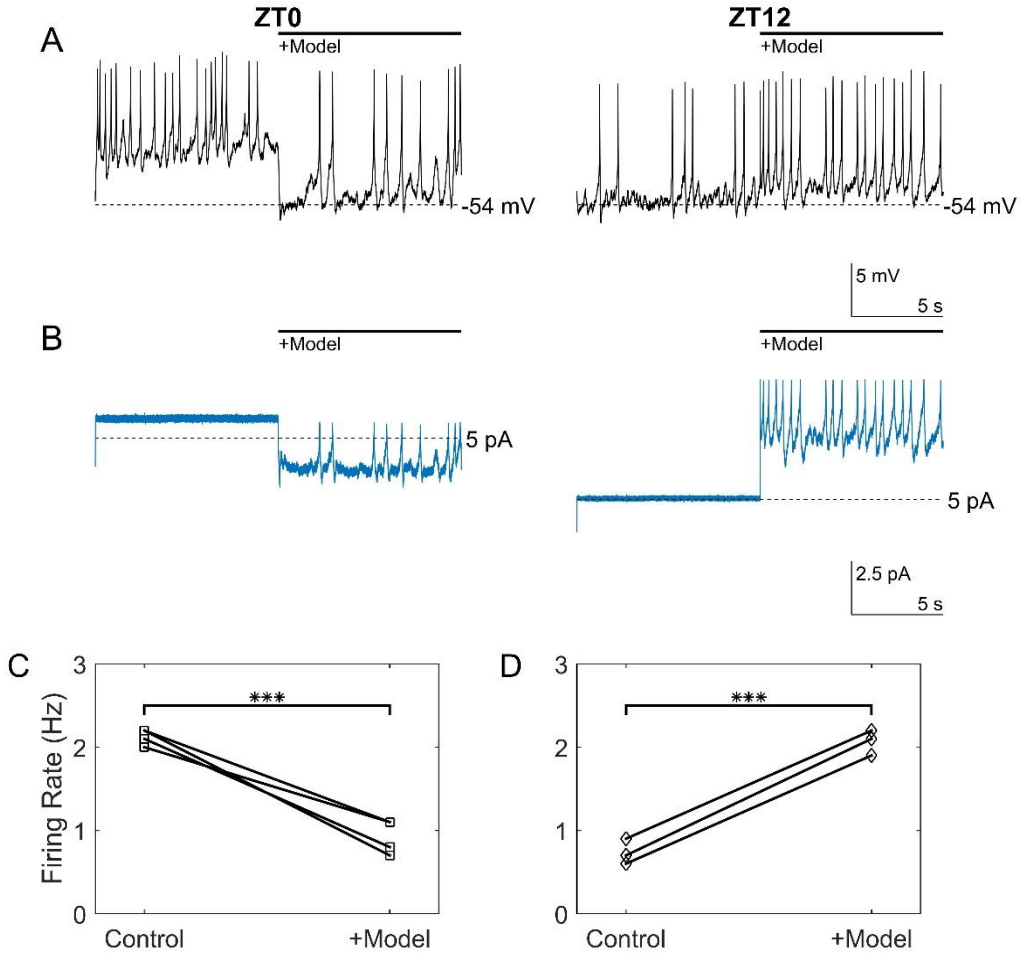

Figure 4.12 Dynamic-clamp switching between morning and evening states.

(A) Representative 20 second epochs of dynamic clamp recordings of LNv electrical activity at ZT0 and ZT12 showing the characteristic firing rates. Removal of Shaw current and introduction of Shal current switch the ZT0 firing rate to the dusk level of ~1 Hz (p=0.0003). Introduction of Shaw current and removal of Shal current switch the ZT12 firing rate to the dawn state of ~2 Hz (p=0.0004). **(B)** Current traces from the respective ZT0 and ZT12 recordings showing the total current injected from the channel models and current-clamp. **(C)** Quantification showing the switch from a dawn to a dusk state (left panel) and from a dusk to a dawn state (right panel). Conductances used are given in Table 2.2 (bottom).

4.3 Discussion

4.3.1 The LNv model

This chapter detailed the development of a model describing the electrical activity of the LNv clock neurons. Neurons of the mammalian SCN have been modelled in a similar fashion previously (Sim and Forger 2007; Belle et al. 2009) and these models have been extended to the dorsal *Drosophila* clock neurons (DN1p) (Flourakis et al. 2015). However, the LNvs have not been modelled in the same fashion despite a wealth of electrophysiological data, indicating a gap in understanding of the system. Indeed, networks of SCN neurons have been modelled by extension of these models (Diekman and Forger 2009); an approach that could be taken in future to extend this model.

The model itself is based on the previous Sim-Forger SCN model and utilises new electrophysiological data to model the activity of separate voltage-gated potassium channels. This allows a more detailed and nuanced study of the behaviour of each individual channel, as in the case of Shaw and Shal shown here. The whole-cell model of action potential firing (equation 4.18) is particularly useful in showing that the anti-phase oscillation of Shaw and Shal current is sufficient to create the changing electrical activity observed in experimental data. Whilst this does not exclude the possible involvement of other channels in this effect, it does place Shaw and Shal as potential targets for modulating the system in subtle ways rather than simply silencing the neurons. This idea of Shaw and Shal oscillation has even allowed the alteration of circadian locomotor rhythms and longevity in flies (see Chapter 5).

4.3.2 Limitations of the model

A limitation of this model is the absence of tractable data on the sodium and calcium channels for modelling, as detailed previously (Figure 3.13). Due to this lack, the model presented in this chapter (equation 4.18) uses the

sodium and calcium channels of the original Sim-Forger model (Sim and Forger 2007).

The sodium channel was itself based on previous SCN experimental data (Jackson 2004) and so represents a mammalian voltage-gated sodium channel. *Drosophila* have only one voltage-gated sodium channel known as *paralytic (para)* or Na_V1 (Miyazaki et al. 1996), however it is subject to alternative splicing. The lack of electrophysiological data means that the correct splice isoform(s) has not been identified, yet some data is known from heterologous expression of splice variants in *Xenopus* oocytes (Olson et al. 2008; Lin et al. 2009).

The main effect of the loss of sodium channel data is on the amplitude of the neuronal spikes (Figure 4.4). This, along with the fact that the recorded data are of somatic spikes, means that the model spike amplitudes are larger than those recorded. Nonetheless, the model used here is similar to the *Drosophila para* splice forms reported and so remains somewhat consistent. Still, future studies could investigate how different splice forms might affect neuronal behaviour in the model or which splice form is present within the LNvs by electrophysiology or molecular techniques such as RNA-seq. One possible approach is to look more closely at the larval LNvs (Figure 3.14) to determine if they are more tractable for analysis of sodium currents.

The calcium channel used in the model is based on previous data (Pennartz et al. 2002; Jackson 2004) of L-type calcium currents and extends this with modelling of E_{Ca} to reflect changes in calcium levels (Ikeda et al. 2003), although this extra functionality is not utilised in the LNv model. In the mammalian SCN, rhythmic oscillations in intracellular calcium concentrations have been reported with peaks during the day (Colwell 2000; Ikeda et al. 2003). Indeed, entry of calcium through voltage-gated calcium channels has been shown to be required for molecular functions of the circadian clock (Lundkvist et al. 2005).

Mammalian voltage-gated calcium channels are broadly split into three categories: L-type (Ca_V1), N/P/Q-type (Ca_V2), and T-type (Ca_V3) based on different pharmacology and kinetics (for review see Catterall, 2011). The *Drosophila* genome does contain homologues of the major N-type, L-type, and T-type voltage-gated calcium channels; the N-type channel *cacophony* is possibly the most well understood and it has been indicated to be expressed in the LNvs (Kula-Eversole et al. 2010) making it feasibly the best candidate. Although, the T-type channel Ca-α1T has been shown to be expressed throughout the fly brain and have a role in promoting wakefulness (Jeong et al. 2015).

Nevertheless, there is little to indicate how consistent the calcium channel model used is with LNv physiology. This perhaps is the main limitation of the model at this point. Especially since calcium levels are likely very important as a link between electrical activity and the circadian molecular clock (Harrisingh et al. 2007; Petrzilka et al. 2009) - potentially by stabilisation of PER and TIM by calcineurin (Kweon et al. 2018) - and the large-conductance calcium-activated potassium channel (BK) homologue *slowpoke* (*slo*) and small conductance channel (SK) could be important to LNv behaviour (Sheeba, Fogle, et al. 2008; Panda et al. 2002; Meredith et al. 2006; Whitt et al. 2016; Belle et al. 2009) as the *slowpoke* null-mutant has shown disruption in accumulation of PDF of the dorsal protocerebrum (Fernandez et al. 2007).

Another point to note about the model is that, due to spatial restrictions of the space clamp, the electrophysiological data used to generate the model is predominantly from the cell soma. This means that the model itself should be seen as a model of the cell soma only; this is reflected in the cell capacitance; the model uses a value of 3.7 pF that was obtained from modelling. Assuming a specific cell membrane capacitance of 1 $\mu F/cm^2$ (Hodgkin et al. 1952), the capacitance of the 10-11 μm diameter soma of the l-LNvs would be roughly 3.4-3.8 pF, consistent with the model.

Despite the previously discussed limitations, the model has helped to further understanding of the mechanism underlying circadian variation in LNv action

potential frequency. With the use of electrophysiological data, the model has shown how Shaw and Shal currents are particularly important in regulating this circadian electrical activity and how changes in the conductance of these channels may be a central principle in normal function. Indeed, the approach used to generate the model also serves as a guide for future investigations into this system, as well as other systems and organisms. Certainly, subsequent modelling with this approach has been useful in the understanding of human essential tremor (Chapter 6).

4.3.3 Dynamic clamp

The model has also allowed for the successful implementation of dynamic clamp in the LNvs; to our knowledge, this is the first time in *Drosophila* and also in circadian rhythm research. This means that the electrical activity of the LNvs can be modulated in real-time. Here we used the dynamic clamp set-up to rescue pharmacological block of Shaker, Shab, Shaw, and Shal as well as rescuing the functional removal of Shaw and Shal by dominant negative subunits (Figures 4.10-11). These rescues verified our channel models in a physiological setting. The models also made it possible to switch the LNvs between dawn and dusk electrical states (Figure 4.12), further suggesting that the changes in Shaw and Shal are sufficient to recapitulate the changes seen in whole cell behaviour.

In the dynamic clamp switching experiments (Figures 4.10 and 4.12), some current injection was used to endure repetitive action potential firing behaviour during the comparatively long experiments. While currents remained constant between drug application and model application (meaning that model channel currents were the only change on applying the model), this is a potential limitation of the study at present as the difference between control and model conditions includes potential current-clamp differences independent of channel behaviour. Future dynamic clamp studies on this should improve on this methodology to develop proper reproducibility and clear interpretation.

In summary, the electrophysiological data gathered previously (see Chapter 3) has been used to generate a mathematical model of LNv activity utilising the Hodgkin-Huxley formalism. The model shows that Shaw and Shal are active in shaping the action potential when they are most expressed and that the circadian changes in Shaw and Shal are sufficient to recapitulate the changes detected in action potential firing rate.

Chapter 5 – Behaviour

This chapter describes behavioural data relating to the circadian locomotor behaviour of various flies as well as their longevity. Section 5.1 provides background to circadian rhythms, the use of this analysis in *Drosophila*, and the role of the clock neurons. Section 5.2 provides results of experiments investigating perturbations of LNv function in circadian rhythms and longevity. Section 5.3 discusses these results.

5.1 Introduction

5.1.1 Circadian rhythms and longevity of *Drosophila* and the LNvs

The sleep/wake cycle is perhaps the most obvious example of a circadian rhythm (see Chapter 1); characteristics of sleep are physical quiescence, a species-specific posture, and an increased arousal threshold. In mammals, sleep can be further divided into stages of rapid eye movement (REM) sleep or non-REM sleep. *Drosophila* display many features of sleep similar to mammals (Shaw et al. 2000; Hendricks et al. 2000) including both homeostatic and circadian drives (Borbély et al. 1989) and distinct sleep stages (Yap et al. 2017). The precise function of sleep remains elusive but has been strongly linked to memory and cognitive performance (Berry et al. 2015).

Under laboratory conditions, *Drosophila* display a largely diurnal pattern of sleep that is highly crepuscular, meaning there is a large increase in behaviour at the twilight periods of dawn and dusk (Vanin et al. 2012). Male flies also exhibit a ‘siesta’ period in the middle of the day consisting of increased sleep, although this is mainly linked to male flies and is temperature-dependent (Roessingh et al. 2015; Lamaze et al. 2017).

The most well-established way to assay circadian activity is through the *Drosophila* activity monitor (DAM) system (Section 2.4.2), looking at the circadian rhythm of locomotor behaviour. The easily recognisable morning and evening peaks of diurnal activity lend themselves well to investigating circadian rhythms and are tractable to analysis such as autocorrelation analysis. As such, studies into the circadian locomotion of fruit flies are well-established (Reiter 1978), forming a crucial part of the discovery of the first bona fide clock gene and behavioural mutant in any organism, called period (Konopka and Benzer 1971). Since then circadian locomotor assays have continued to illuminate components of sleep/wake regulations including various ion channels such as Shaker (Cirelli et al. 2005), the Shaker accessory subunit Hyperkinetic (D. Bushey et al. 2007; Bushey et al. 2010), and Ca-α1T (Jeong et al. 2015) as well as the LNv neurons themselves (Parisky et al. 2008).

The control of circadian locomotor rhythms and sleep in *Drosophila* is often attributed to a dual-oscillator model of morning (M) and evening (E) cells (Aschoff 1966; Pittendrigh and Daan 1976); the M cells are largely the LNvs, whereas the E cells are the LNds and the fifth s-LNv, which does not express PDF (Grima et al. 2004; Stoleru et al. 2004). Interestingly, the control of sleep has shown some distinction from control of circadian locomotor behaviour. The l-LNvs have been reported to be wake-promoting neurons (Parisky et al. 2008) and indeed hyperexcitation of these neurons leads to increased nocturnal behaviour (Sheeba et al. 2008). However, a pathway running from the s-LNvs has also been suggested to modulate rest-activity rhythms (King et al. 2017). This pathway moves from the s-LNvs to the DN1 and then to diuretic hormone 44 (Dh44) expressing neurons of the pars intercerebralis, a region considered as a functional homologue of the mammalian hypothalamus (Cavanaugh et al. 2014; Guo et al. 2016). Nevertheless, when this pathway is disrupted, rest-activity rhythms are more pronounced than those of PDF or PDF receptor mutants (Cavanaugh et al. 2014) suggesting that there are further signals downstream of the PDF-positive LNvs that are involved in regulation of these rhythms.

The in-depth study of sleep itself is, however, a comparatively new field of research. The main characteristics of sleep are sustained physical quiescence, a species-specific posture, an increased threshold of arousal, and a reversibility of this state on waking. In humans this is often shown with polysomnographic data, which is not available in *Drosophila*. However, *Drosophila* have been found to display some of these characteristics (Hendricks et al. 2000; Shaw et al. 2000) with the most identifiable feature being quiescence. Experimentally, circadian studies tend to rely on the definition of sleep as any period of inactivity longer than 5 minutes (Cirelli 2003), allowing the DAM system to give an estimation of sleep.

With their relatively short lifespan, it is also more reasonable to follow individual flies over the course of their lifetime. This allows the examination of how various interventions affect health and overall longevity. For example, *period* mutants and *cycle*-null mutants both showed a shortened lifespan (Klarsfeld and Rouyer 1998; Hendricks et al. 2003). The underlying basis for this may be due to neuroprotective roles against oxidative stress (Krishnan et al. 2009) and neurodegeneration (Krishnan et al. 2012). Additionally, period was reported to be important in divisions of intestinal stem cells and can affect aging (Karpowicz et al. 2013). This means that circadian rhythms and components of the molecular clock are involved in the regulation of *Drosophila* longevity. While presence of predators is not a factor in the longevity of laboratory flies, it should also be noted that in the wild circadian rhythms may be important for longevity in evasion of predators.

5.2 Results

5.2.1 Effects of Shaw or Shal dominant negative transgenes in the LNvs on circadian locomotor behaviour

The current of the Kv channels Shaw and Shal was functionally removed by targeted expression of the dominant negative transgenes ShawTR and Shalp14, respectively, in the LNvs through the *PDF-GAL4* driver. The averaged activity of the flies was visualised by using overall actograms and histograms of the LD and DD periods (Figure 5.1). Under LD conditions, the wild-type and mutant flies showed similarly rhythmic activity profiles with prominent morning and evening peaks. However, the peaks of activity appeared larger when the Shaw dominant negative is expressed (Figure 5.1B). Under DD conditions, the histograms still showed some distinction between day and night (Figure 5.1C). In particular, the morning and evening peaks were still separated by a distinct siesta phase. Again, the activity was elevated with expression of the Shaw dominant negative and in this case the evening peak appeared broader.

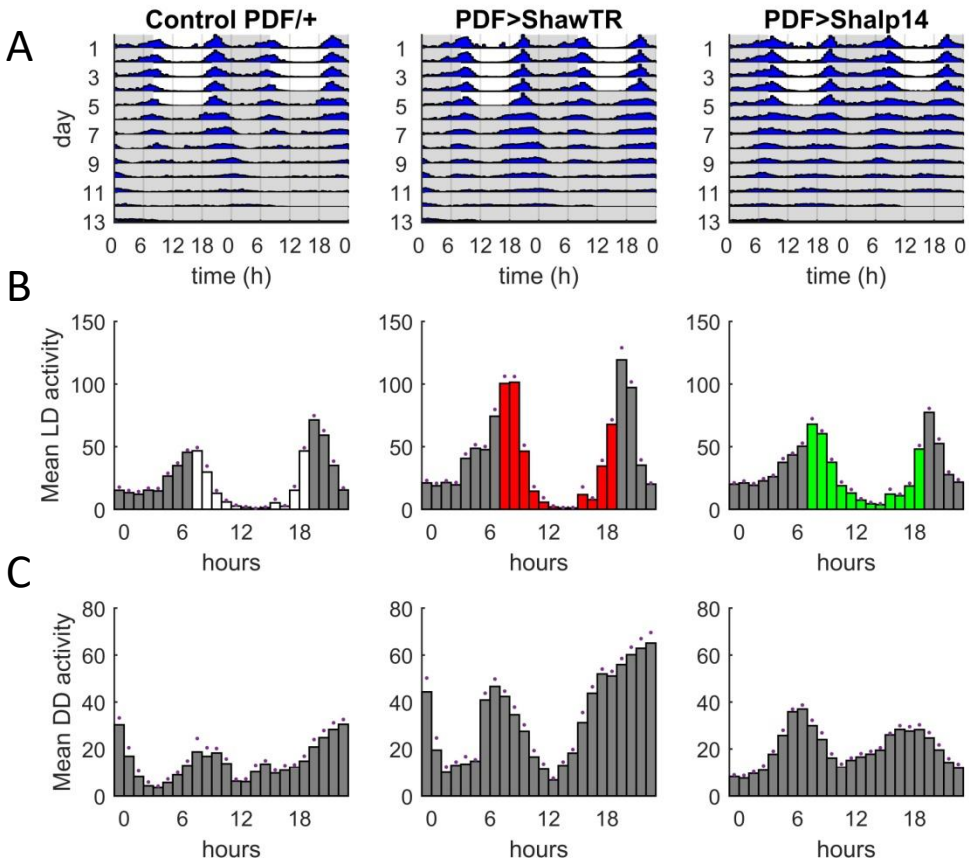

Figure 5.1 Activity patterns of Shaw and Shal mutant flies.

A) Mean actograms of control flies (n=16) and flies expressing either Shaw (n=14) or Shal (n=21) dominant negative transgenes in LNvs. **B)** Mean histograms over the five days of LD. **C)** Mean histograms between the third and fifth days of DD. Activity was measured in beam crosses per 30 min bin. Grey shading indicates the dark phase, white or colour shading indicates the light phase. Dots indicate SEM.

As seen in the LD and DD histograms, the overall activity of the mutant flies was different to that of the controls (Figure 5.2A). The total activity of the Shaw dominant negative flies was significantly increased in both the day and the night. Similarly, the activity of the Shal dominant negative flies was also increased in both the day and the night. However, despite this change in activity, the strength of rhythmicity of the flies was largely unaffected as shown by the mean RS values (for RS see Chapter 2.3) (Figure 5.2B). There was a slight increase in the period of the Shaw dominant negative flies, but no change was observed in the Shal dominant negative flies. There was also no change in the rhythm strength or the proportion of rhythmic flies.

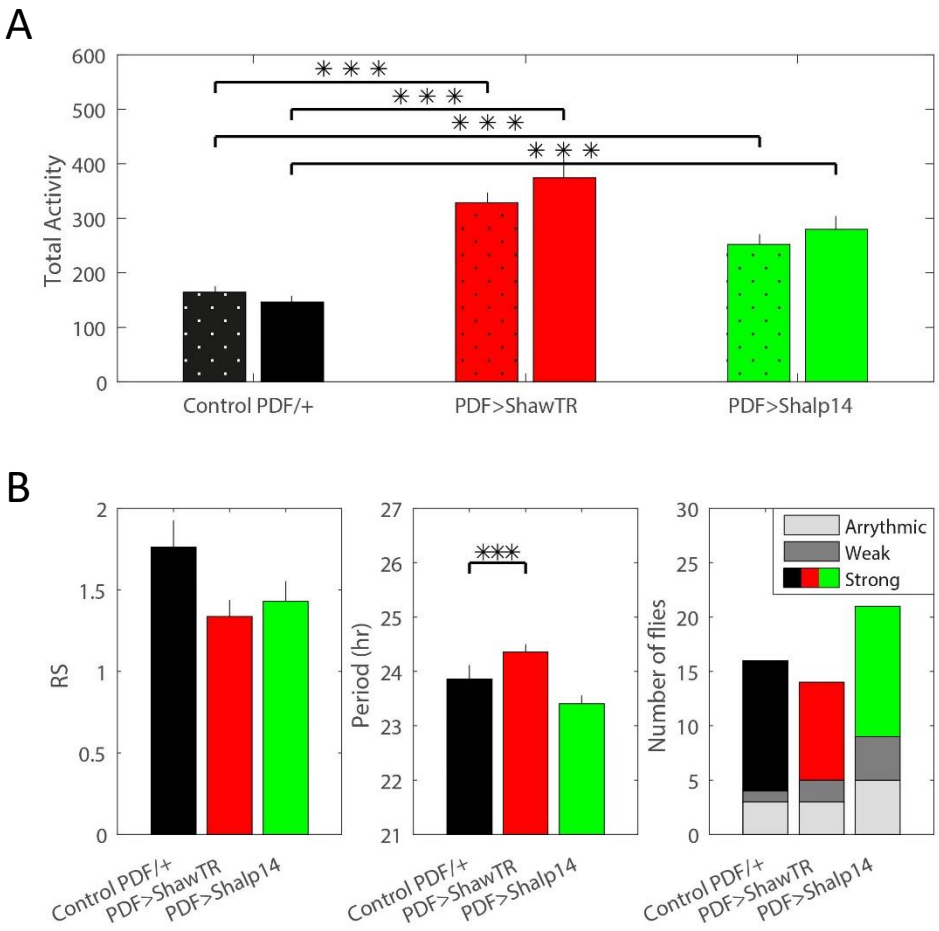

Figure 5.2 Activity and rhythmicity of Shaw and Shal mutant flies.

A) Mean total activity in the day (dotted bar) and the night (plain bar) for control flies (n=16), and flies expressing Shaw (n=14) or Shal (n=21) dominant negative transgenes in the LNvs. Activity of Shaw flies is increased in both day ($p<0.0001$) and night ($p<0.0001$). Activity of Shal flies is also increased in both day ($p=0.0003$) and night ($p<0.0001$). **B)** The mean RS and period of DD activity rhythms and proportion of flies displaying strong or weak rhythms or arrhythmicity. The period of Shaw flies is slightly increased ($p<0.0001$) but the strength of the rhythms is not significantly different as shown by the RS (Rhythm Statistic, see Chapter 2.3) values.

The sleep traces (Figure 5.3A) showed particular differences in the night-time sleep compared with controls. Quantification of the day and night sleep (Figure 5.3B) showed significant decreases in the night-time sleep of both Shaw and Shal dominant negative flies along with a decrease in the day-time sleep of Shal dominant negative flies. In terms of individual sleep bouts (Figure 5.3C), the mean number of sleep bouts was not significantly changed, but in the Shal dominant negative flies the mean length was decreased.

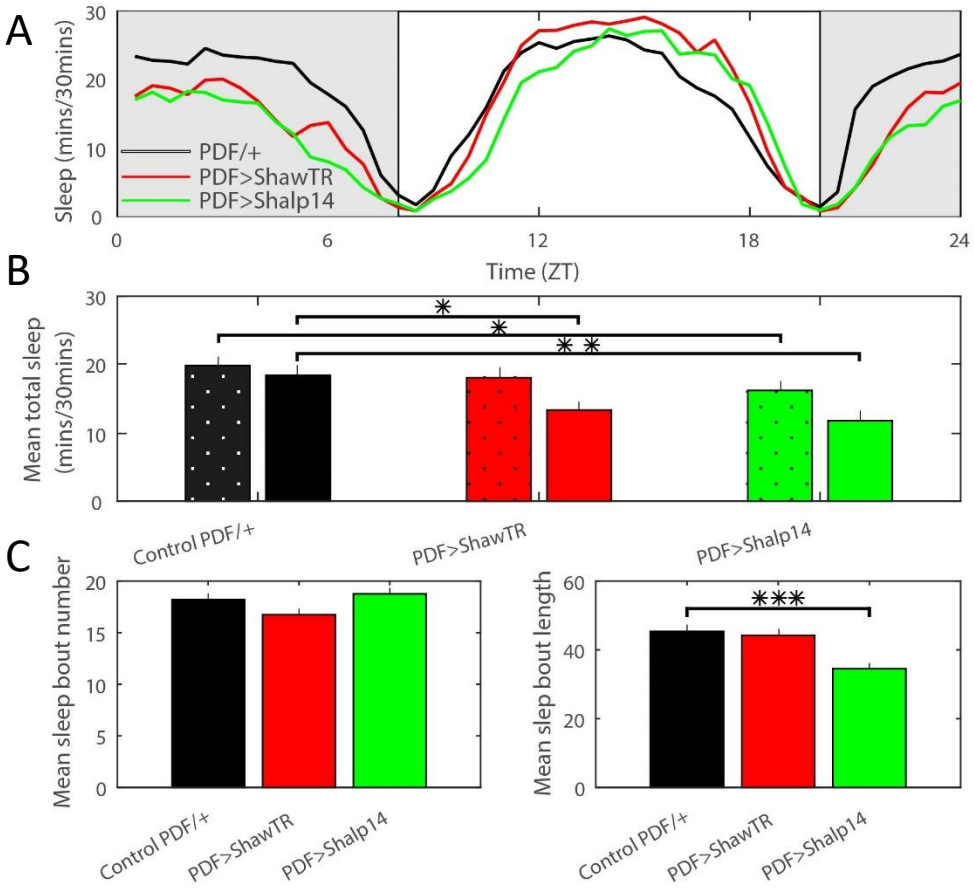

Figure 5.3 Sleep of Shaw and Shal mutant flies.

A) Mean sleep trace for control flies (n=16) and flies expressing either Shaw (n=14) or Shal (n=21) dominant negative transgenes in the LNvs. **B)** The mean day (dotted bar) and night (plain bar) sleep over the five days of LD. There are decreases in night-time sleep of both Shaw (p=0.0349) and Shal (p=0.0062) flies and a decrease in day-time sleep of Shal flies (p=0.0418). **C)** Mean sleep bout number and length. Mean bout length is decreased in Shal flies (p<0.0001).

5.2.2 Effects of *CLK* or *CYC* dominant negative transgenes in the LNvs on circadian locomotor behaviour

The molecular clock of the LNvs was also stopped by expression of the dominant negative transgenes for the core clock proteins *CLK* and *CYC* (Figure 5.4). In LD conditions (Figure 5.4A & B), the flies maintained rhythmic activity with noticeable morning and evening peaks, although the activity was increased especially in the *CYC* mutant. In DD conditions (Figure 5.4C), the rhythmicity of the *CLK* and *CYC* dominant negative flies was abolished, and the activity levels were consistently higher compared to controls.

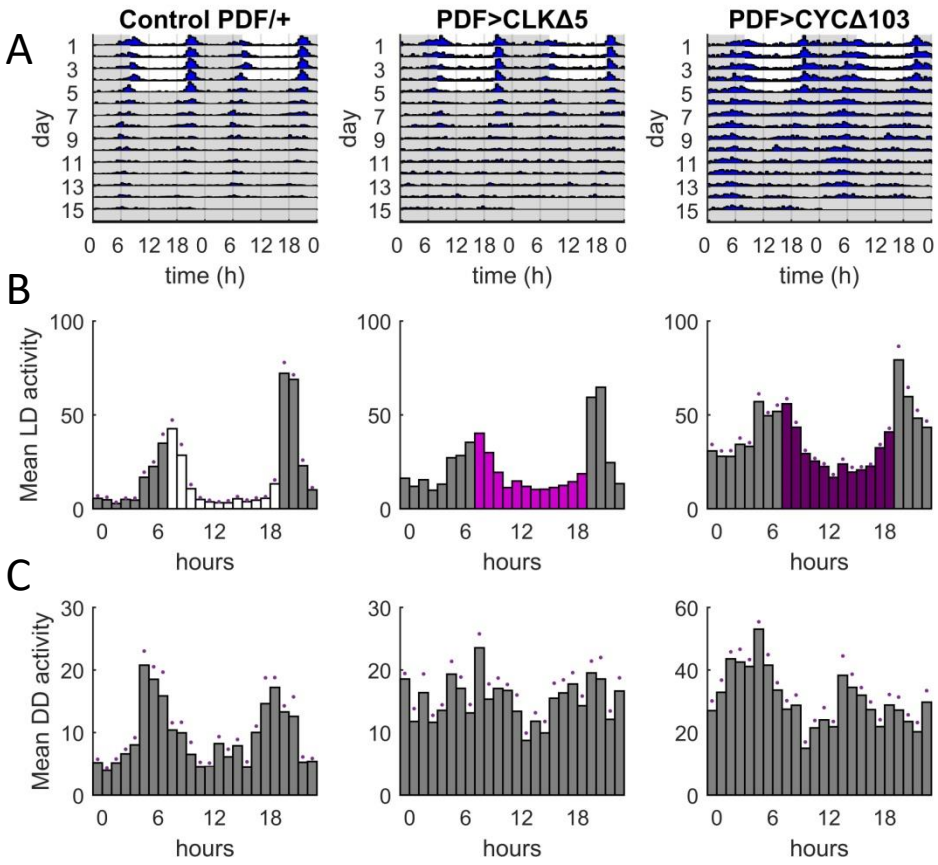

Figure 5.4 Activity patterns of CLOCK and CYCLE mutant flies.

A) Mean actograms of control flies (n=21) and flies expressing either *CLK* (n=24) or *CYC* (n=27) dominant negative transgenes. Activity is double-plotted to demonstrate rhythms more clearly; this means that each day is plotted twice, i.e. the first row is days 1 and 2 and the second row is days 2 and 3. **B)** Mean histograms over the five days of LD. **C)** Mean histograms between the third and fifth days of DD. Activity was measured in beam crosses per 30 min bin. Grey shading indicates the dark phase, white or colour shading indicates the light phase. Dots indicate SEM.

The activity counts (Figure 5.5) showed similar increases as Shaw and Shal mutants. The total day and night activities were significantly increased in the *CYC* mutants (Figure 5.5A). The *CLK* mutants showed a small but not significant increase in both day and night activity, although this was not significant. The strength of rhythms was significantly reduced in both *CLK* and *CYC* mutants as shown by RS values. This was also reflected in the absence of any strongly or even weakly rhythmic flies in either treatment group (Figure 5.5B).

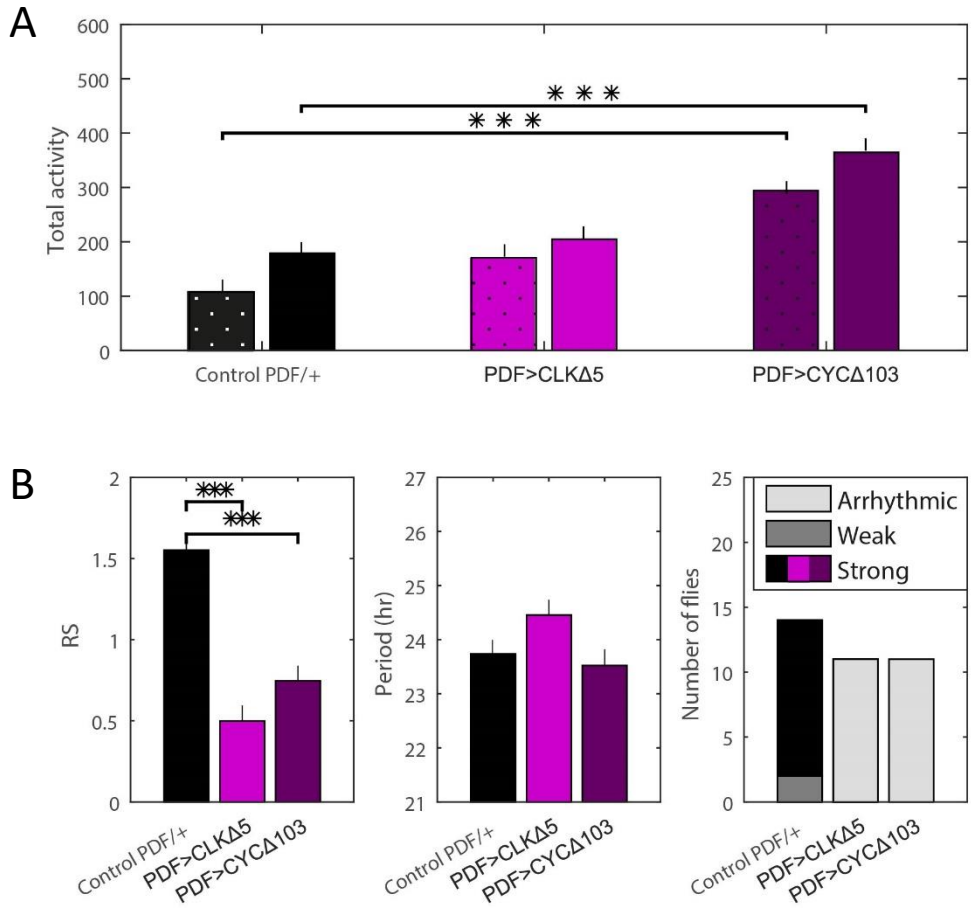

Figure 5.5 Activity and rhythmicity of CLOCK and CYCLE mutant flies.

A) Mean total activity in the day (dotted bar) and the night (plain bar) for control flies (n=21), and flies expressing *CLK* (n=24) or *CYC* (n=27) dominant negative transgenes. Day (p-0.0002) and night (p=0.0008) activity are increased in *CYC* mutants but not in *CLK* mutant (day: p=0.2567, night: p=0.5725). **B)** The mean RS and period of DD activity rhythms and proportion of flies displaying strong or weak rhythms or arrhythmicity. Rhythm strength is reduced in both *CLK* (p<0.0001) and *CYC* mutants (p<0.0001) as shown by RS values.

The effect of the molecular clock dominant negative transgenes on sleep (Figure 5.6) was again similar to that seen with the Shaw and Shal dominant negatives. The sleep trace (Figure 5.6A) and quantification (Figure 5.6B) showed significant decreases in both day and night sleep for both *CLK* and *CYC* dominant negative transgenes. Again, the number of sleep bouts was unaffected, but the mean length of sleep bouts was decreased in both *CLK* and *CYC* mutants.

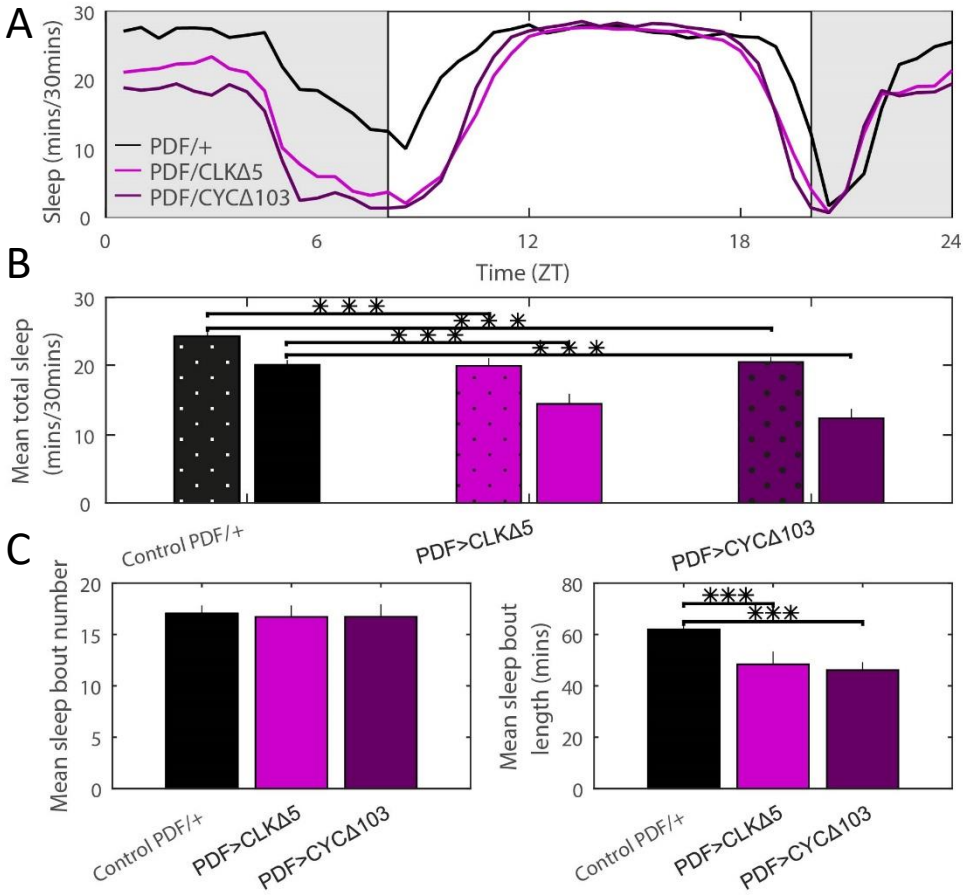

Figure 5.6 Sleep in *clock* and *cycle* mutant flies.

A) Mean sleep trace for control flies (n=21) and flies expressing either *CLK* (n=24) or *CYC* (n=27) dominant negative transgenes. **B)** The mean day (dotted bar) and night (plain bar) sleep over the five days of LD. Sleep is reduced in both *CLK* (day: $p<0.0001$, night: $p<0.0001$) and *CYC* mutants (day: $p=0.0002$, night: $p<0.0001$). **C)** Mean sleep bout number and length. Bout length is decreased in both *CLK* ($p<0.0001$) and *CYC* mutants ($p<0.0001$).

5.2.3 Effects of Shaw or Shal dominant negative transgenes in all clock neurons on circadian locomotor behaviour

Expression of Shaw and Shal dominant negative transgenes in all clock neurons through the TIM driver resulted in a similar pattern of activity changes (Figure 5.7). Under LD conditions (Figure 5.7A & B), the morning and evening peaks remained prominent with increased activity in the dark phase. Under DD conditions (Figure 5.7C), there was not much visible change to the pattern of activity compared with controls.

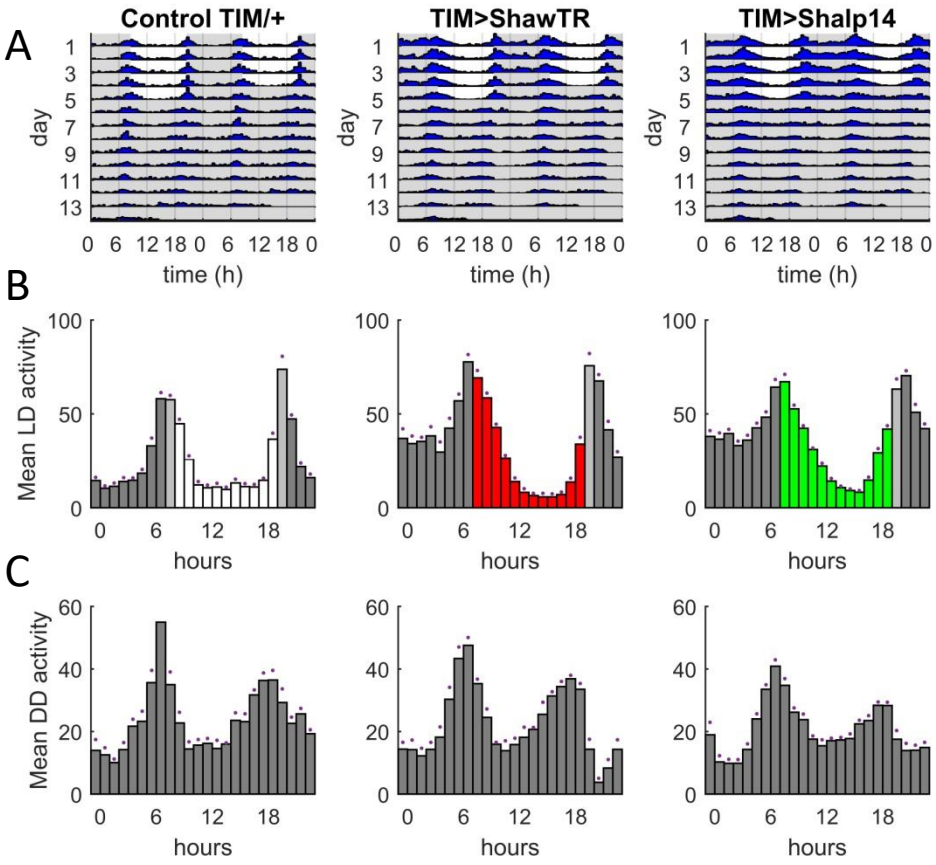

Figure 5.7 Activity patterns of Shaw and Shal dominant negative transgenes in all clock neurons.

A) Mean actograms of control flies (n=21) and flies expressing either Shaw (n=15) or Shal (n=25) dominant negative transgenes with the *tim* driver for all clock neurons. **B)** Mean histograms over the five days of LD. **C)** Mean histograms between the third and fifth days of DD. Activity was measured in beam crosses per 30 min bin. Grey shading indicates the dark phase, white or colour shading indicates the light phase. Dots indicate SEM.

As indicated by the histograms, the activity of the flies was altered (Figure 5.8). The total night activity was significantly increased for both Shaw and Shal dominant negatives with a small increase in the day activity of Shal dominant negative flies. Similar to the expression of these transgenes in PDF neurons, the rhythmicity was only slightly reduced in Shal dominant negative flies but otherwise the rhythm strength and proportion of rhythmic flies was unaffected (Figure 5.8B).

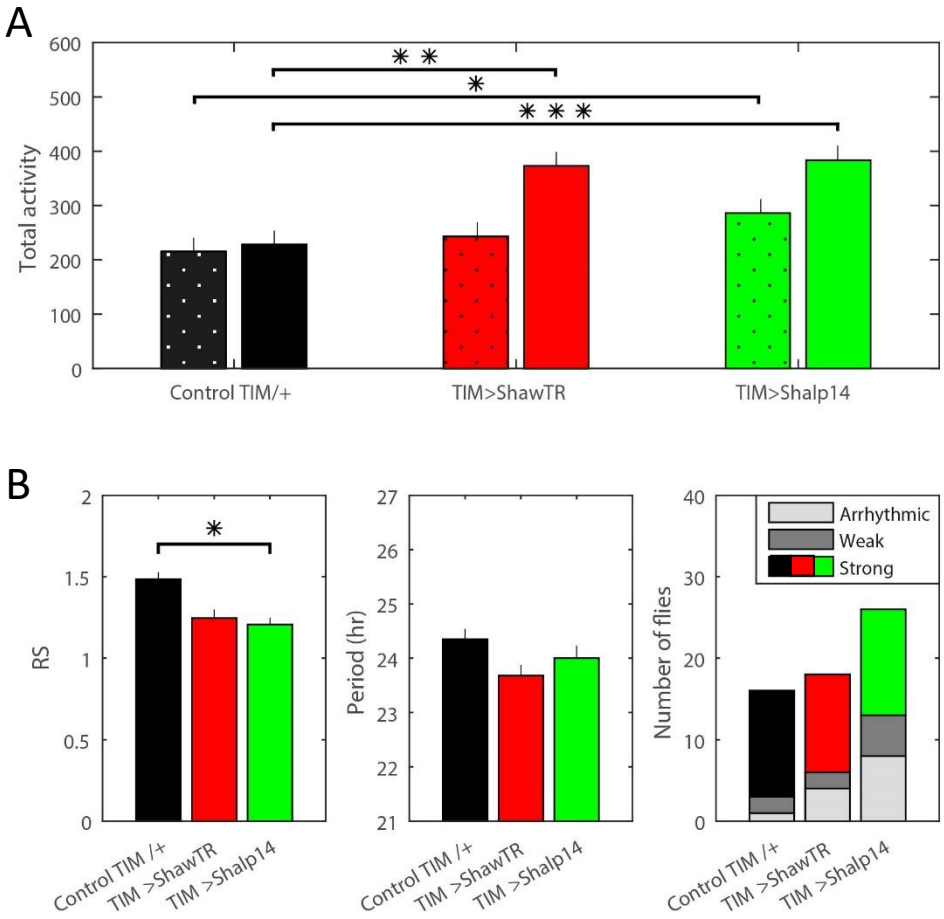

Figure 5.8 Activity and rhythmicity of Shaw and Shal dominant negative transgenes in all clock neurons.

A) Mean total activity in the day (dotted bar) and the night (plain bar) for control flies (n=21), and flies expressing Shaw (n=15) or Shal (n=25) dominant negative transgenes in all clock neurons. Night activity is increased in Shaw (p=0.0011) and Shal flies (p<0.0001). Day activity is increased in Shal flies (p=0.0315). **B)** The mean RS and period of DD activity rhythms and proportion of flies displaying strong or weak rhythms or arrhythmicity. RS is reduced in Shal flies (p=0.0423).

The sleep phenotype (Figure 5.9) reiterated the effect of the electrical manipulation with decreases in both day and night sleep in the Shaw and Shal flies. The effect on sleep bouts was more complex (Figure 5.9C). While the mean number of bouts was decreased in both Shaw and Shal flies, the mean length of bouts was increased in Shaw flies but decreased in Shal flies.

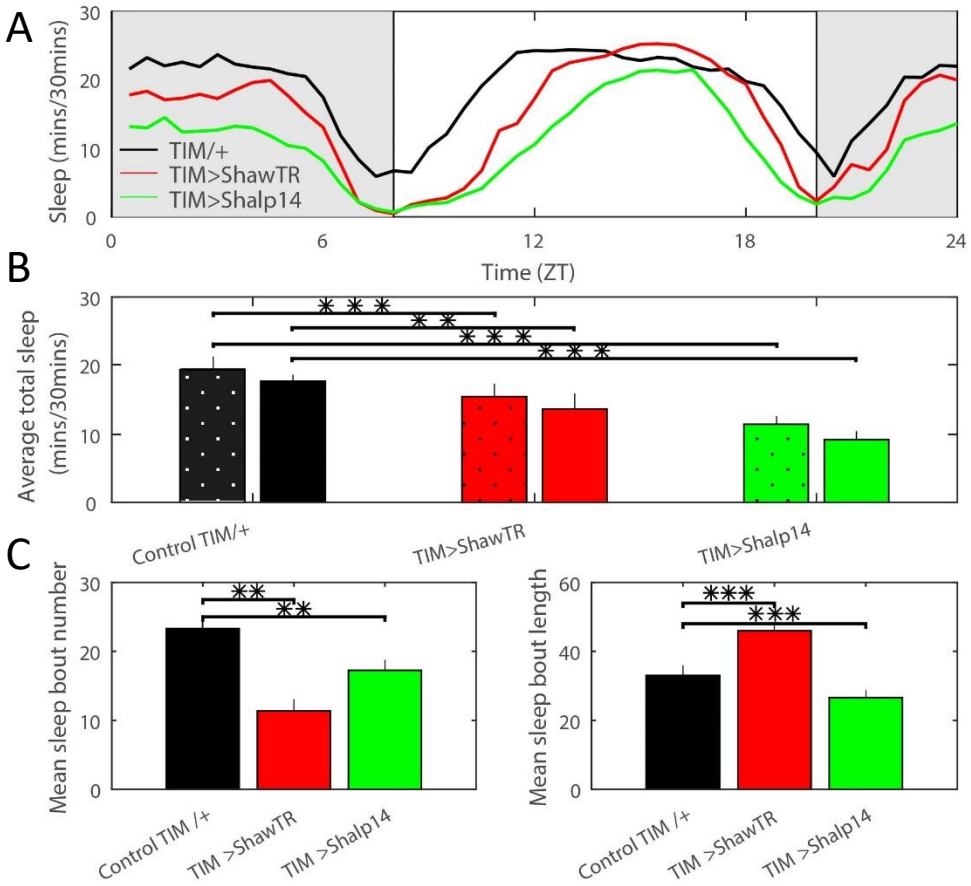

Figure 5.9 Sleep of Shaw and Shal dominant negative transgenes in all clock neurons.

A) Mean sleep trace for control flies (n=21) and flies expressing either Shaw (n=15) or Shal (n=25) dominant negative transgenes in all clock neurons. **B)** The mean day (dotted bar) and night (plain bar) sleep over the five days of LD. Day and night sleep are reduced in Shaw (day: $p<0.0001$, night: $p=0.0038$) and Shal flies (day: $p<0.0001$, night: $p<0.0001$). **C)** Mean sleep bout number and length. Sleep bout number is reduced (Shaw: $p=0.0059$, Shal: $p=0.0017$) and bout length is altered (Shaw: $p<0.0001$, Shal: $p<0.0001$).

5.2.4 Longevity of ion channel and molecular clock manipulations

Expression of the Shaw, Shal, CLK, and CYC dominant negative transgenes not only had an effect on behaviour, but also on overall lifespan. While the removal of Shaker and Shab current by *RNAi* (Figure 5.10A) did not affect longevity, expression of Shaw, Shal, CLK, or CYC dominant negative transgenes resulted in a similar reduction of lifespan.

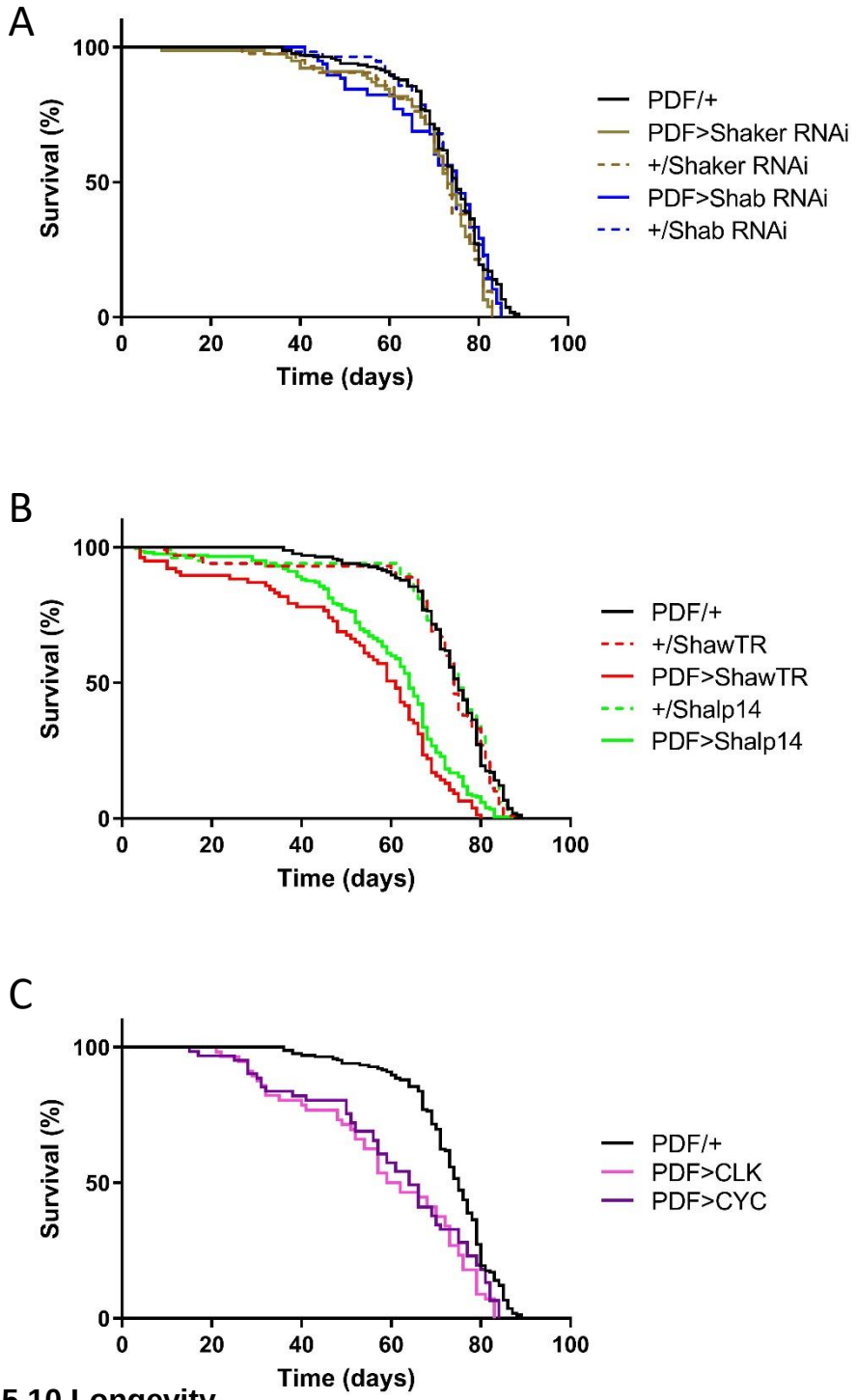

Figure 5.10 Longevity

A) Expression of Shaker (n=77, p=0.1888) or Shab *RNAi* (n=96, p=0.4140) under a PDF driver showed no significant change in longevity compared to undriven Shaker RNAi (n=42) or Shab RNAi (n=56) or PDF/+ controls (n=165). **B)** Expression of Shaw (n=77, p<0.0001) and Shal (n=202, p<0.0001) dominant negative transgenes showed significant decreases in longevity compared with undriven Shaw (n=100), undriven Shal (n=100) or PDF controls (n=165). **C)** Expression of *CYC* (n=61, p=0.0001) and *CLK* (n=56, p<0.0001) dominant negative transgenes showed a decrease in longevity compared with PDF controls (n=165). The decrease is similar between Shaw and Shal dominant negatives and *CYC* and *CLK* dominant negatives.

5.3 Discussion

5.3.1 Effects of Shaw and Shal manipulation

The results presented here indicate a clear effect of manipulating Shaw and Shal in the LNvs (Figures 5.1-3). Namely, an increase in activity and concurrent decrease in sleep without significant change to the rhythmicity of the flies.

A previous study looking at the effects of Shaw (Hodge and Stanewsky 2008) found that expression of the Shaw dominant negative transgene in either all clock neurons or the specifically the LNvs did not lead to drastic changes in rhythmicity, as seen in this thesis. In addition, expression of Shaw *RNAi* within the LNvs decreased sleep significantly and suppressed initiation of the first night-time sleep bout without affecting rhythmicity (Parisky et al. 2008). This is consistent with the finding that expression of the Shaw dominant negative transgene causes a wake-promoting effect. In a similar manner, a recent study using the Shal dominant negative transgene in the LNvs also saw reduced night-time sleep and a wake-promoting effect consistent with the results presented here (Feng et al. 2018).

Hyper-excitation of the LNvs themselves results in increased activity. Excitation by expression of the sodium channel NaChBac resulted in an increase of both day-time and night-time sleep (Sheeba et al. 2008). Similar effects were seen when other drivers were used to target the LNvs, notably the *c929-GAL4* that targets the large LNvs while excluding the small LNvs. Likewise, *RNAi* knock-down of the $GABA_A$ receptor, *resistant to dieldrin* (Rdl), in PDF neurons caused a reduction in sleep (Chung et al. 2009; Parisky et al. 2008). Interestingly, a *Drosophila* model of Parkinson's Disease showed that *PINK1* and *parkin* mutants display elevated locomotor behaviour levels along with hyper-excited LNv activity (Julienne et al. 2017). Together, these results indicate that the l-LNvs are wake-promoting neurons and that altering their activity increases activity and decreases sleep. This agrees with the data presented above where expression of Shaw dominant negative in

either LNvs or all clock neurons leads to increasing locomotor activity. Expression of the Shal dominant negative has been shown to cause a shortened latency to action potential firing and a lower threshold for repetitive firing (Ping et al. 2011; Ping et al. 2015), suggesting that this works to affect behavioural rhythms in a similar manner to the Shaw dominant negative.

In the mammalian SCN, it has been reported that the Shaw homologues Kv3.1b and Kv3.2 are important in the daily rhythm of firing rate of clock neurons (Itri et al. 2005). Here, the fast-delayed rectifier current associated with Kv3 exhibits a diurnal rhythm that is highest during the day, much like Shaw in *Drosophila*. This current is also vital to daily rhythms of motor behaviour as mice lacking both Kv3.1 and Kv3.2 have severely disrupted rhythms of wheel-running behaviour (Kudo et al. 2011). Additionally, the Shal homologues Kv4.1 and Kv4.2 were shown to be associated with an A-type current that again exhibits a diurnal rhythm in the SCN (Itri et al. 2010). Here, Kv4 regulates neuronal firing (Granados-Fuentes et al. 2012; Granados-Fuentes et al. 2015) and knock-down of Kv4.1 increased neuronal firing rates and affected circadian rhythms shortening the period (Hermanstyne et al. 2017). Together, this indicates that there may be some conservation between function of Shaw and Shal in the *Drosophila* clock neurons and Kv3 and Kv4 in the mammalian SCN.

5.3.2 Effects of *CLK* and *CYC* manipulation

The effect of the *CLK* and *CYC* dominant negative transgenes (Figures 5.4-6) mirrors that of the Shaw and Shal effects in the LNvs (Figures 5.1-3) in the increase of activity and decrease of sleep in LD. However, there is the additional effect of the loss of behavioural rhythms in DD shown by the drastic reduction in rhythm strength and loss of strongly rhythmic flies. It has been shown that expression of the *CLK* and *CYC* dominant negative transgenes in the LNvs, and more generally in all clock neurons, abolishes behavioural rhythms in constant darkness (Tanoue et al. 2004).

Whereas the l-LNvs have an established role in promoting wakefulness as described previously, the s-LNvs are more associated with driving rhythmicity in constant conditions. The s-LNvs exhibit robust rhythms of molecular clock components during constant darkness (Grima et al. 2004; Stoleru et al. 2004) and manipulating the period of molecular rhythms in the s-LNvs will cause similar changes in other clock neurons (Shafer and Yao 2014). This indicates that, in DD, the molecular clock of the s-LNvs is important in maintaining rhythmicity. This means that the removal of a functional molecular clock by *CLK* and *CYC* dominant negative transgenes would result in a loss of this ability and hence arrhythmicity in constant darkness, as is observed. This is similar to *pdf* null mutations and ablations of LNv neurons, where rhythmicity in DD is lost (Renn et al. 1999). Hence, loss of LNv communication by PDF reflects that of loss of the molecular clock. Therefore, the rhythmicity effect of the *CLK* and *CYC* mutants is likely due to additional effects on the molecular clock of the s-LNvs.

However, a potential confounding factor is that it has been shown that there is a developmental requirement for CYC in PDF neurons (Goda et al. 2011). In *CYC* mutants, the arborisations are not fully developed and are often largely missing. The neuro-anatomical consequences of blocking CYC (and CLK) function could be changes in Shaw and Shal current by virtue of changing LNv morphology rather than a circadian clock-specific effect. To address, this it would be interesting to investigate the terminal morphology in *CYC* and *CLK* mutants through immunohistochemistry. For example, staining of PDF in the dorsal terminals along with staining of circadian clock components in both controls and *CYC* or *CLK* mutants would show whether there is significant change to the clock or the PDF terminal morphology.

The effect of expressing Shaw or Shal dominant negative transgenes was seen to be an increase in activity without major changes to rhythmicity. Therefore, it is likely that the removal of Shaw or Shal current affects the function of the l-LNvs through changes to excitability, whereas the molecular clock of the s-LNvs and their ability to drive rhythmicity is not significantly affected. This suggests that, at least in the s-LNvs, the Shaw and Shal

channels themselves do not have a role in regulating the molecular clock. However, it may be that there is a regulatory role for Shaw and Shal, but that the removal of one of these channels is not sufficient to create an effect. The continued cycling of the other channel may be enough to mask any effect on rhythmicity, and thus only expression of both Shaw and Shal dominant negative transgenes together would reveal this effect.

5.3.3 Wider effects in the clock using the *tim*-GAL4 driver

The manipulation of Shaw and Shal throughout all clock neurons with the *tim-GAL4* driver (Figures 5.7-9) shows a broadly similar effect seen to that with the *PDF-GAL4* driver. The effect in increasing in activity with no major effect on rhythmicity relates to the role of Shaw and Shal in the LNvs as discussed above. However, when expressing Shaw or Shal dominant negative transgenes in all clock neurons there is the additional effect on sleep bouts (Figure 5.9). While sleep bout number is decreased for both Shaw and Shal, the effect on sleep bout length is different. This indicates that expression of both Shaw and Shal elsewhere in the clock neurons may be important for sleep regulation. However, these channels may be having divergent effects in different sub-groups.

A group of dorsal clock neurons, the DN1s, project to output cells in the pars intercerebralis (PI) that are associated with activity rhythms (Cavanaugh et al. 2014). These PI neurons receive time information from the clock circuitry (Cavey et al. 2016) and secrete DH44, which is a regulator of activity rhythms (Cavanaugh et al. 2014). Also, Shaw has been observed to be expressed in the dorsal clock neurons including the DN1s (Hodge and Stanewsky 2008). Therefore, the inclusion of the DN1s with the *tim-GAL4* driver may be the source of the additional effects of Shaw and Shal disruption on sleep regulation.

5.3.4 Longevity

In terms of the longevity data shown above (Figure 5.10), these data are somewhat surprising given the scope of the manipulation. While the expression of Shaker and Shab *RNAi* in the LNvs does not affect lifespan, the expression of either Shaw or Shal or the molecular clock *CLK* or *CYC* dominant negative transgenes does reduce lifespan. These manipulations target only a small number of neurons in the *Drosophila* brain, and yet affect a fairly drastic influence on the overall longevity of the animal.

Shal has been implicated in *Drosophila* longevity previously (Ping et al. 2015) as expression of the Shal dominant negative driven by *elav-GAL4* significantly decreased longevity. The longevity deficit reported is more severe than that seen here as median lifespan was reduced by roughly five weeks rather than the roughly two weeks observed in this thesis. However, the expression of Shal dominant negative throughout all neurons with *elav-GAL4* is a more drastic manipulation than the more restricted *PDF-GAL4* that only targets 16 neurons. Nevertheless, this suggests that Shal expression in the *Drosophila* brain is linked to longevity and may be important in multiple brain regions due to the different severity of deficits between *PDF-GAL4* and *elav-GAL4* expression.

The similarity between the effects of the Kv channel and molecular clock transgenes indicates a possible cause of the PDF effect on lifespan is disruption to the molecular clock affecting circadian rhythmicity. Yet, it has previously been shown (Hodge and Stanewsky 2008) that expression of the Shaw dominant negative transgene in the LNvs by the driver *PDF-GAL4* does not affect rhythmic accumulation of PDF in the dorsal terminals. The case may be that there is a concurrent change in PDF release and accumulation that means that accumulation appears similar to the wild-type.

One possibility is that release of PDF is not affected, but release of a different transmitter is. It has been previously shown (Yasuyama and Meinertzhagen 2010) that the projections of the LNvs hold both dense-core vesicles containing PDF and small clear vesicles. The transmitter within the small clear vesicles in not known and could feasibly be involved in this lifespan effect.

Deficits in longevity have also been observed with changes in the molecular clock. In flies lacking functional CLK, CYC, or TIM the lifespan was reduced by roughly 15% (Vaccaro et al. 2017). Mutation in CYC was also shown to be related to a shortened lifespan alongside decreased rest in males (Hendricks et al. 2003) and it has also been reported that sleep deprivation in *CYC* mutants past 10 hours causes mortality in the flies (Shaw et al. 2002). This suggests that the loss of sleep seen in all manipulations above may be at least part of the underlying cause of increased mortality.

The fact that the *PDF-GAL4* driver was used in this thesis raises another potential explanation. In addition to the central LNv clock neurons, PDF is expressed in a small number of neurons in the abdominal ganglion (AbPdf neurons), a part of the *Drosophila* ventral nerve chord (Shafer and Yao 2014). These AbPdf neurons project to the hindgut (Nässel et al. 1993) and serve as strong candidates of circulating PDF (Persson et al. 2001). These neurons do not express the core molecular clock genes and are thus not strictly clock neurons. They are also not required for normal circadian locomotor behaviour (Shafer and Yao 2014). However, circulating PDF can adjust the phase of the molecular clock in peripheral sites of pheromone production (Shafer and Taghert 2009). Therefore, these AbPdf neurons could be affecting peripheral clocks or other tissues to create the lifespan effect observed. Nevertheless, very little is known about the AbPdf neurons or the function and effects of circulating PDF levels. Other neurons in the abdominal ganglion express other neuropeptides such as CCAP or juvenile hormone that may be having an effect (Santos et al. 2008). Future studies could target the AbPdf neurons through the driver *Dot-GAL4* to investigate

whether specific manipulation of these neurons recapitulates the effect of *PDF-GAL4* expression of the dominant negative transgenes.

In conclusion, removal of Shaw or Shal current by dominant negative transgenes causes changes in circadian locomotor behaviour consistent with hyperexcitation of the l-LNvs without substantial effect on the rhythmicity of the s-LNvs. In addition, this disruption of Shaw or Shal current in the LNvs has real consequences for the health of the animal as seen by decreases in longevity. This reinforces the concept of Shaw and Shal rhythms in the LNvs being important to the proper functioning of the circadian clock network overall.

Chapter 6 – The Kv9 model of essential tremor

This chapter provides introduction to the neurological condition of essential tremor (ET) in section 6.1.1-3 as well as a previous genetic study into a family of ET patients in section 6.1.4. This study identified a mutation in the human Kv9 channel; section 6.2 outlines the results of experiments investigating the function and consequences of this mutation. The methods used are a combination of those presented previously (see Chapter 2 for more details). Much of the results in this chapter have been previously published (Smith et al. 2018) and are discussed in section 6.3.

6.1 Introduction

6.1.1 Essential tremor

Essential tremor (ET) is a neurological condition characterised by uncontrollable shaking, or 'tremors', of different parts of the body, most commonly the hands or arms. This tremor is distinct from other forms of tremor such as in Parkinson's disease as it is categorised as an 'action' or 'kinetic' tremor, which means that the tremor intensifies with use of the affected muscles whereas the 'resting' tremor of Parkinson's is more notable when at rest (Algarni and Fasano 2018). However, this can be complicated by the fact that rest tremor can also be present in as much as 30% of ET patients (Rajput et al. 2004; Cohen et al. 20003), often presenting later on in the course of the disease.

The term 'essential tremor' has been in use throughout the late 19th and 20th centuries (Louis et al. 2008) but was more firmly established in the mid-20th century (Critchley 1949) to refer to a slowly progressive action tremor that was not associated with any known cause – the term 'essential' is more generally used to describe idiopathic conditions such as essential

hypertension. Indeed, the underlying causes of ET remain unclear. Many cases seem to be familial and so suggest a strong genetic component (Bain et al. 1994; Deng et al. 2007) although environmental causes, such as the toxin harmaline or heavy metals such as mercury and lead, have also been suggested to play a role (Louis 2001). A prominent model of ET pathophysiology posits that the tremor is the result of dysfunction in the inferior olivary nucleus causing rhythmic firing of neurons (Handforth 2012). However, recent studies have proposed that changes in the Purkinje cells themselves and in altered GABA tone (Louis et al. 2014). *Drosophila* themselves do not have an analogous structure to the inferior olivary nucleus controlling motor learning; the main structure for learning in fruit flies is the mushroom bodies, however these are mostly concerned with olfactory learning.

ET is one of the most common neurological diseases; it is thought to affect an estimated 7 million individuals in the US alone (Louis and Ferreira 2010) with an estimated prevalence of 5% in individuals over 65 years old (Deuschl et al. 2015). However, ‘essential tremor’ is considered more of an umbrella term encapsulating symptomatically similar conditions (Marsden 1984; Espay et al. 2017; Hopfner and Deuschl 2018). Nevertheless, it represents a significant burden on many individuals and is therefore an active area of research.

Although ET is classically considered as a monosymptomatic disease, there is a growing appreciation for non-tremor symptoms of ET. In 2001, it was reported that a group of ET patients had deficits in verbal fluency, verbal memory, and working memory (Lombardi et al. 2001). A separate study also found a deficit in attentional and conceptual thinking (Gasparini et al. 2001). In subsequent years it has become apparent that ET patients also experience higher rates of mild cognitive impairment (Sinoff and Badarny 2014), affective disorders such as depression (Fabbrini et al. 2012; Louis, Benito-Leon and Bermejo-Pareja 2007), gait abnormalities (Louis et al. 2012; Roemmich et al. 2013; Lim et al. 2005), and sleep disturbances (Chandran et al. 2012; Sengul et al. 2015).

6.1.2 Current treatments for ET

Existing treatments aim primarily to alleviate difficulties arising from the tremor itself. Certain beta-blockers such as propranolol, which inhibit β-adrenergic receptors, have been indicated for ET although others such as atenolol and pindolol are not effective (Abboud et al. 2011). Propranolol can improve tremor symptoms in around half of patients (Lyons et al. 2003; Hedera et al. 2013). Another drug in common use is primidone, which is an antiepileptic drug with structural similarity to the barbiturates. The effectiveness of primidone in alleviating symptoms is similar to propranolol and together these two drugs form the first-line of treatment. Second-line pharmacological treatments include other antiepileptic drugs such as topiramate, gabapentin, and levetiracetam.

Pharmacologically refractory tremor can also be treated with more invasive techniques. Surgery and subsequent lesioning of the ventral intermediate nucleus of the thalamus has seen some use in treating more severe forms of ET (Kluger et al. 2009). However, deep brain stimulation remains the preferred method for modulating neuronal activity (Benabid et al. 1991; Lorenz and Deuschl 2007). Problems associated with this approach have been the surgical risks of infection and brain haemorrhage alongside difficulties in limiting the electrical stimulation to a specific area, especially when long-term stimulation leads to a reduction in efficacy and so requires increasing stimulation. Possible non-invasive forms of therapy use either highly focussed gamma radiation, termed gamma-knife thalamotomies (Witjas et al. 2015), and focused ultrasound (Fishman and Frenkel 2017). These therapies may avoid some complications associated with surgical invasion but are still in early stages of development.

6.1.3 Research into ET

Despite the apparent strong genetic component of ET, relatively few genes have been identified as contributing to susceptibility. However, previous

studies employing genome-wide linkage scans have indicated a few possibilities associated with certain families of familial ET. A scan in Icelandic families identified a locus on chromosome 3q13 (Gulcher et al. 1997) whilst two scans in North American families indicated loci on chromosomes 2p22-p25 and 6p23 (Higgins et al. 1997; Shatunov et al. 2006). Whilst the locus on chromosome 3q13 has been suggested to involve the dopamine D3 receptor (Lucotte et al. 2006), the pathophysiology of these loci is largely unclear. Using a whole-exome sequencing approach a separate study identified the *fused in sarcoma/translated in liposarcoma* (FUS/TLS) gene located on chromosome 16p11 (Merner et al. 2012), but the pathogenicity of this rare variant is unknown. This last finding was somewhat surprising as FUS/TLS mutations are implicated in amyotrophic lateral sclerosis in some of the mutations identified (Macerollo and Bhatia 2013). Nonetheless, this diversity of loci associated with ET serves to underline the heterogeneity of the condition and also the depth of research needed to understand the pathophysiology and develop appropriate treatments.

Animal models of ET largely follow one of three approaches: (1) a pharmacological model using harmaline; (2) lesions of motor-related brain structures; (3) genetic disruption of particular genes (for a full review see Handforth, 2016). The harmaline model is the most widely used and studied model of ET. Harmaline is an alkaloid found in the Syrian rue plant and has effects as an inhibitor of acetylcholinesterase and monoamine oxidase A (Moloudizargari et al. 2013). It has been found to produce 8-16 Hz tremors in various animals that is kinetic in the same manner as ET (Handforth 2012). The tremor is caused by rhythmic firing of cerebellar circuitry (de Montigny and Lamarre 1973), potentially consistent with human ET. However, this tremor in mice often involves multiple, if not all, limbs and lasts only several hours after injection. Repetitive administration of harmaline also results in tolerance and a gradual loss of the tremor after several treatments (Lutes et al. 1988; Miwa 2007).

Lesions of the deep cerebellar nuclei in monkeys produce an action tremor of roughly 3-7 Hz primarily affecting the upper extremities (Goldberger and

Growden 1971). Rats and cats irradiated soon after birth also develop ataxia and tremor (Anderson and Stromberg 1977). However, damage in these models is often fairly general across the cerebellum and likely represents ataxic tremor that is of limited relevance to ET.

Genetic alteration of GABA control has a number of interesting effects. Mice with a deficiency in GABA transporter type 1 (GAT1) show a tremor, although it is of high frequency at 25-32 Hz (Chiu 2005). Gain of function of the $GABA_A$ receptor is associated with a postural tremor (Homanics et al. 2005). But most interesting is that $GABA_A$ receptor α1 subunit knock-out mice show life-long tremor occurring during actions at a frequency of 19-24 Hz (Kralic et al. 2005; Ogris et al. 2006). Nevertheless, the mice do not respond in exactly the same manner to certain drugs, such as diazepam, as humans and genetic analysis of ET patients failed to find significant association between ET and $GABA_A$ receptor α1 subunit variants (Deng et al. 2006).

6.1.4 New targets of research

A recent study performed whole-exome sequencing in 37 families with early-onset ET and an autosomal-dominant pattern of inheritance (Liu et al. 2016). In two of the independent families, variants of nitric oxide synthase 3 (NOS3) were found to co-segregate with the disease. Other important findings were heterozygous variants in hyaluronan and proteoglycan link protein 4 (HAPLN4) and in ubiquitin-specific protease 46 (USP46). NOS3 is highly expressed in various neurons within the cerebellum (Abbott and Nahm 2004) and has been found to be involved in pathogenesis of Alzheimer's disease and Parkinson's disease (de la Monte, Lu, et al. 2000; de la Monte, Sohn, et al. 2000). HAPLN4 (also known as brain link 2 - BRAL2) and USP46 are also known to be connected to GABAergic neurotransmission in the cerebellum (Bekku et al. 2012; Tomida et al. 2009).

A variant of the KCNS2 gene was also indicated in another family. KCNS2 shows high homology for the *Drosophila* Shab channel (Kv2 ortholog), and

indeed encodes another voltage-gated potassium channel termed Kv9.2. However, this channel is known as a 'silent' channel (Bocksteins 2016), which means that it does not form functional homo-tetramers but instead hetero-multimerises with Kv2 to form functional hetero-tetramers. These silent voltage-gated potassium channels (Kv5-6 and Kv8-9) associate only with Kv2 due to protein interactions (Bocksteins et al. 2014) and have been known to modulate the kinetics of the channel. For example, co-expression of Kv2.1 with Kv9 shifts the voltage-dependence of the channel to more hyperpolarised values (Salinas et al. 1997). The closely related Kv9.1 and Kv9.3 have been reported to, respectively, reduce and increase Kv2 current in heterologous expression studies, along with shifts in inactivation kinetics (Patel et al. 1997; Salinas et al. 1997; Richardson and Kaczmarek 2000).

The missense mutation converted the aspartate residue at position 379 to a glutamate residue (D379E) and was found to alter the structure of the Kv9.2 protein in *in silico* analysis (Liu et al. 2016); the substitution occurs in a highly conserved portion of the KCNS2 gene. A co-localisation between Kv9.2 channels and Kv2.1 and Kv2.2 channels has been observed in Purkinje cells of the cerebellum (Salinas et al. 1997) and dysfunction in the fly homologue of Kv2 (Shab) has been linked to abnormal neuronal activity in motor circuits (Engel and Wu 1992). Together, this study suggests an involvement of cerebellar signalling as has been suggested previously (Louis et al. 2014).

The gradual identification of genes and loci associated with ET have lent weight to the genetic heritability of the disease and suggested possible mechanistic insights. However, an understanding of how each of these gene variants contributes to the pathogenesis of ET is critical in moving the field forward. The KCNS2 mutation offers a particular opportunity for research as it is highly similar to, and can function through the use of, the *Drosophila* Shab channel. *Drosophila* do not themselves possess a Kv9 homologue and so introduction of either the wild-type or mutant human variants of the KCNS2 gene into the *Drosophila* genome can potentially produce a model of this form of ET.

6.2 Results

6.2.1 Electrophysiology of the *Drosophila* essential tremor model

The KCNS2 wild-type and mutant human subunits were introduced into the LNv clock neurons through the *GAL4/UAS* system (as *Drosophila* do not have a Kv9 homologue) and subsequently studied through the use of whole cell patch-clamp (for methods see Section 2.2, for other results see Chapter 3). The response of the LNvs to a standard depolarising pulse in voltage-clamp (Section 2.2.3) was recorded for each of the native Shab channel (*PDF/+*), the Shab channel with the human wild-type Kv9 channel (*PDF>hKv9.2*) and the Shab channel with the mutant Kv9 channel (*PDF>hKv9.2-D379E*) in the absence and presence of the toxin guangxitoxin (GxTX, Section 2.2.5); the difference between the absence and presence of GxTX is taken to be the current of Shab as detailed previously (Section 3.2.1).

The response of the native Shab channel was a non-inactivating current, activating above resting potential as described previously (Section 3.2.1) (Figure 6.1A). Upon introduction of the wild-type hKv9.2 channel (Figure 6.1A), the current becomes inactivating in contrast to the unaltered native Shab channel. This introduction of inactivation similarly occurs with the mutant hKv9.2-D379E channel (Figure 6.1A). Looking at the I-V relationship of each case (Figure 6.1B) shows that the peak current is not reduced by the Kv9 subunits but has potentially shifted to more negative voltages. Displaying the sustained current as a percentage of the peak current (Figure 6.1B right) shows that whereas the native Shab channel is particularly high (85.55%), the wild-type and mutant Kv9 channel reduces this percentage (39.25%). The mutant Kv9 channel is also more severe in this effect than the wild-type (30.48%).

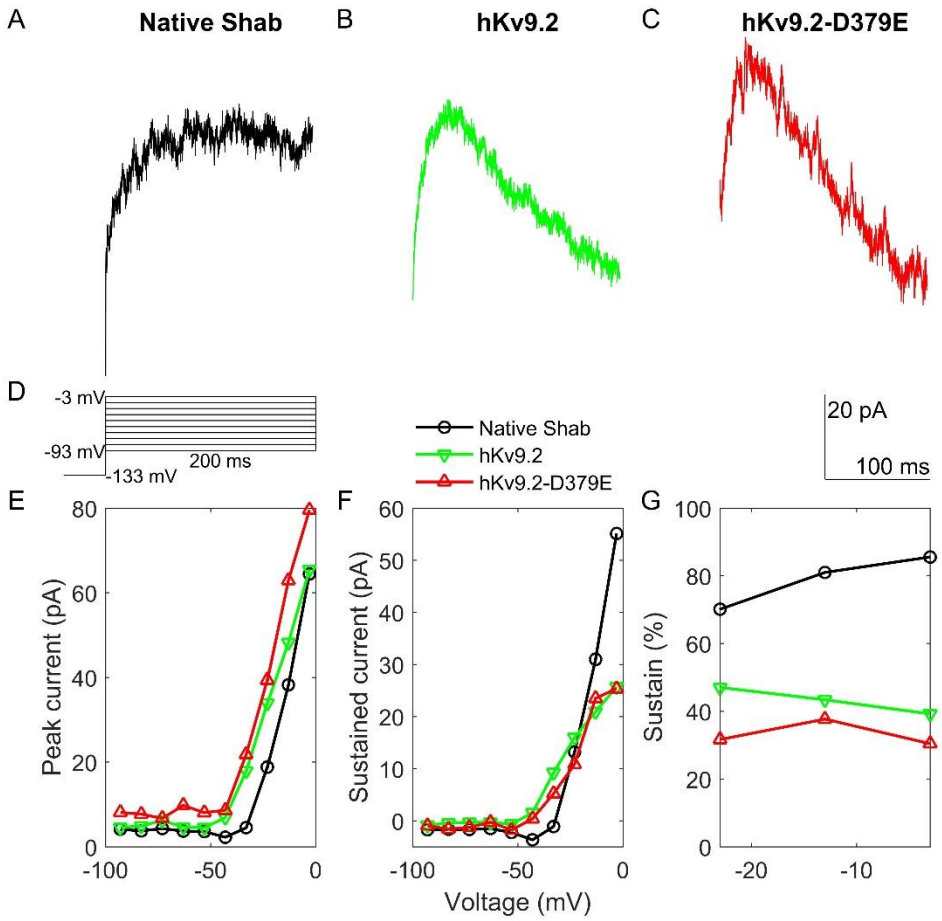

Figure 6.1 The Effect of Kv9 expression on Shab channel kinetics.

A-C) Mean voltage-clamp data of 200 ms depolarisation to -3 mV from -133 mV for the native Shab channel alone (A, n=5), and with human wild-type Kv9 (B, n=5) or human mutant Kv9 (C, n=5). The voltage-clamp protocol (D) is the same as in Figure 3.2C. **E-F)** I-V relationships for peak current (E) and sustained current (F) for each genotype. **G)** The sustained current divided by the peak current gives the sustain percentage, indicating the level of inactivation. Sustained current is measured at the end of the depolarising step (after 180 – 200 ms of depolarisation).

The LNvs expressing the Kv9 subunits also show altered electrical activity in current-clamp consistent with the altered Shab channel currents. The l-LNvs normally show spontaneous action potentials at a frequency of 1-2 Hz depending on the time of day (Section 3.2.1), as is reflected in the controls (Figure 6.2A). When expressing the wild-type Kv9 channel (Figure 6.2B) this increases to around 3-4 Hz; this is somewhat consistent with current-clamp recordings with addition of GxTX to block Shab as detailed previously (Figure 3.5B). For the mutant channel this increases to around 7 Hz (Figure 6.2C), which is higher than control and also higher compared to the wild-type channel.

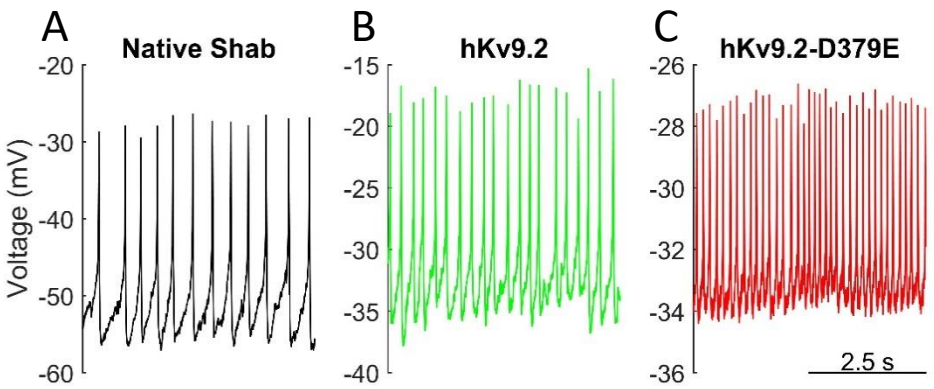

Figure 6.2 The Effect of Kv9 expression on l-LNv firing rate.

Representative 5s epochs of whole-cell current-clamp electrical activity, showing a control firing rate of roughly 2 Hz (A), a rate of roughly 3.5 Hz with the human wild-type Kv9 (B, p=0.0467), and a rate of roughly 7.5 Hz with the human mutant Kv9 (C, p=0.0016). The mutant Kv9 frequency is higher than wild-type Kv9 (p=0.0062).

6.2.2 Computational modelling of the *Drosophila* LNvs

Following a similar approach as previously used for modelling the LNvs (see Chapter 4), this electrophysiological data can be described by the Hodgkin-Huxley formalism (Section 4.1) to model the introduction of the wild-type or mutant Kv9 as a change to the Shab channel (Figure 6.3). The parameters obtained from the model fitting show quantitative differences consistent with the shapes of the channel kinetics. The Kv9 channel subunits both have a more negative voltage of activation (Table 6.1, activation V_h), indicating a shift of the channel activation to more negative voltages. The degree of inactivation is also more striking in the mutant than the wild-type as shown by the higher σ (Table 6.1, inactivation σ).

Using the hKv9.2 and hKv9.2-D379E current descriptions in the whole cell model generated previously (Section 4.2) shows how the simulated behaviour changes to reflect the inclusion of the Kv9 subunits. The experimental data (Figure 6.4A) are consistent with these model descriptions of whole cell activity (Figure 6.4B) showing increased firing rate of spontaneous action potentials. Analysis of the data (Figure 6.4C) shows no significant differences between the experimental data and the model for the controls, wild-type hKv9.2 channel, or the mutant hKv9.2-D379E channel.

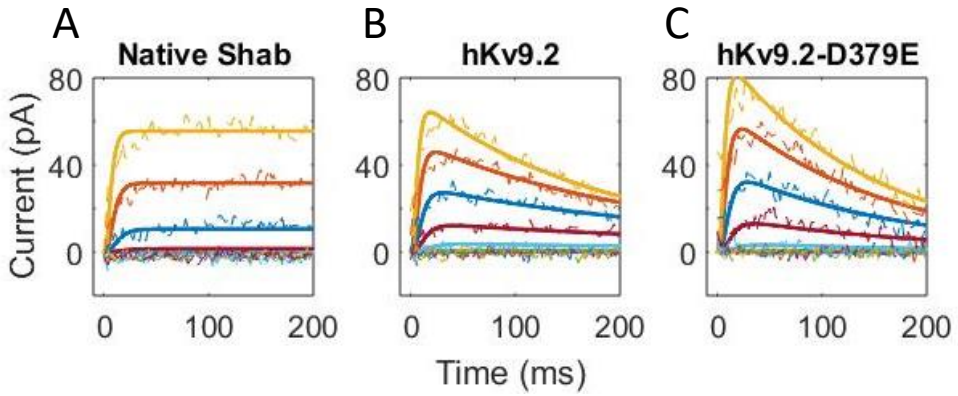

Figure 6.3 Fitting of Hodgkin-Huxley equations to form Kv9 subunit models.

Graphs of the fit between Hodgkin-Huxley equations 4.16 and 4.17 (solid lines) and experimental data (dotted lines) for the three conditions of control (A), human wild-type Kv9 (B), and human mutant Kv9 (C). Fits achieved in the same manner as Figure 4.1.

Activation	Shab (Kv2)	hKv9.2	hKv9.2-D379E
Vh (mV)	-29.69	-45.22	-43.56
K (mV^{-1})	10.49	12.18	14.02
Amp (s^{-1})	30.72	21.61	24.88
Vmax (mV)	-63.69	-73.08	-79.93
σ (mV^{-1})	28.54	38.62	40.84
Inactivation			
Vh (mV)	N/A	-119.05	-128.76
K (mV^{-1})	N/A	31.18	5.31
Amp (s^{-1})	N/A	134.87	131.97
Vmax (mV)	N/A	9.96	5.56
σ (mV^{-1})	N/A	45.19	108.03
Conductance (nS)	0.86	1.73	1.95

Table 6.1 Parameters obtained from fits of Kv9 subunit data.

Individuals parameters for activation and inactivation gate kinetics obtained for Shab (Kv2), human wild-type Kv9 (hKv9.2), and human mutant Kv9 (hKv9.2-D379E). Control condition of Shab is replicated from table 4.1.

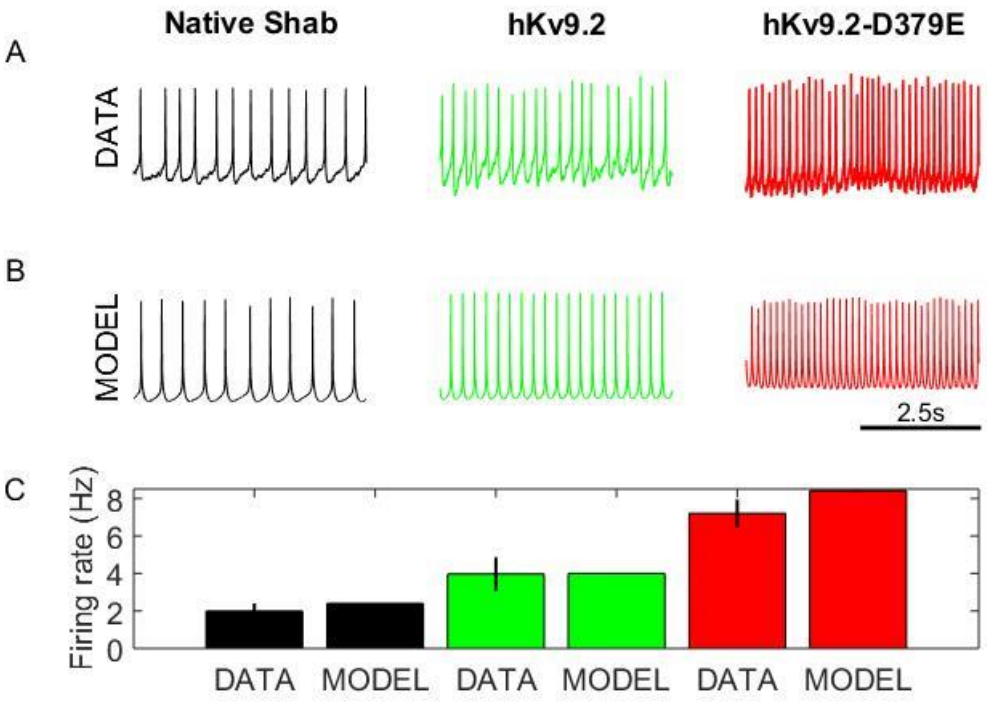

Figure 6.4 Comparison of current-clamp experimental data and model predictions for whole cell action potential firing rate.

A) Representative 5s epochs of whole cell electrical activity, replicated from Figure 6.2. **B)** Whole cell model descriptions of electrical activity for the native Shab channel (left panel) and with human wild-type Kv9 (middle panel) or human mutant Kv9 (right panel). **C)** Quantitative representation of firing rates across genotypes and between experimental data and model descriptions. There is no difference between model data and experimental data (controls: n=6 p=0.3739, wild-type hKv9.2 channel: n=3 p=0.7072, mutant hKv9.2-D379E channel: n=3 p=0.6914).

The advantage of this computational modelling is that the effect of the mutation on channel current within the firing of action potentials can be simulated and hence predicted (Figure 6.5). This shows that the current of the Shab channel activates around the peak of the action potential and itself peaks during the repolarisation phase at around 4.0 pA (Figure 6.5 left panels). When the human wild-type hKv9.2 channel is expressed, the timing of the Shab channel is very similar except that the peak current is lower at around 3.5 pA (Figure 6.5 middle panels). However, in the case of the mutant hKv9.2-D379E channel the greater inactivation has meant that the Shab current is no longer activating during the action potential to the same degree; it has attenuated to $4x10^{-6}$ pA (4 aA) (Figure 6.5 right panels).

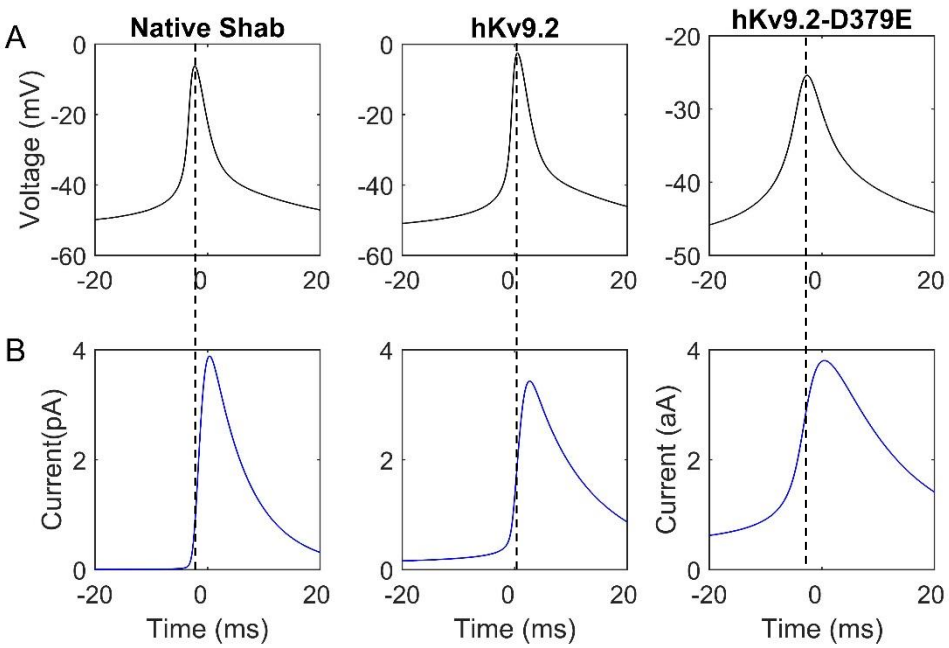

Figure 6.5 Model descriptions of Shab, hKv9.2, and hKv9.2-D379E ion channel model currents during an action potential.

A) Individual action potential within model description of whole cell electrical behaviour (expanded in figure 6.4) for control (left panel) and expression of human wild-type Kv9 (middle panel) or human mutant Kv9 (right panel). **B)** Model description of channel current during the same action potential, respectively, for native Shab (left panel), or with human wild-type Kv9 (middle panel) or human mutant Kv9 (right panel). Note the smaller scale for the hKv9.2-D379E current.

6.2.3 Circadian behaviour and longevity effects

Expression of the Kv9 channel subunits also had behavioural consequences for circadian locomotor behaviour (for methods see Section 2.4.2, for further detail on circadian rhythms see Chapter 5). When driven by the *PDF-GAL4*, expression of the wild-type or mutant Kv9 subunits did not significantly affect the period (Figure 6.6A) or rhythm statistic (see Chapter 2.3) (Figure 6.6B).

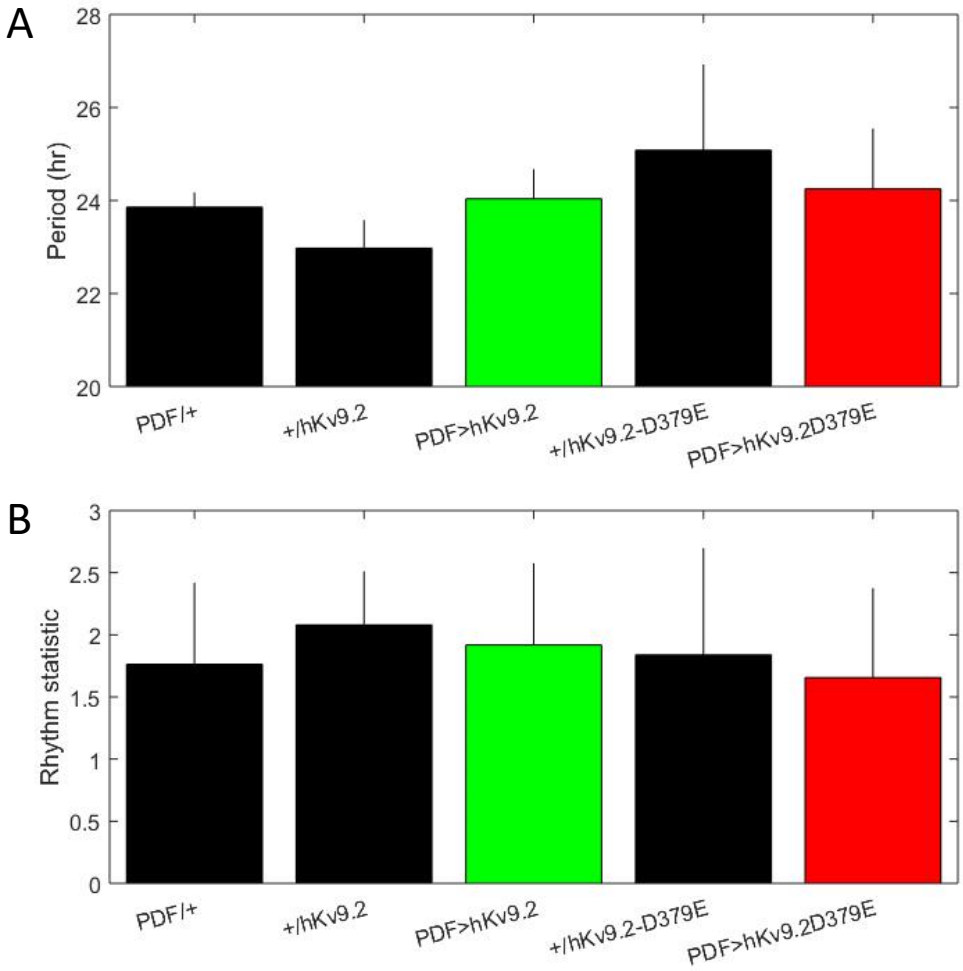

Figure 6.6 Effects of Kv9 subunit expression in LNvs on circadian locomotor period and rhythm statistic.

A) Period of circadian locomotor behaviour for PDF controls (n=16), undriven wild-type (n=19) or mutant (n=17) Kv9, and with expression of human wild-type Kv9 (n=31) or human mutant Kv9 (n=29) in LNvs. **B)** Rhythm statistic as determined by autocorrelation analysis for controls, and with expression of human wild-type Kv9 or human mutant Kv9. No changes seen in period (hKv9.2: p=0.0593, hKv9.2-D379E: p=0.2582) or RS (hKv9.2: p=0.4141, hKv9.2-D379E: p=0.6020).

Significant changes were seen, however, in daily of organisation of behaviour. The diurnal/nocturnal index (D/NI) was reduced for both wild-type and mutant Kv9 subunits compared with undriven controls (Figure 6.7A). Night-time sleep was also reduced for both wild-type and mutant subunits compared with controls (Figure 6.7B). Similarly, night-time activity significantly increased for wild-type and mutant subunits compared with controls (Figure 6.7C). However, in all measures the human wild-type Kv9 and mutant Kv9 subunits did not significantly differ.

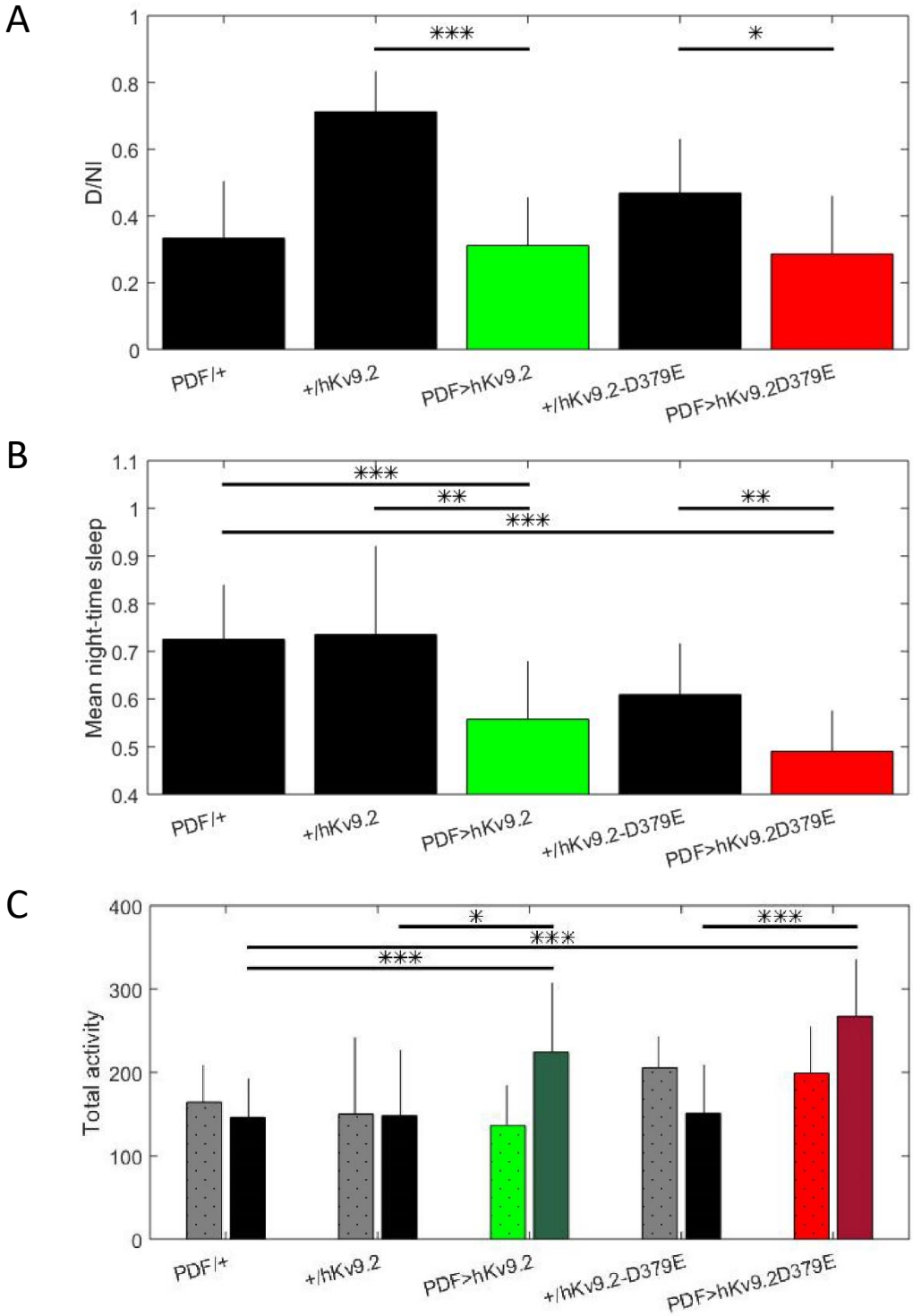

Figure 6.7 Effects of Kv9 subunit expression in LNvs on sleep and activity.

A) Diurnal/nocturnal index (D/NI) for PDF controls (n=16), undriven wild-type (n=19) or mutant (n=17) Kv9, and with expression of human wild-type Kv9 (n=31) or human mutant Kv9 (n=29) in LNvs. There were significant decreases for both wild-type ($p<0.0001$) and mutant Kv9 ($p=0.02$) compared to undriven controls. **B)** Mean night-time sleep for each genotype showing significant decreases between controls and wild-type Kv9 ($p=0.0025$) and mutant Kv9 ($p=0.0026$). **C)** Total day-time (dotted bar) and night-time (plain bar) activity for each genotype showing increases in night-time activity in wild-type ($p=0.0199$) and mutant Kv9 ($p=0.0003$) compared to controls.

Circadian locomotor behaviour is similar when the Kv9 subunits are driven throughout the circadian clock network by the *tim-GAL4* promoter. Circadian period (Figure 6.8A) and rhythm statistic (Figure 6.8B) do not significantly differ between controls, wild-type hKv9.2, and mutant hKv9.2-D379E.

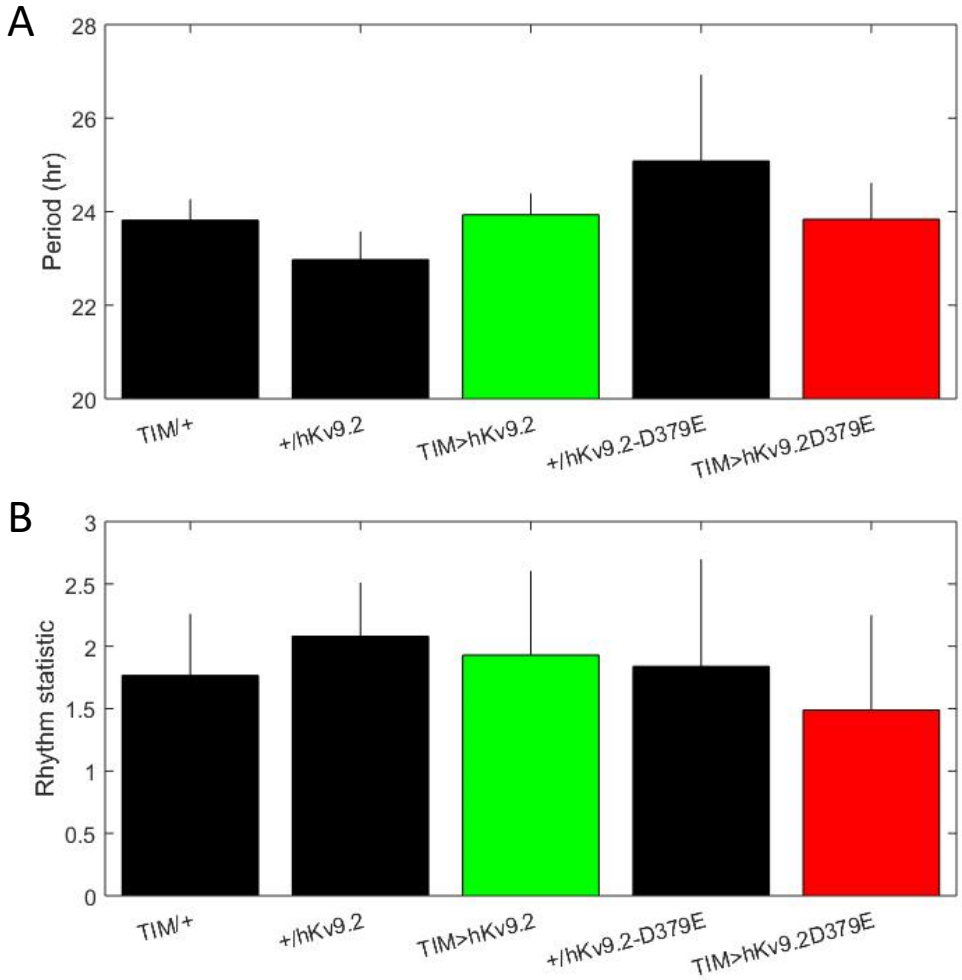

Figure 6.8 Effects of Kv9 subunit expression in all clock neurons on circadian locomotor period and rhythm statistic.

A) Period of circadian locomotor behaviour for TIM controls (n=32), undriven wild-type (n=24) or mutant (n=16) Kv9, and with expression of human wild-type Kv9 (n=15) or human mutant Kv9 (n=13) in all clock neurons. **B)** Rhythm statistic as determined by autocorrelation analysis for controls, and with expression of human wild-type Kv9 or human mutant Kv9.

The balance of night-time and day-time activity is again similar, albeit with smaller effects. The D/NI (Figure 6.9A) was significantly reduced compared to control for the wild-type Kv9 channel. Mean night-time sleep (Figure 6.9B) was also reduced for both wild-type and mutant subunits compared to control. Total activity counts (Figure 6.9C) show increases in night-time activity for wild-type and mutant but the day-time activity remains unaltered for both wild-type and mutant. Comparing this to the PDF driver (Figure 6.7) shows similar results. The *tim-GAL4* control however is fairly active when compared to the *PDF-GAL4* control in both night-time activity and day-time activity making comparison between the genotypes more complex.

Alongside circadian behaviour, longevity is a useful measure of overall health. Longevity assays for *PDF*-driven expression of the Kv9 subunits indicates no significant difference between controls and either the wild-type or mutant Kv9 subunit (Figure 6.10A). *Elav*-driven expression (Figure 6.10B) similarly showed no significant difference for either the wild-type or the mutant. When expression is restricted to the adult stage using the temperature-sensitive inhibitor of GAL4, $GAL80^{ts}$ (Figure 6.10C), both wild-type and mutant are significantly different to controls. $GAL80^{ts}$ inhibits the function of *GAL4* at lower temperatures, hence flies kept at lower temperatures during development do not express the *UAS* transgene. During adulthood flies are raised to higher temperatures (e.g. 30°C) and the *GAL4* becomes functional leading to expression of the *UAS* transgene (Lue et al. 1987).

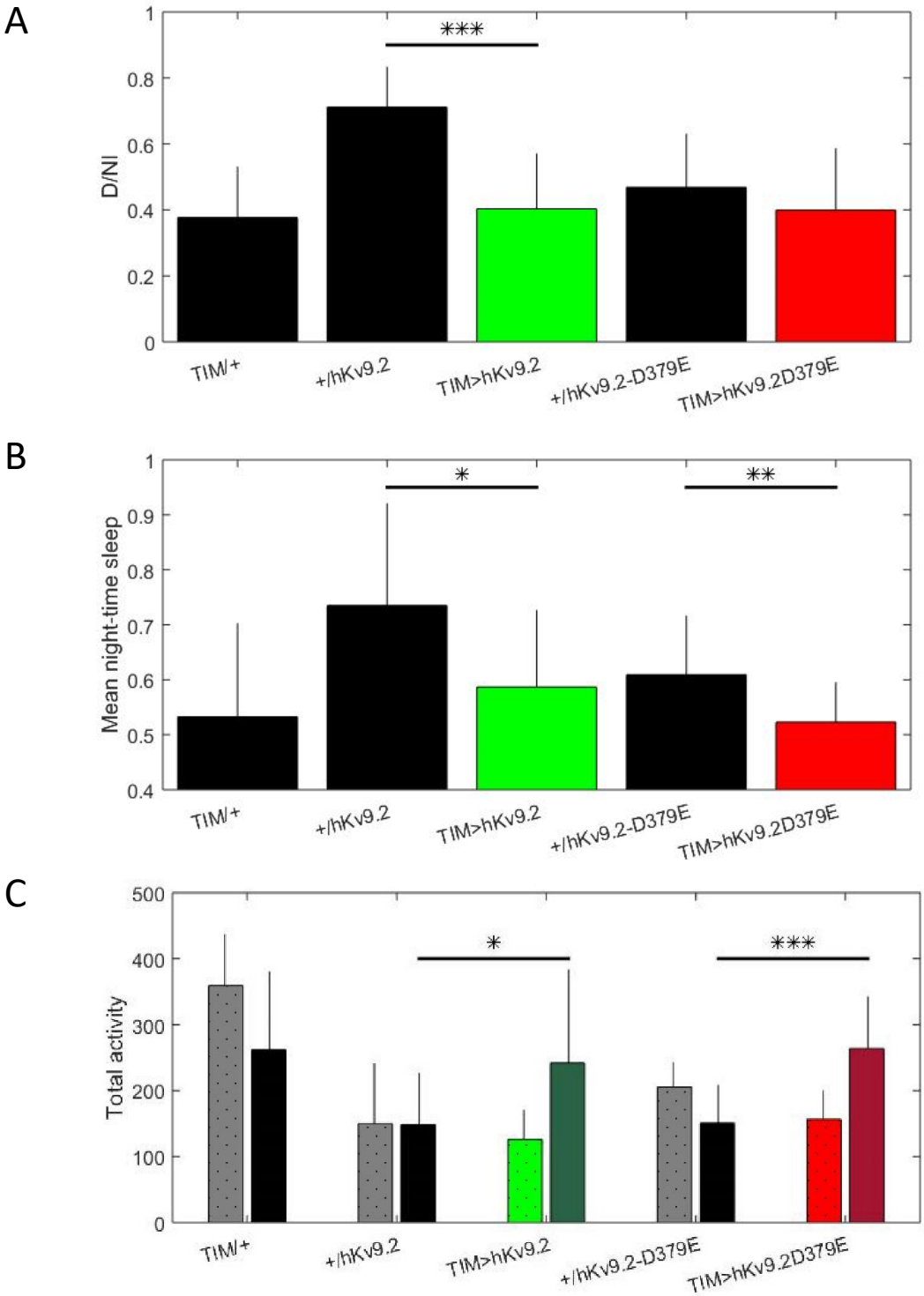

Figure 6.9 Effects of Kv9 subunit expression in clock neurons on sleep and activity.

A) Diurnal/nocturnal index (D/NI) for TIM controls (n=32), undriven wild-type (n=24) or mutant (n=16) Kv9, and with expression of human wild-type Kv9 (n=15) or human mutant Kv9 (n=13) in all clock neurons. There were significant decreases for the wild-type Kv9 ($p<0.0001$). **B)** Mean night-time sleep for each genotype showing significant decreases between control and wild-type ($p=0.0178$) and mutant Kv9 ($p=0.0066$). **C)** Total day-time (dotted bar) and night-time (plain bar) activity for each genotype showing increases in night-time activity in wild-type ($p=0.0403$) and mutant Kv9 ($p=0.0002$) compared to control. Day activity is unaltered (hKv9.2: $p=0.4546$, hKv9.2-D379E: $p=0.0590$).

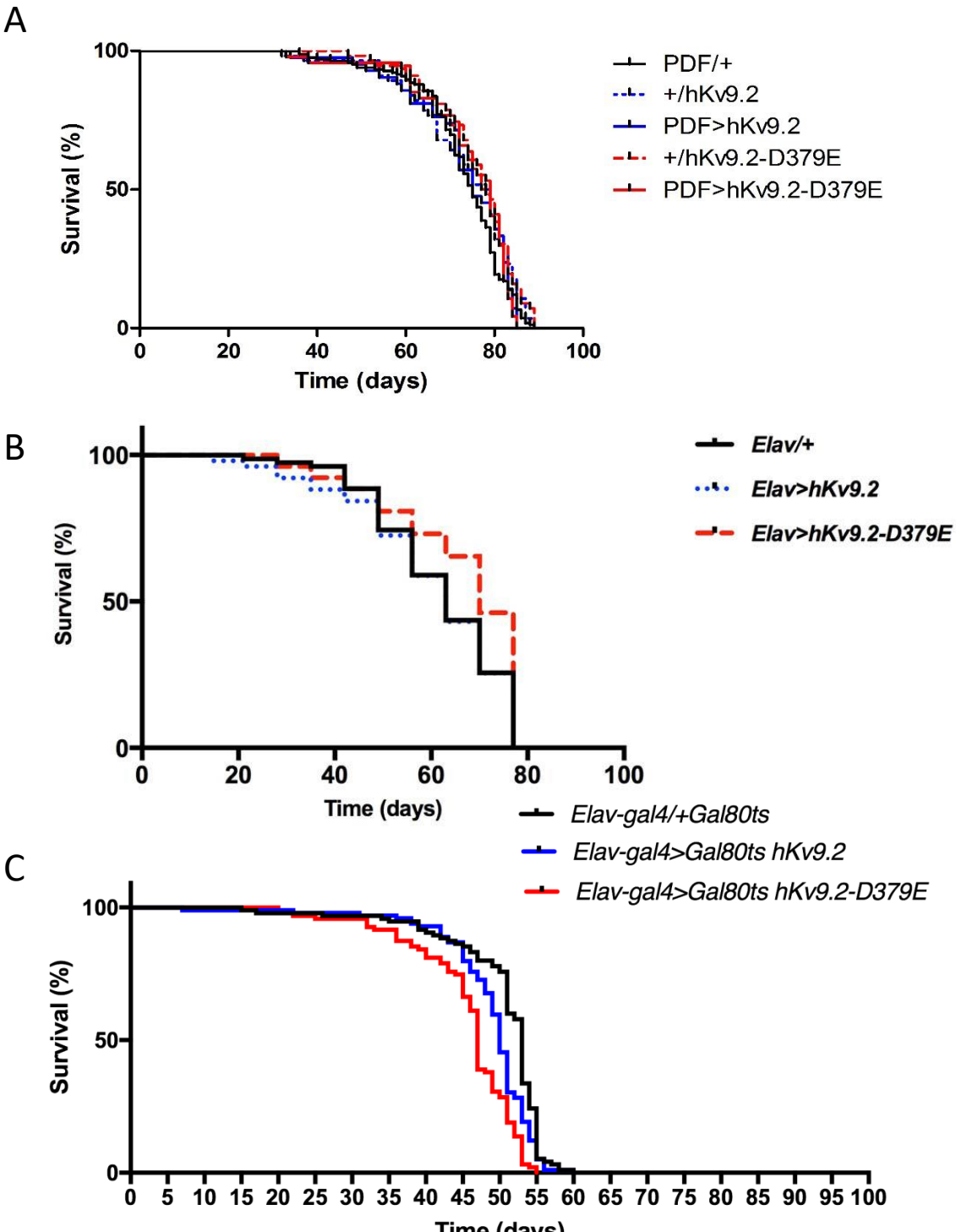

Figure 6.10 Effects of Kv9 subunit expression on longevity

A) Expression of Kv9 subunits in LNvs by *PDF-GAL4* no significant change in longevity (hKv9.2: n=42 p=0.9216, hKv9.2-D379E: n=47 p=0.6852) compared with PDF controls (n=165) or undriven hKv9.2 (n=56) or hKv9.2-D379E controls (n=56). **B)** Expression of Kv9 subunits in all neurons by *Elav-Gal4* shows no significant change (hKv9.2: n=200 p=0.8771, hKv9.2-D379E: n=200 p=0.0656) compared with *Elav-Gal4* controls (n=200). **C)** Expression of Kv9 subunits restricted to the adult stage in all neurons shows some significant difference for the wild-type (n=100, p=0.0012) and the mutant (n=100, p=0.0001) compared to controls (n=100). All *GAL80^{ts}* genotypes have lower longevity than in continuous expression (B). Data in (B) and (C) were gathered by collaborators in Prof Lorraine Clark's lab.

6.3 Discussion

6.3.1 Electrical effects of Kv9 subunits

The results presented reveal differences between the human wild-type hKv9.2 and the mutant hKv9.2-D379E found to be associated with a family of ET patients. In particular, the electrophysiology indicates that the Shab channel is indeed affected by the human wild-type Kv9 subunit, and that the effect of the silent Kv9 subunit is to cause inactivating behaviour that previously was not present in the Shab channel (Figure 6.1). The mutant Kv9 subunit also displays this effect, but perhaps to a larger degree than the wild-type.

Whole cell electrical behaviour was also altered. In normal circumstances, the LNvs spike spontaneously at a rate of 1-2 Hz depending on the time of day as noted previously (Section 3.2.1). The effect of the wild-type Kv9 subunit here was to increase the firing rate of the neurons to around 3-4 Hz. This is consistent with the introduction of inactivation into the channel kinetics as, conceptually, less hyperpolarising potassium current can result in higher excitability. Indeed, the mutant Kv9 subunit displayed an even higher action potential frequency of around 7 Hz (Figure 6.2) alongside a more dramatic inactivation of the channel.

Computational modelling of the Kv9 subunits employed the approach detailed previously (see Chapter 4). Here the model of either wild-type or mutant Kv9 affecting the Shab channel was exchanged with the native Shab channel of the original model. This adapted model was able to recapitulate the electrical behaviour of the spontaneous firing rate for both wild-type and mutant subunits (Figure 6.4). This indicates that the changes to the kinetics, elucidated by voltage-clamp, are sufficient to create the differences in action potential firing rate. In itself this does not exclude the idea that the Kv9 subunits are causing the effects through direct interaction with other channels or proteins. However, it is a good indication that the interaction of

the Kv9 subunits with the Shab channel are the main drivers behind changes in electrical activity.

The advantage of the modelling in allowing predictive description of the channel currents during an action potential deepens the electrophysiological understanding of the model (Figure 6.5). The behaviour of the native Shab channel in activating later in the action potential and being most active during the hyperpolarisation phase is consistent with other reports of Shab and Kv2 behaviours (Peng and Wu 2007; Malin and Nerbonne 2002). It is interesting to note here that when the mutant Kv9 subunit is expressed, the action potential widens despite a simultaneous overall increase in firing rate (Figure 6.5). The widening of the action potential could be due to the loss of Shab current during the repolarisation of the spike, leading to a slower return to baseline. However, while this places the membrane voltage comparatively closer to the threshold potential, it may also affect availability of other ion channels such as sodium or calcium channels.

6.3.2 Behavioural effects of Kv9 subunits

It is interesting that the rhythm statistic and period was unaffected in all cases (Figure 6.6). This indicates that the daily rhythmicity of the LNvs, and the clock network at large, was not altered despite the hyperexcitation of the membrane clock. The s-LNvs are associated with driving rhythmicity in constant conditions (Grima et al. 2004; Stoleru et al. 2004) and so the expectation may have been to see some changes in DD behaviour; although this was not the case.

On the other hand, the l-LNvs are linked to arousal behaviour (Parisky et al. 2008). The observation of disruptions to night-time sleep and increases in night-time behaviour are consistent with this link (Sheeba et al. 2008), as the hyperexcitation of the l-LNvs has potentially contributed to this increased activity (Figure 6.7). An interesting avenue for the future may be to investigate whether hyperexcitation of specifically the s-LNvs or l-LNvs alone

(using *Mai179-GAL4* or *c929-GAL4* drivers) explains the effects seen with the *PDF-GAL4* driver. Such hyperexcitation has been observed to affect night-time activity before (Sheeba et al. 2008). Yet, many studies have relied on expressing channels such as the bacterial sodium channel NaChBac that causes hyperexcitation. Expression of NaChBac itself is a fairly strong perturbation and studies using it tend to show quite extreme effects on electrical activity that are not especially physiologically relevant. In comparison between controls and LNvs expressing NaChBac (Figure 6.11), it can be seen that the amplitude of the spikes is much higher when expressing NaChBac peaking at around 60 mV from a resting potential of around -70 mV. Also, in the presence of NaChBac the spikes have an unusual plateau phase, particularly evident in the night-time recordings. This NaChBac-induced hyperexcitation also caused a disruption of nocturnal sleep and has been associated with complex circadian behaviour patterns (Sheeba et al. 2008). Hence, the use in this study of Kv9 subunits potentially serves as a subtler modulation of the neuronal behaviour.

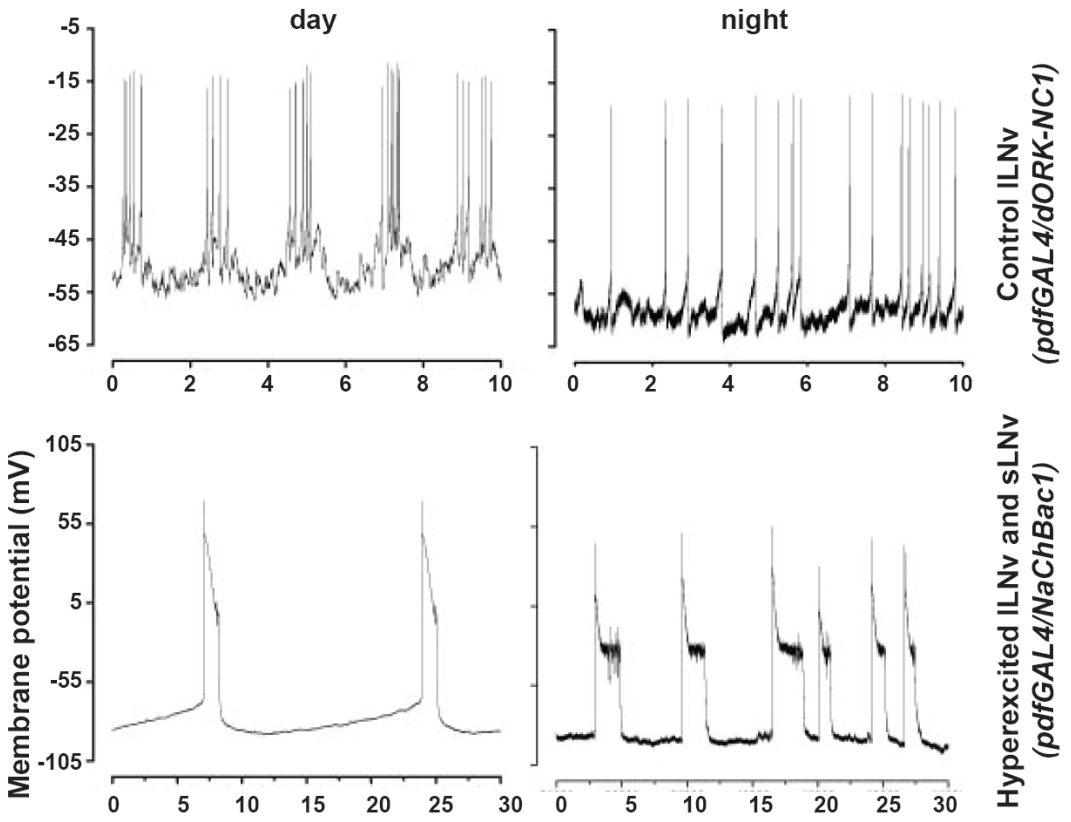

Figure 6.11 Effects of NaChBac expression in LNvs on electrical activity

Recordings during the day (Left column) and the night (right column) in control flies (top row) show normal variation in firing rate and resting membrane potential (figure 3.1). When expressing NaChBac (bottom row), action potentials tend to become much larger and feature an unusual plateau phase. Reproduced from Sheeba et al. 2008, with permission from Elsevier.

It is also interesting that effects on circadian behaviour were perhaps less pronounced with the *tim-GAL4* promoter than the *PDF-GAL4* promoter, despite expression over a larger subset of neurons (Figures 6.8 and 6.9). Shab itself is expressed in a wide range of neurons including clock neurons and so it would stand to reason that either Kv9 subunit could affect a number of neurons. It could also be the case that Shab expression is very low particularly in other clock neurons and so the effect is minimal, or that the effects of Kv9 expression in different subsets conflict with each other and so 'cancel' each other out.

There were no longevity effects observed with expression of Kv9 subunits either restricted to the LNvs or throughout the brain (Figure 6.10). While expression in the LNvs alone may be insufficient to affect health, it is somewhat surprising that pan-neuronal expression is also ineffective since ET and potassium channel dysfunction are associated with reduced longevity (Louis, Benito-Leon, Ottman, et al. 2007; Sheng et al. 2017). When expression was restricted to only adult-stage neurons, significant differences were observed (Figure 6.10C). This may indicate that some compensatory behaviour occurs when the subunits are expressed throughout development. However, decreases seen here in longevity are minimal.

6.3.3 The impact on understanding of essential tremor

So, what does this mean for essential tremor? As described previously, the basis of this mutation is a single family (Liu et al. 2016) and so only directly relates to that one family and that one mutation of the KCNS2 gene. However, while it does not relate to other mutations identified, such as in NOS3 or HAPLN4, it does provide a rough framework and an appreciation that investigating a single mutation can provide insight into the condition as a whole. The study provides functional data that supports the previous study and elucidates some mechanistic detail behind observations of pathogenicity seen in the ET population. It is also consistent with the location of the mutation in the pore domain of KCNS2 and further understanding of the ion channel subunit itself.

Animal models of ET have been lacking to date in mechanistic validity, in that models tend to use methods of creating symptoms of the condition rather than using the underlying causes. The single-gene approach used in this study serves to broaden the knowledge base of the causes of ET and should contribute to future abilities to create models with more mechanistic validity.

The *Drosophila* KCNS2 model of ET shown in this study may however not be the best model for future research. While it displays more mechanistic

validity than other models and indeed displays a lot of face validity, recapitulating effects of the condition such as tremor, it is lacking in other areas. For example, the difference between the physiological effect of the wild-type and mutant Kv9 subunits is fairly subtle with little divergence in longevity, circadian behaviour, or locomotion. This is quite possibly due to the fact that the model represents an over-expression phenotype; the over-expression of either form of the Kv9 subunit creates an effect due to their ectopic expression. The ideal situation would instead be to modify a pre-existing Kv9 subunit to feature the ET mutation. However, *Drosophila* do not possess a Kv9 gene. This was an advantage of using *Drosophila* as native Kv9 would not interfere with expression of the human subunit, but it can also be seen in this way as a disadvantage. One solution to this is using the homology between Kv9 and Shab; by using CRISPR to knock-in the equivalent D379E mutation into Shab this alters the endogenous channel. Although, a draw-back here is that the Shab mutation would affect all Shab-expressing neurons rather than spatially restricting the expression as with *UAS* transgenes.

The mechanistic validity of the model is also limited due to the diverse nature and clinical heterogeneity of the symptoms encapsulated by the term 'essential tremor'. The sheer range of mutations that have been indicated by various studies means that study of one mutation alone only provides one small part of the whole that is required to further treatments of the condition, and thus warrants further investigation into other ion channel genes. Indeed, while this KCNS2 mutation also exhibits non-tremor symptoms such as sleep disturbances and motor defects (Smith et al. 2018), it does not show signs of affective disorders or verbal fluency as have been observed in some human ET patients. The use of *Drosophila* here also limits the relevance of the model to the Purkinje cell degeneration and GABA tone aspects of research into human ET.

Nevertheless, the *Drosophila* model of KCNS2 may serve a purpose beyond modelling of ET. The ability of KCNS2 and its mutation to subtly alter the kinetics of the Shab channel represents an opportunity for use as an

experimental tool. As mentioned previously in discussion, the use of tools such as NaChBac to alter neuronal excitability can be physiologically irrelevant. The subtler effect of KCNS2 can conversely hyperexcite the neuron whilst remaining in physiological ranges of neuronal activity; simply forcing a different state normally available to the neuron rather than a state that would never normally exist.

In summary, the mutation identified in the Kv9 gene KCNS2 (Liu et al. 2016) is associated with altered kinetics of the Shab channel when compared with the wild-type gene. While this mutation represents only one of those associated with essential tremor, it provides some insight into possible mechanisms as the mutation causes hyperexcitability of neurons. The over-expression of this mutation in *Drosophila* clock neurons or neurons in general recapitulates various aspects of ET and presents possible opportunities for elucidating the pathology of ET through development of animal models.

Chapter 7 – Conclusions

This thesis has focused on investigating the circadian variation of LNv clock neuron activity and the physiological functions of that variation. The electrophysiological results presented support the idea that variation in ion channel function underlies the changes in activity. The results of computational modelling further support this idea and allowed for the implementation of dynamic clamp in *Drosophila* to manipulate these neurons directly. Also, this model was utilised in other research to study the effects of a mutation linked with the human essential tremor disorder showing the additional benefits of this modelling approach. Here, I summarise the individual findings from the thesis as a whole.

7.1 General overview

The major finding of the research is the circadian variation in two Kv channels, Shaw and Shal. Isolation of each of the Kv channels by specific pharmacology shows that the current related to Shaker and Shab does not vary depending on time-of-day whereas the current of Shaw and Shal does vary (Figure 3.8). Channel blockers are specific in mammals at this concentration and do not block current when the appropriate channel is functionally removed either by *RNAi* or dominant negative transgene (Figure 3.3B).

Indeed, this cycling of the channel currents is circadian. Cycling of Shaw and Shal currents remains unaltered in the s-LNvs in constant darkness, indicating that it is a true circadian effect (Figure 3.9). This is supported by the observation that a functional clock is required for this cycling as disruption of the molecular clock by dominant negative transgenes (Figure 3.10) abolishes rhythms of Shaw and Shal current. However, the mechanism of channel current cycling remains unclear. As the electrophysiological

techniques used assay only channel function, the underlying basis of this cycling is not well-studied. Possible mechanisms for future investigation include mRNA cycling, ion channel trafficking, redox states, and RNA editing.

The second contribution of this research is the development of the LNv model. The voltage-clamp data acquired from the various Kv channels was used to build channel models that then expanded previous models such as the Sim-Forger model. This makes the model more specific to the *Drosophila* LNv clock neurons and more descriptive as it separates distinct potassium channels. Incorporating the circadian cycling of the Shaw and Shal channels into the whole cell model allowed for a description of spontaneous action potential firing that mirrors the circadian variation experimentally observed in the LNvs (Figure 4.4).

In terms of methodology, this research represents another step forward as it features the successful implementation of dynamic clamp in *Drosophila* and for the study of circadian rhythms. The manipulation of the Kv channels by their channel models allowed for a rescue of pharmacological block that validates the computational channel models in an experimental setting (Figure 4.10). Specific use of Shaw and Shal models also caused a switch in LNv activity between dawn and dusk levels, further suggesting that this cycling is sufficient to create the circadian variation in neuronal activity (Figure 4.12).

The channels are also important physiologically for the whole animal. Functional block of Shaw and Shal channels by dominant negative transgenes causes an increase in activity and decrease in sleep, particularly at night-time (Figures 5.1-3). This effect is similar whether Shaw and Shal are disrupted in the PDF-positive LNvs or in all the clock neurons. This is also seen when the LNv molecular clock is stopped by *clk* or *cyc* dominant negative transgenes, but with an additional effect on rhythmicity (Figures 5.4-6). This suggests a hyperexcitation of l-LNvs via the effect on the membrane clock, with the loss of rhythmicity stemming from disruption of the molecular clock in the s-LNvs. The removal of Shaw or Shal current or the molecular

clock also decreases longevity of flies, potentially via effects on sleep although this is uncertain (Figure 5.10).

The clock neurons represent a good model system for disease states. In the past, the LNvs have been used as models for disease states such as Down's syndrome or Parkinson's disease (Julienne et al. 2017; Lowe et al. 2018). The understanding of the LNv neurons gained here through electrophysiology and computational modelling presented a good opportunity to examine a different ion channel. The identification of a Kv9 channel mutant in essential tremor (a channel not present in *Drosophila*) meant that the wild-type and mutant channels could be expressed in the clock neurons for tractable investigation (see Chapter 6). The Kv9 channel mutation associated with essential tremor was found though the combination electrophysiology and modelling approach to change Shab channel kinetics. This study showed that the mutant Kv9 channel has stronger inactivation kinetics than the wild-type and that this leads to a neuronal hyperexcitation. Hyperexcitation of the LNvs by this alteration of Shab also cause behavioural changes similar to those seen in Shaw and Shal manipulations (see Chapter 3).

7.2 Further remarks and future directions

It is interesting to compare the behavioural data obtained from the various LNv manipulations. To summarise, the disruptions of Shaw and Shal by dominant negative transgenes, Shab by both wild-type and mutant human Kv9 channels, and the molecular clock by dominant negative transgenes in the LNvs all result in increased activity and decreased sleep. As discussed previously (see Chapter 5), this likely relates to the l-LNvs and their role in promoting wakefulness.

One difference between the conditions are that only the molecular clock manipulations cause a change in rhythmicity that is most probably due to

affecting the s-LNvs and their role in driving rhythmicity in constant darkness. Another striking difference is that Shaw, Shal, and molecular clock manipulations in the LNvs cause a consistent shortening of lifespan that is not seen when Shab is manipulated through the Kv9 channels. This may indicate a particular circadian effect of the LNvs on longevity that is not affected by the constant effect of Kv9 wild-type or mutant channels. However, mechanisms underlying this have not been elucidated.

Expression of the various manipulations using the *PDF* promoter means that all LNvs are affected. Hence it cannot be said whether the l-LNvs or the s-LNvs are more important in the disruption of longevity. Future work may use the drivers *C929-GAL4* (l-LNvs) and *Mai179-GAL4* (s-LNvs, LNds) to separate these effects and determine the relative importance of each cell type to the resulting behavioural defects.

The wider context of this work in general reinforces the literature. In particular, the behavioural effects confirm and expand on the understanding of the role of the l-LNvs in promoting wakefulness (Parisky et al. 2008; Sheeba, Fogle, et al. 2008) without being vital neurons in driving rhythmicity. The observation that this can be achieved by a variety of manipulations, most notably of specific Kv channels, expands on the workings of the LNvs and offers new potential ways of modulating their activity.

The main contribution of this thesis is the circadian variation of Shaw and Shal underlying LNv activity variations. This finding integrates both electrophysiology and computation modelling to achieve a novel implementation of dynamic clamp. The marriage of both practical and computational techniques is a particular strength as each supports the other.

As discussed previously (see Chapter 4), the model does have limitations. One notable drawback is the absence of tractable sodium and calcium channel data for modelling. This is currently a technical limitation as obtaining electrophysiological data has proven particularly challenging. One potential approach uses the larval LNvs as they are less widely arborised

and may be more manageable. Preliminary study of the larval LNvs shows that, while less accessible than in the adult, they are tractable for electrophysiology (Figure 3.12). The larval LNvs also exhibit similar activity to their counterparts in the adult stage and so further work could identify if sodium and calcium data can be recorded. However, any work must also address the issue of whether the electrophysiology remains constant between larval and adult stages.

A second approach utilises the characterisation of *para* channel splice forms in *Xenopus* oocytes (Lin et al. 2009) by estimating which splice isoform is the main contributor, either by molecular techniques such as RNA-seq or by computationally fitting each form to available electrophysiological data to determine the most likely candidate. This would then allow that particular splice form to be modelled and replace the existing sodium channel in the whole cell model of the LNvs.

The understanding of Shaw and Shal cycling in this thesis is a mostly phenomenological approach, that is that the channel currents have been observed to cycle but there is little data to suggest the mechanisms underlying this. Various potential mechanisms exist and have been discussed (see Chapter 3) and so future work could focus on determining the methods by which the neurons modulate Shaw and Shal current. While the relevance of cycling mRNA levels to cycling protein levels is as yet unclear, the observation of localisation and trafficking of ion channels playing a role makes this a likely candidate. Other post-translational effects such as redox states or phosphorylation may play important roles and could be tractable to enquiry.

A particularly interesting question in this topic is whether the electrical state of the membrane, or indeed the activity of the ion channels themselves, can impact the molecular clock and how this may occur. Previous studies suggest that this may be the case (Mizrak et al. 2012) but to what extent this happens remains to be seen. It would be interesting to see whether manipulation of the Shaw and Shal channels leads to some change in the

cycling of core circadian clock genes such as *clock* or *period* or any defects in circadian phenomena such as the circadian changes in LNv terminal morphology (Gorostiza et al. 2014; Fernandez et al. 2008).

There are potential parallels with mammalian physiology, as the *Drosophila* LNvs and the mammalian SCN bear various similarities. Both groups exhibit circadian oscillations in electrical activity between day and night (Liu et al. 2007; Meijer and Michel 2015; Sheeba et al. 2008; Cao and Nitabach 2008) and have similar functions and roles of the PDF receptor (Peng et al. 2003; Lin et al. 2004) and the VPAC2 receptor (Hyun et al. 2005; Lear et al. 2005; Mertens et al. 2005). In addition, the cycling of Shaw and Shal channels and their mammalian homologues in Kv3 and Kv4, respectively, is another parallel. Similar to Shaw current being highest at dawn, Kv3.1b and Kv3.2 expression peaks during the day increasing their current (Itri et al. 2005). Likewise, the I_A current associated with Kv4 varies with time-of-day as does Shal current (Itri et al. 2010; Hermanstyne et al. 2017; Granados-Fuentes et al. 2012; Granados-Fuentes et al. 2015). These parallels suggest some level of conservation between the *Drosophila* and mammalian clock networks. Further study of each organism will likely inform the other.

In conclusion, this thesis demonstrates that the LNvs are important in the overall *Drosophila* circadian clock network and exhibit a circadian pattern of varying neuronal activity. These circadian changes can be explained by a shifting pattern of ion channel currents, such as Shaw and Shal, which are important for proper function. Disruption of these ion channels has effects in unsettling normal circadian rhythms in behaviour and reducing sleep and longevity. Computational modelling of these effects allowed the generation of a whole cell model of the LNvs, which in turn successfully enabled the implementation of dynamic clamp to modulate the activity of the LNvs in real-time.

Reference List

Abbott, L. and Nahm, S., 2004. Neuronal nitric oxide synthase expression in cerebellar mutant mice. *Cerebellum*, 3(3), pp.141–51.

Abboud, H., Ahmed, A., and Fernandez, H.H., 2011. Essential tremor: Choosing the right management plan for your patient. *Cleveland Clinic Journal of Medicine*, 78(12), pp.821–828.

Abruzzi, K.C., Zadina, A., Luo, W., Wiyanto, E., Rahman, R., Guo, F., Shafer, O., and Rosbash, M., 2017. RNA-seq analysis of Drosophila clock and non-clock neurons reveals neuron-specific cycling and novel candidate neuropeptides. *PLoS Genetics*, 13(2), pp.1–23.

Algarni, M. and Fasano, A., 2018. The overlap between Essential tremor and Parkinson disease [Online]. *Parkinsonism and Related Disorders*, 46, pp.S101–S104. Available from: https://doi.org/10.1016/j.parkreldis.2017.07.006.

Andersen, O. and Koeppe, R., 1992. Molecular determinants of channel function. *Physiol Rev*, 72, pp.S89-158.

Anderson, W. and Stromberg, M., 1977. Effects of low-level x-irradiation on cat cerebella at different postnatal intervals. I. Quantitative evaluation of morphological changes. *J Comp Neurol*, 171(1), pp.17–37.

Aschoff, J., 1966. Circadian activity pattern with two peaks. *Ecology*, 47, pp.225–49.

Bain, P., Findley, L., Thompson, P., Gresty, M., Rothwell, J., Harding, A., and Marsden, C., 1994. A study of hereditary essential tremor. *Brain*, 117, pp.805–24.

Baranauskas, G., Tkatch, T., Nagata, K., Yeh, J., and Surmeier, D., 2003. Kv3.4 subunits enhance the repolarizing efficiency of Kv3.1 channels in fast-spiking neurons. *Nat Neurosci*, 6(3), pp.258–66.

Baumann, a, Grupe, A., Ackermann, A., and Pongs, O., 1988. Structure of the voltage-dependent potassium channel is highly conserved from Drosophila to vertebrate central nervous systems. *The EMBO journal*, 7(8), pp.2457–2463.

Baxter, D., Canavier, C., Clark, J.J., and Byrne, J., 1999. Computational model of the serotonergic modulation of sensory neurons in Aplysia. *J Neurophysiol*, 82, pp.2914–35.

Bean, B.P., 2007. The action potential in mammalian central neurons. *Nature Reviews Neuroscience*, 8(6), pp.451–465.

Bean, R.C., Shepherd, W., Chan, H., and Eichner, J., 1969. Discrete Conductance Fluctuations in Lipid Bilayer Protein Membranes [Online]. *The Journal of General Physiology*, 53(6), pp.741–757. Available from: http://www.jgp.org/cgi/doi/10.1085/jgp.53.6.741.

Bekku, Y., Saito, M., Moser, M., Fuchigami, M., Maehara, A., Anakayama, M., Kusachi, S., Ninomiya, Y., and Oohashi, T., 2012. Bral2 is indispensable for the proper localization of brevican and the structural integrity of the perineuronal net in the brainstem and cerebellum. *J Comp Neurol*, 520(8), pp.1721–36.

Belle, M.D.C., 2015. Circadian Tick-Talking Across the Neuroendocrine System and Suprachiasmatic Nuclei Circuits: The Enigmatic Communication Between the Molecular and Electrical Membrane Clocks. *Journal of Neuroendocrinology*, 27(7), pp.567–576.

Belle, M.D.C. and Diekman, C.O., 2018. Neuronal oscillations on an ultra-slow timescale: Daily rhythms in electrical activity and gene expression in the mammalian master circadian clockwork. *European Journal of Neuroscience*, (October 2017), pp.1–22.

Belle, M.D.C., Diekman, C.O., Forger, D.B., and Piggins, H.D., 2009. Daily electrical silencing in the mammalian circadian clock. *Science*, 326(5950), pp.281–284.

Benabid, A., Pollak, P., Gervason, C., Hoffman, D., Gao, D., Hommel, M., Perret, J., and de Rougemont, J., 1991. Long-term suppression of tremor by chronic stimulation of the ventral intermediate thalamic nucleus. *Lancet*, 337(8738), pp.403–6.

Benishin, C.G., Sorensen, R.G., Brown, W.E., Krueger, B.K., and Blaustein, M.P., 1988. Four polypeptide components of green mamba venom selectively block certain potassium channels in rat brain synaptosomes. [Online]. *Molecular pharmacology*, 34(2), pp.152–9. Available from: http://www.ncbi.nlm.nih.gov/pubmed/2457792.

Berger, S.D. and Crook, S.M., 2015. Modeling the Influence of Ion Channels on Neuron Dynamics in Drosophila [Online]. *Frontiers in Computational Neuroscience*, 9(November), pp.1–20. Available from: http://journal.frontiersin.org/Article/10.3389/fncom.2015.00139/abstract.

Bergquist, S., Dickman, D.K., and Davis, G.W., 2011. A Hierarchy of Cell Intrinsic and Targe-Derived Homeostatic Signalling. *Neuron*, 66(2), pp.220–234.

Berry, J., Cervantes-Sandoval, I., Chaktaborty, M., and Davis, R.L., 2015. Sleep Facilitates Memory by Blocking Dopamine Neuron-Mediated Forgetting. *Cell*, 161(7), pp.1656–67.

Berty, H., Shi, H., and Lyons-Weiler, J., 2010. Determining the statistical significance of survivorship prediction models. *J Eval Clin Pract*, 16(1), pp.155–65.

Bocksteins, E., 2016. Kv5, Kv6, Kv8, and Kv9 subunits: No simple silent bystanders [Online]. *The Journal of General Physiology*, 147(2), pp.105–125. Available from: http://www.jgp.org/lookup/doi/10.1085/jgp.201511507.

Bocksteins, E., Mayeur, E., Van Tilborg, A., Regnier, G., Timmermans, J.P., and Snyders, D.J., 2014. The subfamily-specific interaction between Kv2.1 and Kv6.4 subunits is determined by interactions between the N- And C-termini. *PLoS ONE*, 9(6).

Borbély, A., Achermann, P., Trachsel, L., and Tobler, I., 1989. Sleep initiation and initial sleep intensity: interactions of homeostatic and circadian mechanisms. *J Biol Rhythms*, 4(2), pp.149–60.

Borg-Graham, L., 1991. Modeling the nonlinear conductances of excitable membranes. In: *Cellular andMolecular Neurobiology: A Practical Approach.* pp.247–275.

Botes, D., Carlsson, F., Jouber, F., Louw, A., Strydom, A., Strydom, D., and Viljoen, C., 1974. Letter: Nomenclature of snake venom toxins. *Toxicon*, 12(2), pp.99–101.

Bouskila, Y. and Dudek, F., 1995. A rapidly activating type of outward rectifier K+ current and A-current in rat suprachiasmatic nucleus neurones. *J Physiol*, 488(2), pp.339–50.

Box, G. and Draper, N., 1987. *Empirical Model-Building and Response Sirfaces*. Wiley.

Brand, A.H. and Perrimon, N., 1993. Targeted gene expression as a means of altering cell fates and generating dominant phenotypes. [Online]. *Development (Cambridge, England)*, 118(2), pp.401–15. Available from: http://www.ncbi.nlm.nih.gov/pubmed/8223268.

Brown, T.M. and Piggins, H.D., 2007. Electrophysiology of the suprachiasmatic circadian clock. *Progress in Neurobiology*, 82(5), pp.229–255.

Buhl, E., Bradlaugh, A., Ogueta, M., Chen, K.-F., Stanewsky, R., and Hodge, J.J.L., 2016. Quasimodo mediates daily and acute light effects on *Drosophila* clock neuron excitability [Online]. *Proceedings of the National Academy of Sciences*, 113(47), pp.13486–13491. Available from: http://www.pnas.org/lookup/doi/10.1073/pnas.1606547113.

Buhr, E.D. and Takahashi, J.S., 2013. Molecular components of the mammalian circadian clock. *Handbook of Experimental Pharmacology*, 217(217), pp.3–27.

Burioka, N., Fukuoka, Y., Koyanagi, S., Miyata, M., Takata, M., Chikumi, H., Takane, H., Watanabe, M., Endo, M., Sako, T., Suyama, H., Ohdo, S., and Shimizu, E., 2010. Asthma: Chronopharmacotherapy and the molecular clock [Online]. *Advanced Drug Delivery Reviews*, 62(9–10), pp.946–955. Available from: http://dx.doi.org/10.1016/j.addr.2010.03.012.

Bushey, D., Huber, R., Tononi, G., and Cirelli, C., 2007. Drosophila Hyperkinetic Mutants Have Reduced Sleep and Impaired Memory [Online]. *Journal of Neuroscience*, 27(20), pp.5384–5393. Available from: http://www.jneurosci.org/cgi/doi/10.1523/JNEUROSCI.0108-07.2007.

Bushey, D., Huber, R., Tononi, G., and Cirelli, C., 2007. Drosophila Hyperkinetic mutants have reduced sleep and impaired memory. *The Journal of neuroscience : the official journal of the Society for Neuroscience*, 27(20), pp.5384–5393.

Bushey, D., Hughes, K.A., Tononi, G., and Cirelli, C., 2010. Sleep, aging, and lifespan in Drosophila. *BMC Neuroscience*, 11.

Cao, G. and Nitabach, M.N., 2008. Circadian control of membrane excitability in Drosophila melanogaster lateral ventral clock neurons Guan. *J Neurosci*, 19(25), pp.389–399.

Catterall, W., 2011. Voltage-gated calcium channels. *Cold Spring Harb Perspect Biol*, 3(8), p.a003947.

Cavanaugh, D.J., Geratowski, J.D., Wooltorton, J.R.A., Jennifer, M., Hector, C.E., Zheng, X., Johnson, E.C., Eberwine, J., and Sehgal, A., 2014. Identification of a circadian output circuit for rest:activity rhythms in Drosophila. *Cell*, 157(3), pp.689–701.

Cavey, M., Collins, B., Bertet, C., Blau, J., Dhabi, A., Emirates, U.A., Dhabi, A., and Emirates, U.A., 2016. Circadian rhythms in neuronal activity propagate through output circuits. *Nat Neurosci*, 19(4), pp.587–595.

Ceriani, M.F., Hogenesch, J.B., Yanovsky, M., Panda, S., Straume, M., and Kay, S.A., 2002. Genome-wide expression analysis in Drosophila reveals genes controlling circadian behavior. *J Neurosci*, 22(21), pp.9305–19.

Chagot, B., Escoubas, P., Villegas, E., Bernard, C., Ferrat, G., Corzo, G., Lazdunski, M., and Darbon, H., 2004. Solution structure of Phrixotoxin 1, a specific peptide inhibitor of Kv4 potassium channels from the venom of the theraphosid spider Phrixotrichus auratus. [Online]. *Protein science : a publication of the Protein Society*, 13(5), pp.1197–208. Available from: http://www.pubmedcentral.nih.gov/articlerender.fcgi?artid=2286752&tool=pmcentrez&rendertype=abstract.

Chandran, V., Pal, P., Reddy, J., Thennarasu, K., Yadav, R., and Shivashankar, N., 2012. Non-motor features in essential tremor. *Acta Neurol Scand*, 125(2), pp.332–7.

Chen, C., Buhl, E., Xu, M., Croset, V., Rees, J.S., Lilley, K.S., Benton, R., Hodge, J.J.L., and Stanewsky, R., 2015. Drosophila Ionotropic Receptor 25a mediates circadian clock resetting by temperature [Online]. *Nature*, 527(7579), pp.516–520. Available from: http://dx.doi.org/10.1038/nature16148.

Chen, K.F., Peschel, N., Zavodska, R., Sehadova, H., and Stanewsky, R., 2011. QUASIMODO, a novel GPI-anchored Zona Pellucida protein involved in light input to the drosophila circadian clock [Online]. *Current Biology*, 21(9), pp.719–729. Available from: http://dx.doi.org/10.1016/j.cub.2011.03.049.

Chiu, C.-S., 2005. GABA Transporter Deficiency Causes Tremor, Ataxia, Nervousness, and Increased GABA-Induced Tonic Conductance in Cerebellum [Online]. *Journal of Neuroscience*, 25(12), pp.3234–3245. Available from: http://www.jneurosci.org/cgi/doi/10.1523/JNEUROSCI.3364-04.2005.

Choi, C., Cao, G., Tanenhaus, A.K., McCarthy, E. v., Jung, M., Schleyer, W., Shang, Y., Rosbash, M., Yin, J.C.P., and Nitabach, M.N., 2012. Autoreceptor Control of Peptide/Neurotransmitter Corelease from PDF Neurons Determines Allocation of Circadian Activity in Drosophila. *Cell Reports*, 2(2), pp.332–344.

Chung, B., Kilman, V., Keath, J., Pitman, J., and Allada, R., 2009. The GABAA Receptor RDL Acts in Peptidergic PDF Neurons to Promote Sleep in Drosophila. *Curr Biol*, 19(5), pp.386–90.

Cirelli, C., 2003. Searching for sleep mutants of Drosophila melanogaster. *BioEssays*, 25(10), pp.940–949.

Cirelli, C., Bushey, D., Hill, S., Huber, R., Kreber, R., Ganetzky, B., and Tononi, G., 2005. Reduced sleep in Drosophila Shaker mutants. *Nature*, 434(7037), pp.1087–1092.

Claridge-Chang, a, Wijnen, H., Naef, F., Boothroyd, C., Rajewsky, N., and Young, M.W., 2001. Circadian regulation of gene expression systems in the Drosophila head. *Neuron*, 32(4), pp.657–671.

Clark, T.G., Bradburn, M.J., Love, S.B., and Altman, D.G., 2003. Survival Analysis Part I: Basic concepts and first analyses. *British Journal of Cancer*, 89(2), pp.232–238.

Cobb, M., 2002. Timeline: exorcizing the animal spirits: Jan Swammerdam on nerve function. *Nat Rev Neurosci*, 3(5), pp.395–400.

Coetzee, W.A., AMARILLO, Y., CHIU, J., CHOW, A., LAU, D., McCORMACK, T., MORENA, H., NADAL, M.S., OZAITA, A., POUNTNEY, D., SAGANICH, M., MIERA, E.V.-S., and RUDY, B., 1999. Molecular Diversity of K+ Channels [Online]. *Annals of the New York Academy of Sciences*, 868, pp.233–255. Available from: http://doi.wiley.com/10.1111/j.1749-

6632.1999.tb11293.x.

Cohen, O., Pullman, S., Jurewicz, E., Watner, D., and Louis, E.D., 20003. Rest tremor in patients with essential tremor: prevalence, clinical correlates, and electrophysiologic characteristics. *Arch Neurol*, 60(3), pp.405–10.

Cole, K. and Moore, J., 1960. Potassium ion current in the squid giant axon: dynamic characteristic. *Biophys J*, 1, pp.1–14.

Colwell, C.S., 2000. Circadian modulation of calcium levels in cells in the suprachiasmatic nucleus. *Eur J Neurosci*, 12(2), pp.571–6.

Colwell, C.S., 2011. Linking neural activity and molecular oscillations in the SCN. *Nat Rev Neurosci*, 12(10), pp.553–69.

Covarrubias, M., Wei, A., and Salkoff, L., 1991. Shaker, Shal, Shab, and Shaw express independent K+ current systems. *Neuron*, 7(5), pp.763–773.

Critchley, M., 1949. Observations on essential (heredofamial) tremor. *Brain*, 72, pp.113–39.

Curtis, H. and Cole, K., 1940. Membrane action potentials from the squid giant axon. *J Cell Comp Physiol*, 15, pp.147–57.

Deng, H., Le, W., and Jankovic, J., 2007. Genetics of essential tremor. *Brain*, 130, pp.1456–64.

Deng, H., Xie, W., Le, W., Huang, M., and Jankovic, J., 2006. Genetic analysis of the GABRA1 gene in patients with essential tremor. *Neurosci Lett*, 401(1), pp.16–9.

Depetris-chauvin, A., Berni, J., Aranovich, E.J., Muraro, N.I., Beckwith, J., and Ceriani, M.F., 2011. Adult-specific electrical silencing of pacemaker neurons uncouples the molecular oscillator from circadian outputs. *Curr Biol*, 21(21), pp.1783–1793.

Destexhe, A. and Huguenard, J., 2000. Nonlinear thermodynamic models of voltage-dependent currents. *J Comput Neurosci*, 9, pp.259–70.

Deuschl, G., Petersen, I., Lorenz, D., and Christensen, K., 2015. Tremor in the elderly: Essential and aging-related tremor. *Mov Disord*, 30(10), pp.1327–34.

Dhooge, a., Govaerts, W., and Kuznetsov, Y. a., 2003. MATCONT: A MATLAB package for numerical bifurcation analysis of ODEs [Online]. *ACM Transactions on Mathematical Software*, 29(2), pp.141–164. Available from: http://portal.acm.org/citation.cfm?doid=779359.779362.

Diekman, C.O., Belle, M.D.C., Irwin, R.P., Allen, C.N., Piggins, H.D., and Forger, D.B., 2013. Causes and Consequences of Hyperexcitation in Central Clock Neurons. *PLoS Computational Biology*, 9(8).

Diekman, C.O. and Forger, D.B., 2009. Clustering predicted by an electrophysiological model of the suprachiasmatic nucleus. *J Biol Rhythms*, 24(4), pp.322–33.

Diochot, S., Drici, M.D., Moinier, D., Fink, M., and Lazdunski, M., 1999. Effects of phrixotoxins on the \uppercaseKv4 family of potassium channels and implications for the role of \uppercaseIto1 in cardiac electrogenesis. [Online]. *British journal of pharmacology*, 126, pp.251–263. Available from: papers2://publication/uuid/679DF8FF-B9AE-4100-A24E-6DAFED09D0D7.

Diochot, S., Schweitz, H., Béress, L., and Lazdunski, M., 1998. Sea anemone peptides with a specific blocking activity against the fast inactivating potassium channel Kv3.4. *Journal of Biological Chemistry*, 273(12), pp.6744–6749.

Duffy, J., 2002. GAL4 system in Drosophila: a fly geneticist's Swiss army knife. *Genesis*, 34(1), pp.1–15.

Emery, P., 2012. Circadian rhythms: An electric jolt to the clock [Online]. *Current Biology*, 22(20), pp.R876–R878. Available from: http://dx.doi.org/10.1016/j.cub.2012.08.003.

Engel, J. and Wu, C., 1992. Interactions of membrane excitability mutations affecting potassium and sodium currents in the flight and giant fiber escape systems of Drosophila. *J Comp Physiol A*, 171(1), pp.93–104.

Erisir, A., Lau, D., Rudy, B., and Leonard, C., 1999. Function of specific K(+) channels in sustained high-frequency firing of fast-spiking neocortical interneurons. *J Neurophysiol*, 82(5), pp.2476–89.

Espay, A., Lang, A., Erro, R., Merola, A., Fasano, A., Berardelli, A., and Bhatia, K., 2017. Essential pitfalls in "essential" tremor AJ [Online]. *Mov Disord*, 32(3), pp.325–31. Available from: http://www.pubmedcentral.nih.gov/articlerender.fcgi?artid=3572699&tool=pmcentrez&rendertype=abstract.

Fabbrini, G., Berardelli, I., Falla, M., Moretti, G., Pasquini, M., Altieri, M., Defazio, G., Biondi, M., and Berardelli, A., 2012. Psychiatric disorders in patients with essential tremor. *Parkinsonism and Related Disorders*, 18(8), pp.971–3.

Feng, G., Zhang, J., Li, M., Shao, L., Yang, L., Song, Q., and Ping, Y., 2018. Control of sleep onset by Shal/K_v4 channels in *Drosophila* circadian neurons [Online]. *The Journal of Neuroscience*, pp.0777-18. Available from: http://www.jneurosci.org/lookup/doi/10.1523/JNEUROSCI.0777-18.2018.

Fernandez, M., Berni, J., and Ceriani, M.F., 2008. Circadian Remodeling of Neuronal Circuits Involved in Rhythmic Behavior. *PLoS Biology*, 6(3), p.e69.

Fernandez, M. d. l. P., Chu, J., Villella, A., Atkinson, N., Kay, S.A., and Ceriani, M.F., 2007. Impaired clock output by altered connectivity in the circadian network [Online]. *Proceedings of the National Academy of Sciences*, 104(13), pp.5650–5655. Available from: http://www.pnas.org/cgi/doi/10.1073/pnas.0608260104.

Fischer, J., Giniger, E., Maniatis, T., and Ptashne, M., 1988. GAL4 activates transcription in Drosophila. *Nature*, 332(6167), pp.853–6.

Fishman, P. and Frenkel, V., 2017. Focused Ultrasound: An Emerging Therapeutic Modality for Neurologic Disease. *Neurotherapeutics*, 14(2), pp.393–404.

FitzHugh, R., 1955. Mathematical models of threshold phenomena in the nerve membrane. *Bull. Math. Biophysics*, 17, pp.257–78.

FitzHugh, R., 1961. Impulses and physiological states in theoretical models of nerve membrane. *Biophys J*, 1, pp.445–66.

Flourakis, M., Kula-Eversole, E., Hutchison, A.L., Han, T.H., Aranda, K., Moose, D.L., White, K.P., Dinner, A.R., Lear, B.C., Ren, D., Diekman, C.O., Raman, I.M., and Allada, R., 2015.

A Conserved Bicycle Model for Circadian Clock Control of Membrane Excitability [Online]. *Cell*, 162(4), pp.836–848. Available from: http://dx.doi.org/10.1016/j.cell.2015.07.036.

Forrest, M., 2015. Simulation of alcohol action upon a detailed Purkinje neuron model and a simpler surrogate model that runs >400 times faster. *BMC Neuroscience*, 16, p.27.

Frazzini, V., Guarnieri, S., Bomba, M., Navarra, R., Morabito, C., Mariggiò, M.A., and Sensi, S.L., 2016. Altered Kv2.1 functioning promotes increased excitability in hippocampal neurons of an Alzheimer's disease mouse model. *Cell Death and Disease*, 7(2), pp.1–12.

Frisch, B., Hardin, P.E., Hamblen-Coyle, M.J., Rosbash, M., and Hall, J.C., 1994. A promoterless period gene mediates behavioral rhythmicity and cyclical per expression in a restricted subset of the drosophila nervous system. *Neuron*, 12(3), pp.555–570.

Galvani, L., 1791. De viribus electricitatis in motu musculari commentarius. *Bon Sci Art Inst Acad Comm*, 7, pp.363–418.

Gandini, M.A., Sandoval, A., and Felix, R., 2014. Patch-clamp recording of voltage-sensitive Ca2+ channels. *Cold Spring Harbor Protocols*, 2014(4), pp.329–335.

Gasparini, M., Bonifati, V., Fabrizio, E., Fabbrini, G., Brusa, L., Lenzi, G., and Meco, G., 2001. Frontal lobe dysfunction in essential tremor: a preliminary study. *J Neurol*, 248(5), pp.399–402.

Gasque, G., Labarca, P., Reynaud, E., and Darszon, A., 2005. Shal and Shaker Differential Contribution to the K+ Currents in the Drosophila Mushroom Body Neurons [Online]. *Journal of Neuroscience*, 25(9), pp.2348–2358. Available from: http://www.jneurosci.org/cgi/doi/10.1523/JNEUROSCI.4384-04.2005.

Gibbs, J.E. and Ray, D.W., 2013. The role of the circadian clock in rheumatoid arthritis. *Arthritis Research and Therapy*, 15(1), pp.1–9.

Goaillard, J.-M. and Marder, E., 2006. Dynamic Clamp Analyses of Cardiac, Endocrine, and Neural Function [Online]. *Physiology*, 21(3), pp.197–207. Available from: http://physiologyonline.physiology.org/cgi/doi/10.1152/physiol.00063.2005.

Goda, T., Mirowska, K., Currie, J., Kim, M.H., Rao, N.V., Bonilla, G., and Wijnen, H., 2011. Adult circadian behavior in Drosophila requires developmental expression of cycle, but not period. *PLoS Genetics*, 7(7).

Goldberger, M. and Growden, J., 1971. Tremor at rest following cerebellar lesions in monkeys: effect of L-DOPA administration. *Brain Res*, 27(1), pp.183–7.

Goodman, C.S. and Heitler, W.J., 1979. Electrical properties of insect neurones with spiking and non-spiking somata: normal, axotomized, and colchicine-treated neurones. *The Journal of experimental biology*, 83, pp.95–121.

Gorostiza, E., Depetris-chauvin, A., Frenkel, L., Pirez, N., and Ceriani, M.F., 2014. Circadian pacemaker neurons change synaptic contacts across the day. *Curr Biol*, 24(18), pp.2161–7.

Granados-Fuentes, D., Hermanstyne, T.O., Carrasquillo, Y., Nerbonne, J.M., and Herzog, E.D., 2015. IA Channels Encoded by Kv1.4 and Kv4.2 Regulate Circadian Period of PER2

Expression in the Suprachiasmatic Nucleus Daniel. , 30(5), pp.396–407.

Granados-Fuentes, D., Norris, A.J., Carrasquillo, Y., Nerbonne, J.M., and Herzog, E.D., 2012. IA Channels Encoded by Kv1.4 and Kv4.2 Regulate Neuronal Firing in the Suprachiasmatic Nucleus and Circadian Rhythms in Locomotor Activity [Online]. *Journal of Neuroscience*, 32(29), pp.10045–10052. Available from: http://www.jneurosci.org/cgi/doi/10.1523/JNEUROSCI.0174-12.2012.

Grima, B., Chélot, E., Xia, R., and Rouyer, F., 2004. Morning and evening peaks of activity rely on different clock neurons of the Drosophila brain. *Nature*, 431(7010), pp.869–873.

Gu, H. and O'Dowd, D.K., 2006. Cholinergic Synaptic Transmission in Adult Drosophila Kenyon Cells In Situ [Online]. *Journal of Neuroscience*, 26(1), pp.265–272. Available from: http://www.jneurosci.org/cgi/doi/10.1523/JNEUROSCI.4109-05.2006.

Guckenheimer, J. and Labouriau, J., 1993. Bifurcation of the Hodgkin and Huxley equations: A new twist. *Bltn Mathcal Biology*, 55, p.937.

Gulcher, R., Jonsson, P., Kong, A., Kristjansson, K., Frigge, M., Karasson, A., Einarsdottir, I., Stefansson, H., Einarsdottir, A., Sigurthoardottir, S., Baldursson, S., Bjornsdottir, S., Hrafnkelsdottir, S., Jakobsson, F., Benedickz, J., and Stefansson, K., 1997. No TitleMapping of a familial essential tremor gene, FET1, to chromosome 3q13. *Nat Genet*, 17(1), pp.84–7.

Guo, F., Yu, J., Jung, H.J., Abruzzi, K.C., Luo, W., Griffith, L.C., and Rosbash, M., 2016. Circadian neuron feedback controls the Drosophila sleep-activity profile. *Nature*, 536(7616), pp.292–297.

Gupta, K., Zamanian, M., Bae, C., Milescu, M., Krepkiy, D., Tilley, D.C., Sack, J.T., Yarov-Yarovoy, V., Kim, J. Il, and Swartz, K.J., 2015. Tarantula toxins use common surfaces for interacting with Kv and ASIC ion channels. *eLife*, 4(MAY), pp.1–20.

Handforth, A., 2012. Harmaline tremor: underlying mechanisms in a potential animal model of essential tremor. [Online]. *Tremor and Other Hyperkinetic Movements (N Y)*, 2, pp.02-92-769–1. Available from: http://www.pubmedcentral.nih.gov/articlerender.fcgi?artid=3572699&tool=pmcentrez&rendertype=abstract.

Handforth, A., 2016. Linking Essential Tremor to the Cerebellum-Animal Model Evidence. *Cerebellum*, 15(3), pp.285–98.

Harbour, V.L., Weigl, Y., Robinson, B., and Amir, S., 2014. Phase Differences in Expression of Circadian Clock Genes in the Central Nucleus of the Amygdala , Dentate Gyrus , and Suprachiasmatic Nucleus in the Rat. , 9(7), pp.1–9.

Harris, R., Sims, S., Parr, J., and Davies, N., 2015. Impact of 12h shift patterns in nursing: A scoping review [Online]. *International Journal of Nursing Studies*, 52(2), pp.605–634. Available from: http://dx.doi.org/10.1016/j.ijnurstu.2014.10.014.

Harrisingh, M.C., Wu, Y., Lnenicka, G.A., and Nitabach, M.N., 2007. Intracellular Ca2+ Regulates Free-Running Circadian Clock Oscillation In Vivo [Online]. *Journal of Neuroscience*, 27(46), pp.12489–12499. Available from: http://www.jneurosci.org/cgi/doi/10.1523/JNEUROSCI.3680-07.2007.

Harvey, A.L., 2001. Twenty years of dendrotoxins. *Toxicon*, 39(1), pp.15–26.

Harvey, A.L. and Karlsson, E., 1980. Dendrotoxin from the venom of the green mamba, Dendroaspis angusticeps. A neurotoxin that enhances acetylcholine release at neuromuscular junction. *Naunyn Schmiedebergs Arch Pharmacol*, 312(1), pp.1–6.

Hastings, M.H., Maywood, E.S., and Brancaccio, M., 2018. Generation of circadian rhythms in the suprachiasmatic nucleus [Online]. *Nature Reviews Neuroscience*, p.1. Available from: http://www.nature.com/articles/s41583-018-0026-z.

Hedera P et al., 2013. Journal of Central Nervous System Disease. *Journal of central nervous disease*, pp.43–55.

Hegde, P., Gu, G., Chen, D., Free, S.J., and Singh, S., 1999. Mutational Analysis of the Shab-encoded Delayed Rectifier K+ Channels in Drosophila [Online]. *Journal of Biological Chemistry*, 274(31), pp.22109–22113. Available from: http://www.jbc.org/cgi/doi/10.1074/jbc.274.31.22109.

Helfrich-Förster, C., 1997. Development of pigment-dispersing hormone-immunoreactive neurons in the nervous system of Drosophila melanogaster. *J Comp Neurol*, 380(3), pp.335–54.

Helfrich-Förster, C., Stengl, M., and Homberg, U., 1998. Organization of the circadian system in insects. *Chronobiology International*, 15(6), pp.567–594.

Helfrich-Förster, C., Yoshii, T., Wülbeck, C., Grieshaber, E., Rieger, D., Bachleitner, W., Cusumano, P., and Rouyer, F., 2007. The lateral and dorsal neurons of Drosophila melanogaster: New insights about their morphology and function. *Cold Spring Harbor Symposia on Quantitative Biology*, 72, pp.517–525.

Hendricks, J.C., Finn, S.M., Panckeri, K.A., Chavkin, J., Williams, J.A., Sehgal, A., and Pack, A.I., 2000. Rest in Drosophila is a sleep-like state. *Neuron*, 25(1), pp.129–138.

Hendricks, J.C., Lu, S., Kume, K., Yin, J., Yang, Z., and Sehgal, A., 2003. Gender dimorphism in the role of cycle (BMAL1) in rest, rest regulation, and longevity in Drosophila melanogaster. *J Biol Rhythms*, 18(1), pp.12–25.

Henslee, E.A., Crosby, P., Kitcatt, S.J., Parry, J.S.W., Bernardini, A., Abdallat, R.G., Braun, G., Fatoyinbo, H.O., Harrison, E.J., Edgar, R.S., Hoettges, K.F., Reddy, A.B., Jabr, R.I., von Schantz, M., O'Neill, J.S., and Labeed, F.H., 2017. Rhythmic potassium transport regulates the circadian clock in human red blood cells [Online]. *Nature Communications*, 8(1), p.1978. Available from: http://www.nature.com/articles/s41467-017-02161-4.

Hermanstyne, T.O., Granados-Fuentes, D., Mellor, R.L., Herzog, E.D., and Nerbonne, J.M., 2017. Acute Knockdown of Kv4.1 Regulates Repetitive Firing Rates and Clock Gene Expression in the Suprachiasmatic Nucleus and Daily Rhythms in Locomotor Behavior [Online]. *Eneuro*, 4(June), p.ENEURO.0377-16.2017. Available from: http://eneuro.sfn.org/lookup/doi/10.1523/ENEURO.0377-16.2017.

Herrington, J., 2007. Gating modifier peptides as probes of pancreatic β-cell physiology. *Toxicon*, 49(2), pp.231–238.

Herrington, J., Zhou, Y.P., Bugianesi, R.M., Dulski, P.M., Feng, Y., Warren, V.A., Smith, M.M., Kohler, M.G., Garsky, V.M., Sanchez, M., Wagner, M., Raphaelli, K., Banerjee, P.,

Ahaghotu, C., Wunderler, D., Priest, B.T., Mehl, J.T., Garcia, M.L., McManus, O.B., Kaczorowski, G.J., and Slaughter, R.S., 2006. Blockers of the delayed-rectifier potassium current in pancreatic β-cells enhance glucose-dependent insulin secretion. *Diabetes*, 55(4), pp.1034–1042.

Higgins, J., Pho, L., and Nee, L., 1997. A gene (ETM) for essential tremor maps to chromosome 2p22-p25. *Mov Disord*, 12(6), pp.859–64.

Hill, T. and Chen, Y., 1972. On the theory of ion transport across nerve membranes. VI. Free energy and activation free energies of conformational change. *Proc Natl Acad Sci U S A*, 69, pp.1723–6.

Hille, B., 1966. Common mode of action of three agents that decrease the transient change in sodium permeability in nerves. *Nature*, 210(5042), pp.1220–2.

Hille, B., 1967. The selective inhibition of delayed potassium currents in nerve by tetraethylammonium ion. *J Gen Physiol*, 50(5), pp.1287–302.

Hille, B., 1968. Pharmacological modifications of the sodium channels of frog nerve. *J Gen Physiol*, 51(2), pp.199–219.

Hladky, S.B. and Haydon, D.A., 1970. Discreteness of conductance change in bimolecular lipid membranes in the presence of certain antibiotics. *Nature*, 225(5231), pp.451–453.

Hodge, J.J. and Stanewsky, R., 2008. Function of the Shaw potassium channel within the Drosophila circadian clock. *PLoS ONE*, 3(5).

Hodge, J.J.L., 2009. Ion channels to inactivate neurons in Drosophila [Online]. *Frontiers in Molecular Neuroscience*, 2(August), pp.1–10. Available from: http://journal.frontiersin.org/article/10.3389/neuro.02.013.2009/abstract.

Hodge, J.J.L., Choi, J.C., O'Kane, C.J., and Griffith, L.C., 2005. Shaw potassium channel genes in Drosophila [Online]. *Journal of Neurobiology*, 63(3), pp.235–254. Available from: http://doi.wiley.com/10.1002/neu.20126.

Hodgkin, A.L. and Huxley, A.F., 1939. Action potentials recorded from inside a nerve fibre. *Nature*, 144, pp.710–11.

Hodgkin, A.L. and Huxley, A.F., 1952a. A quantitative description of membrane current and its application to conduction and excitation in nerve. *Bulletin of Mathematical Biology*, 52(1–2), pp.25–71.

Hodgkin, A.L. and Huxley, A.F., 1952b. Currents carried by sodium and potassium ions through the membrane of the giant axon of Loligo. *J Physiol*, 116, pp.449–72.

Hodgkin, A.L., Huxley, A.F., and Katz, B., 1952. Measurement of current-voltage relations in the membrane of the giant axon of Loligo. *J Physiol*, 116(4), pp.424–48.

Homanics, G., Elsen, F., Ying, S., Jenkins, A., Ferguson, C., Sloat, B., Yuditskaya, S., Goldstein, P., Kralic, J., Morrow, A., and Harrison, N., 2005. A gain-of-function mutation in the GABA receptor produces synaptic and behavioral abnormalities in the mouse. *Genes Brain Behav*, 4(1), pp.10–9.

Hopfner, F. and Deuschl, G., 2018. Is essential tremor a single entity? *Eur J Neurol*, 25(1),

pp.71–82.

Huang, H., Tan, B.Z., Shen, Y., Tao, J., Jiang, F., Sung, Y.Y., Ng, C.K., Raida, M., Köhr, G., Higuchi, M., Fatemi-Shariatpanahi, H., Harden, B., Yue, D.T., and Soong, T.W., 2012. RNA Editing of the IQ Domain in Cav1.3 Channels Modulates Their Ca2+-Dependent Inactivation [Online]. *Neuron*, 73(2), pp.304–316. Available from: http://www.pubmedcentral.nih.gov/articlerender.fcgi?artid=3271027&tool=pmcentrez&rendertype=abstract [Accessed 11 January 2014].

Huang, Y., Ainsley, J.A., Reijmers, L.G., and Jackson, F.R., 2013. Translational Profiling of Clock Cells Reveals Circadianly Synchronized Protein Synthesis. *PLoS Biology*, 11(11).

Hurley, J., Loros, J., and Dunlap, J., 2016. Circadian Oscillators: Around the Transcription-Translation Feedback Loop and on to Output [Online]. *Trends Biochem Sci*, 41(10), pp.834–846. Available from: https://academic.oup.com/sleep/article/doi/10.1093/sleep/zsw002/2957267/Prevalence-of-Circadian-Misalignment-and-Its.

Hyun, S., Lee, Y., Hong, S.T., Bang, S., Paik, D., Kang, J., Shin, J., Lee, J., Jeon, K., Hwang, S., Bae, E., and Kim, J., 2005. Drosophila GPCR han is a receptor for the circadian clock neuropeptide PDF. *Neuron*, 48(2), pp.267–268.

Ikeda, M., Sugiyama, T., Wallace, C., Gompf, H., Yoshioka, T., Miyawaki, A., and Allen, C., 2003. Circadian dynamics of cytosolic and nuclear Ca2+ in single suprachiasmatic nucleus neurons. *Neuron*, 38, pp.253–63.

Ingleby, L., Maloney, R., Jepson, J., Horn, R., and Reenan, R., 2009. Regulated RNA editing and functional epistasis in Shaker potassium channels. *The Journal of general physiology*, 133(1), pp.17–27.

Itri, J.N., Michel, S., Vansteensel, M.J., Meijer, J.H., and Colwell, C.S., 2005. Fast Delayed Rectifier Potassium Current Required for Circadian Neural Activity. *Nat Neurosci*, 8(5), pp.650–656.

Itri, J.N., Vosko, A.M., Schroeder, A., Dragich, J.M., Michel, S., and Colwell, C.S., 2010. Circadian Regulation of A-Type Potassium Currents in the Suprachiasmatic Nucleus [Online]. *Journal of Neurophysiology*, 103(2), pp.632–640. Available from: http://jn.physiology.org/cgi/doi/10.1152/jn.00670.2009.

Jackson, A.C., 2004. Mechanism of Spontaneous Firing in Dorsomedial Suprachiasmatic Nucleus Neurons [Online]. *Journal of Neuroscience*, 24(37), pp.7985–7998. Available from: http://www.jneurosci.org/cgi/doi/10.1523/JNEUROSCI.2146-04.2004.

Jan, L.Y. and Jan, Y.N., 2012. Voltage-gated potassium channels and the diversity of electrical signalling. *The Journal of physiology*, 590(11), pp.2591–2599.

Jaramillo, A.M., Zheng, X., Zhou, Y., Amado, D.A., Sheldon, A., Sehgal, A., and Levitan, I.B., 2004. Pattern of distribution and cycling of SLOB, Slowpoke channel binding protein, in Drosophila. *BMC Neuroscience*, 14, pp.1–14.

Jegla, T. and Salkoff, L., 1997. A novel subunit for shal K+ channels radically alters activation and inactivation. [Online]. *Journal of Neuroscience*, 17(1), pp.32–44. Available from: http://www.ncbi.nlm.nih.gov/pubmed/8987734.

Jeong, K., Lee, S., Seo, H., Oh, Y., Jang, D., Choe, J., Kim, D., Lee, J.H., and Jones, W.D., 2015.

Ca-α1T, a fly T-type Ca 2+ channel, negatively modulates sleep [Online]. *Scientific Reports*, 5, pp.1–13. Available from: http://dx.doi.org/10.1038/srep17893.

Johnson, F., Eyring, H., and Stover, B., 1974. *The theory of rate processes in biology and medicine*. John Wiley and Sons, New York.

Johnston, J., Forsythe, I.D., and Kopp-Scheinpflug, C., 2010. Going native: Voltage-gated potassium channels controlling neuronal excitability. *Journal of Physiology*, 588(17), pp.3187–3200.

Julienne, H., Buhl, E., Leslie, D.S., and Hodge, J.J.L., 2017. Drosophila PINK1 and parkin loss-of-function mutants display a range of non-motor Parkinson's disease phenotypes [Online]. *Neurobiology of Disease*, 104, pp.15–23. Available from: http://dx.doi.org/10.1016/j.nbd.2017.04.014.

Kaneko, M., Helfrich-Förster, C., and Hall, J.C., 1997. Spatial and temporal expression of the period and timeless genes in the developing nervous system of Drosophila: newly identified pacemaker candidates and novel features of clock gene product cycling. [Online]. *The Journal of neuroscience : the official journal of the Society for Neuroscience*, 17(17), pp.6745–60. Available from: http://www.ncbi.nlm.nih.gov/pubmed/9254686.

Karpowicz, P., Zhang, Y., Hogenesch, J.B., Emery, P., and Perrimon, N., 2013. The Circadian Clock Gates the Intestinal Stem Cell Regenerative State. *Cell Reports*, 3(4), pp.996–1004.

Kawasaki, F., Felling, R., and Ordway, R., 2000. A temperature-sensitive paralytic mutant defines a primary synaptic calcium channel in Drosophila. *J Neurosci*, 20, pp.4885–9.

Kimm, T., Khaliq, Z.M., and Bean, B.P., 2015. Differential Regulation of Action Potential Shape and Burst-Frequency Firing by BK and Kv2 Channels in Substantia Nigra Dopaminergic Neurons [Online]. *Journal of Neuroscience*, 35(50), pp.16404–16417. Available from: http://www.jneurosci.org/cgi/doi/10.1523/JNEUROSCI.5291-14.2015.

King, A., Barber, A., Smith, A., Dreyer, A., Sitaraman, D., Nitabach, M.N., Cavanaugh, D.J., and Sehgal, A., 2017. A Peptidergic Circuit Links the Circadian Clock to Locomotor Activity. *Curr Biol*, 27(13), pp.1915–27.

Klarsfeld, A. and Rouyer, F., 1998. Effects of circadian mutations and LD periodicity on the life span of Drosophila melanogaster. *J Biol Rhythms*, 13(6), pp.471–8.

Kluger, B., Klepitskaya, O., and Okun, M., 2009. Surgical treatment of movement disorders. *Neurol Clin*, 27(3), pp.633–77.

Knutsson, A. and Kempe, A., 2014. Shift work and diabetes - A systematic review. *Chronobiology International*, 31(10), pp.1146–1151.

Kolda, T., Lewis, R., and Torczon, V., 2003. Optimization by Direct Search: New Perspectives on Some Classical and Modern Methods [Online]. *SIAM Review*, 45(3), pp.385–482. Available from: https://doi.org/10.1137/S003614450242889.

Kononenko, N.I. and Dudek, F.E., 2006. Persistent calcium current in rat suprachiasmatic nucleus neurons. *Neuroscience*, 138, pp.377–88.

Konopka, R.J. and Benzer, S., 1971. Clock mutants of Drosophila melanogaster. [Online].

Proceedings of the National Academy of Sciences of the United States of America, 68(9), pp.2112–6. Available from: http://www.pubmedcentral.nih.gov/articlerender.fcgi?artid=389363&tool=pmcentrez&rendertype=abstract.

Kralic, J.E., Criswell, H.E., Osterman, J.L., Buckley, T.K.O., Wilkie, M.E., Matthews, D.B., Hamre, K., Breese, G.R., Homanics, G.E., and Morrow, a L., 2005. Genetic essential tremor in γ -aminobutyric acid A receptor α 1 subunit knockout mice. *Journal of Clinical Investigation*, 115(3), pp.774–779.

Krishnan, N., Kretzschmar, D., Rakshit, K., Chow, E., and Giebultowicz, J.M., 2009. The circadian clock gene period extends healthspan in aging Drosophila melanogaster. *Aging*, 1(11), pp.937–948.

Krishnan, N., Rakshit, K., Chow, E., Wentzell, J.S., Kretzschmar, D., and Giebultowicz, J.M., 2012. Loss of circadian clock accelerates aging in neurodegeneration- prone mutants. *Neurobiology of Disease*, 45(3), pp.1129–1135.

Kudo, T., Loh, D.H., Kuljis, D., Constance, C., and Colwell, C.S., 2011. Fast delayed rectifier potassium current: critical for input and output of the circadian system Takashi. *J Neurosci*, 31(8), pp.2746–55.

Kuhlman, S.J. and McMahon, D.G., 2004. Rhythmic regulation of membrane potential and potassium current persists in SCN neurons in the absence of environmental input. *European Journal of Neuroscience*, 20(4), pp.1113–1117.

Kula-Eversole, E., Nagoshi, E., Shang, Y., Rodriguez, J., Allada, R., and Rosbash, M., 2010. Surprising gene expression patterns within and between PDF-containing circadian neurons in Drosophila [Online]. *Proceedings of the National Academy of Sciences*, 107(30), pp.13497–13502. Available from: http://www.pnas.org/cgi/doi/10.1073/pnas.1002081107.

Kumar, S., Chen, D., and Sehgal, A., 2012. Dopamine acts through Cryptochrome to promote acute arousal in Drosophila. *Genes and Development*, 26(11), pp.1224–1234.

Kweon, S., Lee, J., Lim, C., and Choe, J., 2018. High-Amplitude Circadian Rhythms in Drosophila Driven by Calcineurin-Mediated Post-translational Control of sarah. *Genetics*, 209(3), pp.815–28.

de la Monte, S., Lu, B., Sohn, Y., Etienne, D., Kraft, J., Ganju, N., and Wands, J., 2000. Aberrant expression of nitric oxide synthase III in Alzheimer's disease: relevance to cerebral vasculopathy and neurodegeneration. *Neurbiol Aging*, 21(2), pp.309–19.

de la Monte, S., Sohn, Y., Etienne, D., Kraft, J., and Wands, J., 2000. Role of aberrant nitric oxide synthase-3 expression in cerebrovascular degeneration and vascular-mediated injury in Alzheimer's disease. *Ann N Y Acad Sci*, 903, pp.61–71.

Lago, J., Rodriguez, L.P., Blanco, L., Vieites, J.M., and Cabado, A.G., 2015. Tetrodotoxin, an extremely potent marine neurotoxin: Distribution, toxicity, origin and therapeutical uses. *Marine Drugs*, 13(10), pp.6384–6406.

Lamaze, A., Öztürk-Çolak, A., Fischer, R., Peschel, N., Koh, K., and Jepson, J., 2017. Regulation of sleep plasticity by a thermo-sensitive circuit in Drosophila. *Scientific Reports*, 7, p.40304.

Lapicque, L., 1907. Recherches quantitatives sur l'excitation électrique des nerfs traitée comme une polarisation. *Journal de Physiologie et de Pathologie Générale*, 9, pp.620–635.

Lear, B.C., Merrill, C.E., Lin, J.M., Schroeder, A., Zhang, L., and Allada, R., 2005. A G Protein-coupled receptor, groom-of-PDF, is required for PDF neuron action in circadian behavior. *Neuron*, 48(2), pp.221–227.

Levine, J.D., Funes, P., Dowse, H.B., and Hall, J.C., 2002. Signal analysis of behavioral and molecular cycles. *BMC Neuroscience*, 3, pp.1–25.

Lien, C.-C. and Jonas, P., 2003. Kv3 potassium conductance is necessary and kinetically optimized for high-frequency action potential generation in hippocampal interneurons. *The Journal of neuroscience : the official journal of the Society for Neuroscience*, 23(6), pp.2058–2068.

Lien, C.-C., Martina, M., Schultz, J.H., Ehmke, H., and Jonas, P., 2002. Gating, modulation and subunit composition of voltage-gated K(+) channels in dendritic inhibitory interneurones of rat hippocampus. *J Physiol*, 538, pp.405–19.

Lim, E.-S., Seo, M.-W., Woo, S.-R., Jeong, S.-Y., and Jeong, S.-K., 2005. Relationship between essential tremor and cerebellar dysfunction according to age. [Online]. *Journal of clinical neurology (Seoul, Korea)*, 1(1), pp.76–80. Available from: http://www.pubmedcentral.nih.gov/articlerender.fcgi?artid=2854933&tool=pmcentrez&rendertype=abstract.

Lin, W.-H., Wright, D.E., Muraro, N.I., and Baines, R.A., 2009. Alternative Splicing in the Voltage-Gated Sodium Channel DmNav Regulates Activation, Inactivation, and Persistent Current. *J Neurophysiol*, 102(3), pp.1994–2006.

Lin, Y., Stormo, G.D., and Taghert, P.H., 2004. The Neuropeptide Pigment-Dispersing Factor Coordinates Pacemaker Interactions in the Drosophila Circadian System [Online]. *Journal of Neuroscience*, 24(36), pp.7951–7957. Available from: http://www.jneurosci.org/cgi/doi/10.1523/JNEUROSCI.2370-04.2004.

Lindblad, D., Murphey, C., Clark, J., and WR, G., 1996. A model of the action potential and underlying membrane currents in a rabbit atrial cell. *Am J Physiol*, 271, pp.1666–96.

Linford, N.J., Bilgir, C., Ro, J., and Pletcher, S.D., 2013. Measurement of Lifespan in Drosophila melanogaster [Online]. *Journal of Visualized Experiments*, (71), pp.1–9. Available from: http://www.jove.com/video/50068/measurement-of-lifespan-in-drosophila-melanogaster.

Liu, A., Welsh, D., Ko, C., Tran, H., Zhang, E., Priest, A., Buhr, E., Singer, O., Meeker, K., Verma, I., Doyle, F., Takahashi, J.S., and Kay, S., 2007. Intercellular coupling confers robustness against mutations in the SCN circadian clock network. *Cell*, 129(3), pp.605–16.

Liu, X., Hernandez, N., Kisselev, S., Floratos, A., Sawle, A., Ionita-Laza, I., Ottman, R., Louis, E.D., and Clark, L.N., 2016. Identification of candidate genes for familial early-onset essential tremor [Online]. *European Journal of Human Genetics*, 24(7), pp.1009–1015. Available from: http://dx.doi.org/10.1038/ejhg.2015.228.

Lombardi, W.J., Woolston, D.J., Roberts, J.W., and Gross, R.E., 2001. Cognitive deficits in

patients with essential tremor [Online]. *Neurology*, 57(5), pp.785–790. Available from: http://www.neurology.org/cgi/doi/10.1212/WNL.57.5.785.

Lorenz, D. and Deuschl, G., 2007. Update on pathogenesis and treatment of essential tremor. *Curr Opin Neurol*, 20(4), pp.447–52.

Louis, E.D., 2001. Etiology of essential tremor: should we be searching for environmental causes? *Mov Disord*, 16(5), pp.822–9.

Louis, E.D., Benito-Leon, J., and Bermejo-Pareja, F., 2007. Self-reported depression and anti-depressant medication use in essential tremor: cross-sectional and prospective analyses in a population-based study. *Eur J Neurol*, 14(10), pp.1138–46.

Louis, E.D., Benito-Leon, J., Ottman, R., and Bermejo-Pareja, F., 2007. A population-based study of mortality in essential tremor. *Neurology*, 69(21), pp.1982–9.

Louis, E.D., Broussolle, E., Goetz, C.G., Krack, P., Kaufmann, P., and Mazzoni, P., 2008. Historical underpinnings of the term essential tremor in the late 19th century. *Neurology*, 71(11), pp.856–859.

Louis, E.D. and Ferreira, J., 2010. How common is the most common adult movement disorder? Update on the worldwide prevalence of essential tremor. *Mov Disord*, 25(5), pp.534–41.

Louis, E.D., Lee, M., Babij, R., Ma, K., Cortés, E., Vonsattel, J.P.G., and Faust, P.L., 2014. Reduced Purkinje cell dendritic arborization and loss of dendritic spines in essential tremor. *Brain*, 137(12), pp.3142–3148.

Louis, E.D., Rao, K., and Gerbin, M., 2012. Functional Correlates of Gait and Balance Difficulty in Essential Tremor: Balance Confidence, Near Misses and Falls. *Gait Posture*, 35(1), pp.43–7.

Lowe, S., Hodge, J.J.L., and Usowicz, M., 2018. A third copy of the Down syndrome cell adhesion molecule (Dscam) causes synaptic and locomotor dysfunction in Drosophila. *Neurobiol Dis*, 110, pp.93–101.

Lucotte, G., Lagarde, J., Funalot, B., and Sokoloff, P., 2006. Linkage with the Ser9Gly DRD3 polymorphism in essential tremor families. *Clin Genet*, 69(5), pp.437–40.

Lue, N.F., Chasman, D.I., Buchman, a R., and Kornberg, R.D., 1987. Interaction of GAL4 and GAL80 gene regulatory proteins in vitro. *Molecular and cellular biology*, 7(10), pp.3446–3451.

Lundkvist, G.B., Kwak, Y., Davis, E., Tei, H., and Block, G., 2005. A Calcium Flux Is Required for Circadian Rhythm Generation in Mammalian Pacemaker Neurons [Online]. *Journal of Neuroscience*, 25(33), pp.7682–7686. Available from: http://www.jneurosci.org/cgi/doi/10.1523/JNEUROSCI.2211-05.2005.

Lutes, J., Lorden, J., Beales, M., and Oltmans, G., 1988. Tolerance to the tremorogenic effects of harmaline: evidence for altered olivo-cerebellar function. *Neuropharmacology*, 27(8), pp.849–55.

Lyons, K., Pahwa, R., Comella, C., Eisa, M., Elble, R., Fahn, S., Jankovic, J., Juncos, K., Koller, W., Onda, W., Sethi, K., Stern, MB, Tanner, C., Tintner, R., and Watts, R., 2003. Benefits and risks of pharmacological treatments for essential tremor. *Drug Saf*, 26(7),

pp.461–81.

Macerollo, A. and Bhatia, K., 2013. FUS gene mutations cause essential tremor: a surprise but also confirms genetic heterogeneity of essential tremor. *Mov Disord*, 28(3), p.290.

MacKinnon, R., 1991. Determination of the subunit stoichiometry of a voltage-activated potassium channel. *Nature*, 350(6315), pp.232–5.

Maffie, J. and Rudy, B., 2008. Weighing the evidence for a ternary protein complex mediating A-type K+ currents in neurons. *J Physiol*, 586(23), pp.5609–23.

Maguire, S. and Sehgal, A., 2015. Heating and cooling the Drosophila melanogaster clock Sarah. *Current Opinion in Insect Science*, 1(7), pp.71–75.

De Mairan, M., 1729. Observation Botanique. *Histoire de l'Acadmie Royale*, pp.35–36.

Malin, S. and Nerbonne, J., 2002. Delayed rectifier K+ currents, IK, are encoded by Kv2 alpha-subunits and regulate tonic firing in mammalian sympathetic neurons. *J Neurosci*, 22(23), pp.10094–105.

Marsden, C., 1984. The pathophysiology of movement disorders. *Neurol Clin*, 2(3), pp.435–59.

Martina, M., Metz, A., and Bean, B.P., 2007. Voltage-dependent potassium currents during fast spikes of rat cerebellar Purkinje neurons: inhibition by BDS-I toxin. *J Neurphysiol*, 97(1), pp.563–71.

Martina, M., Schultz, J.H., Ehmke, H., Monyer, H., and Jonas, P., 1998. Functional and molecular differences between voltage-gated K+ channels of fast-spiking interneurons and pyramidal neurons of rat hippocampus. [Online]. *The Journal of neuroscience : the official journal of the Society for Neuroscience*, 18(20), pp.8111–25. Available from: http://www.ncbi.nlm.nih.gov/pubmed/9763458.

Masri, S., Kinouchi, K., and Sassone-Corsi, P., 2015. Circadian clocks, epigenetics, and cancer. *Current Opinion in Oncology*, 27(1), pp.50–56.

Mauvoisin, D., Wang, J., Jouffe, C., Martin, E., Atger, F., Waridel, P., Quadroni, M., Gachon, F., and Naef, F., 2014. Circadian clock-dependent and -independent rhythmic proteomes implement distinct diurnal functions in mouse liver [Online]. *Proceedings of the National Academy of Sciences*, 111(1), pp.167–172. Available from: http://www.pnas.org/cgi/doi/10.1073/pnas.1314066111.

McDonald, M.J. and Rosbash, M., 2001. Microarray analysis and organization of circadian gene expression in Drosophila. *Cell*, 107(5), pp.567–578.

Meijer, J.H. and Michel, S., 2015. Neurophysiological analysis of the suprachiasmatic nucleus: a challenge at multiple levels. *Methods Enzymol*, 552, pp.75–102.

Meijer, J.H. and Michel, S., 2015. *Neurophysiological analysis of the suprachiasmatic nucleus: A challenge at multiple levels*. 1st ed. Elsevier Inc. Available from: http://dx.doi.org/10.1016/bs.mie.2014.11.001.

Melinek, R. and Muller, K.J., 1996. Action potential initiation site depends on neuronal excitation. *The Journal of neuroscience : the official journal of the Society for Neuroscience*, 16(8), pp.2585–2591.

Meredith, A.L., Wiler, S., Miller, B., Takahashi, J.S., Fodor, A., Ruby, N.F., and Aldrich, R.W., 2006. BK calcium-activated potassium channels regulate circadian behavioral rhythms and pacemaker output. *Nat Neurosci*, 9(8), pp.1041–9.

Merner, N.D., Girard, S.L., Catoire, H., Bourassa, C. V., Belzil, V. V., Rivière, J.B., Hince, P., Levert, A., Dionne-Laporte, A., Spiegelman, D., Noreau, A., Diab, S., Szuto, A., Fournier, H., Raelson, J., Belouchi, M., Panisset, M., Cossette, P., Dupré, N., Bernard, G., Chouinard, S., Dion, P.A., and Rouleau, G.A., 2012. Exome sequencing identifies FUS mutations as a cause of essential tremor. *American Journal of Human Genetics*, 91(2), pp.313–319.

Mertens, I., Vandingenen, A., Johnson, E.C., Shafer, O.T., Li, W., Trigg, J.S., De Loof, A., Schoofs, L., and Taghert, P.H., 2005. PDF receptor signaling in Drosophila contributes to both circadian and geotactic behaviors. *Neuron*, 48(2), pp.213–219.

Metaxakis, A. and Partridge, L., 2013. Dietary Restriction Extends Lifespan in Wild-Derived Populations of Drosophila melanogaster. *PLoS ONE*, 8(9).

Mezan, S., Feuz, J.D., Deplancke, B., and Kadener, S., 2016. PDF Signaling Is an Integral Part of the Drosophila Circadian Molecular Oscillator [Online]. *Cell Reports*, 17(3), pp.708–719. Available from: http://dx.doi.org/10.1016/j.celrep.2016.09.048.

Miskiewicz, K., Pyza, E., and Schürmann, F.W., 2004. Ultrastructural characteristics of circadian pacemaker neurones, immunoreactive to an antibody against a pigment-dispersing hormone in the fly's brain. *Neuroscience Letters*, 363(1), pp.73–77.

Miwa, H., 2007. Rodent models of tremor. *Cerebellum*, 6(1), pp.66–72.

Miyazaki, M., Ohyama, K., Dunlap, D., and Matsumura, F., 1996. Cloning and sequencing of the para-type sodium channel gene from susceptible and kdr-resistant German cockroaches (Blattella germanica) and house fly (Musca domestica). *Mol Gen Genet*, 252(1), pp.61–8.

Mizrak, D., Ruben, M., Myers, G.N., Rhrissorrakrai, K., Gunsalus, K.C., and Blau, J., 2012. Electrical activity can impose time of day on the circadian transcriptome of pacemaker neurons [Online]. *Current Biology*, 22(20), pp.1871–1880. Available from: http://dx.doi.org/10.1016/j.cub.2012.07.070.

Moloudizargari, M., Mikaili, P., Aghajanshakeri, S., Asghari, M., and Shayegh, J., 2013. Pharmacological and therapeutic effects of Peganum harmala and its main alkaloids. *Pharamcogn Rev*, 7(14), pp.199–212.

de Montigny, C. and Lamarre, Y., 1973. Rhythmic activity induced by harmaline in the olivo-cerebello-bulbar system of the cat. *Brain Res*, 53(1), pp.81–95.

Morris, C. and Lecar, H., 1981. Voltage oscillations in the barnacle giant muscle fiber. *Biophys J*, 35(1), pp.193–213.

Murray, J.M., Sletten, T.L., Magee, M., Gordon, C., Lovato, Nicole, D., Bartlett, D.J., Kennaway, D.J., Lack, L.C., Grunstein, R.R., Lockley, S.W., and Rajaratnam, S.M.W., 2017. Prevalence of Circadian Misalignment and Its Association with Depressive Symptoms in Delayed Sleep Phase Disorder Short Title : Circadian Misalignment in DSPD [Online]. *Sleep*, 114(1–3), pp.1–35. Available from: https://academic.oup.com/sleep/article/doi/10.1093/sleep/zsw002/2957267/Prevalence-of-Circadian-Misalignment-and-Its.

Nadal, M., Ozaita, A., Amarillo, Y., MIERA, E.V.-S., Ma, Y., Mo, W., Goldberg, E., Misumi, Y., Ikehara, Y., Neubert, T., and Rudy, B., 2003. The CD26-related dipeptidyl aminopeptidase-like protein DPPX is a critical component of neuronal A-type K+ channels. *Neuron*, 37(3), pp.449–61.

Nagumo, J., Arimoto, S., and Yoshizawa, S., 1962. An active pulse transmission line simulating nerve axon. *Proc IRE*, 50, pp.2061–70.

Nakahata, Y., Yoshida, M., Takano, A., Soma, H., Yamamoto, T., Yasuda, A., Nakatsu, T., and Takumi, T., 2008. A direct repeat of E-box-like elements is required for cell-autonomous circadian rhythm of clock genes. *BMC Molecular Biology*, 9, pp.1–11.

Nakamura, Y., Nakajima, S., and Grundfest, H., 1965. The action of tetrodotoxin on electrogenic components of squid giant axons. *J Gen Physiol*, 48(6), pp.975–96.

Narahashi, T., Moore, J., and Scott, W., 1964. Tetrodotoxin blockage of sodium conductance increase in lobster giant axons. *J Gen Physiol*, 47, pp.965–74.

Nässel, D., Shiga, S., Morherr, C., and Rao, K., 1993. Pigment-dispersing hormone-like peptide in the nervous system of the flies Phormia and Drosophila: immunocytochemistry and partial characterization. *J Comp Neurol*, 331(2), pp.183–98.

Neher, E. and Sakmann, B., 1976. Single-channel currents recorded from membrane of denervated frog muscle fibres. *Nature*, 260, pp.799–802.

Ni, J.-Q., Zhou, R., Czech, B., Liu, L.-P., Holderbaum, L., Yang-zhou, D., Shim, H., Tao, R., Handler, D., and Karpowicz, P., 2011. A genome-scale shRNA resource for transgenic RNAi in Drosophila. *Nat Methods*, 8(5), pp.405–407.

Nitabach, M.N., Blau, J., and Holmes, T.C., 2002. Electrical Silencing of Drosophila Pacemaker Neurons Stops the Free-Running Circadian Clock [Online]. *Cell*, 109, pp.485–495. Available from: https://ac.els-cdn.com/S0092867402007377/1-s2.0-S0092867402007377-main.pdf?_tid=191a407f-2f36-4e51-b468-c0c04bc18151&acdnat=1520814518_8b6e01a8d692d51fc76ec3f96a9757e8.

Nitabach, M.N., Sheeba, V., Vera, D., Blau, J., and Holmes, T.C., 2005. Membrane electrical excitability is necessary for the free-running larval Drosophila circadian clock. *J Neurobiol*, 62(1), pp.1–13.

Nitabach, M.N., Wu, Y., Sheeba, V., Lemon, W., Strumbos, J., Zelensky, P., White, B., and Holmes, T.C., 2006. Electrical hyperexcitation of lateral ventral pacemaker neurons desynchronizes downstream circadian oscillators in the fly circadian circuit and induces multiple behavioral periods. *J Neurosci*, 26(2), pp.479–89.

Noguchi, T., Leise, T., Kingsbury, N., Diemer, T., Wang, L., Henson, M., and Welsh, D., 2017. Calcium circadian rhythmicity in the suprachiasmatic nucleus: cell autonomy and network modulation. *eNeuro*, 4, pp.16–17.

Nygren, A., Fiset, C., Firek, L., Clark, J., Lindblad, D., Clark, R., and Giles, W., 1998. Mathematical model of an adult human atrial cell: The role of K+ currents in repolarization. *Circ Res*, 82, pp.63–81.

O'Dowd, D.K. and Aldrich, R.W., 1988. Voltage-clamp analysis of sodium channels in wild-type and mutant Drosophila neurons. [Online]. *The Journal of neuroscience : the official journal of the Society for Neuroscience*, 8(10), pp.3633–43. Available from:

http://www.ncbi.nlm.nih.gov/pubmed/2848103.

O'Neill, J. and Reddy, A., 2011. Circadian clocks in human red blood cells [Online]. *Nature*, 469(7331), pp.498–503. Available from: http://www.nature.com/nature/journal/v469/n7331/abs/nature09702.html.

Ogris, W., Lehner, R., Fuchs, K., Furtmuller, B., Hoger, H., Homanics, G., and Sieghart, W., 2006. Investigation of the abundance and subunit composition of GABAA receptor subtypes in the cerebellum of alpha1-subunit-deficient mice. *J Neurochem*, 96(1), pp.136–47.

Olson, R., Liu, Z., Nomura, Y., Song, W., and Dong, K., 2008. Molecular and functional characterization of voltage-gated sodium channel variants from Drosophila melanogaster. *Insect Biochemistry and Molecular Biology*, 38(5), pp.604–610.

Pak, M.D., Baker, K., Covarrubias, M., Butler, a, Ratcliffe, a, and Salkoff, L., 1991. mShal, a subfamily of A-type K+ channel cloned from mammalian brain. [Online]. *Proceedings of the National Academy of Sciences of the United States of America*, 88(10), pp.4386–90. Available from: http://www.pubmedcentral.nih.gov/articlerender.fcgi?artid=51664&tool=pmcentrez&rendertype=abstract.

Pallotta, B. and Wagoner, P., 1992. Voltage-dependent potassium channels since Hodgkin and Huxley. *Physiol Rev*, 72(4), pp.S49-67.

Panda, S., Hogenesch, J.B., and Kay, S.A., 2002. Circadian rhythms from flies to human. *Nature*, 417(6886), pp.329–335.

Parisky, K.M., Agosto, J., Pulver, S.R., Shang, Y., Hodge, J.J.L., Kang, K., Liu, X., Garrity, P.A., and Griffith, L.C., 2008. PDF cells are a GABA-responsive wake-promoting component of the Drosophila sleep circuit Katherine. *Neuron*, 60(4), pp.672–682.

Park, D. and Griffith, L.C., 2006. Electrophysiological and Anatomical Characterization of PDF-Positive Clock Neurons in the Intact Adult *Drosophila* Brain [Online]. *Journal of Neurophysiology*, 95(6), pp.3955–3960. Available from: http://www.physiology.org/doi/10.1152/jn.00117.2006.

Park, J.H., Helfrich-Förster, C., Lee, G., Liu, L., Rosbash, M., and Hall, J.C., 2000. Differential regulation of circadian pacemaker output by separate clock genes in Drosophila [Online]. *Proc Natl Acad Sci U S A*, 97(7), pp.3608–3613. Available from: http://www.ncbi.nlm.nih.gov/entrez/query.fcgi?cmd=Retrieve&db=PubMed&dopt=Citation&list_uids=10725392.

Patel, A.J., Lazdunski, M., and Honoré, E., 1997. Kv2.1/Kv9.3, a novel ATP-dependent delayed-rectifier K+ channel in oxygen-sensitive pulmonary artery myocytes. [Online]. *The EMBO journal*, 16(22), pp.6615–25. Available from: http://www.pubmedcentral.nih.gov/articlerender.fcgi?artid=1170266&tool=pmcentrez&rendertype=abstract.

Patton, A., Chesham, J.E., and Hastings, M.H., 2016. Combined pharmacological and genetic manipulations unlock unprecedented temporal elasticity and reveal phase- specific modulation of the molecular circadian clock of the mouse suprachiasmatic nucleus. *J Neurosci*, 36, pp.9326–41.

Peng, H., Chung, P., Long, F., Qu, L., Jenett, A., Seeds, A.M., Myers, E.W., and Simpson, J.H.,

2011. BrainAligner: 3D registration atlases of *Drosophila* brains. *Nature methods*, 8(6), pp.493–498.

Peng, I.-F. and Wu, C.-F., 2007. Differential contributions of Shaker and Shab K+ currents to neuronal firing patterns in Drosophila. *Journal of neurophysiology*, 97(1), pp.780–794.

Peng, I.-F. and Wu, C.-F., 2007. Drosophila cacophony Channels: A Major Mediator of Neuronal Ca2+ Currents and a Trigger for K+ Channel Homeostatic Regulation [Online]. *Journal of Neuroscience*, 27(5), pp.1072–1081. Available from: http://www.jneurosci.org/cgi/doi/10.1523/JNEUROSCI.4746-06.2007.

Peng, Y., Stoleru, D., Levine, J.D., Hall, J.C., and Rosbash, M., 2003. Drosophila free-running rhythms require intercellular communication. *PLoS Biology*, 1(1), pp.32–40.

Pennartz, C., de Jeu, M., Bos, N., Schaap, J., and Geurtsen, A., 2002. Diurnal modulation of pacemaker potentials and calcium current in the mammalian circadian clock. *Nature*, 416, pp.286–90.

Persson, M., Eklund, M., Dircksen, H., Muren, J., and Nässel, D., 2001. Pigment-dispersing factor in the locust abdominal ganglia may have roles as circulating neurohormone and central neuromodulator. *J Neurobiol*, 48(1), pp.19–41.

Peto, R., Pike, M., Armitage, P., Breslow, N., Cox, D., Howard, S., Mantel, N., McPherson, K., Peto, J., and Smith, P., 1977. Design and analysis of randomized clinical trials requiring prolonged observation of each patient. II. analysis and examples. *Br J Cancer*, 35(1), pp.1–39.

Petrzilka, S., Taraborrelli, C., Cavadini, G., Fontana, A., and Birchler, T., 2009. Clock gene modulation by TNF-alpha depends on calcium and p38 MAP kinase signaling. *J Biol Rhythms*, 24(4), pp.283–94.

Pickard, G. and Sollars, P., 2012. Intrinsically photosensitive retinal ganglion cells. *Rev Physiol Biochem Pharmacol*, 162, pp.59–90.

Ping, Y., Hahm, E.T., Waro, G., Song, Q., Vo-Ba, D.A., Licursi, A., Bao, H., Ganoe, L., Finch, K., and Tsunoda, S., 2015. Linking Aβ42-Induced Hyperexcitability to Neurodegeneration, Learning and Motor Deficits, and a Shorter Lifespan in an Alzheimer's Model. *PLoS Genetics*, 11(3), pp.1–25.

Ping, Y., Waro, G., Licursi, A., Smith, S., Vo-Ba, D.A., and Tsunoda, S., 2011. Shal/Kv4 channels are required for maintaining excitability during repetitive firing and normal locomotion in Drosophila. *PLoS ONE*, 6(1), pp.15–20.

Pittendrigh, C. and Daan, S., 1976. A functional analysis of circadian pacemakers in nocturnal rodents. V. Pacemaker structure: a clock for all seasons. *J Comp Physiol*, 106(3), pp.333–5.

Prentice, R. and Marek, P., 1979. A qualitative discrepancy between censored data rank tests. *Biometrics*, 35(4), pp.861–7.

Prinz, A.A., Abbott, L.F., and Marder, E., 2004. The dynamic clamp comes of age. *Trends in Neurosciences*, 27(4), pp.218–224.

Rajput, A., Robinson, C., and Rajput, A., 2004. Essential tremor course and disability: A clinicopathologic study of 20 cases. *Neurology*, 62(6), pp.932–6.

Reiter, L., 1978. Use of activity measures in behavioral toxicology. *Environmental Health Perspectives*, VOL. 26(October), pp.9–20.

Renn, S.C.P., Park, J.H., Rosbash, M., Hall, J.C., and Taghert, P.H., 1999. A pdf neuropeptide gene mutation and ablation of PDF neurons each cause severe abnormalities of behavioral circadian rhythms in Drosophila. *Cell*, 99(7), pp.791–802.

Richardson, F. and Kaczmarek, L., 2000. Modification of delayed rectifier potassium currents by the Kv9.1 potassium channel subunit. *Hear Res*, 147(1), pp.21–30.

Rieckhof, G., Yoshihara, M., Guan, Z., and Littleton, J., 2003. Presynaptic N-type calcium channels regulate synaptic growth. *J Biol Chem*, 278, pp.41099–108.

Rieger, D., 2006. Functional Analysis of Circadian Pacemaker Neurons in Drosophila melanogaster [Online]. *Journal of Neuroscience*, 26(9), pp.2531–2543. Available from: http://www.jneurosci.org/cgi/doi/10.1523/JNEUROSCI.1234-05.2006.

Robles, M.S., Cox, J., and Mann, M., 2014. In-Vivo Quantitative Proteomics Reveals a Key Contribution of Post-Transcriptional Mechanisms to the Circadian Regulation of Liver Metabolism. *PLoS Genetics*, 10(1).

Roemmich, R.T., Zeilman, P.R., Vaillancourt, D.E., Okun, M.S., and Hass, C.J., 2013. Gait variability magnitude but not structure is altered in essential tremor. *Journal of Biomechanics*, 46(15), pp.2682–2687.

Roessingh, S., Wolfgang, W., and Stanewsky, R., 2015. Loss of Drosophila melanogaster TRPA1 Function Affects 'Siesta' Behavior but Not Synchronization to Temperature Cycles. *J Biol Rhythms*, 30(6), pp.492–505.

Rubaiy, H., 2017. A Short Guide to Electrophysiology and Ion Channels. *J Pharm Pharm Sci*, 20, pp.48–67.

Ruben, M., Drapeau, M.D., Mizrak, D., and Blau, J., 2012. A mechanism for circadian control of pacemaker neuron excitability Marc. , 27(5), pp.353–364.

Rudy, B. and McBain, C.J., 2001. Kv3 channels: voltage-gated K+ channels designed for high-frequency repetitive firing. *Trends in neurosciences*, 24(9), pp.517–526.

Ryan, M.Y., Maloney, R., Reenan, R., and Horn, R., 2008. Characterization of five RNA editing sites in Shab potassium channels. *Channels (Austin, Tex.)*, 2(3), pp.202–209.

Ryglewski, S. and Duch, C., 2009. Shaker and Shal Mediate Transient Calcium-Independent Potassium Current in a Drosophila Flight Motoneuron. *J Neurophysiol*, 102(6), pp.3673–88.

Salinas, M., Duprat, F., Heurteaux, C., Hugnot, J., and Lazdunski, M., 1997. New modulatory alpha subunits for mammalian Shab K+ channels. *J Biol Chem*, 272(39), pp.24371–9.

Salkoff, L. and Wyman, R., 1981. Genetic modification of potassium channels in Drosophila Shaker mutants. *Nature*, 293(5829), pp.228–230.

Santos, J., Vomel, M., Struck, R., Homberg, U., Nassel, D., and Wegener, C., 2008. Neuroarchitecture of aminergic systems in the larval ventral ganglion of Drosophila melanogaster. *PLoS ONE*, 3(3).

Schmutz, I., Chavan, R., Ripperger, J.A., Maywood, E.S., Jurik, A., Stauffer, A., Delorme, J.E.,

and Moosmang, S., 2015. Europe PMC Funders Group A Specific Role for the REV-ERB α controlled L-type Voltage Gated Calcium Channel Ca V 1 . 2 in Resetting the Circadian Clock in the Late Night. , 29(4), pp.288–298.

Schoenmakers, T., Visser, G., Flik, G., and Theuvenet, A., 1992. CHELATOR: an improved method for computing metal ion concentrations in physiological solutions. *Biotechniques*, 12(6), pp.870–4.

Schubert, F.K., Hagedorn, N., Yoshii, T., Helfrich-Förster, C., and Rieger, D., 2018. Neuroanatomical details of the lateral neurons of Drosophila melanogaster support their functional role in the circadian system. *Journal of Comparative Neurology*, 526(7), pp.1209–1231.

Sehgal, A., Price, J., and Young, M.W., 1992. Ontogeny of a biological clock in Drosophila melanogaster. *Proceedings of the National Academy of Sciences of the United States of America*, 89(February), pp.1423–1427.

Sengul, Y., Sengul, H., Yucekaya, S., Yucel, S., Bakim, B., Pazarci, N., and Özdemir, G., 2015. Cognitive functions, fatigue, depression, anxiety, and sleep disturbances: assessment of nonmotor features in young patients with essential tremor. *Acta Neurol Belg*, 115(3), pp.281–7.

Shafer, O.T., Rosbash, M., and Truman, J.W., 2002. Sequential nuclear accumulation of the clock proteins period and timeless in the pacemaker neurons of Drosophila melanogaster. *The Journal of neuroscience : the official journal of the Society for Neuroscience*, 22(14), pp.5946–5954.

Shafer, O.T. and Taghert, P.H., 2009. RNA-interference knockdown of drosophila pigment dispersing factor in neuronal subsets: The anatomical basis of a neuropeptide's circadian functions. *PLoS ONE*, 4(12).

Shafer, O.T. and Yao, Z., 2014. Pigment-dispersing factor signaling and circadian rhythms in insect locomotor activity [Online]. *Current Opinion in Insect Science*, 1, pp.73–80. Available from: http://dx.doi.org/10.1016/j.cois.2014.05.002.

Shatunov, A., Sambuughin, N., Jankovic, J., Elble, R., Lee, H., Singleton, A., Dagvadorj, A., Ji, J., Zhang, Y., Kimonis, V., Hardy, J., Hallett, M., and Goldfarb, L., 2006. Genomewide scans in North American families reveal genetic linkage of essential tremor to a region on chromosome 6p23. *Brain*, 129, pp.2318–31.

Shaw, P.J., Cirelli, C., Greenspan, R.J., and Tononi, G., 2000. Correlates of sleep and waking in *Drosophila melanogaster*. *Science (New York, N.Y.)*, 287(2000), pp.1834–1837.

Shaw, P.J., Tononi, G., Greenspan, R.J., and Robinson, D.F., 2002. Stress response genes protect against lethal effects of sleep deprivation in Drosophila [Online]. *Nature*, 417(6886), pp.287–291. Available from: http://www.nature.com/doifinder/10.1038/417287a.

Sheeba, V., Fogle, K.J., Kaneko, M., Rashid, S., Chou, Y., and Vijay, K., 2008. Large Ventral Lateral Neurons Modulate Arousal and Sleep in Drosophila. *Curr Biol*, 18(20), pp.1537–1545.

Sheeba, V., Gu, H., Sharma, V.K., Dowd, D.K.O., and Todd, C., 2008. Circadian- and Light-Dependent Regulation of Resting Membrane Potential and Spontaneous Action Potential Firing of Drosophila Circadian Pacemaker Neurons. *J Neurophysiol*, 99(2),

pp.976–988.

Sheng, Y., Tang, L., Kang, L., and Xiao, R., 2017. Membrane ion Channels and Receptors in Animal lifespan Modulation. *J Cell Physiol*, 232(11), pp.2946–56.

Shirakawa, T., Honma, S., Katsuno, Y., Oguchi, H., and Honma, K., 2000. Synchronization of circadian firing rhythms in cultured rat suprachiasmatic neurons. *Eur J Neurosci*, 12(8), pp.2833–8.

Shu, Y., Duque, A., Yu, Y., Haider, B., and McCormick, D., 2007. Properties of action-potential initiation in neocortical pyramidal cells: evidence from whole cell axon recordings. *J Neurophysiol*, 97, pp.746–60.

Sigworth, F. and Neher, E., 1980. Single Na+ channel currents observed in cultured rat muscle cells. *Nature*, 287, pp.447–9.

Sim, C.K. and Forger, D.B., 2007. Modeling the electrophysiology of suprachiasmatic nucleus neurons. *Journal of Biological Rhythms*, 22(5), pp.445–453.

Singh, A. and Singh, S., 1999. Unmasking of a novel potassium current in Drosophila by a mutation and drugs. *J Neurosci*, 19(16), pp.6838–43.

Sinoff, G. and Badarny, S., 2014. Mild cognitive impairment, dementia, and affective disorders in essential tremor: a prospective study. [Online]. *Tremor and other hyperkinetic movements (New York, N.Y.)*, 4, p.227. Available from: http://www.pubmedcentral.nih.gov/articlerender.fcgi?artid=4069695&tool=pmcentrez&rendertype=abstract.

Skarzyński, T., 1992. Crystal structure of alpha-dendrotoxin from the green mamba venom and its comparison with the structure of bovine pancreatic trypsin inhibitor. [Online]. *Journal of molecular biology*, 224(3), pp.671–83. Available from: http://www.ncbi.nlm.nih.gov/pubmed/1373774.

Smith, P., Arias, R., Sonti, S., Odgerel, Z., Santa-Maria, I., McCabe, B.D., Tsaneva-Atanasova, K., Louis, E.D., Hodge, J.J.L., and Clark, L.N., 2018. A Drosophila Model of Essential Tremor. *Scientific reports*, 8(1), p.7664.

Softky, W. and Koch, C., 1993. The highly irregular firing of cortical cells is inconsistent with temporal integration of random EPSPs. *J Neurosci*, 13(1), pp.334–50.

Solc, C. and Aldrich, R., 1988. Voltage-Gated Drosophila Potassium Channels in Larval CNS Neurons of Drosophila. *The Journal of Neuroscience*, 8(7), pp.2556–70.

Stanewsky, R., Kaneko, M., Emery, P., Beretta, B., Wager-Smith, K., Kay, S.A., Rosbash, M., and Hall, J.C., 1998. The cry(b) mutation identifies cryptochrome as a circadian photoreceptor in Drosophila. *Cell*, 95(5), pp.681–692.

Stoleru, D., Peng, Y., Agosto, J., and Rosbash, M., 2004. Coupled Oscillators control morning and evening locomotor behaviour of Drosophila. *October*, 431(October).

Taghert, P.H. and Shafer, O.T., 2006. Mechanisms of clock output in the Drosophila circadian pacemaker system. *Journal of Biological Rhythms*, 21(6), pp.445–457.

Tanoue, S., Krishnan, P., Krishnan, B., Dryer, S.E., and Hardin, P.E., 2004. Circadian Clocks in Antennal Neurons Are Necessary and Sufficient for Olfaction Rhythms in Drosophila.

Curr Biol, 14(1), pp.638–49.

Tempel, B.L., Jan, Y.N., and Jan, L.Y., 1988. Cloning of a probable potassium channel gene from mouse brain. *Nature*, 332(6167), pp.837–839.

Terajima, H., Yoshitane, H., Ozaki, H., Suzuki, Y., Shimba, S., Kuroda, S., Iwasaki, W., and Fukada, Y., 2017. ADARB1 catalyzes circadian A-to-I editing and regulates RNA rhythm. *Nat Genet*, 49(1), pp.146–51.

Tilley, D.C., Eum, K.S., Fletcher-Taylor, S., Austin, D.C., Dupre, C., Patron, L.A., Garcia, R.L., Lam, K., Yarov-Yarovoy, V., Cohen, B.E., and Sack, J.T., 2014. Chemoselective tarantula toxins report voltage activation of wild-type ion channels in live cells [Online]. *Proceedings of the National Academy of Sciences*, 111(44), pp.E4789–E4796. Available from: http://www.pnas.org/cgi/doi/10.1073/pnas.1406876111.

Tomchik, S.M. and Davis, R.L., 2008. Cyclic AMP Imaging Sheds Light on PDF Signaling in Circadian Clock Neurons. *Neuron*, 58(2), pp.161–163.

Tomida, S., Mamiya, T., Sakamaki, H., Miura, M., Aosaki, T., Masuda, M., Niwa, M., Kameyama, T., Kobayahi, J., Iwaki, Y., Imai, S., Ishikawa, A., Abe, K., Yoshimura, T., Nabeshima, T., and Ebihara, S., 2009. Usp46 is a quantitative trait gene regulating mouse immobile behavior in the tail suspension and forced swimming tests. *Nat Genet*, 41(6), pp.688–95.

Troyer, T. and Miller, K., 1997. Physiological gain leads to high ISI variability in a simple model of a cortical regular spiking cell. *Neural Comput*, 9(5), pp.971–83.

Tsien, R.W. and Noble, D., 1969. A transition state theory approach to the kinetics of conductances in excitable membranes. *J Membr Biol*, 1, pp.248–73.

Tsunoda, S. and Salkoff, L., 1995a. Genetic analysis of Drosophila neurons: Shal, Shaw, and Shab encode most embryonic potassium currents [Online]. *The Journal of Neuroscience*, 15(3), pp.1741–1754. Available from: http://www.ncbi.nlm.nih.gov/pubmed/7891132.

Tsunoda, S. and Salkoff, L., 1995b. The major delayed rectifier in both Drosophila neurons and muscle is encoded by Shab. *The Journal of neuroscience : the official journal of the Society for Neuroscience*, 15(July), pp.5209–5221.

Vaccaro, A., Issa, A.R., Seugnet, L., Birman, S., and Klarsfeld, A., 2017. Drosophila Clock Is Required in Brain Pacemaker Neurons to Prevent Premature Locomotor Aging Independently of Its Circadian Function. *PLoS Genetics*, 13(1), pp.1–24.

Vanin, S., Bhutani, S., Montelli, S., Menegazzi, P., Green, E.W., Pegoraro, M., Sandrelli, F., Costa, R., and Kyriacou, C.P., 2012. Unexpected features of Drosophila circadian behavioural rhythms under natural conditions [Online]. *Nature*, 484(7394), pp.371–375. Available from: http://dx.doi.org/10.1038/nature10991.

Verkhratsky, A., Krishtal, O.A., and Petersen, O.H., 2006. From Galvani to patch clamp: The development of electrophysiology. *Pflugers Archiv European Journal of Physiology*, 453(3), pp.233–247.

Vosshall, L.B. and Young, M.W., 1995. Circadian rhythms in drosophila can be driven by period expression in a restricted group of central brain cells. *Neuron*, 15(2), pp.345–360.

Wang, J.W. and Wu, C., 1996. In Vivo Functional Role of the Drosophila Hyperkinetic Gating and Inactivation of Shaker K + Channels [Online]. *Biophysical Journal*, 71(6), pp.3167–3176. Available from: http://dx.doi.org/10.1016/S0006-3495(96)79510-3.

Wang, Q., Abruzzi, K.C., Rosbash, M., and Rio, D.C., 2018. Striking circadian neuron diversity and cycling of Drosophila alternative splicing [Online]. *eLife*, 7, pp.1–35. Available from: https://elifesciences.org/articles/35618.

Wang, S., Bondarenko, V.E., Qu, Y., Morales, M.J., Rasmusson, R.L., and Strauss, H.C., 2004. Activation properties of Kv4.3 channels: Time, voltage and [K+]o dependence. *Journal of Physiology*, 557(3), pp.705–717.

Wang, T.A., Yu, Y. V, Govindaiah, G., Ye, X., Coleman, T.P., Sweedler, J. V, and Cox, C.L., 2012. Circadian Rhythm of Redox State Regulates Excitability in Suprachiasmatic Nucleus Neurons. *Science*, 337(6096), pp.839–842.

Webb, A.B., Angelo, N., Huettner, J.E., and Herzog, E.D., 2009. Intrinsic, nondeterministic circadian rhythm generation in identified mammalian neurons [Online]. *Proceedings of the National Academy of Sciences*, 106(38), pp.16493–16498. Available from: http://www.pnas.org/cgi/doi/10.1073/pnas.0902768106.

Wei, a, Covarrubias, M., Butler, A., Baker, K., Pak, M., and Salkoff, L., 1990. K+ current diversity is produced by an extended gene family conserved in Drosophila and mouse. [Online]. *Science (New York, N.Y.)*, 248(4955), pp.599–603. Available from: http://www.ncbi.nlm.nih.gov/pubmed/2333511.

Whitt, J.P., Montgomery, J.R., and Meredith, A.L., 2016. BK channel inactivation gates daytime excitability in the circadian clock [Online]. *Nature Communications*, 7, pp.1–13. Available from: http://dx.doi.org/10.1038/ncomms10837.

Wicher, D., Walther, C., and Wicher, C., 2001. Non-synaptic ion channels in insects - Basic properties of currents and their modulation in neurons and skeletal muscles. *Progress in Neurobiology*, 64(5), pp.431–525.

Wilders, R., 2006. Dynamic clamp: A powerful tool in cardiac electrophysiology. *Journal of Physiology*, 576(2), pp.349–359.

Wilson, R.I., Turner, G.C., and Laurent, G., 2004. Transformation of Olfactory Drosophila Antennal Lobe. *Science*, 303(January), pp.366–370.

Witjas, T., Carron, R., Krack, P., Eusebio, A., Vaugoyeau, M., Hariz, M., Azulay, J., and Regis, J., 2015. A prospective single-blind study of Gamma Knife thalamotomy for tremor. *Neurology*, 85(18), pp.1562–8.

Wu, Y., Cao, G., and Nitabach, M.N., 2008. Electrical silencing of PDF neurons advances the phase of non-PDF clock neurons in Drosophila. *Journal of Biological Rhythms*, 23(2), pp.117–128.

Yang, Z. and Sehgal, A., 2001. Role of molecular oscillations in generating behavioral rhythms in Drosophila. *Neuron*, 29(2), pp.453–467.

Yap, M.H.W., Grabowska, M.J., Rohrscheib, C., Jeans, R., Troup, M., Paulk, A.C., van Alphen, B., Shaw, P.J., and van Swinderen, B., 2017. Oscillatory brain activity in spontaneous and induced sleep stages in flies [Online]. *Nature Communications*, 8(1), p.1815. Available from: http://www.nature.com/articles/s41467-017-02024-y.

Yasuyama, K. and Meinertzhagen, I.A., 2010. Synaptic connections of PDF-immunoreactive lateral neurons projecting to the dorsal protocerebrum of Drosophila melanogaster. *Journal of Comparative Neurology*, 518(3), pp.292–304.

Yeung, S.Y.M., 2005. Modulation of Kv3 Subfamily Potassium Currents by the Sea Anemone Toxin BDS: Significance for CNS and Biophysical Studies [Online]. *Journal of Neuroscience*, 25(38), pp.8735–8745. Available from: http://www.jneurosci.org/cgi/doi/10.1523/JNEUROSCI.2119-05.2005.

Yu, D., Feng, C., and Guo, A., 1999. Altered outward K+currents in Drosophila larval neurons of memory mutants rutabaga and amnesiac. *Journal of Neurobiology*, 40(2), pp.158–170.

Zhang, L., Chung, B.Y., Lear, B.C., Kilman, V.L., Liu, Y., Mahesh, G., Meissner, R., Hardin, P.E., and Allada, R., 2011. Signaling to Produce Robust Daily Behavior in Drosophila. , 20(7), pp.591–599.

Appendix

Section A1 ‘FconMain1’ gives the main script for fitting of electrophysiological data. Section A2 ‘CostFun1’ gives the function used by FconMain1 to generate the model fit of the data from the current parameters. Sections A3 ‘ODEm’ and A4 ‘ODEh’ give the differential equations used by CostFun1 in generating the channel current. Section A5 gives the particle swarm optimisation function for global fitting of the data. Section A6 ‘LNVmodel’ gives the function that describes the whole cell activity. Section A7 ‘MODEL.mat’ describes a data file containing the model parameters.

A1 FconMain1

```
% fmincon Main script file written by Saeed A. Mahar 14
February, 2014

clc, clearvars -except results hopes scores i, close all;

% Parameters bounds
%      1     2     3       4        5             6     7
8       9        10           11          12   13
%      Vh_m  k_m   Amp_m   Vmax_m   sigma_m       Vh_n  k_n
amp_n   Vmax_n   sigma_n    Gmax_Kv7    p_m  p_n
UB = [  -20    25     35     -50      245          -10   65
155      10       150          5        3    1];
LB = [  -50     1     10    -300       21         -140    1
1     -80         2        0.1        3    1];

% Generates random initial parameters values
x_0 = rand(1,13);
x0 = x_0.*(UB-LB)+LB;

% Number of variables
nvars = 13;

% Calling MATLAB fmincon function
[x,fval,exitflag,output,reason,final_pop] =
fmincon(@CostFun1,x0,[],[],[],[],LB,UB,[],[]);

result = x;
```

A2 CostFun1

```
% CostFun.m created by Saeed A. Mahar September 20, 2013 to
find the minimum of Objective function

function Score = CostFun1(Pars)

load 'KV1.mat'
%IK = KV9MU;
HP = V(1:10,1);
Vt = V(1:10,2);
t = T;

m0 = m_0(Pars(1:2), HP);
h0 = h_0(Pars(6:7), HP);

[t,m]  = ode23t(@ODEm,t,m0,[],Pars(1:5), Vt);
[t,n]  = ode23t(@ODEh,t,h0,[],Pars(6:10), Vt);

g   = Pars(11);
p   = Pars(12);
q   = Pars(13);

% HH formalism current (I) equation to calculate current
Ek = -90;
I = g*(m.^p.*n.^q)'.*((Vt-Ek)*ones(1,length(t)));

I_intrp = interp1(T,IK(:,1:10),t,'spline');

% Cost function fitness score
Score = norm(abs((I_intrp)'-(I)),2)     % 2 norm

%figure(1)
plot(t,I,'r.-','linewidth',2); hold on;
ax = gca;
ax.ColorOrderIndex = 1;
```

```
plot(t(1:10:end),IK(1:10:end,1:10),'k--','linewidth',0.1);
hold off;
%xlim([-10 200])
%ylim([-20 120])
xlim([-20 200])
ylim([-10 120])
xlabel('Time (ms)'), ylabel('I (pA)')
title(Score)
drawnow;
end
```

A3 ODEm

```
% ODE function representing channel activation gate variable
(m) written in Hodgkin-Huxley formalism

function [dxdt] = ODEm( ~, x0 , p, V)
vh = p(1);
k  = p(2);
a  = p(3);
b  = p(4);
c  = p(5);
infx = 1./(1+exp(-(V-vh)/k));
taux = a*exp(-((V-b)/c));

% Output
dxdt = (infx-x0)./taux;
end
```

A4 ODEh

```
% This is a function file for inactivation gate

function [dhdt] = ODEh( ~, h0, p, V)
vh = p(1);
k  = p(2);
a  = p(3);
b  = p(4);
c  = p(5);

infh = 1./(1+exp((V-vh)/k));
tauh = 0.51+a*exp(-((V-b)/c));

dhdt = (infh-h0)./tauh;
end
```

A5 Particle Swarm Optimisation

```
function [finalsolns, globals, solns1, solns2, solns3, solns4,
solns5] = particleswarm(parts)


tic;


%Upper and lower bounds


%                    Activation
Inactivation
%      Vh_m  k_m   Amp_m   Vmax_m   sigma_m       Vh_n  k_n
amp_n   Vmax_n   sigma_n    Gmax_Kv7    p_m  p_n
UB = [  -35.2 8.9     10    -166      190          -55    7.5
10     -16.6       9.1         90        3    1];
LB = [  -35.2 6.9    0.1    -306       30          -53    3.5
0.1     -36.6       5.1          30        3    1];


Parsna = [-35.2 7.9 1 -286 160 -62 5.5 1 -26.6 7.1 3 1 60];


%Load in experimental data


load('KV1.mat');
%IK = IK(:,1:10);


%Initialise matrices


iters = 30;
solns = zeros(parts,14);
solns(:,1:13) = rand(parts,13);
v = zeros(parts,13);
omega = 0.2;                                %Inertia
psi1 = 0.3;                                 %global weighting
psi2 = 0.2;                                 %personal
weighting
```

```
globals = zeros(1,iters);

%Generate initial solution particles

solns(:,1) = solns(:,1).*(UB(1)-LB(1))+LB(1);
solns(:,2) = solns(:,2).*(UB(2)-LB(2))+LB(2);
solns(:,3) = solns(:,3).*(UB(3)-LB(3))+LB(3);
solns(:,4) = solns(:,4).*(UB(4)-LB(4))+LB(4);
solns(:,5) = solns(:,5).*(UB(5)-LB(5))+LB(5);
solns(:,6) = solns(:,6).*(UB(6)-LB(6))+LB(6);
solns(:,7) = solns(:,7).*(UB(7)-LB(7))+LB(7);
solns(:,8) = solns(:,8).*(UB(8)-LB(8))+LB(8);
solns(:,9) = solns(:,9).*(UB(9)-LB(9))+LB(9);
solns(:,10) = solns(:,10).*(UB(10)-LB(10))+LB(10);
solns(:,11) = solns(:,11).*(UB(11)-LB(11))+LB(11);
solns(:,12) = solns(:,12).*(UB(12)-LB(12))+LB(12);
solns(:,13) = solns(:,13).*(UB(13)-LB(13))+LB(13);

%Calculate fitness of initial particles
HP = V(1:10,1);
Vt = V(1:10,2);
t = T;
Ek = 52;
for i=1:parts
    m0 = m_0(solns(i,1:2), HP);
    h0 = h_0(solns(i,6:7), HP);
    [t,m]  = ode23t(@ODEm,t,m0,[],solns(i,1:5), Vt);
    [t,n]  = ode23t(@ODEh,t,h0,[],solns(i,6:10), Vt);
    g   = solns(i,11);
    p   = solns(i,12);
    q   = solns(i,13);
    I = g*(m.^p.*n.^q)'.*((Vt-Ek)*ones(1,length(t)));
```

```
    I_intrp = interp1(T,IK(:,1:10),t,'spline');
    Score = norm(abs((I_intrp)'-(I)),2);
    solns(i,14) = Score;
end

%Update global best and personals

best = min(solns(:,14));
bestrow = solns(:,14)==best;
globalbest = solns(bestrow,:);

personals = solns;

%%Particle Swarm Optimisation

for j=1:iters

    %calculate velocities
    U1 = rand(parts,13);
    U2 = rand(parts,13);

    for n=1:parts
        for m=1:13

            v(n,m) = omega*v(n,m) +
psi1*U1(n,m)*(globalbest(m)-solns(n,m)) +
psi2*U2(n,m)*(personals(n,m)-solns(n,m));

        end
    end

    %Update particles
```

```
    solns(:,1:13) = solns(:,1:13) + v(:,1:13);

    %Re-calculate fitness

    for i=1:parts
            try
                m0 = m_0(solns(i,1:2), HP);
                h0 = h_0(solns(i,6:7), HP);
                [t,m]  = ode23t(@ODEm,t,m0,[],solns(i,1:5),
Vt);
                [t,n]  = ode23t(@ODEh,t,h0,[],solns(i,6:10),
Vt);
                g   = solns(i,11);
                p   = solns(i,12);
                q   = solns(i,13);
                I = g*(m.^p.*n.^q)'.*((Vt-
Ek)*ones(1,length(t)));
                I_intrp = interp1(T,IK(:,1:10),t,'spline');
                Score = norm(abs((I_intrp)'-(I)),2);
                solns(i,14) = Score;
            catch
                %If ODE fails, particle is randomised to
create new
                %particle
                solns(i,1) = solns(i,1).*(UB(1)-LB(1))+LB(1);
                solns(i,2) = solns(i,2).*(UB(2)-LB(2))+LB(2);
                solns(i,3) = solns(i,3).*(UB(3)-LB(3))+LB(3);
                solns(i,4) = solns(i,4).*(UB(4)-LB(4))+LB(4);
                solns(i,5) = solns(i,5).*(UB(5)-LB(5))+LB(5);
                solns(i,6) = solns(i,6).*(UB(6)-LB(6))+LB(6);
                solns(i,7) = solns(i,7).*(UB(7)-LB(7))+LB(7);
                solns(i,8) = solns(i,8).*(UB(8)-LB(8))+LB(8);
                solns(i,9) = solns(i,9).*(UB(9)-LB(9))+LB(9);
```

```
                solns(i,10) = solns(i,10).*(UB(10)-
LB(10))+LB(10);
                solns(i,11) = solns(i,11).*(UB(11)-
LB(11))+LB(11);
                solns(i,12) = solns(i,12).*(UB(12)-
LB(12))+LB(12);
                solns(i,13) = solns(i,13).*(UB(13)-
LB(13))+LB(13);
            end
    end

    %Update personal bests and global best

    if min(solns(:,14))<globalbest(14)
        best = min(solns(:,14));
        bestrow = solns(:,14)==best;
        globalbest = solns(bestrow,:);
    end

    for p=1:parts
        if solns(p,14)<personals(p,14)
            personals(p,:) = solns(p,:);
        end
    end
    globals(j) = globalbest(14);
    disp(num2str(j))
    if j==1
        solns1 = solns;
    elseif j==2
        solns2 = solns;
    elseif j==3
        solns3 = solns;
    elseif j==4
        solns4 = solns;
```

```
    elseif j==5
        solns5 = solns;
    end
end

finalsolns = solns;
disp(['Best solution is:' num2str(globalbest)])
load('MODEL.mat');
disp(['Solutions should be:' num2str(Parsna) ' '])
plot(globals)

toc
```

A6 LNVmodel

```
function varargout = LNVmodel


%
%LNVmodel (Written by P Smith, University of Bristol)
%Models activity of Drosophila LNV neuron
%
%*Call function --> LNVmodel;
%
%*Assign output --> [vrec,I1,I2,I3,I4] = LNVmodel;
%Returns membrane potential (vrec)
%        Kv1 current (I1)
%        Kv2 current (I2)
%        Kv3 current (I3)
%        Kv4 current (I4)
%
%Enter time of day as a response in the form of ZTX (zeitgeber
time)
%Where ZT0 is sunrise/lights-on and ZT12 is sunset/lights-off
%ZT24 is the same as ZT0
%
%Enter form of Kv2 model as either 1, 2, or 3
%Where 1 is the normal native Kv2 current
%      2 is the native Kv2 with human wild-type Kv9
%      3 is the native Kv2 with human mutant Kv9 (c379E)



%frequency = zeros(1,24);
%k41a = zeros(24,1000001);
%k42a = zeros(24,1000001);

%for iters=1:24
```

```
%% Parameters


C=3.7;


call = 'What is the time (ZT)? [Input: 0-24]:';
%User input for time of day
ZT = input(call);


% Integration settings


DT=0.01;
t0=0;
tf=12000;
%Time is in ms
t=t0:DT:tf;
numT=length(t);


load('MODEL.mat');
%Loads channel parameters
Pars1 = KV1;
Pars3 = KV32;
Pars4 = KV4;


Ena=52; Ek=-90; El=-7; Eca=132;
%Reversal potentials based on Nernst equation


g_leak = ((0.0043*cos(0.2618*ZT))+0.0906);
%Use user input to calculate the conductances
kv3 = ((0.07075*cos(0.2618*ZT))+0.09575);
%for Kv3, Kv4, and the leak conductance
kv4 = ((0.225*-cos(0.2618*ZT))+0.275);
g_k3 = kv3*Pars3(11); g_k4 = kv4*Pars4(11);
g_ca=3.86;  g_k1 = Pars1(11);
%Major fixed conductances
```

```
sigma=0.05; iapp = zeros(numT,1);
%Noise setting


%Choose a Kv2 current

kv2call = 'What form of Shab? (1=Native, 2=With hKv9WT, 3=With
hKv9MU):';

kv2choice = input(kv2call);

if     kv2choice == 1;
%Normal Kv2 current

    Pars2 = KV2; g_na=60; iapp(:) = -4.97;

elseif kv2choice == 2;
%Kv2 with human wild-type Kv9

    Pars2 = KV9W; g_na=62; iapp(:) = -4.8;

elseif kv2choice == 3;
%Kv2 with mutant c379E Kv9

    Pars2 = KV9M; g_na=58.9; iapp(:) = -4.32; g_ca=g_ca*0.73;
g_k3=g_k3*1.1;

else

    disp('*Inappropriate answer.')

    disp('*Enter Kv2 type as either: 1, 2, or 3.')

    disp('*Please try again.')

    return

end

    g_k2 = Pars2(11);


% Initial conditions


v=-55;

mna=0.22; hna=0.02; mca=0.09; hca=0.032;

mk1=0.13; hk1=0.31; mk2 = 0.2; hk2 = 0.46;

mk4 = 0.45; hk4 = 0.85; mk3 = 0.52; hk3 = 0.985;


vrec=zeros(numT,1);
%Handles used to retrieve variables for the entire run

vrec(1)=v;
```

```
na1=zeros(numT,1);

na2=zeros(numT,1);

ca1=zeros(numT,1);

ca2=zeros(numT,1);

k11=zeros(numT,1);

k12=zeros(numT,1);

k21=zeros(numT,1);

k22=zeros(numT,1);

k31=zeros(numT,1);

k32=zeros(numT,1);

k41=zeros(numT,1);

k42=zeros(numT,1);

leak=zeros(numT,1);

I1=zeros(numT,1);

I2=zeros(numT,1);

I3=zeros(numT,1);

I4=zeros(numT,1);

%% Integrate using Euler-Maruyama method


for ix=2:numT

    %% gating functions


    % sodium activation

    mna_inf = 1/(1+exp(-(v+35.2)/7.9));
% In the form; 1./(1+exp(-(V-vh)/k))

    tau_mna = exp(-(v+286)/160);
%              a*exp(-((V-b)/c))


    % sodium inactivation

    hna_inf = 1/(1+exp((v+62)/5.5));
% In the form; 1./(1+exp((V-vh)/k));

    tau_hna = 0.51+exp(-(v+26.6)/7.1);
%              a*exp(-((V-b)/c));
```

```
% calcium activation
mca_inf = 1/(1+exp(-(v+25)/7.5));
tau_mca = 3.1;

% calcium inactivation
hca_inf = 1/(1+exp((v+260)/65));
tau_hca = exp(-(v-444)/220);

% potassium1 activation
mk1_inf = 1/((1+exp(-(v-Pars1(1))/Pars1(2))));
tau_mk1 = Pars1(3)*exp(-((v-Pars1(4))/Pars1(5)));

% potassium1 inactivation
hk1_inf = 1/((1+exp((v-Pars1(6))/Pars1(7))));
tau_hk1 = Pars1(8)*exp(-((v-Pars1(9))/Pars1(10)));

% potassium2 activation
mk2_inf = 1/((1+exp(-(v-Pars2(1))/Pars2(2))));
tau_mk2 = Pars2(3)*exp(-((v-Pars2(4))/Pars2(5)));

% potassium2 inactivation
hk2_inf = 1/((1+exp((v-Pars2(6))/Pars2(7))));
tau_hk2 = Pars2(8)*exp(-((v-Pars2(9))/Pars2(10)));

% potassium3 activation
mk3_inf = 1/((1+exp(-(v-Pars3(1))/Pars3(2))));
tau_mk3 = Pars3(3)*exp(-((v-Pars3(4))/Pars3(5)));

% potassium3 inactivation
hk3_inf = 1/((1+exp((v-Pars3(6))/Pars3(7))));
tau_hk3 = Pars3(8)*exp(-((v-Pars3(9))/Pars3(10)));
```

```
% potassium4 activation
mk4_inf = 1/((1+exp(-(v-Pars4(1))/Pars4(2))));
tau_mk4 = Pars4(3)*exp(-((v-Pars4(4))/Pars4(5)));

% potassium4 inactivation
hk4_inf = 1/((1+exp((v-Pars4(6))/Pars4(7))));
tau_hk4 = Pars4(8)*exp(-((v-Pars4(9))/Pars4(10)));

% ionic currents;
Ina = g_na*(mna^3)*hna*(v-Ena);
Ica = g_ca*mca*hca*(v-Eca);
Ik1 = g_k1*(mk1^4)*hk1*(v-Ek);
Ik2 = g_k2*(mk2^4)*(hk2^Pars2(13))*(v-Ek);
Ik3 = g_k3*(mk3^4)*hk3*(v-Ek);
Ik4 = g_k4*(mk4^4)*hk4*(v-Ek);
Ileak = g_leak*(v-El);

%% Differential equations

dv=(iapp(ix)-Ina-Ica-Ik1-Ik2-Ik3-Ik4-Ileak)/C;
dmna=(mna_inf-mna)/tau_mna;
dhna=(hna_inf-hna)/tau_hna;
dmca=(mca_inf-mca)/tau_mca;
dhca=(hca_inf-hca)/tau_hca;
dmk1=(mk1_inf-mk1)/tau_mk1;
dhk1=(hk1_inf-hk1)/tau_hk1;
dmk2=(mk2_inf-mk2)/tau_mk2;
dhk2=(hk2_inf-hk2)/tau_hk2;
dmk3=(mk3_inf-mk3)/tau_mk3;
dhk3=(hk3_inf-hk3)/tau_hk3;
dmk4=(mk4_inf-mk4)/tau_mk4;
dhk4=(hk4_inf-hk4)/tau_hk4;
```

```
    W=(rand-0.5);


    v=v+dv*DT+(sigma*sqrt(DT)*W);
    mna=mna+dmna*DT;
    hna=hna+dhna*DT;
    mca=mca+dmca*DT;
    hca=hca+dhca*DT;
    mk1=mk1+dmk1*DT;
    hk1=hk1+dhk1*DT;
    mk2=mk2+dmk2*DT;
    hk2=hk2+dhk2*DT;
    mk3=mk3+dmk3*DT;
    hk3=hk3+dhk3*DT;
    mk4=mk4+dmk4*DT;
    hk4=hk4+dhk4*DT;


    I1(ix) = Ik1;
%Handles used to retrieve channel currents for the entire run
    I2(ix) = Ik2;
    I3(ix) = Ik3;
    I4(ix) = Ik4;


    vrec(ix)=v;
%Handles used to retrieve variables for the entire run
    na1(ix)=hna;
    na2(ix)=mna;
    ca1(ix)=hca;
    ca2(ix)=mca;
    k11(ix)=hk1;
    k12(ix)=mk1;
    k21(ix)=hk2;
    k22(ix)=mk2;
```

```
    k31(ix)=hk3;
    k32(ix)=mk3;
    k41(ix)=hk4;
    k42(ix)=mk4;
    leak(ix)=Ina;

end

%% Creating Figures

%pks =
findpeaks(vrec,'minPeakProminence',10,'Annotate','Extents');
%Calculates AP frequency of the run
%freq = length(pks)/10;
%frequency(iters) = freq
%k41a(iters,:) = k41(:);
%k42a(iters,:) = k42(:);

%end

%time = 0:0.00001:10; %for secs

set(0,'DefaultFigureWindowStyle','docked')
%Automatically docks subsequent figures

%To return to normal use:

%    figure()
%plots of gating variable phase-planes
%    subplot(2,2,1)
%    plot(k11(5:end),k12(5:end),'r')
%    title('Kv1')
%    ylabel('Inactivation')
%    subplot(2,2,2)
```

```
%    plot(k21(5:end),k22(5:end),'b')
%    title('Kv2')
%    subplot(2,2,3)
%    plot(k31(5:end),k32(5:end),'g')
%    title('Kv3')
%    ylabel('Inactivation')
%    xlabel('Activation')
%    subplot(2,2,4)
%    plot(k41(5:end),k42(5:end),'m')
%    title('Kv4')
%    xlabel('Activation')


%    figure()
%Plots of individual channel currents
%    subplot(2,1,1)
    plot(t,vrec);
    %title(['ZT',num2str(ZT),' Frequency ' num2str(freq) '
Hz'])
%    ylabel('Voltage (mV)')
%    subplot(2,1,2)
%    plot(t,I1,'Color',[0.5 0.3 0.1])
%    hold on
%    plot(t,I2,'b')
%    plot(t,I3,'r')
%    plot(t,I4,'g')
%    legend('Shaker','Shab','Shaw','Shal')
%    ylabel('Current(pA)')
%    xlabel('Time (ms)')
%
%    figure()
%Standard voltage plot of action potentials
%    plot(t,vrec);
%    title(['ZT',num2str(ZT),' Frequency ' num2str(freq) '
Hz'])
```

```
%    set(gca,'XTick',[0 2000 4000 6000 8000 10000])
%    set(gca,'XTickLabel',[0 2 4 6 8 10])
%    xlabel('Time (s)')
%    ylabel('Voltage (mV)')

%% Returning Outputs

    nOutputs = nargout;
    varargout = cell(1,nOutputs);
if nOutputs == 1
    varargout{1} = vrec;
elseif nOutputs == 2
    varargout{1} = vrec;
    varargout{2} = I1;
elseif nOutputs == 3
    varargout{1} = vrec;
    varargout{2} = I1;
    varargout{3} = I2;
elseif nOutputs == 4
    varargout{1} = vrec;
    varargout{2} = I1;
    varargout{3} = I2;
    varargout{4} = I3;
elseif nOutputs == 5
    varargout{1} = vrec;
    varargout{2} = I1;
    varargout{3} = I2;
    varargout{4} = I3;
    varargout{5} = I4;
end

end
```

A7 MODEL.mat

```
>> KV1

KV1 =

  -34.1761    9.7511    1.7929   -4.0678   73.8824  -93.1913
54.4931   22.1871   35.8125   52.0401    2.3466    4.0000
1.0000

>> KV2

KV2 =

  -29.6885   10.4942   30.7235  -63.6872   28.5394  -54.1081
22.4825    4.9594  -66.1917   52.4741    0.8639    4.0000
0

>> KV32

KV32 =

  -57.3022   14.6255    0.0307   20.0280  238.5817  -25.8216
2.4999  154.8312  159.8190  167.0988    1.3950    4.0000
1.0000

>> KV4

KV4 =

  -48.6331    7.6498    0.0541  -74.8583   61.5381  -43.0546
1.7309   44.5164  -66.2372  180.1061    1.2524    4.0000
1.0000

>> KV9W

KV9W =

  -45.2175   15.1802   21.6077  -73.0761   38.6172 -119.0544
31.1842  134.8676    9.9556   45.1851    1.7307    4.0000
1.0000

>> KV9M

KV9M =

  -43.5607   14.0186   24.8813  -79.9314   40.8414 -128.7633
5.3088  131.9673    5.5594  108.0317    1.9532    4.0000
1.0000
```